frontiers | Research Topics

Systems biology of maturation and senescence in horticultural plants

Edited by
Peitao Lü, Ji Tian, Cai-Zhong Jiang, Barbara Blanco-Ulate and Macarena Farcuh

Published in
Frontiers in Plant Science

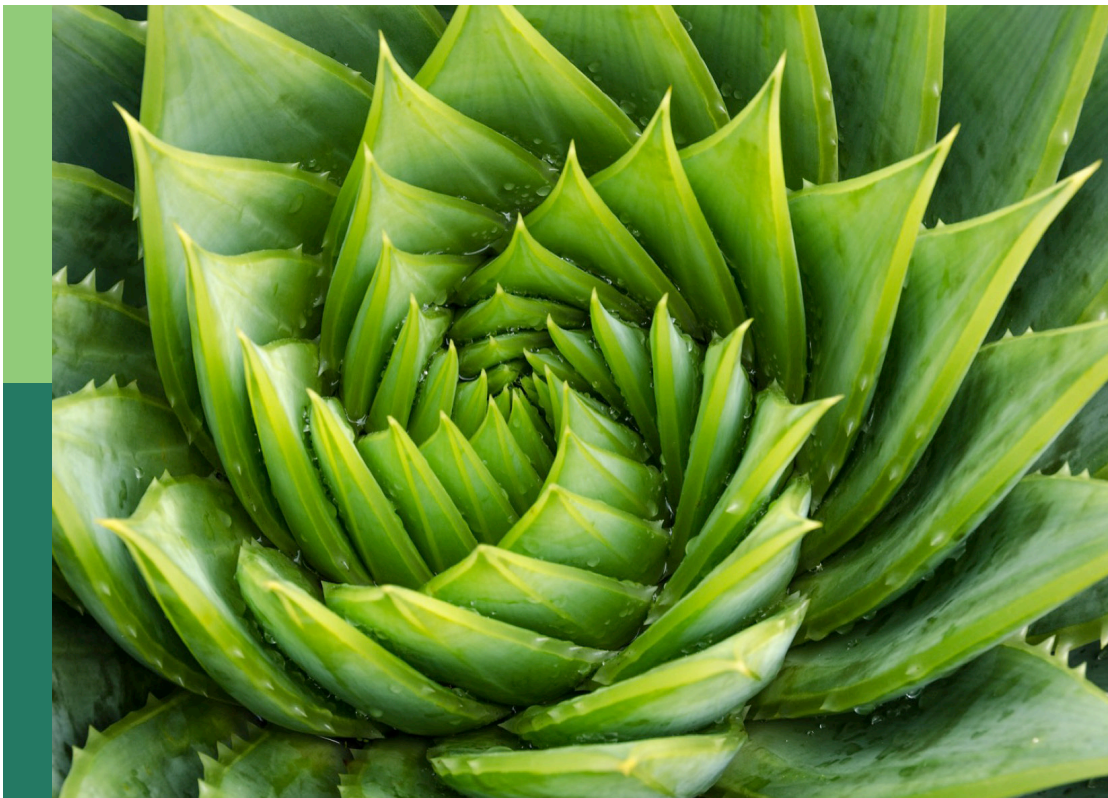

ISSN 1664-8714
ISBN 978-2-83251-377-4
DOI 10.3389/978-2-83251-377-4

About Frontiers

Frontiers is more than just an open access publisher of scholarly articles: it is a pioneering approach to the world of academia, radically improving the way scholarly research is managed. The grand vision of Frontiers is a world where all people have an equal opportunity to seek, share and generate knowledge. Frontiers provides immediate and permanent online open access to all its publications, but this alone is not enough to realize our grand goals.

Frontiers journal series

The Frontiers journal series is a multi-tier and interdisciplinary set of open-access, online journals, promising a paradigm shift from the current review, selection and dissemination processes in academic publishing. All Frontiers journals are driven by researchers for researchers; therefore, they constitute a service to the scholarly community. At the same time, the *Frontiers journal series* operates on a revolutionary invention, the tiered publishing system, initially addressing specific communities of scholars, and gradually climbing up to broader public understanding, thus serving the interests of the lay society, too.

Dedication to quality

Each Frontiers article is a landmark of the highest quality, thanks to genuinely collaborative interactions between authors and review editors, who include some of the world's best academicians. Research must be certified by peers before entering a stream of knowledge that may eventually reach the public - and shape society; therefore, Frontiers only applies the most rigorous and unbiased reviews. Frontiers revolutionizes research publishing by freely delivering the most outstanding research, evaluated with no bias from both the academic and social point of view. By applying the most advanced information technologies, Frontiers is catapulting scholarly publishing into a new generation.

What are Frontiers Research Topics?

Frontiers Research Topics are very popular trademarks of the *Frontiers journals series*: they are collections of at least ten articles, all centered on a particular subject. With their unique mix of varied contributions from Original Research to Review Articles, Frontiers Research Topics unify the most influential researchers, the latest key findings and historical advances in a hot research area.

Find out more on how to host your own Frontiers Research Topic or contribute to one as an author by contacting the Frontiers editorial office: frontiersin.org/about/contact

Systems biology of maturation and senescence in horticultural plants

Topic editors

Peitao Lü — Fujian Agriculture and Forestry University, China
Ji Tian — Beijing University of Agriculture, China
Cai-Zhong Jiang — Crops Pathology and Genetics Research Unit, Agricultural Research Service (USDA), United States
Barbara Blanco-Ulate — University of California, Davis, United States
Macarena Farcuh — University of Maryland, College Park, United States

Citation

Lü, P., Tian, J., Jiang, C.-Z., Blanco-Ulate, B., Farcuh, M., eds. (2023). *Systems biology of maturation and senescence in horticultural plants*.
Lausanne: Frontiers Media SA. doi: 10.3389/978-2-83251-377-4

Table of contents

frontiers | Frontiers in Plant Science

TYPE Editorial
PUBLISHED 05 January 2023
DOI 10.3389/fpls.2022.1123695

OPEN ACCESS

EDITED AND REVIEWED BY
Zoran Nikoloski,
Max Planck Institute of Molecular Plant Physiology, Germany

*CORRESPONDENCE
Peitao Lü
ptlv@fafu.edu.cn

†These authors have contributed equally to this work

SPECIALTY SECTION
This article was submitted to Plant Systems and Synthetic Biology, a section of the journal Frontiers in Plant Science

RECEIVED 14 December 2022
ACCEPTED 20 December 2022
PUBLISHED 05 January 2023

CITATION
Lü P, Tian J, Jiang C-Z, Blanco-Ulate B and Farcuh M (2023) Editorial: Systems biology of maturation and senescence in horticultural plants. *Front. Plant Sci.* 13:1123695. doi: 10.3389/fpls.2022.1123695

Editorial: Systems biology of maturation and senescence in horticultural plants

Peitao Lü[1*†], Ji Tian[2†], Cai-Zhong Jiang[3,4], Barbara Blanco-Ulate[4] and Macarena Farcuh[5]

[1]College of Horticulture, Fujian Agriculture and Forestry University, Fuzhou, China, [2]Department of Horticulture, Beijing University of Agriculture, Beijing, China, [3]Crops Pathology and Genetics Research Unit, United States Department of Agriculture-Agricultural Research Service (USDA-ARS), Davis, CA, United States, [4]Department of Plant Sciences, University of California, Davis, Davis, CA, United States, [5]Department of Plant Science and Landscape Architecture, University of Maryland, College Park, MD, United States

KEYWORDS

horticultural plant, maturation, senescence, systems biology, omics

Editorial on the Research Topic
Systems biology of maturation and senescence in horticultural plants

Plant organ maturation and senescence is a terminal and irreversible developmental process that transforms organs from nutrient assimilation to quality formation or nutrient reallocation, which is essential for the value of horticultural plants (Guo et al., 2021). The onset and progression of organ maturation and senescence in horticultural plants is regulated by endogenous and environmental cues. This process involves highly complex and ordered genetic programs closely coordinated by multidimensional regulation, including chromatin status, (post)transcriptional regulation, and (post) translational regulation (Woo et al., 2019). Over the last two decades, significant breakthroughs in revealing the molecular mechanisms underlying organ maturation and senescence have benefited from the identification and functional determination of key genes in some model plants, such as fruit ripening genes in tomato, flower senescence-associated genes (SAGs) in petunia and leaf SAGs in Arabidopsis (Guo et al., 2021). However, although some of the mechanisms of maturation and senescence have been dissected in model plants, these mechanisms are not always universal and are limited to the regulation of several key genes. Therefore, studies in this field are still challenging in other horticultural plants.

To address these questions, we established this Research Topic, aiming to gather a broad range of genetic, epigenetic, transcriptomic, and metabolomic studies related to organ maturation and senescence in horticultural plants. This collection includes 8 original research articles covering multi-omics in the regulation of organ abscission in ornamental plants (Jiang et al.; Wang et al.; Zhang et al.), functional regulation of key genes for ripening and bolting in fruit and vegetable (Chen et al.; Cheng et al.; Huang et al.), and functional compounds characterization in beverage and medicinal plants (Wang et al.; Zhou et al.). These studies featured diverse horticultural plants, including

rose, tea, marijuana, lettuce, strawberry, crabapple and red apple. In addition, we received one review on the internal and external factors regulating leaf senescence thereby influencing the quality and yield of horticultural plants (Zhao et al.). Here, we highlighted the main points of these contributed articles as follows:

Organ abscission in horticultural plants is one of the signs of maturation and senescence. However, premature abscission affects the quality of ornamental plants (Ito and Nakano, 2015). Wang et al. found that the abscission zone had been established at the base of the fruit pedicels of the fruit-abscission cultivars through the anatomical observation of different ornamental crabapple cultivars. Using biochemical assays and comparative transcriptomics, they further reported that fruit-abscission susceptible cultivars had significantly higher accumulation of hydrolases activity, which may be due to cross-talks among phytohormones and a few key transcription factors (TFs) that play important regulatory roles in this process. In rose petal abscission studies, Jiang et al. performed a comprehensive analysis of shedding at the translational and post-translational levels using transcriptome, proteome, and ubiquitome data. Based on a series analyses, they conclude that the accumulation of peroxidase (POD) may be related to the deposition of lignin, forming a protective layer during petal shedding. Zhang et al. analyzed the effect of silver thiosulfate (STS), a commonly used chemical to block the action of ethylene, on petal abscission in cut rose at transcriptomic and metabolomic levels. They demonstrated that STS significantly delayed rose petal abscission by reducing pectinase and cellulase activities thereby preventing cell wall degradation. They also identified a few important metabolites and revealed insights into STS-delayed rose petal abscission. Their findings provide valuable clues for subsequent studies of petal abscission in ethylene-sensitive flowers.

Plant development or stress-induced maturation and senescencein horticultural plants are accompanied by global changes in metabolites and gene expression. Cheng et al. investigated the molecular divergences at three fruit ripening stages in red apple. By comparing metabolites of these developmental stages, they hypothesized that there may be a competitive relationship between anthocyanins and flavonols in the biosynthesis during fruit ripening. They further identified members of the bZIP and MYB families as hub transcription factors that regulate anthocyanins and flavonols biosynthesis based on transcriptome and chromatin accessibility data. In diploid strawberry genome, Huang et al. identified 8 *Cellulose synthase* (*CesA*) genes and 25 *Cellulose synthase-like* (*Csl*) genes and characterized the function of *FveCesA4* involved in the regulation of fruit ripening by transient overexpression and knock-down experiments. Meanwhile, based on weighted gene co-expression network analysis (WGCNA) and gene silencing, Chen et al. demonstrated that a transcription factor LsMYB15 may play an important role in the melatonin-induced bolting delay in response to high temperature stress in lettuce. These studies show that multifaceted research approaches have been well applied to the study of maturation and senescence and can functionally elucidate regulatory mechanisms governing this process in horticultural plants.

The maturation process of horticultural plants is accompanied by the formation of functional compounds. In recent years, the identification of functional substances has received more and more attention in beverage and medicinal plants (Ghoshal and Kansal, 2019). Zhou et al. analyzed the composition of lipids in the albino tea and their changes in response to light by lipidomics combined with transcriptomics. They found that three key lipid components were significantly associated with the chlorophyll SPAD and suggested that *HY5* and *GLIP* may be hub genes involved lipid regulation *via* WGCNA. Furthermore, Wang et al. identified 42 MATEs in *Cannabis sativa* genome and revealed that several candidate *CsMATEs* may be involved in the biosynthesis of cannabinoids in different tissues and under UV-B treatment. These studies have laid a potential foundation for the exploration of functional compounds in horticultural plants.

The study of leaf senescence has long been a hot field. Zhao et al. discussed the crosstalk between leaf senescence and the quality, productivity and stress tolerance in horticultural plants. The authors highlighted the importance of hormones (ethylene, ABA and cytokinins), genes (TFs and SAGs) and abiotic stresses (temperature, light and moisture) to provide insights into the regulation of leaf senescence, thereby maximizing quality and yield and enhancing stress tolerance.

The maturation and senescence of horticultural plants is highly ordered and complex. Most contributors to this Research Topic analyzed the plasticity and complexity mechanisms of maturation and senescence of horticultural plants from a systems perspective and a multi-omics approach. We hope that these studies will contribute to improve the quality and yield of horticultural crops and provide useful information for genome-wide biodesign-based molecular breeding.

Author contributions

PL wrote the manuscript. All authors contributed to the article and approved the submitted version.

Funding

This work was supported by the Construction of Plateau Discipline of Fujian Province, China (102/71201801101) and the Leading Innovative Talents Introduction and Cultivation Project, Changzhou, China (CQ20220018) to PL; by Beijing

nova program (Z201100006820142) and the Supporting Plan for Cultivating High-level Teachers in Colleges and Universities in Beijing (CIT&TCD201904054) to JT; by start-up funds from the College of Agriculture and Natural Resources and the Department of Plant Science and Landscape Architecture (UMD) to MF.

Conflict of interest

The authors declare that the research was conducted in the absence of any commercial or financial relationships that could be construed as a potential conflict of interest.

Publisher's note

All claims expressed in this article are solely those of the authors and do not necessarily represent those of their affiliated organizations, or those of the publisher, the editors and the reviewers. Any product that may be evaluated in this article, or claim that may be made by its manufacturer, is not guaranteed or endorsed by the publisher.

References

Ghoshal, G. G., and Kansal, S. K. (2019). "The emerging trends in functional and medicinal beverage research and its health implication," in *Functional and medicinal beverages: Volume 11: The science of beverages*. Eds. A. M. Grumezescu and A. M. Holban (Academic Press), 41–71. doi: 10.1016/B978-0-12-816397-9.00002-9

Guo, Y., Ren, G., Zhang, K., Li, Z., Miao, Y., and Guo, H. (2021). Leaf senescence: progression, regulation, and application. *Mol. Horticult.* 1, 5. doi: 10.1186/s43897-021-00006-9

Ito, Y., and Nakano, T. (2015). Development and regulation of pedicel abscission in tomato. *Front. Plant Sci.* 6. doi: 10.3389/fpls.2015.00442

Woo, H. R., Kim, H. J., Lim, P. O., and Nam, H. G. (2019). Leaf senescence: systems and dynamics aspects. *Annu. Rev. Plant Biol.* 70, 347–376. doi: 10.1146/annurev-arplant-050718-095859

frontiers | Frontiers in Plant Science

ORIGINAL RESEARCH
published: 28 June 2022
doi: 10.3389/fpls.2022.921021

LsMYB15 Regulates Bolting in Leaf Lettuce (*Lactuca sativa* L.) Under High-Temperature Stress

*Li Chen, Mengnan Xu, Chaojie Liu, Jinghong Hao, Shuangxi Fan and Yingyan Han**

Beijing Key Laboratory of New Technology in Agricultural Application, National Demonstration Center for Experimental Plant Production Education, Beijing University of Agriculture, Beijing, China

High temperature is one of the primary environmental stress factors affecting the bolting of leaf lettuce. To determine the potential role of melatonin in regulating high-temperature induced bolting in leaf lettuce (*Lactuca sativa* L.), we conducted melatonin treatment of the bolting-sensitive cultivar "S39." The results showed that 100 μmol L^{-1} melatonin treatment significantly promoted growth, and melatonin treatment delayed high-temperature-induced bolting in lettuce. RNA-seq analysis revealed that the differentially expressed genes (DEGs) involved in "plant hormone signal transduction" and "phenylpropanoid biosynthesis" were significantly enriched during high-temperature and melatonin treatment. Quantitative reverse transcription polymerase chain reaction (qRT-PCR) analysis suggested that the expression patterns of abscisic acid (ABA)-related genes positively correlated with stem length during leaf lettuce development. Furthermore, weighted gene co-expression network analysis (WGCNA) demonstrated that MYB15 may play an important role in melatonin-induced resistance to high temperatures. Silencing the *LsMYB15* gene in leaf lettuce resulted in early bolting, and exogenous melatonin delayed early bolting in leaf lettuce at high temperatures. Our study provides valuable data for future studies of leaf lettuce quality.

Keywords: melatonin, leaf lettuce, high temperature, bolting, ABA-related gene

OPEN ACCESS

Edited by:
Peitao Lü,
Fujian Agriculture and Forestry University, China

Reviewed by:
Tao Wu,
Hunan Agricultural University, China
Wang Huasen,
Zhejiang Agriculture and Forestry University, China

****Correspondence:***
Yingyan Han
hyybac@126.com

Specialty section:
This article was submitted to Plant Systems and Synthetic Biology, a section of the journal Frontiers in Plant Science

Received: *15 April 2022*
Accepted: *30 May 2022*
Published: *28 June 2022*

Citation:
Chen L, Xu M, Liu C, Hao J, Fan S and Han Y (2022) LsMYB15 Regulates Bolting in Leaf Lettuce (Lactuca sativa L.) Under High-Temperature Stress. Front. Plant Sci. 13:921021. doi: 10.3389/fpls.2022.921021

INTRODUCTION

Leaf lettuce (*Lactuca sativa* L.) is an annual vegetable crop of the Asteraceae family. It produces a range of organic compounds, such as proteins, fiber, phenols, and others, and has both edible and medicinal value (Chadwick et al., 2016). As the cultivation of leaf lettuce expands year on year and development continues, it has become one of the most-consumed leafy vegetables in the world (Viacava et al., 2017). Leaf lettuce is primarily cultivated in polytunnels and similar facilities and is prone to bolting (producing a flowering stem prematurely) at high temperatures during cultivation. Bolting is accelerated under high-temperature conditions, which causes leaves to become bitter-tasting and limits crop marketability (Han et al., 2021a,b). Therefore, delayed bolting and flowering are preferred in lettuce for maximizing harvestable yield while maintaining culinary quality.

Leaf lettuce is a cruciferous vegetable and self-pollinating plant whose flowering is accelerated under longer day lengths and higher ambient temperatures (Uwimana et al., 2012).

Premature flowering limits vegetative growth, and thus the accumulation of sufficient resources for sustained growth. Plants undergo profound physiological changes when transitioning from vegetative to reproductive growth. Due to its importance in both basic and translational biology, flowering time has been extensively studied in model plant species, particularly in *Arabidopsis thaliana* (thale cress; Han et al., 2021a,b). Research has shown that, in *Arabidopsis*, at least six genetic pathways regulate the transition to flowering, including the photoperiod, vernalization, autonomous, ambient temperature, age-dependent, and gibberellin (GA) pathways, which coordinate with one another to regulate flowering (Izawa, 2020). The signals from flowering pathways, such as *FLOWERING LOCUS T* (*FT*), *SUPPRESSOR OF OVEREXPRESSION OF CO1* (*SOC1*), and *LEAFY* (*LFY*), are integrated into the genetic network of flowering (Jutarou et al., 2021). Among these integrons, the florigen gene *FT* is the central node of floral transition, whose transcriptional expression is positively regulated by zinc finger transcription factor *CONSTANS* (*CO*), while negatively regulated by *FLOWERING LOCUS C* (*FLC*; Zong et al., 2021). It has been widely reported that different environmental factors affect plant flowering by regulating the expression of floral integrons and stimulating changes in plant hormone levels (Zou et al., 2020). Increasing evidence suggests that flowering time is associated with plant hormones (Ying et al., 2014). In *Arabidopsis*, it has been found that the target of the repressive function of abscisic acid (ABA) is the flowering-promoting gene *SOC1*. One report has it that the CORONATINE INSENSITIVE1 (COI1)-dependent signaling pathway delays the flowering time by inhibiting the expression of the florigen gene FLOWERING *LOCUS T* (*FT*). This proved that the APETALA2 transcription factor (TFs) TARGET OF EAT1 (TOE1) and TOE2 interact with JAZ (Jasmonate-Zim domain) protein and repress the transcription of FT (Zhai et al., 2015). Therefore, understanding the crosstalk between hormones and flowering-related genes is of great importance for elucidating the regulatory mechanisms of bolting and flowering in plants.

In vegetable cultivation and production, leafy vegetables that can bolt include, primarily, Chinese cabbage, beets, spinach, celery, onion, and lettuce. The "low-temperature vernalization" types of cruciferous vegetables have been extensively studied. In *Arabidopsis*, *FRIGIDA* (*FRI*) and *FLOWERING LOCUS C* (*FLC*) are important genes regulating the vernalization pathway, and mechanistically interact to control flowering time (Schon et al., 2021). *FLC* acts as a strong repressor of floral transition; before vernalization, expression of *FLC* is increased, and plants cannot bloom. When plant vernalization is completed, expression of *FLC* decreases, and the plants bloom. In Chinese cabbage (*Brassica rapa* ssp. *chinensis*), *BcFLC2* plays a key role in flowering regulation as a negative regulator by controlling the expression of *BcSOC1*, *BcSPL15*, *BcMAF2*, *BcTEM1*, and other genes closely related to flowering (Huang et al., 2018). The vernalization response in biennial beets (*Beta vulgaris*) is mediated by the *FT* homolog *BvFT1*, which, in contrast to the promotive action of *FT* in *Arabidopsis*, functions as a repressor of flowering (Pin et al., 2010).

High temperature is one of the primary environmental stress factors that affect the normal growth and development of plants (Chen et al., 2017). Studies have found that environmental temperature regulation of plant flowering is affected by multiple pathways. At ambient temperatures, *FLC* expression is quantitatively modulated by a chromatin-silencing mechanism, and the effect of chromatin on transcription and co-transcriptional processing is of central importance to the regulation of gene expression. The FT protein, acting as a florigen, is translocated from mature leaves to the shoot apex, simultaneously forming a complex with FLOWERING LOCUS D (FD). *SOC1* is first evoked in the shoot apex during the floral switch process (Kong et al., 2016). The FT-FD dimer and *SOC1* activate the downstream genes *LEAFY* (*LFY*), *AP1*, and *FRUITIFUL* (*FUL*) to define floral characteristics. *FLC* interacts with *SHORT VEGETATIVE PHASE* (*SVP*) to inhibit *SOC1* transcription by directly combining with the *SOC1* promoter in the vegetative phase, among which *SVP*, *FLM*, and their homologous genes play a key role (Balanzà et al., 2014). *SVP* is a flowering suppressor that inhibits plant flowering by combining with *FT* and *SCO1* gene promoter elements. The autonomous regulatory factors *FCA* and *FVE* participate in the environmental temperature regulation pathway by inhibiting *SVP* (Kong et al., 2016). In *Arabidopsis*, high temperatures reduce SVP-FLC and promote flowering (Jones et al., 2020). *SOC1* contributes to the GA-regulated floral transition, and *SOC1* expression is increased in response to GA treatments. Studies have shown that the *LsFT* gene is involved in the process of high temperatures promoting bolting and flowering in leaf lettuce, and using RNA interference (RNAi) technology to knock down *LsFT*, the *LsSOC1* gene leads to delayed bolting and insensitivity to high temperatures (Chen et al., 2017, 2018).

Melatonin (*N*-acetyl-5-methoxytryptamine) was first discovered in plants in 1995 (Kanwar et al., 2018), and whether melatonin is universally present and what its function is in plants has subsequently attracted widespread attention. The presence of melatonin was reported in all plants tested and in different parts of plants, including roots, stems, leaves, flowers, fruits, and seeds (Arnao and Hernández-Ruiz, 2020; Onik et al., 2020), where the focus was on the effects of exogenous melatonin on plant growth, morphogenesis, and certain environmental stresses (Sun et al., 2020). Melatonin's actions include its ability to act as a plant biostimulator against stress, both biotic and abiotic, its ability to regulate plant growth, and its ability to regulate the processes of plant vegetative development (Arnao and Hernández-Ruiz, 2018, 2019; Jahan et al., 2021a). In studies of senescence in kiwifruit leaves, due to the enhanced scavenging activity of the antioxidant enzymes peroxidase (POD), superoxide dismutase (SOD), and catalase (CAT), membrane damage was reduced, and reduction in the hydrogen peroxide (H_2O_2) content effectively delayed senescence (Liang et al., 2018). In general, cold, heat, salinity, drought, UV radiation, and chemical toxicity are countered or mitigated by the presence of melatonin (Arnao and

Hernández-Ruiz, 2018; Choi and Back, 2019; Moustafa-Farag et al., 2019). Melatonin promotes the relationship between the growth of maize seedlings and the pathways related to nitrogen metabolism, coordinating the growth and development of maize seedlings and resulting in increased plant survival rates, higher shoot and deeper root growth, and improved photosynthetic efficiency (Erdal, 2019). Melatonin also promotes the relationship between grape seedling growth and sugar metabolism, improving the resistance of grape seedlings, accompanied by improved chloroplast and stomatal morphologies (Zhong et al., 2020).

In this study, in order to obtain insights into transcriptional regulation by melatonin treatment on early bolting and flowering in leaf lettuce under high-temperature stress, we used RNA sequencing (RNA-seq) analysis to study exogenous melatonin at high temperatures in the bolting-sensitive lettuce cultivar "S39." Transcriptome analysis revealed that plant hormone signals, including ABA, ethylene, and GA signals, are involved in this process. The level of *LsMYB15*, an ABA-related gene, increases significantly during this process. Based on an analysis of the genes in the stem length-related gene module and using weighted gene co-expression network analysis (WGCNA), we determined that *LsMYB15* plays an important regulatory function in bolting in leaf lettuce. We propose that *LsMYB15* could be a useful and effective genetic resource for the improvement of leaf lettuce quality.

MATERIALS AND METHODS

Plant Materials and Growing Conditions

The bolting-sensitive *L. sativa* cultivar S39 was selected and grown at the Beijing University of Agriculture Experimental Station under greenhouse conditions [seeds provided by Cathay Green Seeds (Beijing) Co., Ltd.]. The photoperiod was 16 h/8 h (light/dark), the light intensity was maintained at 200 μmol m^{-2} s^{-1}, the temperature was maintained at 20°C/15°C (day/night), and the relative humidity was 60–65%. Pest control and water management were carried out according to standard practices. A total of 300 uniform and disease-free plump seeds were selected, which were then immersed in 9 cm-diameter petri dishes filled with filter paper moistened with distilled water. The dishes were then placed in a lighted incubator in order to germinate. Following the development of a white radical, the seeds were transplanted into a plug tray and placed in a lighted incubator for cultivation.

Melatonin Treatment

When the leaf lettuce seedlings had reached the three-leaf-center stage, they were transplanted to a nutrition bowl 11 cm (diameter) × 12 cm (height), which remained in the light incubator; plants displaying consistent growth conditions were selected for testing. In October 2020, when the seedlings reached the five-leaf-center stage, they were subjected to a day/night temperature setting of 20°C/15°C, a photoperiod of 16 h/8 h, a light intensity of 200 μmol m^{-2} s^{-1}, and a relative humidity of 60–65%. Following initiation of the treatment, melatonin (Sigma-Aldrich, Shanghai, China) was sprayed onto the plants with a small sprayer at 9:00 a.m. on the morning of treatment at concentrations of 0, 10, 50, 100, and 150 μmol L^{-1}. Wearing gloves, the spray was applied evenly to leaf surfaces until the surfaces were wet but not dripping. Exogenous melatonin was applied every 3 days, and following treatment for 15 days, the plants were sampled at approximately 9:00 a.m., we selected leaves that had been subjected to different concentrations of melatonin in order to determine the physiological indicators of the indices of the primary functional leaves.

In February 2021, when the seedlings had reached the five-leaf-center stage, they were subjected to a day/night temperature setting of 35°C/30°C, a photoperiod of 16 h/8 h, a light intensity of 200 μmol m^{-2} s^{-1}, and a relative humidity of 60–65% for high-temperature treatment. Following initiation of the heat treatment, solutions of 0 μmol L^{-1} melatonin (H) and 100 μmol L^{-1} melatonin (HM) were sprayed onto the plants using the same small sprayer at 9:00 a.m. Again wearing gloves, the spray was applied evenly to the leaf surfaces until the surfaces were wet but not dripping. Exogenous melatonin was applied every 3 days, and the plants were subjected to high-temperature treatment for 30 days and sampled at approximately 9:00 a.m. The leaf lettuce was then immediately frozen in liquid nitrogen and stored at 80°C for further analysis. We selected leaves (in triplicate) at 0, 6, 9, 15, 18, and 27 days that showed obvious changes in phenotype, and the physiological indicators of the indices of the primary functional leaves were determined and subjected to RNA-seq analysis.

RNA Extraction and qRT-PCR Analysis

An RNA extraction kit (Aidlab, Beijing, China) was used to extract total RNA from lettuce leaves according to the manufacturer's instructions, and RNA was converted into complementary DNA (cDNA) using an Access RT-PCR system (Promega Corporation, Madison, WI, United States). qRT-PCR and SYBR Green qPCR Mix (Takara Bio Inc., Shiga, Japan) and a Bio-Rad CFX96 real-time PCR system (Bio-Rad, Hercules, CA, United States) were used to analyze gene expression levels. The US National Center for Biotechnology Information (NCBI) primer basic local alignment search tool (BLAST) algorithm[1] was used to design PCR primers, which are listed in **Supplementary Table 3**. Next, 10 μl 2 × SYBR Green qPCR Mix (Takara Bio Inc.), 7 μl ddH_2O, 1 μl upstream primer, 1 μl downstream primer, and 1 μl 100 ng cDNA were added to tubes, for a total volume of 20 μl. After mixing the reaction, the program was set to 95°C for 30 s, 95°C for 10 s, 60°C for 15 s, and 72°C for 30 s for 39 cycles. Following completion of the amplification cycle and cooling to 60°C, the DNA product was denatured by heating it to 95°C, and a melting curve was generated after the operation was completed. The leaf lettuce 18S ribosomal RNA gene was used as an internal control to normalize transcript levels, and $2^{(-\Delta\Delta Ct)}$ analysis was used to calculate the transcript levels.

[1]https://www.ncbi.nlm.nih.gov/tools/primer-blast

RNA-Seq Library Preparation and Sequencing

RNA library preparation and sequencing were carried out. The preliminary quality inspection included Nanodrop detection, agarose gel electrophoresis detection, and Agilent 2100 detection, which were used to determine RNA concentration, RNA integrity, and RNA integrity number (RIN), respectively. A 1% agarose gel was used to test for RNA degradation and contamination. If the RNA bands were clear, it was taken that there were no impurities or contamination. The RNA 6000 Nano kit was used for testing, the kurtosis of the sample was concentrated, and the RNA degradation rate was low, generally meeting the requirements for standard library construction. According to the recommendation of the manufacturer (Shanghai Majorbio Biopharm Technology Co., Ltd), 33 sequencing libraries were generated, the libraries were sequenced on an Illumina HiSeq platform (Illumina, Inc., San Diego, CA, United States), and paired-end reads were generated. SeqPrep software[2] and Sickle[3] were used to perform quality control on the original sequencing data to obtain high-quality quality control data (clean data) to ensure the accuracy of subsequent analytic results.

Differential Expression Analysis

After obtaining the read counts of genes, the differential expression of genes between samples was analyzed to identify differentially expressed genes (DEGs) between samples, and the functions of differential genes were investigated. The differential expression module selects the DESeq2 software to analyze the raw counts. The default parameters are $p < 0.05$ & $|\log2FC| >= 1$; to control the probability or frequency of errors in the overall inference result, the p value obtained by the statistical test was subjected to multiple test corrections, which is known as the p-adjust value. The platform uses BH (FDR for correction with Benjamini/Hochberg) for multiple test corrections of data. At values of $p < 0.05$, genes were considered differentially expressed.

GO and KEGG Cluster Analysis of Differentially Expressed Genes

The gene ontology (GO) database[4] was used to analyze genes and gene products according to their participation in biological processes (BPs), molecular functions (MFs), and cellular components (CCs), which were classified and annotated according to these three aspects. For $p < 0.05$, DEGs were considered significantly enriched. Kyoto Encyclopedia of Genes and Genomes (KEGG)[5] to perform KEGG pathway enrichment analysis on the genes in the gene set. The calculation principle is the same as that used in the GO function enrichment analysis. Fisher's exact test was used for enrichment analysis. The Benjamini–Hochberg (BH) multiple calibration method was chosen to check the p values. For corrected $p < 0.05$, the KEGG pathway that meets this condition was considered to be significantly enriched in the gene set.

Co-expression Analysis of Transcription Factors and Phenotypic Data (WGCNA)

Weighted gene co-expression network analysis (WGCNA) was used to identify modules of highly correlated genes based on the FPKM data.[6] After obtaining the gene modules that are commonly expressed, we linked the modules to the phenotypic information of interest to explore whether the expression of transcription factors is related to high-temperature bolting genes.

Construction of and Infection With *LsMYB15* VIGS Vectors

The 340-bp open reading frames of *LsMYB15* were used to design the primers (**Supplementary Table 3**). The fragments were then cloned from the S39 cDNA. The cloned fragments and pTRV2 empty vector were digested with EcoR1 endonuclease and BmaH1 endonuclease. Following purification, the fragments were ligated and transformed to obtain a recombinant plasmid. The identified recombinant plasmid was transformed into the *Agrobacterium* strain GV3101, and an infection solution was prepared. The infection buffer consisted of 10 mM $MgCl_2$, 10 mM MES, and 20 mM acetosyringone.

Three groups of plants were set up: a blank control group, in which the plants received no injection (WT); a negative control group, in which pTRV2 and pTRV1 empty vectors were mixed in a 1:1 ratio and injected into the plants (TRV2); and an experimental group, in which pTRV2-*LsMYB15* and pTRV1 empty vectors were mixed in a 1:1 ratio and injected (TRV2-*LsMYB15*; Wang et al., 2021). After 1 week of infection, the plants were held at 35°C for 1 week, and the other growth conditions remained unchanged. Plant morphological changes were monitored, including weekly measurements of stem length. After 1 week of high-temperature treatment, the new leaves that grew following the injection were randomly selected, then tested using the characteristic tobacco rattle virus (TRV) primers to determine whether the TRV virus had been transferred into the plants, and finally treated with exogenous melatonin. The cDNA of the young leaves was used to detect the effects by PCR and qRT-PCR using gene-specific primers. To observe morphological changes in the gene-silenced plants, the stem lengths of the plants that were infected for 1 week were measured.

Enzyme-Linked Immunosorbent Assay

An Enzyme-Linked Immunosorbent Assay (ELISA) test kit (Thermo Fisher Technology Co., Ltd., Shanghai, China) was used for testing in accordance with the manufacturer's instructions. The determination of antioxidant enzymes and the extraction and determination of endogenous hormones were both determined by ELISA. First, 0.1 g of lettuce leaves was weighed and ground into a powder using liquid nitrogen. The standard was then diluted, and samples were added according

[2]https://github.com/jstjohn/SeqPrep
[3]https://github.com/najoshi/sickle
[4]http://www.geneontology.org
[5]http://www.genome.jp/kegg
[6]https://horvath.genetics.ucla.edu/html/CoexpressionNetwork/Rpackages/WGCNA/

to the operating procedure and incubated at 37°C for 30 min. Each well was filled with a washing solution, incubated for 30 s, and the washing solution then discarded, which was repeated five times. A 50-μl volume of enzyme-labeled reagent was added to each well, except for blank wells, and incubated at 37°C for 30 min. The washing was repeated five times. Next, 50 μl of developer A and 50 μl of developer B were added to each well, the plate was gently shaken, and the color was developed at 37°C for 10 min in the dark. Finally, 50 μl of stop solution was added to each well to stop the reaction (in this case, the blue color turned yellow to indicate that the reaction had stopped). Measurements were then taken within 15 min. The blank well was adjusted to zero, and the absorbance/optical density (OD) of each well in sequence was measured at a wavelength of 450 nm. The OD values of plant ascorbate peroxidase (APX; EC 1.11.1.11), plant superoxide dismutase (SOD; EC 1.15.1.1), plant catalase (CAT; EC 1.11.1.6), plant peroxidase (POD; EC 1.11.1.7), phenylalanine ammonia lyase (PAL; EC 4.3.1.5), and plant polyphenol oxidase (PPO; EC 1.10.3.1) were measured at 290, 560, 240, 450, 290, and 420 nm, respectively. The ODs increased by 0.01, 0.01, 0.01, 0.01, 0.01, and 0.001 units (U), respectively.

Data Analysis

Experimental data were analyzed using one-way ANOVA followed by Tukey's multiple range test to compare differences between the significance of the difference was $p \leq 0.05$ or $p \leq 0.01$. Origin 95, Microsoft Excel 2016 and IBM SPSS Statistics 22 were used for analysis.

RESULTS

Effects of Treatment With Different Concentrations of Melatonin on Growth and Development in Leaf Lettuce

To examine the potential role of melatonin in regulating the bolting-sensitive plant line S39, we treated plants with different concentrations of exogenous melatonin (0, 10, 50, 100, and 150 μmol L^{-1}), and then housed them under controlled-temperature conditions (20°C) for 15 days (**Figure 1A**). The results showed that exogenous melatonin significantly altered the blade length and blade width of leaf lettuce (**Figure 1B**). Specifically, a melatonin concentration of 100 μmol L^{-1} increased the leaf length and leaf width of leaf lettuce by 45 and 52%, respectively, compared to those treated with the lower concentrations. Therefore, we inferred that exogenous melatonin affected the growth and development of leaf lettuce. The preliminary experiment indicated that 100 μmol L^{-1} melatonin significantly enhanced growth vigor compared to the other treatment groups, and the plants grew very well. However, a melatonin concentration of 150 μmol L^{-1} resulted in serious wilting. To verify whether melatonin also affected the growth and development of leaf lettuce under high-temperature conditions, we selected 100 μmol L^{-1} melatonin for subsequent studies.

Transcriptome Analysis of Leaf Lettuce Treated With Melatonin and Subjected to High Temperatures

Leaf lettuce is susceptible to high-temperature stress during cultivation, which causes bolting and flowering, reducing the yield. Therefore, we treated plants with 100 μmol L^{-1} melatonin to further observe whether melatonin affected the growth of lettuce under high-temperature conditions. Furthermore, we treated leaf lettuce with 100 μmol L^{-1} melatonin at high temperatures during the growth period (the control group was not treated with exogenous melatonin under the same conditions) and found that phenotypes changed significantly at 0, 6, 9, 15, 18, and 27 days. Compared to the new phenotype, under the high-temperature treatment, the control group without exogenous melatonin bolted significantly faster than the treatment group with exogenous melatonin. Moreover, exogenous melatonin-treated lettuce leaves were larger and greener than those in the control group (**Figures 2A,B**). Therefore, we selected the S39 cultivar for transcriptome analysis in order to understand the exogenous melatonin regulation network of bolting during leaf lettuce development at high temperatures. Total RNA was extracted from three biological replicates of six different leaf developmental stages of S39 and used to generate cDNA libraries, which were subjected to paired-end sequencing using Illumina high-throughput RNA sequencing. After removing reads derived from rRNA and those of low quality, the total length of clean reads ranged from 45,664,626 to 63,758,324 among the different libraries, and almost 67% of the sequenced reads could be aligned to the apple genome (**Supplementary Table 1**). A Pearson correlation analysis indicated that the three libraries from the biological replicates of each developmental stage had highly consistent transcriptome profiles (**Supplementary Figure 1**).

Identification of Genes With Differential Expression During Leaf Development Under Melatonin Treatment

Fragments per kilobase of transcript per million mapped reads (FPKM) values were used to investigate transcript differences. As a result, 399 genes (ratio > 2.0, $p < 0.05$) were found to be upregulated and 506 genes (ratio < 0.5, $p < 0.05$) were downregulated in HM6 vs. H6. The DEGs at this stage were the lowest; 1,374 genes (ratio > 2.0, $p < 0.05$) were upregulated and 968 genes (ratio < 0.5, $p < 0.05$) were downregulated in HM9 vs. H9; 1,352 genes (ratio > 2.0, $p < 0.05$) were upregulated and 1,034 genes (ratio < 0.5, $p < 0.05$) were downregulated in HM15 vs. H15 (**Figures 2C,D**); 2,182 genes (ratio > 2.0, $p < 0.05$) were upregulated and 1,167 genes (ratio < 0.5, $p < 0.05$) were downregulated in HM18 vs. H18. The expression level of upregulated differential genes was the highest, and 2,099 genes (ratio > 2.0, $p < 0.05$) were upregulated and 2,960 genes (ratio < 0.5, $p < 0.05$) were downregulated in HM27 vs. H27. The DEGs were the most abundant at this stage (**Figures 2C,D**). Therefore, we focused on the analysis of the HM27 vs. H27 stage with the highest expression of DEGs in order to determine the causes of leaf lettuce phenotypic changes.

DEGs (ratio > 2.0 or ratio < 0.5, $p < 0.05$) were classified into different functional categories based on their GO annotations.

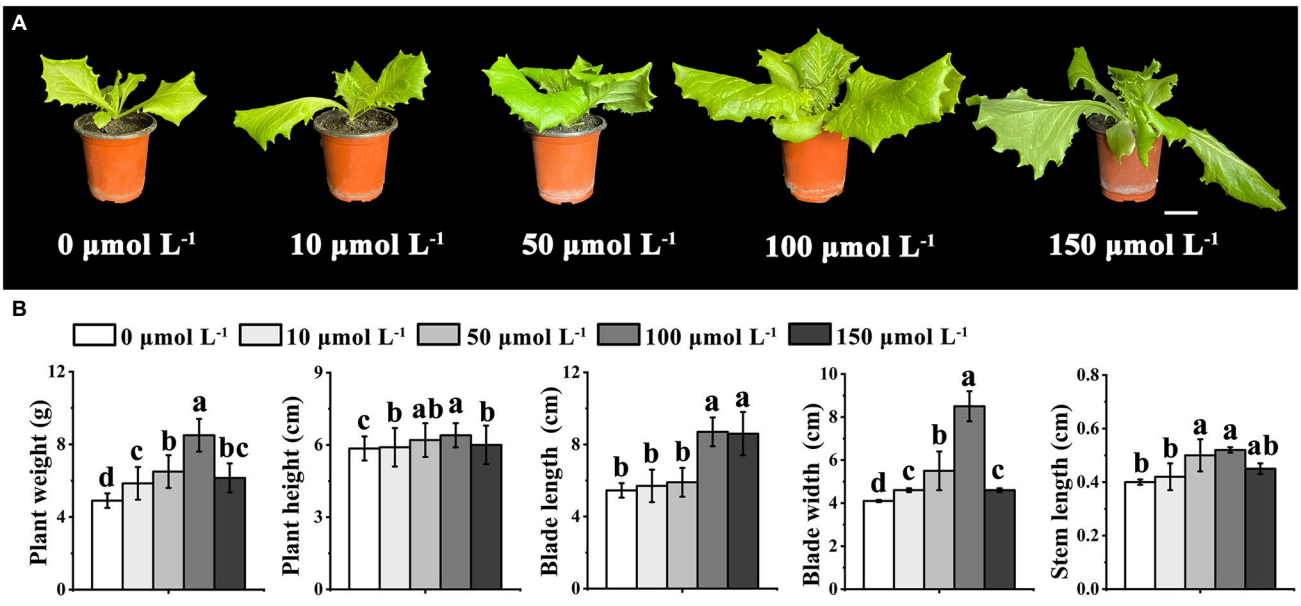

FIGURE 1 | Effects of different concentrations of melatonin treatment under control temperature (20°C) on growth and development in leaf lettuce. **(A)** Leaf lettuce of the bolting-sensitive line S39 treated with 0, 10, 50, 100, and 150 μmol L^{-1} melatonin, corresponding to the morphological features of five different concentrations. Scale bars = 5 cm. **(B)** The weight, height, blade length, blade width, and steam length of leaf lettuce in five different concentrations of melatonin. Different letters above the bars indicate significantly different values ($p < 0.05$) calculated using one-way analysis of variance (ANOVA) followed by a Tukey's multiple range test.

The numbers of DEGs involved in "metabolic processes" (MPs), BPs, "catalytic activity" (CA), and MF were largest in HM27 vs. H27 (**Figure 3A**). In all the treatments, most DEGs were from the BP and MF categories. KEGG is a pathway-related database that provides a classification for biologically complex patterns. Notably, KEGG terms associated with "plant hormone signal transduction," "starch and sucrose metabolism," and "phenylpropanoid biosynthesis" were enriched in HM27 vs. H27 and in HM9 vs. H9, which are stages that are significantly affected by variations in bolting (**Figure 3B**). Genes involved in "plant hormone signal transduction" were also enriched in HM27 vs. H27 and in HM9 vs. H9, including several plant hormone signal transduction and response proteins, including ABA-related genes, auxin-responsive genes, ethylene signal transduction pathway genes, and ethylene-responsive genes (**Supplementary Table 2**). These results suggested that, at high temperatures, exogenous melatonin not only plays an important role in leaf development but also affects bolting.

Identification of Important Modules and Genes for Bolting Accumulation in Leaf Lettuce Using WGCNA Analysis

Weighted gene co-expression network analysis (WGCNA) is a method for identifying networks of genes with certain associated functions or traits and for revealing putative hub genes with particular influence (Horvath et al., 2008; Yang et al., 2018). To identify genes associated with bolting in leaf lettuce, we identified co-expressed gene sets by applying WGCNA (**Figure 4A**) to examine the genes expressed after excluding those with low FPKM values (average FPKM <1) and/or a low coefficient of variation (<1) across all development stages. The 38,915 DEGs in the five different treatment regimes that met these stringent criteria were categorized into 35 co-expression modules (**Figure 4B**).

Next, we measured the weight, height, blade length, blade width, and steam length of leaf lettuce. The steam length of leaf lettuce treated with melatonin at high temperatures was shorter than that not treated with melatonin (**Figures 4C,D**). An analysis of the relationship between modules and stem length revealed that the Turquoise ($r = 0.87$, $p = 3e{-}06$) module and the Blue module ($r = 0.75$, $p = 3e{-}04$) were highly correlated with bolting (**Figure 4B**).

Genes associated with the "protein processing in endoplasmic reticulum," "ubiquitin-mediated proteolysis," "photosynthesis-antenna proteins," "MAPK signaling pathway-plant," and the "phosphatidylinositol-signaling system" categories were enriched in the Turquoise and Blue modules. Additionally, genes in the "oxidative phosphorylation," "glutathione metabolism," "porphyrin and chlorophyll metabolism," and "carotenoid biosynthesis" categories were also enriched in the Turquoise and Blue modules, which are all processes that have been associated with leaf lettuce bolting (**Supplementary Figure 2**).

To validate expression of the DEGs and bolting-related genes from the Turquoise and Blue modules, qRT-PCR in leaf lettuce was carried out for nine representative genes. The expression levels of the bolting-related genes *LsMYB15* (LG3315676, XP_023766862.1), *LsbHLH35* (LG5484648, PLY83907.1), *LsZAT10* (LG198317, XP_023764915.1), *LsNCED3* (LG7647715, PLY98266.1), *LsDPBF3* (LG8689275, XP_023768520.1), *LsWNK6* (LG4344685, XP_023729088.1), *LsSIZ1* (LG1143132, XP_023733270.1), *LsSPL12* (LG4402676, XP_023741755.1), and *LsAGL27* (LG4402879,

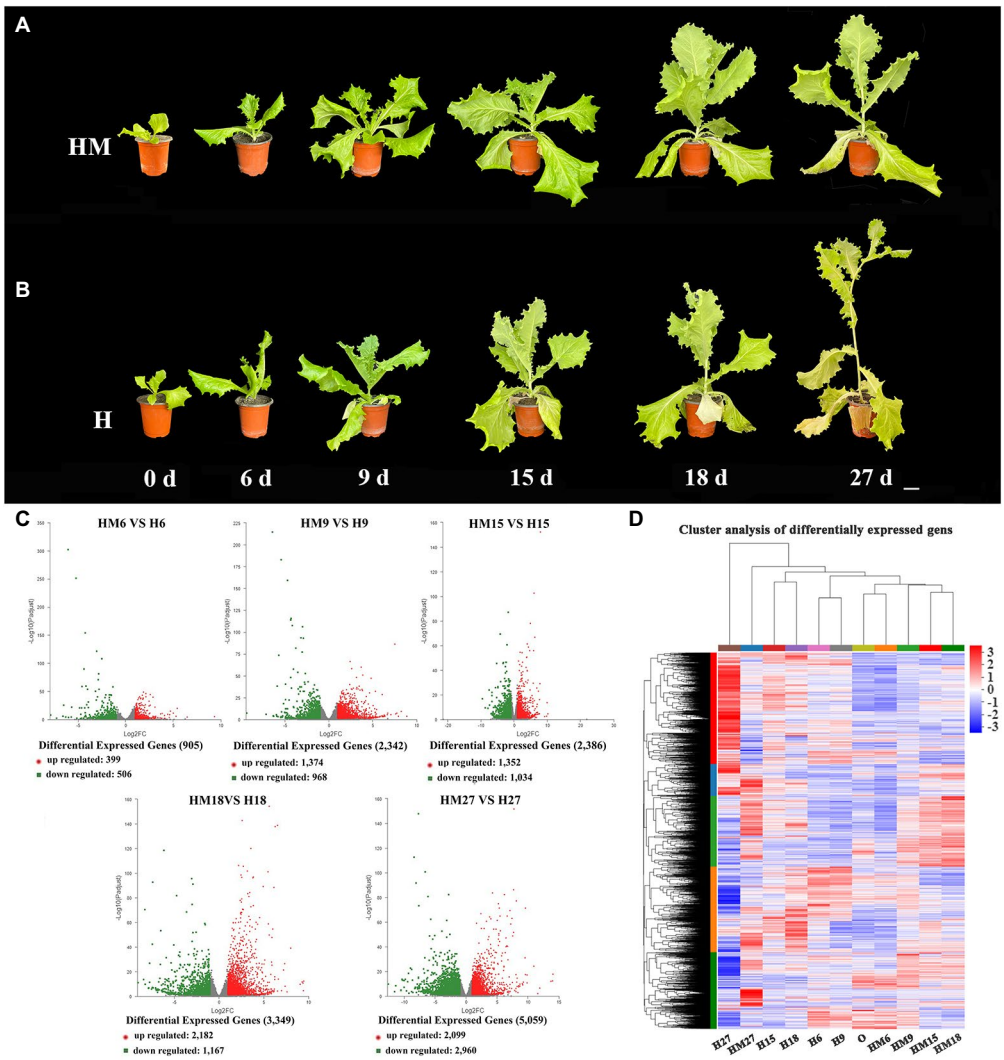

FIGURE 2 | RNA-seq analysis of leaf lettuce treated with 100 μmol L^{-1} melatonin at high temperature during the growth period (the control group did not receive exogenous melatonin under the same conditions). **(A)** In 100 μmol L^{-1} melatonin treatment (HM), the leaf developmental stages of phenotypes changed significantly at 0, 6, 9, 15, 18, and 27 days with different stem lengths, and whole plants were characterized. Scale bars = 5 cm. **(B)** In the control group that did not have exogenous melatonin (H), the leaf developmental stages of phenotypes changed significantly on 0, 6, 9, 15, 18, and 27 days with different stem lengths, and whole plants were characterized. Scale bars = 5 cm. **(C)** Volcano plot visualizing differentially expressed genes (DEGs). The DEGs are shown in red and green. The *x*-axis represents the fold change in HM6 vs. H6, HM96 vs. H9, HM15 vs. H15, HM18 vs. H18 and HM27 vs. H27 (on a log2 scale), and the *y*-axis represents the negative log10-transformed *p* values ($p < 0.05$) of the t test for determining differences between the samples. **(D)** Cluster analysis of DEGs during different leaf treatments.

XP_023741806.1) were examined. A correlation analysis showed that the expression of these nine genes was closely related to bolting (**Figure 5A**). The DEGs between the control and melatonin groups showed that, following melatonin treatment, significant upregulation of the expression of most regulatory genes in the ABA-related genes occurred, except for the *LsSPL12* gene (**Figure 5B**), as determined by RNA-seq. The relative gene expression analysis of selected DEGs (*LsMYB15*, LG3315676) indicated high integrity and correlation between the transcriptome analyses from the RNA-seq and qRT-PCR results (**Figure 5C**). This result indicated that inhibiting bolting in leaf lettuce was positively affected by melatonin treatment as a result of it increasing the expression of ABA-related genes.

Silencing of *LsMYB15* Expression in Leaf Lettuce Alters the Occurrence of Bolting

Under drought or cold conditions, ABA is often recruited as the primary signal for increasing the transcription levels of stress-responsive genes that may confer protection to assaulted plants (Agurla et al., 2018; Li et al., 2021). MYB transcription factors have been found to play important roles in many physiological processes under normal and adverse growth conditions (Guo et al., 2017). MYB15 is a member of the R2R3 MYB family of transcription factors in *Arabidopsis* (Ding et al., 2009). However, the role of MYB15 in high-temperature stress has not been previously reported. In the work reported below, we provide evidence

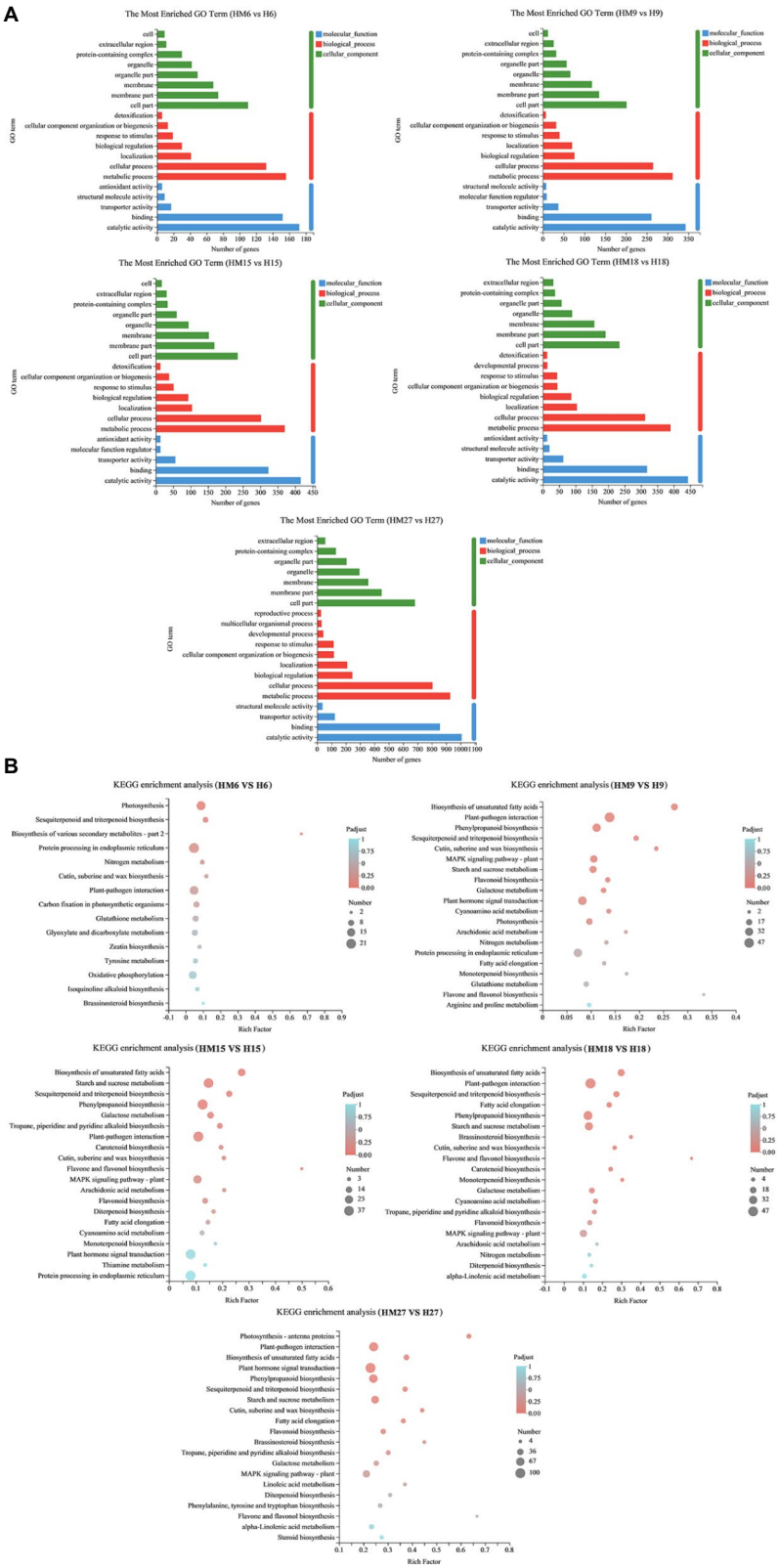

FIGURE 3 | GO classification and KEGG pathway enrichment of differentially expressed genes (DEGs) in lettuce leaves. **(A)** GO classification of DEGs. **(B)** KEGG pathway enrichment of DEGs. "MH" represents 100 μmol L^{-1} melatonin treatment under high temperature, and "H" represents no exogenous melatonin treatment under high temperature.

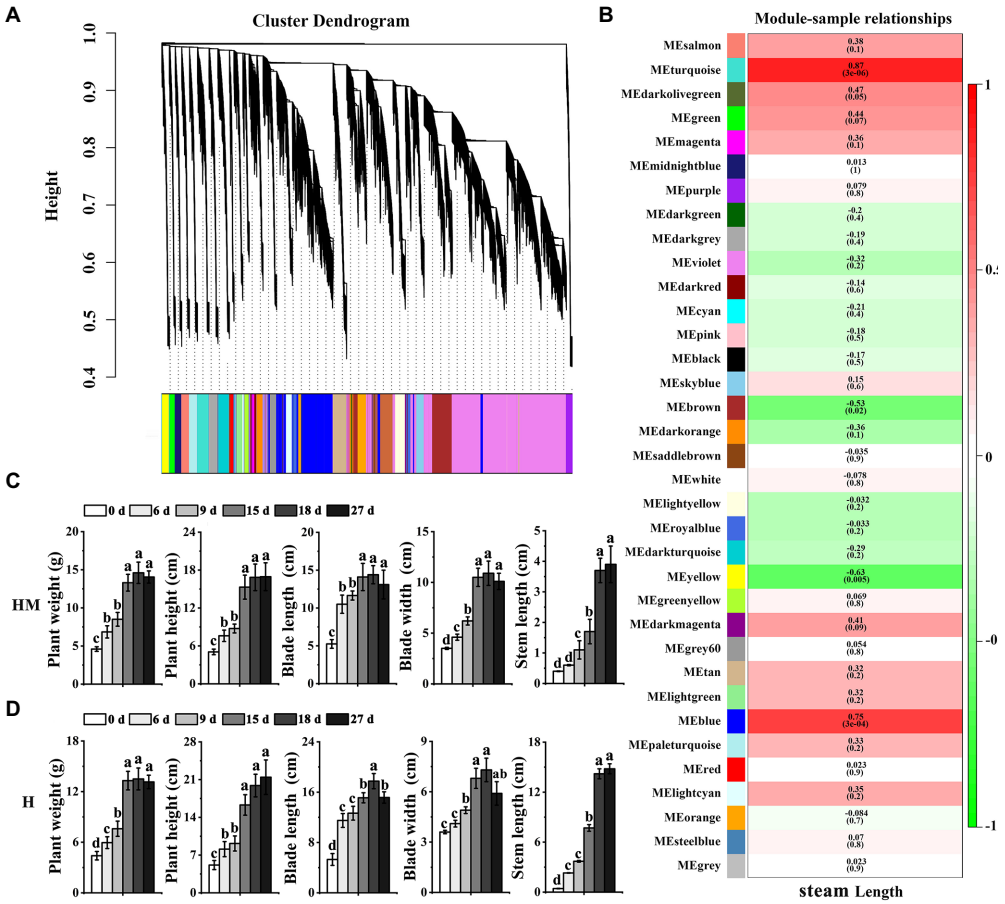

FIGURE 4 | Network analysis dendrogram showing modules identified by weighted gene co-expression network analysis (WGCNA). **(A)** Dendrogram plot with color annotation. **(B)** Module-bolting correlations and corresponding *p* values (in parentheses). The left panel shows the seven modules. The color scale on the right shows module trait correlation from 1 (green) to 1 (red). **(C)** The weight, height, blade length, blade width, and steam length of leaf lettuce in five developmental stages with exogenous melatonin at high temperature. "MH" represents 100 μmol L^{-1} melatonin treatment under high temperature. **(D)** The weight, height, blade length, blade width, and steam length of leaf lettuce in five developmental stages without exogenous melatonin at high temperature. "H" represents no exogenous melatonin treatment under high temperature. Different letters above the bars indicate significantly different values ($p < 0.05$) calculated using one-way analysis of variance (ANOVA) followed by a Tukey's multiple range test.

showing that silencing of *LsMYB15* leads to bolting in leaf lettuce. To further elucidate the role of the *LsMYB15* genes, we suppressed their expression in leaves of the bolting-sensitive S39 lettuce cultivar using virus-induced gene silencing (VIGS) in the TRV vector.

The leaf lettuce plants infiltrated with the virus containing TRV2-*LsMYB15* under high-temperature conditions and exposed to exogenous melatonin administration, along with a control group that did not receive exogenous melatonin or the viral construct, developed a bolting phenotype 7 days post-infection. In contrast, plants infiltrated with the empty vector pTRV2 did not bolt (**Supplementary Table 3**). The rapid bolting in plants expressing TRV2-*LsMYB15* was then examined in the control (**Figures 6A,B**). qRT-PCR revealed that the TRV2-*LsMYB15* transcript levels in the *LsMYB15*-silenced plants decreased by approximately 90% compared to the control plantlets. From the above phenotypic and physiological analyses, the expression levels of ABA-related genes in *LsMYB15*-silenced plants are of great significance. For this purpose, qRT-PCR was used to analyze and compare the gene transcription levels between the *LsMYB15*-silenced plants and the control plants (**Supplementary Table 4**). Based on the results from three independent analyses, we found that the transcription levels of three genes (*LsMYB15*, *LsCOR15A*, and *LsRD29A*) in the *LsMYB15*-silenced plants were significantly reduced in the presence of exogenous melatonin compared to the melatonin-treated control plants treated similarly. The transcript levels of *LsMYB15*, *LsCOR15A*, and *LsRD29A* were also significantly lower in the *LsMYB15*-silenced plants than in the control group in the absence of exogenous melatonin (**Figure 6C**). Taken together, we further hypothesized that *LsMYB15* plays a role in transcriptional regulation *via* modulation of bolting and indirect gene regulation, which could be the cause of the altered bolting in leaf lettuce.

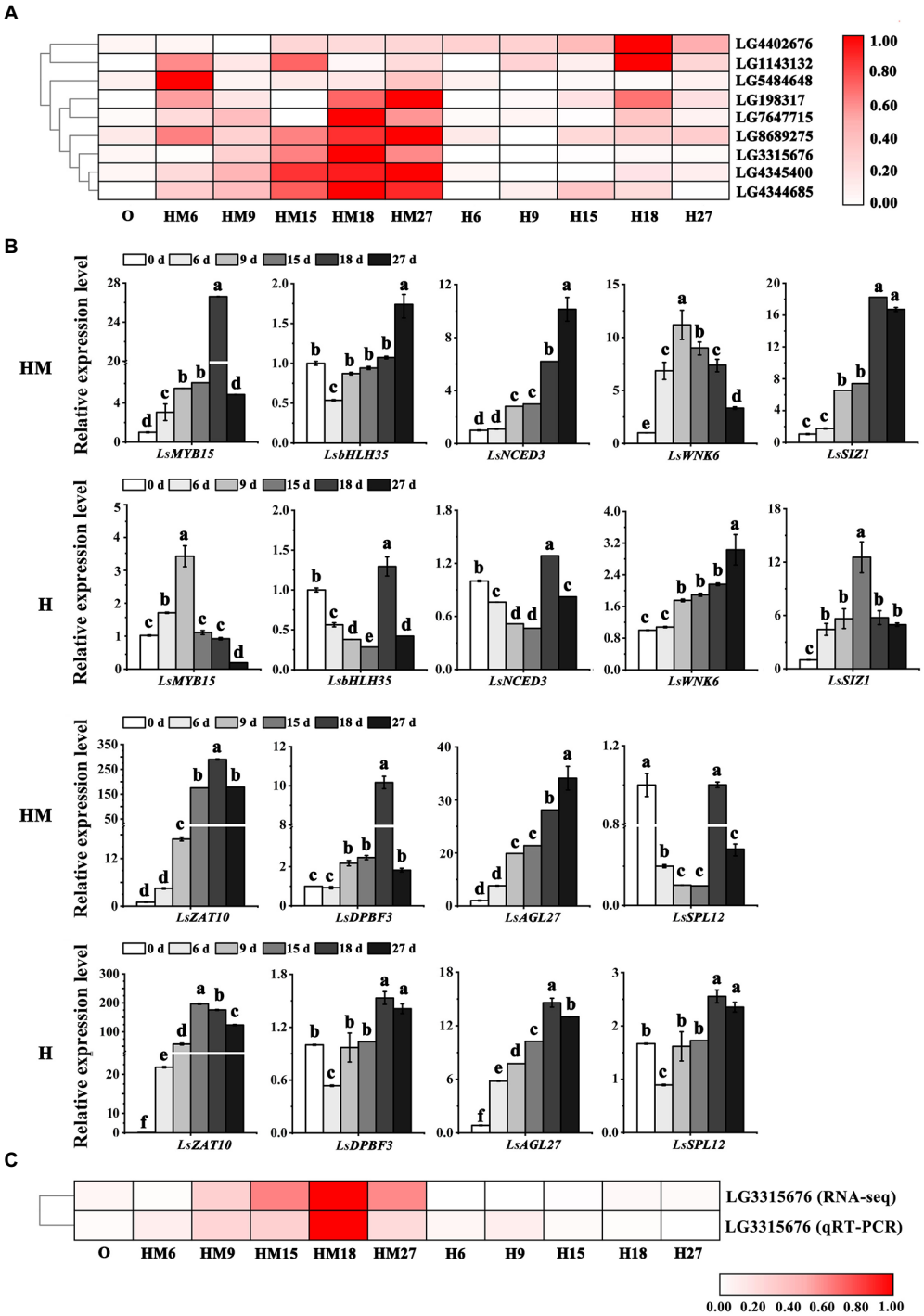

FIGURE 5 | Identification and analysis of bolting-related genes. **(A)** Heatmaps describing the expression profiles of candidate genes related to bolting-related genes. **(B)** Validation of RNA-seq expression profiles *via* qRT-PCR. **(C)** Correlation analysis between ABA-related genes and expression of the related candidate *LsMYB15* (LG3315676) *via* RNA-seq and qRT-PCR data. "MH" represents 100 μmol L^{-1} melatonin treatment under high temperature, and "H" represents no exogenous melatonin treatment under high temperature. Different letters above the bars indicate significantly different values ($p < 0.05$) calculated using one-way analysis of variance (ANOVA) followed by Tukey's multiple range test.

The results of antioxidant enzyme activity measurements showed that APX, SOD, CAT, POD, and PAL activities exhibited a steady increase in both the control plants and the melatonin-treated leaf lettuce, with no significant difference between WT and TRV2, but PPO activity decreased rapidly (**Figure 6D**).

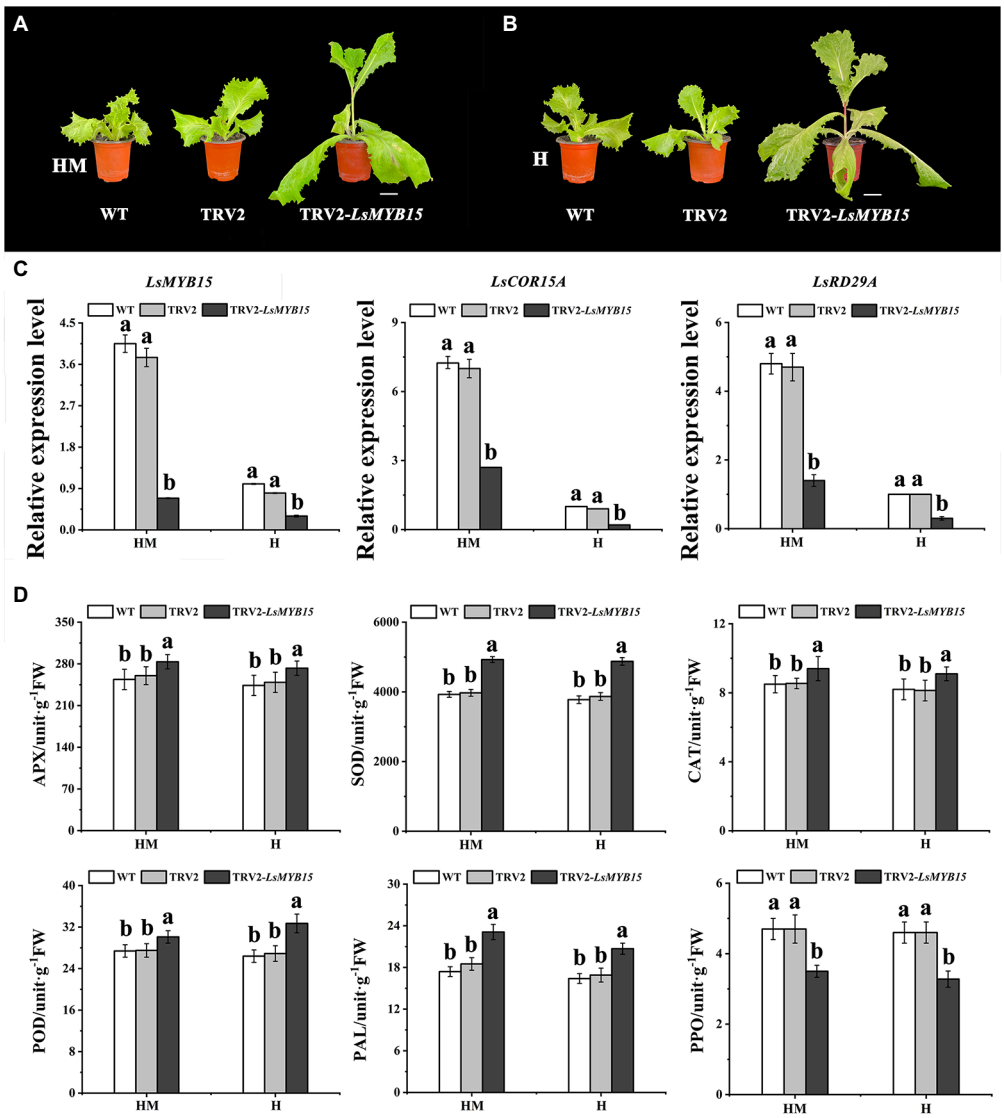

FIGURE 6 | Silencing of *LsMYB15* genes in the bolting-sensitive line S39. **(A)** Under high-temperature conditions, the exogenous melatonin administration constructs developed a bolting phenotype 7 days postinfection. Scale bars = 5 cm. **(B)** Under high-temperature conditions, the control group that did not have exogenous melatonin construct developed a bolting phenotype 7 days postinfection. Scale bars = 5 cm. **(C)** Relative expression levels in inoculated TRV2-*LsMYB15* plants were determined using qRT-PCR to determine transcription levels of three genes (*LsMYB15*, *LsCOR15A*, and *LsRD29A*) in leaf lettuce plants. **(D)** Activities of APX, SOD, CAT, POD, PAL, and PPO during heat treatment of control and melatonin-treated leaf lettuce. Bars indicate the standard error from each mean of three independent replications. Mean values with the same letter are not significantly different ($p < 0.05$). An increase in absorbance of 0.01 at 290 nm, 0.01 at 560 nm, 0.01 at 240 nm, 0.01 at 450 nm, 0.01 at 290 nm and 0.001 at 420 nm per min was defined as one unit (U) of APX, SOD, CAT, POD, PAL, and PPO activity, respectively. "MH" represents 100 μmol L^{-1} melatonin treatment under high temperature, and "H" represents no exogenous melatonin treatment under high temperature. Error bars indicate the SEM of three replicate measurements. Different letters above the bars indicate significantly different values ($p < 0.05$) calculated using one-way analysis of variance (ANOVA) followed by Tukey's multiple range test.

DISCUSSION

Effects of Melatonin on Leaf Lettuce Under High-Temperature Stress

Melatonin is considered a potential plant growth regulator that enhances plant growth. Nevertheless, the role of melatonin in mediating the stress response in different plant species and growth cycles still needs to be explored. Melatonin can enhance the tolerance of plants to abiotic stresses such as drought, salt, ambient temperature, and heavy metals in different ways (Wang et al., 2017a,b; Sun et al., 2020). For example, in rice seedlings, exogenous melatonin treatment under salt stress increased the net photosynthetic rate of rice and enhanced the absorption and transmission of light energy, increasing the relative water content and sucrose and starch contents and improving the salt tolerance of rice (Yan et al., 2021). In wheat (*Triticum aestivum* L.), the application of melatonin reduced oxidative stress by lowering thiobarbituric acid-reactive substances

and H_2O_2 content, increasing the activity of antioxidant enzymes and of photosynthesis and carbohydrate metabolism and actively improving heat resistance (Iqbal et al., 2021).

In conclusion, melatonin is extensively involved in the plant stress response, regulating growth and development and protecting plants from abiotic stress. High temperature is one of the primary environmental stress factors that affect the normal growth and development of leaf lettuce. Leaf lettuce growth temperatures above 30°C result in early bolting, and bolting reduces both plant quality and yields (Chen et al., 2017). Therefore, we selected 100 μmol L^{-1} melatonin at high temperatures during the growth period (the control group was not treated with exogenous melatonin under the same conditions) for further research. We found that the growth of leaf lettuce recovered following melatonin treatment at high temperatures, while the speed of bolting was significantly faster in the control group than in the treatment group. In addition, exogenous melatonin-treated lettuce leaves were larger and greener than those in the control group, with the most significant leaf width being 49% higher than that of the control group (**Figures 2A–D**). These results demonstrated that melatonin is involved in the stress response of leaf lettuce, regulating its growth and development and protecting leaf lettuce from high-temperature stress.

Plant Hormones Play an Important Role in Enhancing Plant Growth and Stress Resistance

Phytohormones participate in various processes throughout a plant's lifecycle. Studies have shown that five classical plant hormones, including auxins, cytokinins, GAs, ABA, and ethylene, play important roles in plant growth and stress responses, as well as brassinosteroids, jasmonic acid, salicylic acid, strigolactones, and peptides (Wang et al., 2017a,b; Zhao et al., 2021). For example, in cucumber seedlings, indoleacetic acid—acting as a downstream signaling molecule—is involved in H_2S-induced tolerance to chilling (Zhang et al., 2020). In *Arabidopsis*, high temperature promotes ABA accumulation, and elevated ABA levels trigger the upregulation of ABA enzyme biosynthesis genes, improving plant heat tolerance during growth (Gupta et al., 2020). In conclusion, hormones play a key role in adaptation to abiotic stress during plant growth and development. In this study, the number of DEGs involved in "plant hormone signal transduction" was significantly enhanced, as determined by KEGG analysis (**Supplementary Figure 2**). Using WGCNA, some of the genes screened from the high-correlation modules, including *MYB15*, *bHLH35*, *ZAT10*, *NCED3*, *DPBF3*, *WNK6*, *SIZ1*, and *SPL12*, were all ABA-related and have been reported to regulate plant growth and stress tolerance by regulating the ABA pathway (**Figure 5**). In perennial ryegrass (*Lolium perenne*) leaves, exogenous melatonin reduced the ABA content, delaying senescence. The reduction in ABA was correlated with downregulation of two ABA biosynthesis genes (*LpZEP* and *LpNCED1*), which were upregulated by heat stress, although melatonin suppressed this effect. Thus, the response of ABA in heat-induced senescence was delayed by melatonin through the reduction in ABA biosynthesis and the downregulation of signaling pathway factors (Zhang et al., 2017). We believe, therefore, that ABA plays an important role in the growth and development of lettuce under high-temperature conditions.

Melatonin exerts its effects by regulating various elements related to interfering with the activities of other phytohormones. For example, studies have found that, following exogenous melatonin treatment of tomato (*Solanum lycopersicum*) plants, the expression levels of ABA receptors induced by melatonin were increased and ABA signaling transduction pathways were activated, leading to heat resistance and inhibition of heat-induced senescence in tomato plants (Jahan et al., 2021b). In cucumber (*Cucumis sativus*) seedlings, exogenous melatonin were found to alleviate low-temperature stress by upregulating the expression of *CsZat12* and regulating the metabolism of PA and ABA (Zhao et al., 2017). In conclusion, ABA plays an important role in melatonin therapy and improves the tolerance of plants to abiotic stress. The results of this study demonstrate that melatonin regulates the growth and development of leaf lettuce by regulating the expression of ABA-related genes under high-temperature conditions, consistent with the results of previous studies.

LsMYB15 Regulates Bolting in Leaf Lettuce

The MYB transcription factor plays an important role in plant physiological processes under conditions of treatment with exogenous melatonin. In tea (*Camellia sinensis*) leaves, the increase in lignin content was found to parallel the rise in POD activity following melatonin treatment, which revealed that melatonin could increase lignin accumulation by enhancing POD activity. Additionally, melatonin also modified the expression of MYB transcription factor genes, which were regarded as candidates for the regulation of lignin metabolism in tea leaves (Han et al., 2021a,b). In water bamboo shoots, the transcription factors of *ZlMYB1* and *ZlMYB2* from the MYB family were increased, and melatonin treatment markedly reduced their expression, indicating that melatonin may be a participant in the transcriptional regulation of lignin synthesis (Yang et al., 2022). *LsMYB15* (LG3315676) was selected from the identified DEGs as a putative regulator of bolting using WGCNA. In *Arabidopsis*, *MYB15* is a positive regulator of drought and salt tolerance. Enhanced transcript levels of ABA biosynthesis, signaling, or responsive genes in *MYB15* overexpression lines also lead to increased tolerance to drought and salt stress (Ding et al., 2009; Li et al., 2021). When induced by low-temperature stresses, C-repeat binding factor (CBF) functions as a positive regulator to aid ABA-dependent increases in the expression levels of stress-responsive genes, leading to enhanced tolerance to freezing (Zhou et al., 2011). There were no changes in *COR15A* or *RD29A* in *MYB15*-overexpressing plants, suggesting that the coordination of upstream genes induces downstream genes more effectively with cellular protective functions (Chen et al., 2010). These studies suggest that melatonin treatment directly upregulates defense genes in response to stress through the ABA pathway, decreasing cellular injury.

In this study, *LsMYB15* silencing resulted in decreased expression levels of the downstream genes *LsCOR15A* and *LsRD29A*. These results indicate that *MYB15* may function differently and be involved in separate transcriptional regulation schemes under different stresses. From the results of the phenotypic, physiological, and molecular analyses conducted on leaf lettuce treated with exogenous melatonin under high-temperature conditions, strong positive correlations were observed among *LsMYB15*-silenced genes and reduced expression of the genes involved in ABA signaling (**Figure 6**). Furthermore, downstream stress–response pathways were activated, including those for reduced antioxidant systems, reduced osmoprotectants, enhanced membrane oxidation, and enhanced leaf senescence. In the presence of melatonin, leaf lettuce also bolted. Consequently, *LsMYB15* is likely to be a positive regulator of high-temperature bolting in leaf lettuce.

In conclusion, we have provided evidence that *LsMYB15* regulates bolting in leaf lettuce. These studies provide a more detailed understanding of the high-temperature stress regulatory network during leaf lettuce development and a new perspective for studying bolting and the potential applications of hormone treatment in agriculture.

DATA AVAILABILITY STATEMENT

The datasets presented in this study are publicly available, this data can be found here: https://www.ncbi.nlm.nih.gov/bioproject/PRJNA810911.

AUTHOR CONTRIBUTIONS

LC: data curation, formal analysis, methodology, and writing—original draft. MX: software, resources, and validation. CL: project administration, resources, software, and supervision. JH: methodology and validation. SF: supervision, resources, and funding acquisition. YH: conceptualization, writing—review and editing, and project administration. All authors contributed to the article and approved the submitted version.

FUNDING

Financial support was provided by The National Natural Science Foundation of China (32172607) and the Beijing Municipal Organization Department-Top-notch Young Talents Program (2018000026833ZK76).

ACKNOWLEDGMENTS

We thank Cathay Green Seeds (Beijing) Co., Ltd. for providing experimental resources.

SUPPLEMENTARY MATERIAL

The Supplementary Material for this article can be found online at: https://www.frontiersin.org/articles/10.3389/fpls.2022.921021/full#supplementary-material

REFERENCES

Agurla, S., Gahir, S., Munemasa, S., Murata, Y., and Raghavendra, A. S. (2018). Mechanism of stomatal closure in plants exposed to drought and cold stress: adaptation mechanisms and their applications. *Adv. Exp. Med. Biol.* 1081, 215–232. doi: 10.1007/978-981-13-1244-1_12

Arnao, M. B., and Hernández-Ruiz, J. (2018). Melatonin and its relationship to plant hormones. *Ann. Bot.* 121, 195–207. doi: 10.1093/aob/mcx114

Arnao, M. B., and Hernández-Ruiz, J. (2019). Melatonin and reactive oxygen and nitrogen species: a model for the plant redox network. *Melatonin Res.* 2, 152–168. doi: 10.32794/11250036

Arnao, M. B., and Hernández-Ruiz, J. (2020). Melatonin in flowering, fruit set and fruit ripening. *Plant Reprod.* 33, 77–87. doi: 10.1007/s00497-020-00388-8

Balanzà, V., Martínez-Fernández, I., and Ferrándiz, C. (2014). Sequential action of *FRUITFULL* as a modulator of the activity of the floral regulators *SVP* and *SOC1*. *J. Exp. Bot.* 65, 1193–1203. doi: 10.1093/jxb/ert482

Chadwick, M., Gawthrop, F., Michelmore, R. W., Wagstaff, C., and Methven, L. (2016). Perception of bitterness, sweetness and liking of different genotypes of lettuce. *Food Chem.* 197, 66–74. doi: 10.1016/j.foodchem.2015.10.105

Chen, Z., Han, Y., Ning, K., Ding, Y., Zhao, W., Yan, S., et al. (2017). Inflorescence development and the role of *LsFT* in regulating bolting in lettuce (*Lactuca sativa* L.). *Front. Plant Sci.* 8:2248. doi: 10.3389/fpls.2017.02248

Chen, C. C., Liang, C. S., Kao, A. L., and Yang, C. C. (2010). HHP1, a novel signalling component in the cross-talk between the cold and osmotic signalling pathways in *Arabidopsis*. *J. Exp. Bot.* 61, 3305–3320. doi: 10.1093/jxb/erq162

Chen, Z., Zhao, W., Ge, D., Han, Y., and Wang, Q. (2018). LCM-seq reveals the crucial role of *LsSOC1* in heat-promoted bolting of lettuce (*Lactuca sativa* L.). *Plant J.* 95, 516–528. doi: 10.1111/tpj.13968

Choi, G. H., and Back, K. (2019). Suppression of melatonin 2-hydroxylase increases melatonin production leading to the enhanced abiotic stress tolerance against cadmium, senescence, salt, and tunicamycin in rice plants. *Biomolecules* 9:589. doi: 10.3390/biom9100589

Ding, Z., Li, S., An, X., Liu, X., Qin, H., and Wang, D. (2009). Transgenic expression of *MYB15* confers enhanced sensitivity to abscisic acid and improved drought tolerance in *Arabidopsis thaliana*. *J. Genet. Genomics* 36, 17–29. doi: 10.1016/S1673-8527(09)60003-5

Erdal, S. (2019). Melatonin promotes plant growth by maintaining integration and coordination between carbon and nitrogen metabolisms. *Plant Cell Rep.* 38, 1001–1012. doi: 10.1007/s00299-019-02423-z

Gupta, M. K., Lenka, S. K., Gupta, S., and Rawal, R. K. (2020). Agonist, antagonist and signaling modulators of ABA receptor for agronomic and post-harvest management. *Plant Physiol. Biochem.* 148, 10–25. doi: 10.1016/j.plaphy.2019.12.023

Guo, J., Ling, H., Ma, J., Chen, Y., Su, Y., Lin, Q., et al. (2017). A sugarcane R2R3-MYB transcription factor gene is alternatively spliced during drought stress. *Sci. Rep.* 7:41922. doi: 10.1038/srep41922

Han, R., Truco, M. J., Lavelle, D. O., and Michelmore, R. W. (2021a). A composite analysis of flowering time regulation in lettuce. *Front. Plant Sci.* 12:632708. doi: 10.3389/fpls.2021.632708

Han, M. H., Yang, N., Wan, Q. W., Teng, R. M., and Zhuang, J. (2021b). Exogenous melatonin positively regulates lignin biosynthesis in *Camellia sinensis*. *Int. J. Biol. Macromol.* 179, 485–499. doi: 10.1016/j.ijbiomac.2021.03.025

Horvath, S., Dong, J., and Miyano, S. (2008). Geometric interpretation of gene co-expression network analysis. *PLoS Comput. Biol.* 4:e1000117. doi: 10.1371/journal.pcbi.1000117

Huang, F., Liu, T., Wang, J., and Hou, X. (2018). Isolation and functional characterization of a floral repressor, *BcFLC2*, from Pak-choi (*Brassica rapa* ssp *chinensis*). *Planta* 248, 423–435. doi: 10.1007/s00425-018-2891-0

Iqbal, N., Fatma, M., Gautam, H., Umar, S., and Khan, N. A. (2021). The crosstalk of melatonin and hydrogen sulfide determines photosynthetic performance by regulation of carbohydrate metabolism in wheat under heat stress. *Plan. Theory* 10:1778. doi: 10.3390/plants10091778

Izawa, T. (2020). What is going on with the hormonal control of flowering in plants? *Plant J.* 105, 431–445. doi: 10.1111/tpj.15036

Jahan, M. S., Guo, S., Sun, J., Shu, S., Wang, Y., El-Yazied, A. A., et al. (2021a). Melatonin-mediated photosynthetic performance of tomato seedlings under high-temperature stress. *Plant Physiol. Biochem.* 167, 309–320. doi: 10.1016/j.plaphy.2021.08.002

Jahan, M. S., Shu, S., Wang, Y., Hasan, M. M., and Guo, S. (2021b). Melatonin pretreatment confers heat tolerance and repression of heat-induced senescence in tomato through the modulation of ABA-and GA-mediated pathways. *Front. Plant Sci.* 12:650955. doi: 10.3389/fpls.2021.650955

Jones, D. M., Olson, T., Pullen, N., Wells, R., and Morris, R. J. (2020). The oilseed rape developmental expression resource: a resource for the investigation of gene expression dynamics during the floral transition in oilseed rape. *BMC Plant Biol.* 20:344. doi: 10.1186/s12870-020-02509-x

Jutarou, F., Yuki, O., Ryuhei, T., Kanako, N., and Yohsuke, T. (2021). DELLA degradation by gibberellin promotes flowering via GAF1-TPR-dependent repression of floral repressors in *Arabidopsis*. *Plant Cell* 33, 2258–2272. doi: 10.1093/plcell/koab102

Kanwar, M. K., Yu, J., and Zhou, J. (2018). Phytomelatonin: recent advances and future prospects. *J. Pineal Res.* 65:e12526. doi: 10.1111/jpi.12526

Kong, X., Xi, L., Qu, G. P., Peng, L., and Jing, B. J. (2016). *Arabidopsis* SUMO protease ASP1 positively regulates flowering time partially through regulating FLC stability. *J. Integr. Plant Biol.* 59, 15–29. doi: 10.1111/jipb.12509

Li, D., Peng, S., Chen, S., Li, Z., and Yang, G. (2021). Identification and characterization of 5 walnut *MYB* genes in response to drought stress involved in ABA signaling. *Physiol. Mol. Biol. Plants* 27, 1323–1335. doi: 10.1007/s12298-021-01008-z

Liang, D., Shen, Y., Ni, Z., Wang, Q., Lei, Z., Xu, N., et al. (2018). Exogenous melatonin application delays senescence of kiwifruit leaves by regulating the antioxidant capacity and biosynthesis of flavonoids. *Front. Plant Sci.* 9:426. doi: 10.3389/fpls.2018.00426

Moustafa-Farag, M., Almoneafy, A., Mahmoud, A., Elkelish, A., Arnao, M. B., Li, L., et al. (2019). Melatonin and its protective role against biotic stress impacts on plants. *Biomolecules* 10:54. doi: 10.3389/fpls.2017.02248

Onik, J. C., Wai, S. C., Li, A., Lin, Q., Sun, Q., Wang, Z., et al. (2020). Melatonin treatment reduces ethylene production and maintains fruit quality in apple during postharvest storage. *Food Chem.* 337:127753. doi: 10.1016/j.foodchem.2020.127753

Pin, P. A., Benlloch, R., Bonnet, D., Wremerth-Weich, E., Kraft, T., Gielen, J. J. L., et al. (2010). An antagonistic pair of *FT* homologs mediates the control of flowering time in sugar beet. *Science* 330, 1397–1400. doi: 10.1126/science.1197004

Schon, M., Baxter, C., Xu, C., Enugutti, B., Nodine, M. D., and Ca, D. (2021). Antagonistic activities of cotranscriptional regulators within an early developmental window set *FLC* expression level. *Proc. Natl. Acad. Sci. U. S. A.* 118:e2102753118. doi: 10.1073/pnas.2102753118

Sun, C., Liu, L., Wang, L., Li, B., Jin, C., and Lin, X. (2020). Melatonin: a master regulator of plant development and stress responses. *J. Integr. Plant Biol.* 63, 126–145. doi: 10.1111/jipb.12993

Uwimana, B., Smulders, M. J., Hooftman, D. A., Hartman, Y., Van Tienderen, P. H., Jansen, J., et al. (2012). Crop to wild introgression in lettuce: following the fate of crop genome segments in backcross populations. *BMC Plant Biol.* 12:43. doi: 10.1186/1471-2229-12-43

Viacava, G. E., Roura, S. I., Berrueta, L. A., Iriondo, C., Gallo, B., and Alonso-Salces, R. M. (2017). Characterization of phenolic compounds in green and red oak-leaf lettuce cultivars by UHPLC-DAD-ESI-QToF/MS using MS^E scan mode. *J. Mass Spectrom.* 52, 873–902. doi: 10.1002/jms.4021

Wang, Q., An, B., Shi, H., Luo, H., and He, C. (2017b). High concentration of melatonin regulates leaf development by suppressing cell proliferation and endoreduplication in *Arabidopsis*. *Int. J. Mol. Sci.* 18:991. doi: 10.3390/ijms18050991

Wang, L., Feng, C., Zheng, X., Guo, Y., Zhou, F., Shan, D., et al. (2017a). Plant mitochondria synthesize melatonin and enhance the tolerance of plants to drought stress. *J. Pineal Res.* 63:e12429. doi: 10.1111/jpi.12429

Wang, L., Wu, Y., Du, W., Yan, Z., Qi, Z., Tang, W., et al. (2021). Virus-induced gene silencing (VIGS) analysis shows involvement of the *LsSTPK* gene in lettuce (*Lactuca sativa* L.) in high temperature-induced bolting. *Plant Signal. Behav.* 16:1913845. doi: 10.1080/15592324.2021.1913845

Yan, F., Zhang, J., Li, W., Ding, Y., and Li, G. (2021). Exogenous melatonin alleviates salt stress by improving leaf photosynthesis in rice seedlings. *Plant Physiol. Biochem.* 163, 367–375. doi: 10.1016/j.plaphy.2021.03.058

Yang, B., Han, Y., Wu, W., Fang, X., Chen, H., and Gao, H. (2022). Impact of melatonin application on lignification in water bamboo shoot during storage. *Food Chem. X* 13:100254. doi: 10.1016/j.fochx.2022.100254

Yang, T., Li, K., Hao, S., Zhang, J., Song, T., Tian, J., et al. (2018). The use of RNA sequencing and correlation network analysis to study potential regulators of crabapple leaf color transformation. *Plant Cell Physiol.* 59, 1027–1042. doi: 10.1093/pcp/pcy044

Ying, Y. J., Ma, C., Xu, Y. J., Wei, Q., Imtiaz, M., Lan, H. B., et al. (2014). A zinc finger protein regulates flowering time and abiotic stress tolerance in chrysanthemum by modulating gibberellin biosynthesis. *Plant Cell* 26, 2038–2054. doi: 10.3389/fpls.2016.00682

Zhai, Q., Zhang, X., Wu, F., Feng, H., Deng, L., Xu, L., et al. (2015). Transcriptional mechanism of jasmonate receptor COI1-mediated delay of flowering time in *Arabidopsis*. *Plant Cell* 27, 2814–2828. doi: 10.1105/tpc.15.00619

Zhang, X. W., Liu, F. J., Zhai, J., Li, F. D., and Ai, X. Z. (2020). Auxin acts as a downstream signaling molecule involved in hydrogen sulfide-induced chilling tolerance in cucumber. *Planta* 251:69. doi: 10.1007/s00425-020-03362-w

Zhang, J., Shi, Y., Zhang, X., Du, H., Xu, B., and Huang, B. (2017). Melatonin suppression of heat-induced leaf senescence involves changes in abscisic acid and cytokinin biosynthesis and signaling pathways in perennial ryegrass (*Lolium perenne* L.). *Environ. Exp. Bot.* 138, 36–45. doi: 10.1016/j.envexpbot.2017.02.012

Zhao, B., Liu, Q., Wang, B., and Yuan, F. (2021). Roles of phytohormones and their signaling pathways in leaf development and stress responses. *J. Agric. Food Chem.* 69, 3566–3584. doi: 10.1021/acs.jafc.0c07908

Zhao, H., Zhang, K., Zhou, X., Xi, L., Wang, Y., Xu, H., et al. (2017). Melatonin alleviates chilling stress in cucumber seedlings by up-regulation of *CsZat12* and modulation of polyamine and abscisic acid metabolism. *Sci. Rep.* 7:4998. doi: 10.1038/s41598-017-05267-3

Zhong, L., Lin, L., Yang, L., Liao, M., and Tang, Y. (2020). Exogenous melatonin promotes growth and sucrose metabolism of grape seedlings. *PLoS One* 15:e0232033. doi: 10.1371/journal.pone.0232033

Zhou, M. Q., Shen, C., Wu, L. H., Tang, K. X., and Lin, J. (2011). CBF-dependent signaling pathway: a key responder to low temperature stress in plants. *Crit. Rev. Biotechnol.* 31, 186–192. doi: 10.3109/07388551.2010.505910

Zong, W., Zhao, B., Xi, Y., Bordiya, Y., Mun, H., Cerda, N. A., et al. (2021). DEK domain-containing proteins control flowering time in *Arabidopsis*. *New Phytol.* 231, 182–192. doi: 10.1111/nph.17366

Zou, L. P., Pan, C., Wang, M. X., Cui, L., and Han, B. Y. (2020). Progress on the mechanism of hormones regulating plant flower formation. *Hereditas* 42, 739–751. doi: 10.16288/j.yczz.20-014

Conflict of Interest: The authors declare that the research was conducted in the absence of any commercial or financial relationships that could be construed as a potential conflict of interest.

Publisher's Note: All claims expressed in this article are solely those of the authors and do not necessarily represent those of their affiliated organizations, or those of the publisher, the editors and the reviewers. Any product that may be evaluated in this article, or claim that may be made by its manufacturer, is not guaranteed or endorsed by the publisher.

frontiers | Frontiers in Plant Science

TYPE Original Research
PUBLISHED 16 September 2022
DOI 10.3389/fpls.2022.1013263

OPEN ACCESS

EDITED BY
Ji Tian,
Beijing University of Agriculture, China

REVIEWED BY
Ying Yan Han,
Beijing University of Agriculture, China
Haifeng Jia,
Nanjing Agricultural University, China

*CORRESPONDENCE
Guojun Zhang
zhangguojun-8@163.com
Zunzheng Wei
weizunzheng@163.com

†These authors contributed equally to this work

SPECIALTY SECTION
This article was submitted to Plant Systems and Synthetic Biology, a section of the journal Frontiers in Plant Science

RECEIVED 06 August 2022
ACCEPTED 17 August 2022
PUBLISHED 16 September 2022

CITATION
Wang X, Wang Y, Yan S, Sun X, Liu H, Cheng B, Xu X, Wei Z and Zhang G (2022) A multifaceted comparison between the fruit-abscission and fruit-retention cultivars in ornamental crabapple. *Front. Plant Sci.* 13:1013263. doi: 10.3389/fpls.2022.1013263

A multifaceted comparison between the fruit-abscission and fruit-retention cultivars in ornamental crabapple

Xue Wang[1,2†], Yi Wang[3†], Shufang Yan[4], Xuan Sun[2], Hongyan Liu[2], Beibei Cheng[1], Xingxing Xu[1], Zunzheng Wei[2*] and Guojun Zhang[1*]

[1]College of Horticultural Science and Technology, Hebei Key Laboratory of Horticultural Germplasm Excavation and Innovative Utilization, Hebei Normal University of Science and Technology, Qinhuangdao, China, [2]Institute of Grassland Flowers and Ecology, Beijing Academy of Agriculture and Forestry Sciences, Beijing, China, [3]College of Horticulture, China Agricultural University, Beijing, China, [4]Hebei Academy of Forestry and Grassland Sciences, Hebei Forest City Construction Technology Innovation Center, Shijiazhuang, China

The ornamental crabapple is a multipurpose landscaping tree that bears brilliant fruit throughout the winter. However, whether or not its fruit persists after maturation is specifically correlated to cultivar characteristics. In this work, we screened two different types that display fruit-retention ("Donald Wyman," "Red Jewel," and "Sugar Tyme") and fruit-abscission ("Radiant" and "Flame") in Northern China across the whole winter using multi-year successional records. Fruit-abscission was determined predominantly by the abscission zone established at the base of the pedicel, regardless of fruit size and pedicel length, according to the results of the comparative research. The primary physiological rationale was the accumulation of hydrolases activity (pectinesterase, cellulase, polygalacturonase, and β-glucosidase). Comparative transcriptomics further identified a number of upregulated DEGs involved in the synthesis pathways of canonical phytohormones, such as ethylene, jasmonic acid, abscisic acid, and cytokinin, as well as 12 transcription factors linked in downstream signaling in fruit-abscission cultivars. Finally, a model incorporating multi-layered modulation was proposed for the fruit abscission of ornamental crabapple. This study will serve as the foundation for the development of fruit-viewing crabapples that have an extended ornamental lifetime.

KEYWORDS

ornamental crabapple, fruit abscission, abscission zone, cell wall hydrolase, transcriptomics

Introduction

The ornamental crabapple (*Malus* crabapple) is a superb attractive tree owing to its vividly colored flowers, foliage, and fruits. Currently, the majority of researches are devoted to these features (Goncharovska et al., 2022). Even so, the ornamental crabapple's ability to sustain fruit after blooming is always highlighted as the demand for gardening increases exponentially around the world. The time of fruit abscission, which is a significant determinant of aesthetic value, varies substantially across the present cultivars. While some cultivars of ornamental crabapple lose their fruit in September, other may keep theirs until the next flowering season. Several species, including apple (Heo and Chung, 2019), litchi (Zhao and Li, 2020), pear (Li et al., 2019), and olive (Parra et al., 2020), have had their molecular processes of fruit abscission investigated. However, the internal mechanism of fruit abscission of ornamental crabapple has not been examined. Hence, it is crucial to explore the effect of fruit abscission on ornamental crabapple.

The now-recognized abscission process normally involves four stages (Estornell et al., 2013; Tucker and Kim, 2015; Patharkar and Walker, 2018). The process starts with the differentiation of abruption layers. Several layers of stratified cells are formed before to abscission. Abscission responses to the phytohormone signals constitute the second step (such as decrease in auxin and increase in ethylene). The third stage involves modifying the cell wall and separating the cells. Various enzymes are produced at this step, resulting in the degradation of pectin and polysaccharides in the cell wall. Cell adhesion is eliminated by the degrading of pectin and cellulose by cell wall hydrolase (Zamil and Geitmann, 2017). In grape, cellulase (CX) and polygalacturonase (PG) synthesis is enhanced in the abscission zone (AZ), which facilitates fruit abscission (Wu et al., 2021). Analysis of gene expression in the AZ of litchi small fruit demonstrated that the expression of *LcPG1* is positively related to fruit abscission (Peng et al., 2013). The fourth stage is characterized by fruit abscission differentiation and the formation of a protective layer. The fact that some of the laminate cells are degraded by cell hydrolase and lose adhesion, others form protective layers.

It has been shown that fruit abscission is a highly coordinated biochemical process (Sun et al., 2009). Recent studies have demonstrated that senescence and the fruit abscission process are influenced by a range of elements, hormone being one of the most prominent (Agusti et al., 2012; Gulfishan et al., 2019). According to prior research, ethylene (ET), abscisic acid (ABA), and cytokinin (CTK) may stimulate fruit abscission, but auxin (IAA) and gibberellin (GA) can inhibit fruit abscission (Taylor and Whitelaw, 2001). *MdACS5A* and *MdACO1* in the mature fruit AZ may be associated with the physiological fruit abscission of "Golden delicious" and "Fuji" prior to harvest (Li et al., 2010). Apple fruit abscission and enhanced Acrylonitrile-butadiene-acrylate (ABA) biosynthesis are related with the stimulation of 9-cis-epoxide carotenoid dioxygenase gene that is sensitive to ABA (Giulia et al., 2013). Grape IAA and GA regulate auxin homoeostasis by inhibiting polar auxin transport in order to control abscission. Reduced transcription of four *VvPIN* genes inhibits polar IAA transport, leading to fruit abscission (Kuhn et al., 2016). In apple, the inactive gene of cytokinin dehydrogenase (CKX) was upregulated during fruit shedding induction, indicating that CTK was reduced during this process (Botton et al., 2011). In conclusion, fruit abscission is mediated by the coordinated action of several hormones.

Here, we examined fruit-abscission and fruit-retention cultivars of ornamental crabapple, which, respectively, shed their fruits in the fall and the following spring. Wood slicing technology, RNA-seq, and quantitative real-time PCR (qRT-PCR) were used to compare the two and explore the internal processes determining fruit abscission in ornamental crabapple. This study offered a framework for future research on the morphology, anatomy, and molecular biology of organ abscission in ornamental crabapple and provided the foundation for uncovering the molecular mechanism of organ abscission in ornamental crabapple and developing cultivars with a prolonged ornamental lifecycle.

Materials and methods

Plant materials

In 2011, ornamental crabapple cultivars including "Donald Wyman," "Red Jewel," "Sugar Tyme," "Radiant," and "Flame" were imported from the United States. The grafted seedlings were transplanted to the resource garden at Hebei Normal University of Science & Technology (39°N, 119°E). Each cultivar was planted with five replications, as well as the block layout was completely random. After they were flowered in 2013, the fruit growth was monitored for 5 years, including the fruit ornamental period, the abscission period, and the abscission position on the dwarf shoot.

Depending on whether the fruit falls off in autumn, these ornamental crabapples may be divided into two groups (Supplementary Figure 1A). "Donald Wyman," "Red Jewel," and "Sugar Tyme" are described as fruit-retention cultivars. They retain fruits well throughout the winter, even until March or April of the following year. "Radiant" and "Flame" are fruit-abscission cultivars. Their fruit gradually falls in late September. The AZ between the fruit pedicel and dwarf shoot is more easily to form in fruit-abscission cultivars than fruit-retention cultivars (Supplementary Figure 1B).

Fruits related traits descriptions in ornamental crabapple

According to our previous investigations (Supplementary Table S1), the end of September is a critical time for determining whether ornamental crabapple fruit will fall off. On September 25, 2019, 20 healthy fruits per cultivar were chosen at random from perennial shoots. Trait parameters defined using Guideline for the

Conduct of Tests for Distinctness, Uniformity, and Stability-Ornament Apple (UPOV:TG/192/1). These characteristics comprised the size of fruit and pedicel. The size of fruit includes its length, width, and weight, whereas the size of fruit pedicel includes its length and thickness. The length and width of the fruit, as well as the length and thickness of the fruit pedicel for each individual fruit, were measured using vernier caliper. In addition, a 1–2 cm piece of dwarf shoot and fruit pedicel was cut with a knife and then divided into three parts for extensive evaluation. One part was fixed in a mixture of formaldehyde, acetic acid, and ethanol (FAA) for tissue sectioning, while the other two parts were frozen in liquid nitrogen and stored at −80°C for enzymatic activity assays and RNA extraction.

Anatomical observation of fruit pedicel AZ

Those samples fixed in FAA for 24 h initially were sectioned longitudinally and transversely to a thickness of approximately 8 μm using a microtome. Then, the slices were positioned on the slides. These slides were finally treated with the following reagents in sequence: 1.0% safranin solution, 50% ethanol, 70% ethanol, 85% ethanol, 0.1% solid green solution, 100% ethanol, and resin sealing. These were finally inspected with an Olympus DP 72 light microscope.

Enzyme extraction and activity assay

Pectinesterase (PE), CX, PG, and β-glucosidase (BG) were assayed in accordance with the manufacturer's instructions (Suzhou Keming Biotechnology). Initially, 0.05 g of frozen shoot and fruit pedicels were pulverised with 200 ml of a pretreatment solution in an ice-bath mortar. The supernatant containing the enzyme was then retrieved by centrifuging at 16,000 *g* for 10 min at 4°C. The manufacturer's kit outlines the methods available for the specific examination of each enzyme. The enzyme activity of the PE was examined using titration, while the activities of the other three enzymes were examined using an Enzyme-Linked Sorbent Assay (ELSA), with absorbance values recorded at 620, 540, and 400 nm, respectively. There were three replicates for each sample.

cDNA library preparation and RNA sequencing

RNA extraction was performed using the RNAprep pure Plant Kit (Beijing Tian gen Co., Ltd.). RNA purity and integrity were examined using an Agilent 2100 Bioanalyzer. The cDNA was synthesized with a Thermo Frist Strand cDNA Synthesis Kit (Thermo Fisher Scientific). Using Illumina Truseq RNA Sample Prep Kits (Illumina, Santiago), five cDNA libraries each with roughly 130–150 bp insertion fragments were generated, and subjected to paired-end sequencing on an Illumina HiSeq platform owned by Beijing Biomarker Technologies Co., Ltd. All raw data were deposited to the Genome Sequence Archive (GSA) with the accession number CRA004670.

Sequence assembly, unigenes functional annotation and transcription factor identification

After quality control, we acquired the clean reads for each cultivar and assembled them into non-redundant unigenes using the Trinity platform embedded on the website (http://www.biocloud.net/, Beijing Biomarker Technologies Co., Ltd). These unigenes served as reference repository to examine the variations in gene expression among five cultivars. In addition, these assembled non-redundant unigenes were functionally blasted against a number of databases, including Non-Redundant Protein Sequence (NR), Gene Ontology (GO), Clusters of Orthologous Groups for Eukaryotic Complete Genomes (KOG), Kyoto Encyclopedia of Genes and Genomes (KEGG), Clusters of Orthologous Groups (COG), and Swiss-Prot, among others. Furthermore, homology search for non-redundant unigenes against plant transcription factor databases (Plant TFDB) identified the transcription factor using iTAK software with a significant cut-off of E-value (10E−5; Zheng et al., 2016).

Analysis of gene differential expression

Consensus unigenes of five cultivars were used for the analysis of differentially expressed genes. The EBSeq software (Leng et al., 2013) was used to identify the set of differentially expressed genes (DEGs) among five ornamental crabapples cultivars. The DEGs were screened using the Benjamini-Hochberg-corrected. The false discovery rate (FDR) was as a key indicator. Those consensus unigenes with more than two-fold differential expression and FDR less than 0.01 were considered candidate DEGs.

To calculate consensus unigene expression levels, the number of uniquely aligned fragments was normalized using the FPKM (Fragments Per Kilobase of exon model per Million mapped fragments) value (Mortazavi et al., 2008).

Quantitative PCR analysis

Total RNA extraction and cDNA synthesis for each sample were conducted as in previous RNA library preparation. Candidate genes in the qRT-PCR examination included *McPME12* (Pectinesterase 12), *McBGLU12* (β-glucosidase 12), *McCEL1* (Cellulase 1), *McPG* (Polygalacturonase), *McbHLH75* (Basic helix–loop–helix domain 75), and *McWRKY75* (WRKY transcription factor 75). The gene-specific PCR primers designed

by Primer Premier 5 were presented in Supplementary Table S5. The *McActin* gene was used as an internal reference gene. The relative expression levels of genes were quantified using ABI StepOne Plus equipment. Each sample comprises three biological replicates. Relative expression levels for each gene were analyzed using the $2^{\wedge(-\Delta\Delta Ct)}$ method (Livak and Schmittgen, 2001).

Statistical analysis

All data were analyzed using the IBM SPSS Statistics 20.0 software (SPSS Inc., United States). Significance and multiple comparisons in each cultivar were assessed using ANOVA and Tukey's multiple range test with a significance threshold of 0.05.

Results

Effects of fruit-related traits of ornamental crabapple on fruit abscission

Our prior sequential field observations spanning 5 years suggested that the five cultivars's fruit-shedding periods varied substantially. The fruit abscission phase of "Donald Wyman," "Red Jewel," and "Sugar Tyme" occurred normally in mid-March of the following year. "Radiant" dropped all of its fruit in early October, while "Flame" shed sooner, virtually all of its fruit by the end of September. Since fruit and fruit pedicel characteristics are major determinants of fruit drop, we evaluated the fluctuations in these two related parameters on September 25 for each cultivar. The changes in the two assessed fruit-related variables were showed in Table 1.

Fruit-retention cultivars, including "Donald Wyman," "Red Jewel," and "Sugar Tyme," featured fruit length, width, and weight, respectively, of 10.33–12.37 and 9.99–11.42 mm, and 0.82–1.06 g, while fruit-abscission cultivars, "Radiant" and "Flame," with 11.43–18.73 and 11.47–16.83 mm, and 1.05–3.42 g, respectively (Table 1). "Flame" as a cultivar with early fruit abscission possibly connected with its largest fruit (18.73 mm in length and 16.83 mm in width, respectively) and greatest weight (3.42 g). Even though "Radiant" also lost it fruit earlier in October, its average fruit weight of 1.05 g is comparable to that of fruit-retention cultivars, such as "Doanld Wyman" (1.02 g), "Red Jewel" (0.82 g), and "Sugar Tyme" (1.06 g). Those suggested that fruit size and weight may not be the primary factors of early fruit abscission in "Radiant." The length and thickness of fruit pedicels in the fruit-retention and -abscission cultivars, were 27.91–36.10 and 0.34–0.63 mm, as well as 20.76–39.11 and 0.53–0.66 mm, respectively. The fruit pedicels of the cultivar "Flame" were the shortest (20.76 mm) but the thickest (0.66 mm), while those in the "Radiant" were the longest (39.11 mm) but relatively thicker (0.53 mm). It is rather unexpected that "Donald Wyman" has both the longest (36.10 mm) and thickest (0.63 mm) fruit pedicels. This suggests that fruit abscission is not directly associated with any of these fruit pedicel characteristics. Fruit size and fruit pedicel variation did not change significantly between fruit-retention and -abscission cultivars, according to our results. This is also indicative of the fact that the complex attribute of fruit abscission is substantially determined by the underlying processes specific to the cultivars.

Microstructure observation on fruit AZ in ornamental crabapple

Abscission describes the detachment of plant organs from their parent plant. This procedure frequently occurs at the intersection of two distinct organs in one or more AZ-specific cell layers (Yu and Kellogg, 2018). A microtome wood sectioning technique was utilized to examine the architecture histological appearances in longitudinal and transverse orientations of the AZ in ornamental crabapples (Figure 1).

The attachment of fruit pedicel to the dwarf shoot pith (Figures 1A3–E3) was confirmed by longitudinal slices. Additionally, we observed that the internodes of the shoots were exceedingly short. The epidermis, cortex, bast fibers, secondary bast, secondary xylem, and pith constitute shoot and fruit pedicel, in that order, from the inside out (Figures 1A4–E4,A5–E5). The epidermis and cortex together form a protective layer. The secondary bast mostly transports the products of photosynthesis, while the secondary xylem primarily conveys water and ions and provides structural strength. The pith, which is situated in the center of the vascular column, is composed of cells with thin cell walls and storage capacity. In contrast to the shoot, the fruit pedicel's transverse anatomical structure comprised of the cortex, which, along with the epidermis, served a protective function for the fruit pedicel. In addition, the bast fibers in the fruit pedicel had greatly thicker cell walls, which supported the fruit.

TABLE 1 Fruit-related traits description in fruit-retention and -abscission cultivars of ornamental crabapple.

Cultivars		Fruit size			Fruit pedicel	
		Length (mm)	Width (mm)	Weight (g)	Length (mm)	Thickness (mm)
Fruit-retention cultivars	Donald Wyman	11.09 ± 0.90 bc	11.42 ± 0.95b	1.02 ± 0.18b	36.10 ± 5.64ab	0.63 ± 0.12ab
	Red Jewel	10.33 ± 0.70c	9.99 ± 0.56b	0.82 ± 0.14b	31.69 ± 3.31bc	0.43 ± 0.08 cd
	Sugar Tyme	12.37 ± 1.18b	10.62 ± 0.83b	1.06 ± 0.27b	27.91 ± 3.40c	0.34 ± 0.05d
Fruit-abscission cultivars	Radiant	11.43 ± 0.60bc	11.47 ± 1.22b	1.05 ± 0.33b	39.11 ± 5.75a	0.53 ± 0.08bc
	Flame	18.73 ± 1.68a	16.83 ± 2.09a	3.42 ± 0.95a	20.76 ± 3.14d	0.66 ± 0.13a

10.3389/fpls.2022.1013263

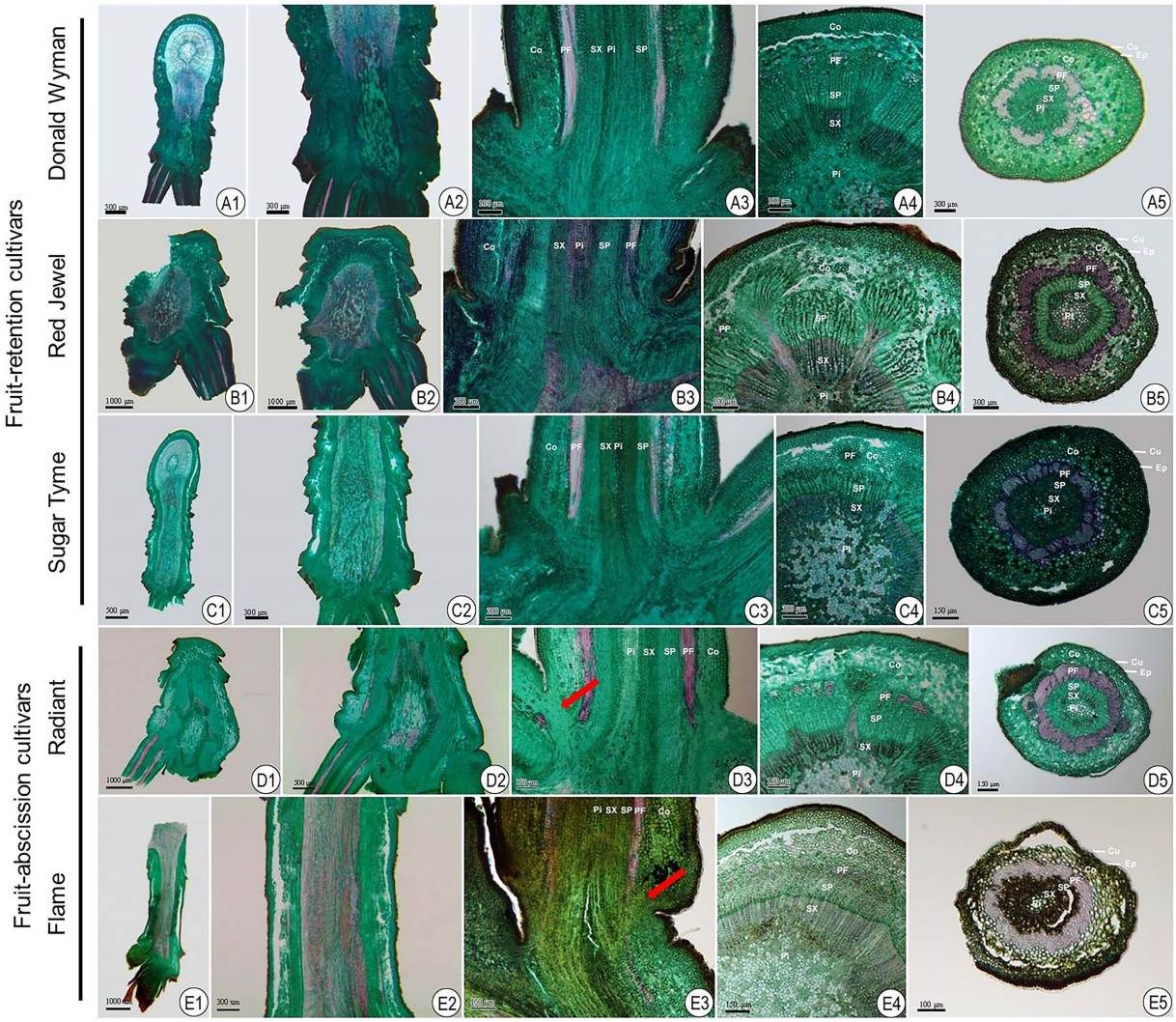

FIGURE 1
Anatomical observations of fruit AZ in fruit-retention and -abscission cultivars of ornamental crabapple. **(A1–A5)** "Donald Wyman"; **(B1–B5)** "Red Jewel"; **(C1–C5)** "Sugar Tyme"; **(D1–D5)** "Radiant"; **(E1–E5)** "Flame." **(A1–E1)** and **(A2–E2)** longitudinal section of attached shoot and fruit pedicels; **(A3–E3)** longitudinal section of fruit pedicels; **(A4–E4)** and **(A5–E5)** transverse section of shoot and fruit pedicels, respectively. Cu, Cuticle; Ep, epidermal cells; Co, cortex; PF, phloem fiber; SP, secondary phloem; SX, secondary xylem; and Pi, pith.

It was further revealed that in fruit-abscission cultivars, the cortical layer at the junction of the fruit pedicel and dwarf shoot had conspicuous microscopic parenchyma cell (Figures 1D3,E3), but in fruit retention cultivars, the cortical cells at the base of the fruit pedicel were homogeneous in size and evenly organization. In these cultivars of fruit-abscission, the abscission layer appears to develop throughout time, indicating that it is the fundamental component of fruit abscission.

Enzyme activity in the AZ of ornamental crabapple fruits

We measured the amounts of four enzymes (PE, CX, PG, and BG) in five ornamental crabapple cultivars's dwarf shoot and fruit pedicel (Figure 2). These results demonstrate that fruit-abscission cultivars ("Flame," "Radiant") possess significantly higher PE, CX, PG, and BG enzyme activities than fruit-retention cultivars ("Donald Wyman," "Red Jewel," and "Sugar Tyme"). The PE and CX enzyme activity of the fruit-abscission cultivars was about 1.5 times that of the fruit-retention cultivars. The activity of PG enzyme was significantly different among the five cultivars, but the enzyme content of the fruit-abscission cultivars was still high. Likewise, we found that the enzyme activity of BG was highest in the "Flame," which may lead to early abscission of the "Flame" fruits (Figure 2). On the basis of these results, the increased activity of hydrolases (such as PE, PG, CX, and BG) degraded the pectin and cellulose in the cell wall, which may be one of the reasons for the fruit abscission of ornamental crabapples.

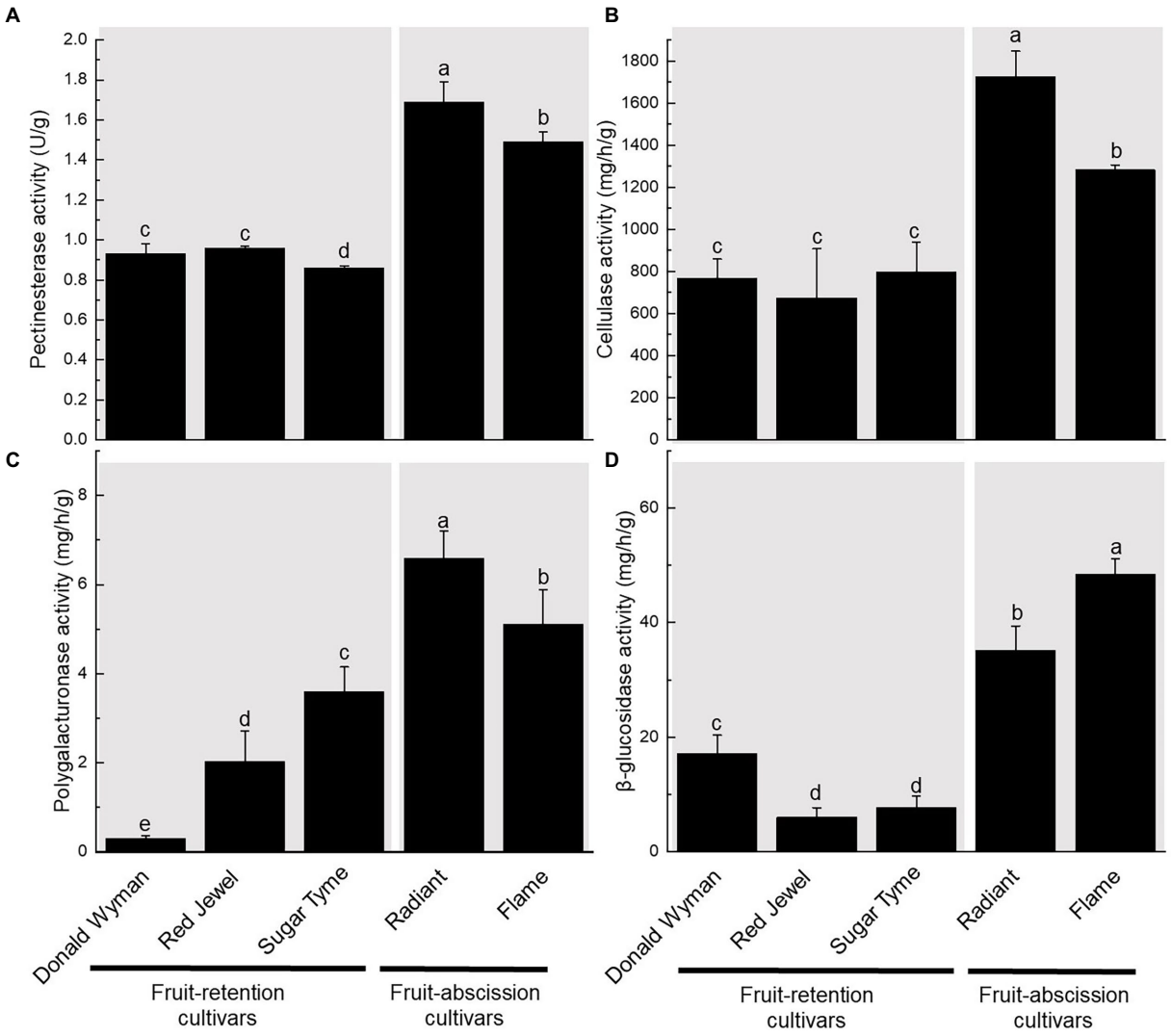

FIGURE 2
Variation in enzyme activity of fruit pedicels in fruit-retention and -abscission cultivars of ornamental crabapple. **(A)** Pectinesterase (PE); **(B)** Cellulase (CX); **(C)** Polygalacturonase (PG); and **(D)** β-glucosidase (BG). Different letters indicate significant differences at $p<0.05$.

Assembly and annotation of unigenes and differential expression analysis

Using RNA-seq, we sequenced five ornamental crabapple cultivars to explore the transcriptional processes underlying the establishment of the AZ, a determinant in fruit abscission. Transcriptome sequencing results for fruit-retention and fruit-abscission cultivars of ornamental crabapple were shown in Supplementary Table S2.

After quality control and data collection, the total clean data were about 51.59 G. with each cultivar ranging between 6.7 and 10.7 Gb. The GC content ranged from 46.39 to 47.84%, while the Q30 content ranged from 91.79 to 94.60%. A total of 44,830 consensus non-redundant unigenes were generated after assembly, of which 55,196 were longer than 1,000 bp and N50 was 1,807 bp. The total length of all unigenes was 51,673,246 bp. The majority of the unigenes were between 300 and 500 bp in length, accounting for 32.15% of the total. The proportions of lengths between 500 and 1,000 bp, 1,000–2,000 bp, and more than 2,000 bp are 27.75, 23.44, and 16.67%, respectively (Supplementary Table S3).

The annotation of unigenes derived from ornamental crabapples was shown in Supplementary Table S4. It was determined that 33,299 consensus unigenes were annotated, with 16,748 (50.30%) having a length more than 1,000 bp and 16,551 (49.70%) with lengths roughly equivalent to 300 bp but less than 1,000 bp. In the NR database, 32,503 unigenes were annotated, accounting for 97.61% of all annotated consensus unigenes. This is followed by Swiss-Prot (19,643, 59.01%), GO (18,270, 54.87%), KOG (18,090, 54.33%), KEGG (12,922, 38.81%), and COG (11,681, 35.08%).

We used in RNA-seq analysis to study the changes in gene expression during fruit shedding in different ornamental

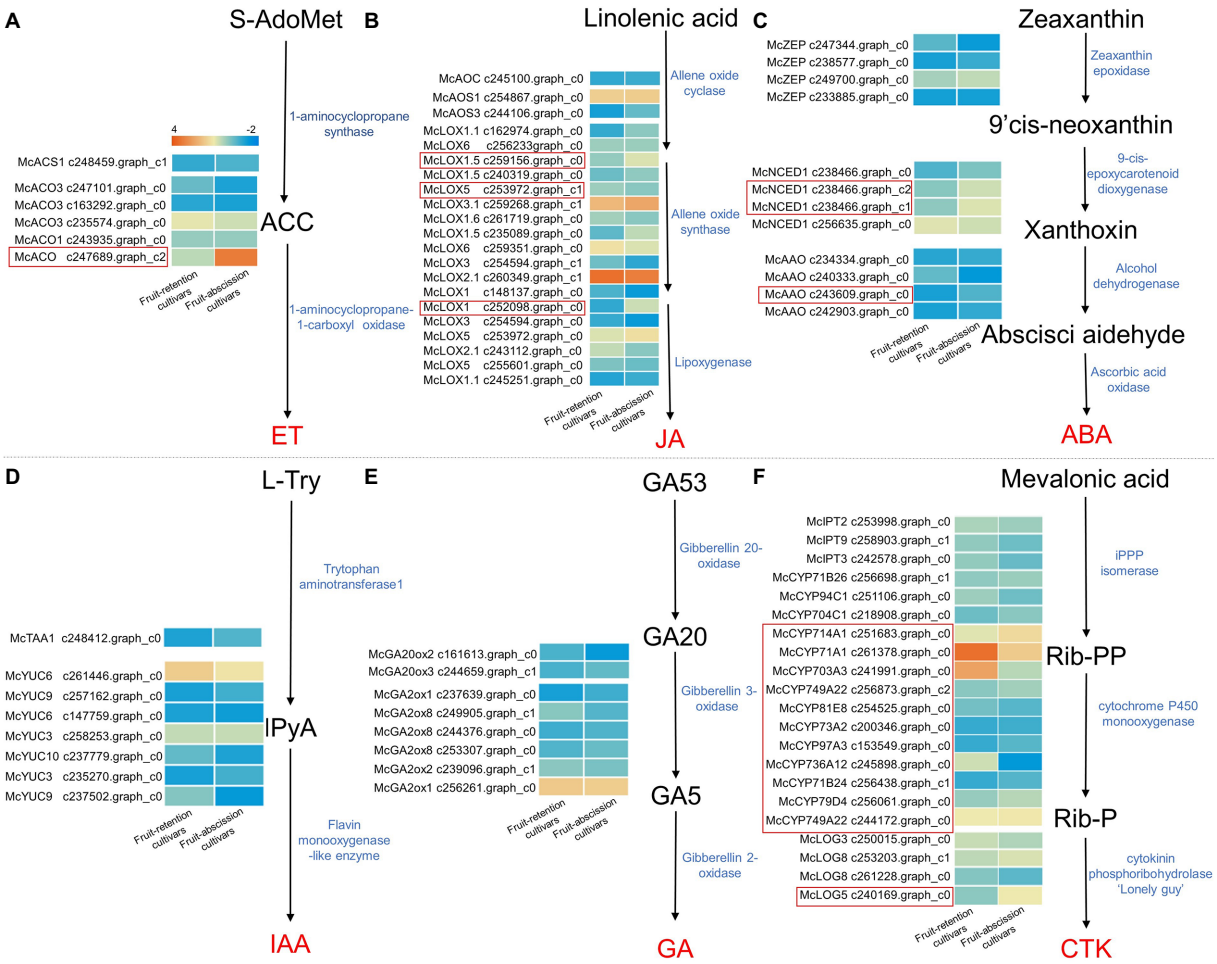

FIGURE 3
Schematics of biosynthesis differential transcript profiles of hormone-related genes. Genes up- or downregulated in all stages in fruit-retention and -abscission cultivars were denoted by light orange and blue, respectively. **(A)** Ethylene; **(B)** Jasmonic acid; **(C)** Abscisic acid; **(D)** Auxin; **(E)** Gibberellin; and **(F)** Cytokinin.

crabapple cultivars, and then revealed the effects of hormones, transcription factors and cell wall hydrolases on fruit abscission. A total of 767 DEGs satisfying the criteria of $\log_2$(Fold Change) ≥ 1 and FRD < 0.01 was identified between fruit-abscission cultivars and fruit-retention cultivars. Of these, 442 DEGs were upregulated whereas 325 were downregulated.

Expression levels of phytohormone synthesis-related genes in the fruit abscission transcriptome

Hormones govern fruit abscission directly and play a crucial function as a signaling component in the fruit abscission process. To identify potential regulatory mechanisms that leading to the fruit abscission of ornamental crabapple, we compared the transcript levels of key enzymes involved in hormone biosynthesis across fruit-retention and -abscission cultivars (Figure 3). The results revealed that synthetases of six hormone biosynthesis pathways were retrieved, among which ET, jasmonic acid (JA), ABA, and CTK synthesis genes were differentially expressed in cultivars with different fruit abscission types.

Consensus unigenes were used to identify the key synthases *McACS1* and *McACOs* in the ethylene biosynthesis pathway. 1-aminocyclopropane-1-carboxylate oxidase (ACO) is a significant rate-limiting enzyme that plays an essential role in ET biosynthesis regulation (Vanderstraeten et al., 2019). The expression of *McACO* varied significantly across ornamental crabapples with different fruit abscission types (Figure 3A). Similarly, *McAOC*, *McAOS1*, *McAOS3*, and *McLOXs* genes were identified in the JA biosynthesis pathway, the expression levels of *McLOX1*, *McLOX1.5*, and *McLOX5* differed significantly across fruit-retention and -abscission cultivars (Figure 3B). In the ABA biosynthesis pathway, *McNCED1* and *McAAOs* revealed significantly variable expression levels, while *McZEPs* was not found (Figure 3C). *McTAA1* and *McYUCs* genes, which encode key enzymes in the IAA synthesis pathway, were identified in the fruit's AZ. However, non-significant differences between their

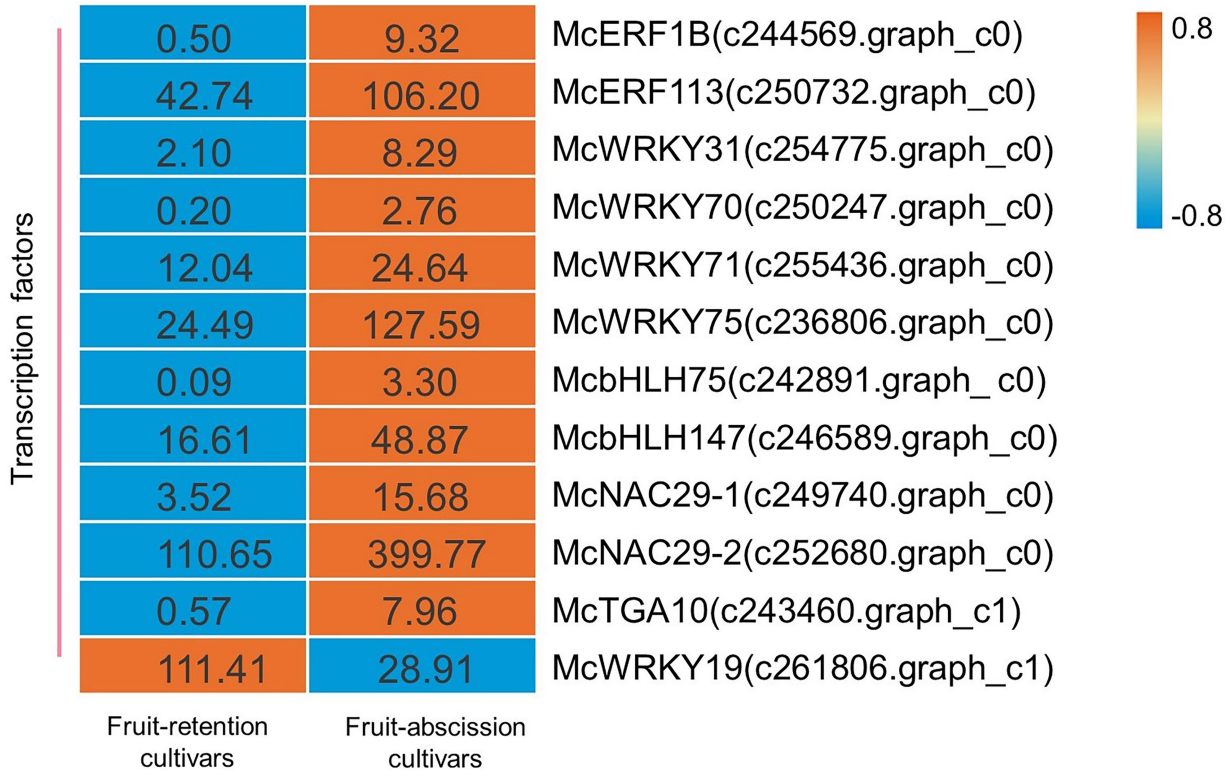

FIGURE 4
Schematics of biosynthesis differential transcript profiles of hormone metabolism-related genes and TFs. Genes up- or downregulated in all stages in fruit-retention and -abscission cultivars are denoted by orange and blue, respectively.

expressions indicate that IAA may not be directly involved in the abscission of ornamental crabapple fruit (Figure 3D). The expression of *McGA20ox2/3* and *McGA2oxs* genes in the GA biosynthesis pathway was not significantly different between the fruit-retention and fruit-abscission cultivars (Figure 3E). For the CTK synthesis pathway, a high number of the *McCYP450s* genes were found with substantial expression differences in different fruit abscission cultivars, but *McIPT2/3/9* and *McLOG3/8* genes showed no significant expression changes (Figure 3F).

In conclusion, the four phytohormones include ET, JA, ABA, and CTK have the potential in the fruit abscission of ornamental crabapple. The considerable differential expression of *McACO*, *McLOX1, McLOX1.5, McLOX5, McNCED1, McAAO, McCYP450s*, and *McLOG5* may have a direct effect on the hormone levels in the AZ. In addition, we hypothesized that IAA and GA have no direct influence on fruit abscission since their synthetic-related genes revealed no significant expression differences. Intriguingly, most of the differentially expressed hormone synthesis genes were upregulated. It is proved that ET, JA, ABA, and CTK may have positive regulatory effects on fruit abscission. Our findings demonstrated the synchronization of multiple hormones that induce fruit abscission in ornamental crabapple.

There is a crucial function for transcription factors throughout every phase of a plant's development (Jiang et al., 2020). Transcriptome data were used to identify the transcription factors (TFs) involved in the regulation of ornamental crabapple fruit abscission, and to explore the regulatory mechanism of phytohormones on signal transduction. Some TFs potentially regulated by hormones were analyzed, and their expression varied across ornamental crabapple cultivars. There were identified 12 TFs including family ERF, WRKY, bHLH, NAC, and TGA. Finally, a heatmap depicting the expression levels of these TFs was shown (Figure 4).

Numerous studies have shown that the aforementioned transcription factor families are connected with the shedding of plant organs. The AP2/ERF family of transcription factors, *RhERF1* and *RhERF4*, has a function in the abscission of petals in Rosa hybrida (Gao et al., 2019). After melon fruit ripens, WRKY transcription factors are activated and engaged in fruit abscission (Corbacho et al., 2017). *CitbHLH1*, a member of the transcription factor family involved in the function of signaling hormones including ET and JA (Sun et al., 2018), may also play a significant role in regulating fruit abscission (Agusti et al., 2012). Likewise, NAC TFs in litchi may be associated with the transcriptional cascade initiated by ET-driven fruit abscission (Li et al., 2015). In addition, TGA TFs in *Arabidopsis* contributed to the establishment of a BOP-dependent AZ, which resulted to the abscission of petals (Corrigan, 2018). Several TFs linked with abscission, including ERF (*McERF1B* c244569.graph_c0, *McERF113* c250732.graph_c0), WRKY (*McWRKY31* c254775.graph_c0, *McWRKY70* c250247.

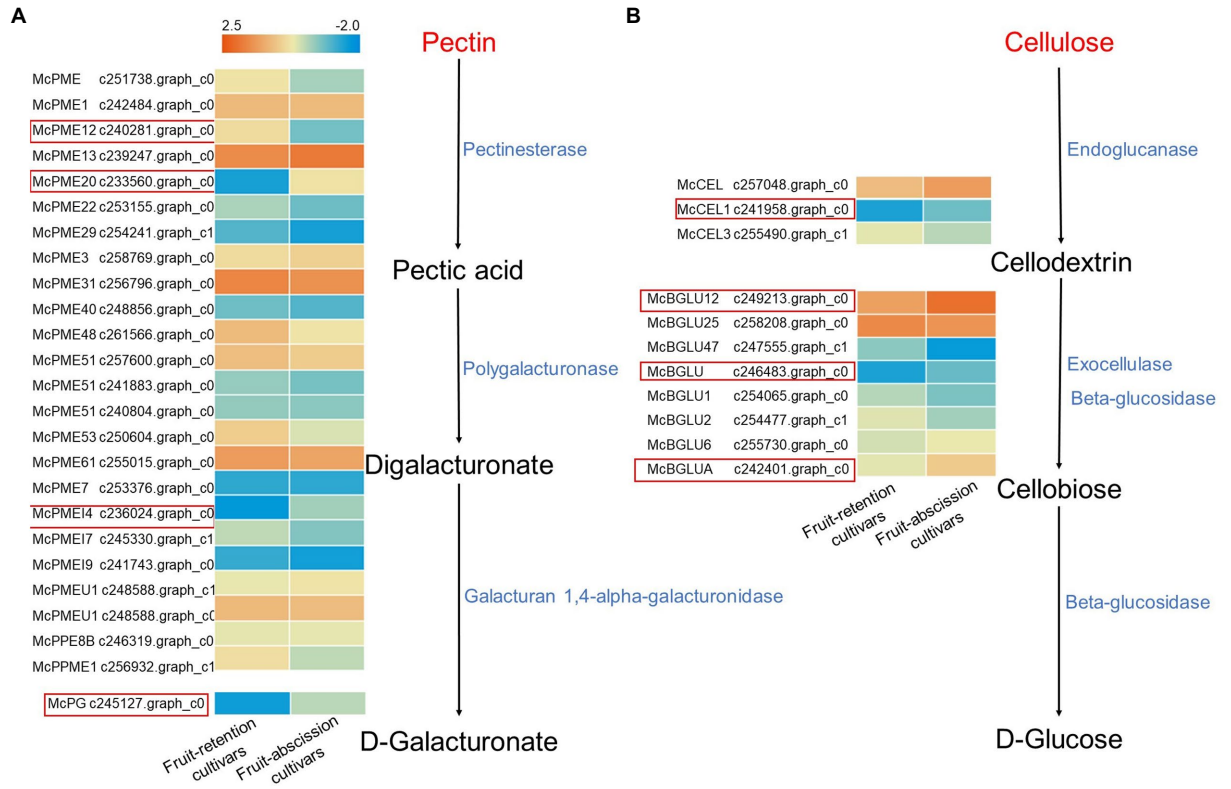

FIGURE 5
Schematics of metabolic differential transcript profiles of cellulose and pectin synthesis related genes. Genes up- or downregulated in all stages in fruit-retention and -abscission cultivars are denoted by light orange and blue, respectively. **(A)** Pentin; **(B)** Cellulose.

graph_c0, *McWRKY71* c255436.graph_c0, and *McWRKY75* c236806.graph_c0), bHLH (*McbHLH75* c242891.graph c0, *McbHLH147* c246589.graph_c0), NAC (*McNAC29-1* c249740. graph_c0, *NAC29-2* c252680.graph_c0), and TGA (*McTGA10* c243460.graph_c1), were upregulated in our research. Furthermore, *McWRKY19* (c261806.graph_c1) was considerably down-regulated in fruit-abscission cultivars. This finding highlighted the function of TFs in the fruit abscission of ornamental crabapple and shed light on the underlying molecular process.

Transcriptome expression trends of plant cell wall hydrolase-related synthetic genes in different fruit abscission types

Pectin and cellulose are the main components of plant cell walls, they sustain the entire cell structure and prevent its degeneration. Pectin in the abscission layer was dissolved during fruit abscission by hydrolases such as CX and PG, which weakens the cell wall and result in fruit abscission (Gulfishan et al., 2019). To further explore the enzymes involved in the degradation of abscission cells, we identified the enzyme-encoded genes in the metabolic pathway of pectin and cellulose in the transcriptome (Figure 5). *McPMEs* (c240281.graph_c0, c233560.graph_c0, c236024.graph_c0), *McPG* (c245127.graph_c0), *McCEL1* (c241958.graph_c0), and *McBGLUs* (c249213.graph_c0, c246483.graph_c0, c242401.graph_c0) were significant expressed in the AZ pectin and cellulose metabolic pathway. Other enzyme-encoded genes were not significantly varied among fruit-retention and -abscission cultivars. The findings confirmed that the buildup of PE and CX in the AZ facilitated the fruit abscission of ornamental crabapple.

Expression validation of differentially expressed cell wall hydrolases and TFs in the transcriptome

To verify the differential expression of cell wall hydrolases and TFs in various abscission type cultivars, six genes were selected: four cell wall hydrolases (*McPME12*, *McCEL1*, *McBGLU12*, and *McPG*) and two TFs (*McbHLH75*, *McWRKY75*). The elevated expression levels of *McPME12*, *McCEL1*, *McBGLU12*, and *McPG* in fruit-abscission cultivars relative to fruit-retention cultivars indicate the importance of cell wall hydrolases in fruit abscission. In addition, the increased expression of *McbHLH75* and *McWRKY75* in fruit-abscission cultivars provides more evidence for the function of TFs in fruit abscission. The identification of expression levels further confirmed the reliability of the transcriptome data (Figure 6).

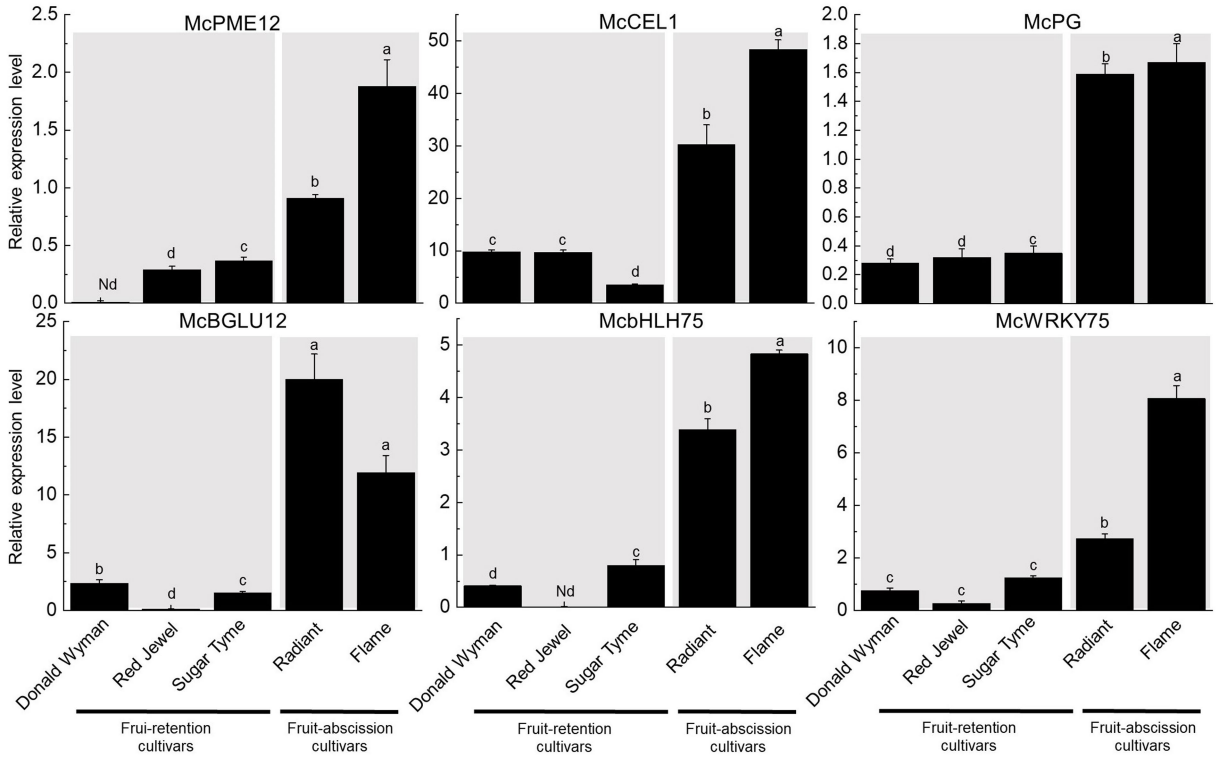

FIGURE 6
Six genes were selected for quantitative real-time PCR (qRT-PCR). The data were normalized by using McActin as an internal reference. Data were represented as mean±SD for three biological replicates.

According to the differences in the expression levels of the above related genes, the response hormones of different abscission cultivars of ornamental crabapple were determined, and finally the abscission was successful. Therefore, we constructed a fruit abscission model of ornamental crabapple to demonstrate the possible internal mechanism affecting fruit abscission of ornamental crabapple (Figure 7).

Discussion

Fruit abscission is a normal physiological phenomenon that is mostly triggered by internal factors. Here, analyzing fruit pedicel length, fruit pedicel thickness, and fruit quality of fruit-retention and -abscission cultivars, we found that the fruit weight of "Radiant" was 1.05 g; the weight of "Flame" was 3.42 g. Interestingly, both "Flame" with the large weight fruit and "Radiant" with the small weight fruit were found that be shedding varieties in our study. Previous research has shown that the small fruit of the citrus variety is late shedding (Ruiz et al., 2001). In citrus, late shedding of small fruit is influenced by carbohydrate supply limitation, and it is speculated that free sugar levels in the peel may be the signal that triggers shedding. However, according to our article, "Radiant" is early shedding variety. These suggested that fruit weight may not be the major determinants in early fruit abscission of ornamental crabapple. The fruit drop of ornamental crabapple may most due to internal factors.

Previous studies have shown a clear correlation between fruit abscission and plant cell structure alterations. During the berry shedding process of different grape varieties, the separation layer's cells expand in volume and become progressively hydrolyzed, or liquefied (Li et al., 2020). PE, PG, CX, and BG affect abscission by degrade the AZ and changing the cell structure (Phetsirikoon et al., 2016; Patharkar and Walker, 2019). The activity of PGs is significantly elevated in the side of secondary xylem where the fruit is attached to the receptacle (Tabuchi et al., 2000). *CsPME1* and *CsPME3* in Valencia orange were differentially expressed and influenced fruit abscission (Joseph et al., 1998). PGs were also seen in the distal and proximal ends of the tomato pedicel explants during the entire shedding process. In tomato, PG is associated with pedicel abscission based on its distribution in isolated areas (Qi et al., 2014). After induction of pedicel shedding, two PG genes, *TAPG1* and *TAPG4*, were more expressed in proximal AZ cells than in distal AZ cells (Kalaitzis et al., 1997). During litchi fruit drop, cell wall degradation and cell separation occurred, as well as an increase in cellulase activity and a reduction in cellulose content. Its two CEL genes (*LcCEL2* and *LcCEL8*) are closely related to shedding (Li et al., 2019). In the calyx ablating region of Valencia orange, the activities of endogenous -1, 4-β-glucanase (cellulase) and polygalacturonidase were dramatically increased

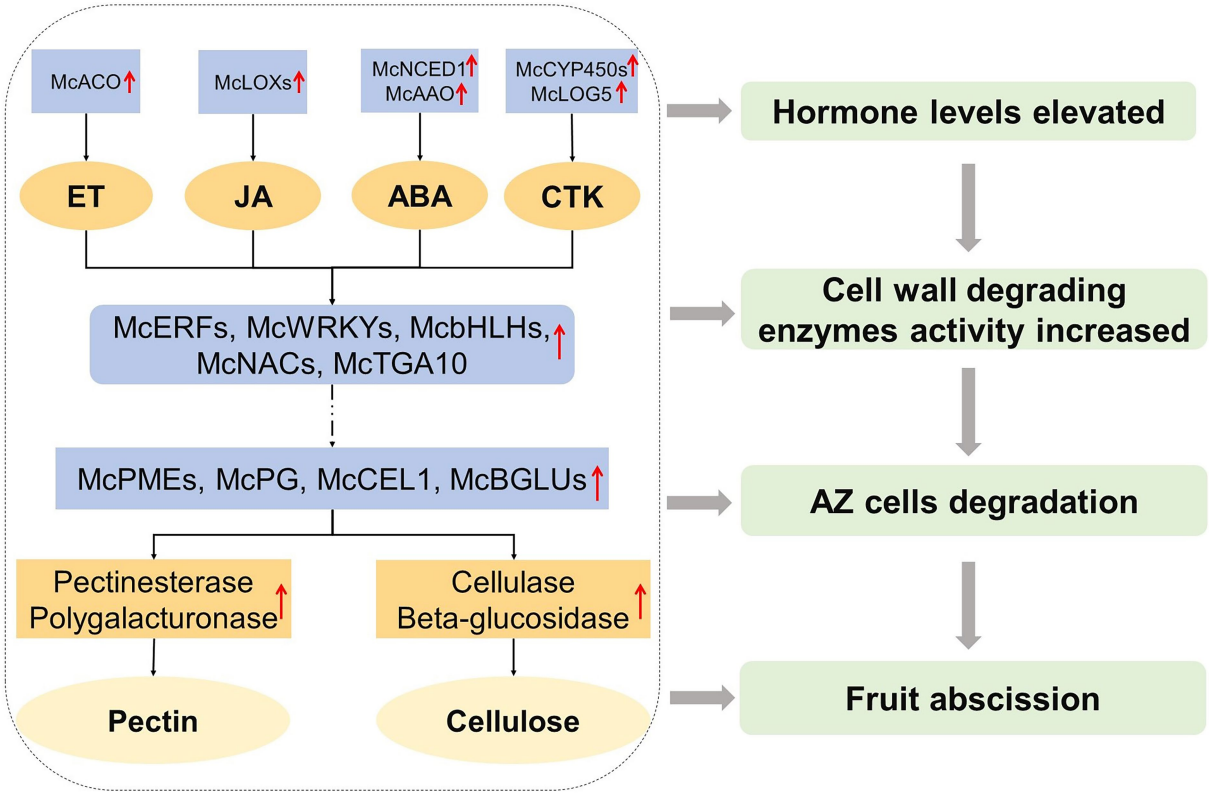

FIGURE 7
A model for regulating fruit abscission in ornamental crabapple was proposed. The expression of ethylene biosynthesis genes, jasmonic acid biosynthesis genes, abscisic acid biosynthesis genes, and cytokinin biosynthesis genes upregulated in AZ during fruit abscission. Cell wall hydrolase-related genes were also upregulated. Solid arrows indicate known mechanisms; broken arrows indicate unknown mechanisms, and red represents upregulation increase events.

(Burns et al., 1998). In this research, fruit-abscission cultivars exhibited significant alterations in PE, CX, PG, and BG. This is roughly consistent with the results of previous studies.

Phytohormones control the fruit abscission. According to their function, different hormones may be split into two categories: one promotes aging, shedding and inhibit growth, while the other inhibits aging and promotes growth. According to prior study, ET can accelerate abscission formation and enhance organ shedding (Bunya-atichart et al., 2011; Meng et al., 2019). In apple, the increase of *MdACO1* (constructional triple reaction 1) was detected in fruit separations (Botton et al., 2011). In litchi, *LcEIL2/3* genes activated *LcCEL2/8*, *LcPG1/2* (cell wall remodeling genes) and *LcACS1/4/7*, *LcACO2/3* (ether biosynthesis genes) through interaction with promoters to affecting the process of fruit shedding (Ma et al., 2020). The expression of *McACO* in our research was significantly increased in fruit-abscission cultivars compared to fruit-retention cultivars, as shown by transcriptome analysis. This further demonstrates the effect ET in fruit abscission, although its precise mechanism requires more research.

Jasmonic acid also has a significant influence in fruit shedding. Methyl jasminate (MeJA) can affect moss's internode growth by interacting with IAA. Furthermore, MeJA can induce the formation of secondary AZs in bryophytes by altering endogenous levels of auxin and JA-related compounds (Dziurka et al., 2022). Simultaneously, MeJA, JA, and 1-aminocyclopropane-1-carboxylic acid (ACC) were administered to grape berries, revealing that ACC could promote MeJA-induced grape shedding (Fidelibus et al., 2022). These findings also indicated that ET and JA may have a synergistic effect on fruit abscission regulation. In this work, JA synthesis genes *McLOX1*, *McLOX1.5*, and *McLOX5* in fruit-abscission cultivars were significantly upregulated. It is shown that JA affected fruit shedding. However, additional research is required to determine if JA and ET may act together to regulation fruit abscission in ornamental crabapple.

Abscisic acid and CTK signaling also play vital roles in the process of fruit abscission. *McNCED1* and *McAAO*, two ABA synthase genes, were identified to be up-regulated in fruit-abscission cultivars of ornamental crabapple. Previous research also showed that *LgAAO3* and *LgNCED* genes were upregulation during longan fruit drop, which resulted from the accumulation of ABA in the AZ (Wei et al., 2021). In addition, the ABA is abundant while CTK is low in litchi fruit, which may influence fruit shedding (Qiu et al., 1998). During rose petal shedding, the *RbLOG* gene, which encodes the cytokinin nucleoside 5′-monophosphate phosphoribosyl hydrolase, is upregulated (Singh et al., 2020). Results from this

study's transcriptome analysis also revealed that differential expression of *McLOG5*, indicating that CTK may play crucial roles in the fruit abscission process of ornamental crabapple. ET may interact with other hormones, such as ABA and CTK (Meir et al., 2010). In fact, once the mechanisms associated with non-dropping fruit are triggered, it seems that the molecular process of both ET and ABA biosynthesis are considerably and rapidly downregulated (Vriezen et al., 2008; Nitsch et al., 2009). Evidently, ET, JA, CTK, and ABA may play a role alone or in concert in the process of ornamental crabapple fruit shedding, and the specific mechanism needs to be explored further.

Transcription factors are considered to be the main switches regulating the cascade in development and various biological processes (Riechmann et al., 2000). During tomato's fruit abscission, ethylene responsiveness factor 52 (*SiERF52*) acts as a central TF to activating CELs and PGs (Nakano et al., 2014). In this study, we also found that *McERF1B*, *McERF113* in ornamental crabapple were upregulated in fruit-abscission varieties. Our findings supported the conclusions of previous research that ET induces fruit abscission. The regulatory action of ET on fruit abscission, which may be mediated through the activation of ERF transcription factors to govern the establishment of the AZ in the fruit pedicel, requires more elaboration. We also discovered that several WRKY transcription factors had significantly variable expression levels in different cultivars of ornamental crabapple. Among them, *McWRKY31/70/71/75* was upregulated while *McWRKY19* was downregulated. This discrepancy in expression pattern may be a result of the distinct transcriptional regulatory functions of WRKY transcription factors. During ET-induced fruit abscission of litchi, the expression levels of *LcbHLH* and *LcNAC* transcription factors in AZ were altered (Li et al., 2015). Similar to the prior findings, we found that the expression levels of bHLH (*McbHLH75/147*) and NAC (*McNAC29-1*, *McNAC29-2*) transcription factors were different in ornamental crabapple with distinct in fruit-abscission cultivars. It is also worth noting that *McTGA10* is a member of the bZIP transcription factor. TGA transcription factor can bind to downstream genes specifically to regulate fruit shedding of *Phaseolus vulgaris* (Sriskantharajah et al., 2021). Therefore, the differential expression of *McTGA10* was anticipated to mediate changes in other genes that affect the fruit abscission of ornamental crabapples. Due to the variable endogenous hormone concentrations in the AZ, different ornamental crabapple cultivars expressed by a large number of TFs in a manner that were distinct from one another. These TFs may stimulate the synthesis of cell wall hydrolases in the fruit AZ of ornamental crabapple.

Following the conclusion of the preceding research, we put forth a hypothesized model in an effort to regulate the fruit abscission of ornamental crabapple (Figure 7). In this paradigm, ET, JA, ABA, and CTK are the primary signaling hormones, and their synthesis genes are upregulated to alter the internal hormone levels. Those phytohormone-related downstream TFs, *McERFs*, *McWRKYs*, *McbHLHs*, *McNACs*, and *McTGA10*, were boosted and played a signal transduction function, collaborating with their downstream genes to increase the expression of cell wall hydrolase production genes (*McPMEs*, *McPG*, *McCEL1*, and *McBGLUs*). Subsequently, the activity of cell wall hydrolases (pectinesterase, polygalacturonase, cellulase, and β-glucosidase) was enhanced to finally degrade the cells in the AZ, resulting in the abscission of ornamental crabapple fruit.

Data availability statement

The data presented in the study are deposited in the Genome Sequence Archive repository, accession number CRA004670.

Author contributions

GZ and XW conceived the study. XW, SY, XS, HL, BC, and XX collected materials and performed experiments. XW, YW, and ZW analyzed the RNA-seq data and drafted the manuscript. XW, YW, ZW, and GZ revised the manuscript. All authors contributed to the article and approved the submitted version.

Funding

This work was supported by the Hebei Provincial Department of Science and Technology Project (21326301D), National "Twelfth Five-Year" Plan for Science and Technology Support (2012AA102002-5) and Hebei University Horticultural Crop Breeding Application Technology R & D Center (YF201404). The funders had no role in study design, data collection and analysis, decision to publish, or preparation of the manuscript.

Conflict of interest

The authors declare that the research was conducted in the absence of any commercial or financial relationships that could be construed as a potential conflict of interest.

Publisher's note

Supplementary material

The Supplementary material for this article can be found online at: https://www.frontiersin.org/articles/10.3389/fpls.2022.1013263/full#supplementary-material

SUPPLEMENTARY FIGURE S1
Comparison of the different period of ornamental crabapple fruit. **(A)** Show the changes of fruit growth status of five cultivars of ornamental crabapple from August to November. Fruit abscission fell off completely in October **(B)**. The location of fruit-retention cultivars and the location of fruit-abscission cultivars.

References

Agusti, J., Gimeno, J., Merelo, P., Serrano, R., Cercos, M., Conesa, A., et al. (2012). Early gene expression events in the laminar abscission zone of abscission-promoted citrus leaves after a cycle of water stress/rehydration: involvement of *CitbHLH1*. *J. Exp. Bot.* 63, 6079–6091. doi: 10.1093/jxb/ers270

Botton, A., Eccher, G., Forcato, C., Ferrarini, A., Begheldo, M., Zermiani, M., et al. (2011). Signaling pathways mediating the induction of apple fruitlet abscission. *BMC Plant Biol.* 155, 185–208. doi: 10.1104/pp.110.165779

Bunya-atichart, K., Ketsa, S., and Van Doorn, W. G. (2011). Ethylene-sensitive and ethylene-insensitive abscission in *Dendrobium*: correlation with polygalacturonase activity. *Postharvest Biol. Technol.* 60, 71–74. doi: 10.1016/j.postharvbio.2010.11.006

Burns, J. K., Lewandowski, D. J., Nairn, C. J., and Brown, G. (1998). Endo-1, 4-β-glucanase gene expression and cell wall hydrolase activities during abscission in Valencia orange. *Physiol. Plant.* 102, 217–225. doi: 10.1034/j.1399-3054.1998.1020209.x

Corbacho, J., Romojaro, F., Pech, J. C., Latché, A., and Gomez-Jimenez, M. C. (2017). Early transcriptomic events involved in melon mature-fruit abscission. *Acta Hortic.* 1151, 127–134. doi: 10.17660/actahortic.2017.1151.21

Corrigan, L. (2018). *Investigating How Boundary Genes Control Abcission in Arabidopsis thaliana*. Ottawa, Canada: Carleton University.

Dziurka, M., Góraj-Koniarska, J., Marasek-Ciolakowska, A., Kowalska, U., Saniewski, M., Ueda, J., et al. (2022). A possible mode of action of methyl jasmonate to induce the secondary abscission zone in stems of *Bryophyllum calycinum*: relevance to plant hormone dynamics. *Plants Theory* 11:360. doi: 10.3390/plants11030360

Estornell, L. H., Agustí, J., Merelo, P., Talón, M., and Tadeo, F. R. (2013). Elucidating mechanisms underlying organ abscission. *Plant Sci.* 199-200, 48–60. doi: 10.1016/j.plantsci.2012.10.008

Fidelibus, M. W., Petracek, P., and McArtney, S. (2022). Jasmonic acid activates the fruit-pedicel abscission zone of 'Thompson seedless' grapes, especially with co-application of 1-aminocyclopropane-1-carboxylic acid. *Plants Theory* 11:1245. doi: 10.3390/plants11091245

Gao, Y., Liu, Y., Liang, Y., Lu, J., Jiang, C., Fei, Z., et al. (2019). Rosa hybrida RhERF1 and RhERF4 mediate ethylene-and auxin-regulated petal abscission by influencing pectin degradation. *Plant J.* 99, 1159–1171. doi: 10.1111/tpj.14412

Giulia, E., Alessandro, B., Mariano, D., Andrea, B., Benedetto, R., and Angelo, R. (2013). Early induction of apple fruitlet abscission is characterized by an increase of both isoprene emission and abscisic acid content. *BMC Plant Biol.* 161, 1952–1969. doi: 10.1104/pp.112.208470

Goncharovska, I., Vladimyr, K., Antonyuk, G., Catalina, D., and Sestras, A. F. (2022). Flower and fruit morphological characteristics of different crabapple genotypes of ornamental value. *Notul. Sci. Biol.* 14:10684. doi: 10.15835/nsb14110684

Gulfishan, M., Jahan, A., Bhat, T. A., and Sahab, D. (2019). "Plant senescence and organ abscission" in *Senescence Signalling and Control in Plants*. eds. M. Sarwat and N. Tuteja (India: Academic Press), 255–272.

Heo, S., and Chung, Y. S. (2019). Validation of MADS-box genes from apple fruit pedicels during early fruit abscission by transcriptome analysis and real-time PCR. *Genes Genomics* 41, 1241–1251. doi: 10.1007/s13258-019-00852-4

Jiang, C., Zhang, H., Ren, J., Dong, J., Zhao, X., Wang, X., et al. (2020). Comparative transcriptome-based mining and expression profiling of transcription factors related to cold tolerance in Peanut. *Int. J. Mol. Sci.* 21:1921. doi: 10.3390/ijms21061921

Joseph, N. C., Lewandowski, D. J., and Burns, J. K. (1998). Genetics and expression of two pectinesterase genes in Valencia orange. *Physiol. Plant.* 102, 226–235. doi: 10.1034/j.1399-3054.1998.1020210.x

Kalaitzis, P., Solomos, T., and Tucker, M. L. (1997). Three different polygalacturonases are expressed in tomato leaf and flower abscission, each with a different temporal expression pattern. *Plant Physiol.* 113, 1303–1308. doi: 10.1104/pp.113.4.1303

Kuhn, N., Serrano, A., Abello, C., Arce, A., Espinoza, C., Gouthu, S., et al. (2016). Regulation of polar auxin transport in grapevine fruitlets (Vitis vinifera L.) and the proposed role of auxin homeostasis during fruit abscission. *BMC Plant Biol.* 16:234. doi: 10.1186/s12870-016-0914-1

Leng, N., Dawson, J. A., Thomson, J. A., Ruotti, V., Rissman, A. I., Smits, B. M., et al. (2013). EBSeq: an empirical Bayes hierarchical model for inference in RNA-seq experiments. *Bioinformatics* 29, 2073–1043. doi: 10.1093/bioinformatics/btt337

Li, M., Huang, Z., You, X., Zhang, Y., Wei, P., Zhou, K., et al. (2020). Relationships between cell structure alterations and berry abscission in table grapes. *Front. Nutr.* 7:69. doi: 10.3389/fnut.2020.00069

Li, C., Wang, Y., Ying, P., Ma, W., and Li, J. (2015). Genome-wide digital transcript analysis of putative fruitlet abscission related genes regulated by ethephon in litchi. *Front. Plant Sci.* 6:502. doi: 10.3389/fpls.2015.00502

Li, C. Q., Zhao, M. L., Ma, X. S., Wen, Z. X., Ying, P. Y., Peng, M. J., et al. (2019). The HD-zip transcription factor *LcHB2* regulates litchi fruit abscission through the activation of two cellulase genes. *J. Exp. Bot.* 70, 5189–5203. doi: 10.1093/jxb/erz276

Li, J., Zhu, H., and Yuan, R. (2010). Profiling the expression of genes related to ethylene biosynthesis, ethylene perception, and cell wall degradation during fruit abscission and fruit ripening in apple. *J. Am. Soc. Hortic. Sci.* 135, 391–401. doi: 10.21273/JASHS.135.5.391

Livak, K. J., and Schmittgen, T. D. (2001). Analysis of relative gene expression data using real-time quantitative PCR and the $2^{-\Delta\Delta CT}$ method. *Methods* 25, 402–408. doi: 10.1006/meth.2001.1262

Ma, X., Yuan, Y., Wu, Q., Wang, J., Li, J., and Zhao, M. (2020). *LcEIL2/3* are involved in fruitlet abscission via activating genes related to ethylene biosynthesis and cell wall remodeling in litchi. *Plant J.* 103, 1338–1350. doi: 10.1111/tpj.14804

Meir, S., Philosoph-Hadas, S., Sundaresan, S., Selvaraj, K. S., Burd, S., Ophir, R., et al. (2010). Microarray analysis of the abscission-related transcriptome in the tomato flower abscission zone in response to auxin depletion. *Plant Physiol.* 154, 1929–1956. doi: 10.1104/pp.110.160697

Meng, J., Zhou, Q., Zhou, X., Fang, H. X., and Ji, S. J. (2019). Ethylene and 1-MCP treatments affect leaf abscission and associated metabolism of Chinese cabbage. *Postharvest Biol. Technol.* 157, 110963. doi: 10.1016/j.postharvbio.2019.110963

Mortazavi, A., Williams, B. A., McCue, K., Schaeffer, L., and Wold, B. (2008). Mapping and quantifying mammalian transcriptomes by RNA-Seq. *Nat. Methods* 5, 621–628. doi: 10.1038/nmeth.1226

Nakano, T., Fujisawa, M., Shima, Y., and Ito, Y. (2014). The AP2/ERF transcription factor SlERF52 func-tions in flower pedicel abscission in tomato. *J. Exp. Bot.* 65, 3111–3119. doi: 10.1093/jxb/eru154

Nitsch, L. M. C., Oplaat, C., Feron, R., Ma, Q., Wolters-Arts, M., Hedden, P., et al. (2009). Abscisic acid levels in tomato ovaries are regulated by *LeNCED1* and *SlCYP707A1*. *Planta* 229, 1335–1346. doi: 10.1007/s00425-009-0913-7

Parra, R., Paredes, M. A., Labrador, J., Nunes, C., Coimbra, M. A., Fernandez-Garcia, N., et al. (2020). Cell wall composition and ultrastructural immunolocalization of pectin and arabinogalactan protein during *Olea europaea* L. fruit abscission. *Plant Cell Physiol.* 61, 814–825. doi: 10.1093/pcp/pcaa009

Patharkar, O. R., and Walker, J. C. (2018). Advances in abscission signaling. *J. Exp. Bot.* 69, 733–740. doi: 10.1093/jxb/erx256

Patharkar, O. R., and Walker, J. C. (2019). Connections between abscission, dehiscence, pathogen defense, drought tolerance, and senescence. *Plant Sci.* 284, 25–29. doi: 10.1016/j.plantsci.2019.03.016

Peng, G., Wu, J., Lu, W., and Li, J. (2013). A polygalacturonase gene clustered into clade E involved in lychee fruitlet abscission. *Sci. Hortic.* 150, 244–250. doi: 10.1016/j.scienta.2012.10.029

Phetsirikoon, S., Paull, R. E., Chen, N., Ketsa, S., and Doorn, W. G. V. (2016). Increased hydrolase gene expression and hydrolase activity in the abscission zone involved in chilling-induced abscission of *Dendrobium* flowers. *Postharvest Biol. Technol.* 117, 217–229. doi: 10.1016/j.postharvbio.2016.03.002

Qi, M. F., Xu, T., Chen, W. Z., and Li, T. L. (2014). Ultrastructural localization of polygalacturonase in ethylene stimulated abscission of tomato pedicel explants. *Sci. World J.* 2014:389896. doi: 10.1155/2014/389896

Qiu, Y. P., Xu, X., and Wang, B. Q. (1998). Endogenous hormone balance in three types of litchi fruit and their fruit set mechanism. *Guoshu Kexue* 15, 39–43.

Riechmann, J. L., Heard, J., Martin, G., Reuber, L., Jiang, C. Z., Keddie, J., et al. (2000). Arabidopsis transcription factors: genome-wide comparative analysis among eukaryotes. *Science* 290, 2105–2110. doi: 10.1126/science.290.5499.2105

Ruiz, R., Garcıa-Luis, A., Monerri, C., and Guardiola, J. (2001). Carbohydrate availability in relation to fruitlet abscission in citrus. *Ann. Bot.* 87, 805–812. doi: 10.1006/anbo.2001.1415

Singh, P., Bharti, N., Singh, A. P., Tripathi, S. K., Pandey, S. P., Chauhan, A. S., et al. (2020). Petal abscission in fragrant roses is associated with large scale differential

regulation of the abscission zone transcriptome. *Sci. Rep.* 10:17196. doi: 10.1038/s41598-020-74144-3

Sriskantharajah, K., El Kayal, W., Torkamaneh, D., Ayyanath, M. M., Saxena, P. K., Sullivan, A. J., et al. (2021). Transcriptomics of improved fruit retention by hexanal in 'Honeycrisp' reveals hormonal crosstalk and reduced cell wall degradation in the fruit abscission zone. *Int. J. Mol. Sci.* 22:8830. doi: 10.1104/pp.007971

Sun, L., Bukovac, M. J., Forsline, P. L., and Nocker, S. (2009). Natural variation in fruit abscission-related traits in apple (*Malus*). *Euphytica* 165, 55–67. doi: 10.1007/s10681-008-9754-x

Sun, X., Wang, Y., and Sui, N. (2018). Transcriptional regulation of bHLH during plant response to stress. *Biochem. Biophys. Res. Commun.* 503, 397–401. doi: 10.1016/j.bbrc.2018.07.123

Tabuchi, T., Ito, S., and Arai, N. (2000). Development of the abscission zones in j-2^{in} pedicels of Galapagos wild tomatoes. *J. Jpn. Soc. Hortic. Sci.* 69, 443–445. doi: 10.2503/jjshs.69.443

Taylor, J. E., and Whitelaw, C. A. (2001). Signals in abscission. *New Phytol.* 151, 323–340. doi: 10.1046/j.0028-646x.2001.00194.x

Tucker, M. L., and Kim, J. (2015). Abscission research: what we know and what we still need to study. *Stewart Postharv. Rev.* 11, 1–7. doi: 10.2212/spr.2015.2.1

Vanderstraeten, L., Depaepe, T., Bertrand, S., and Van Der Straeten, D. (2019). The ethylene precursor ACC affects early vegetative development independently of ethylene signaling. *Front. Plant Sci.* 10:1591. doi: 10.3389/fpls.2019.01591

Vriezen, W. H., Feron, R., Maretto, F., Keijman, J., and Mariani, C. (2008). Changes in tomato ovary transcriptome demonstrate complex hormonal regulation of fruit set. *New Phytol.* 177, 60–76. doi: 10.1111/j.1469-8137.2007.02254.x

Wei, H. Y., Li, Z. Z., Qiu, S. X., and Sheng, Y. S. (2021). Changes of fruit abscission and carbohydrate, ABA and related genes expression in the pericarp and fruit abscission zone of longan under starvation stress. *Acta Hortic. Sinica* 48:1457. doi: 10.16420/j.issn.0513-353x.2020-0538

Wu, P., Xin, F., Xu, H., Chu, Y., Du, Y., Tian, H., et al. (2021). Chitosan inhibits postharvest berry abscission of 'Kyoho' table grapes by affecting the structure of abscission zone, cell wall degrading enzymes and SO2 permeation. *Postharvest Biol. Technol.* 176:111507. doi: 10.1016/j.postharvbio.2021.111507

Yu, Y., and Kellogg, E. A. (2018). Inflorescence abscission zones in grasses: diversity and genetic regulation. *Annu. Plant Rev.* 1, 1–35. doi: 10.1002/9781119312994.apr0619

Zamil, M., and Geitmann, A. (2017). The middle lamella-more than a glue. *Phys. Biol.* 14:015004. doi: 10.1088/1478-3975/aa5ba5

Zhao, M., and Li, J. (2020). Molecular events involved in fruitlet abscission in litchi. *Plan. Theory* 9:151. doi: 10.3390/plants9020151

Zheng, Y., Jiao, C., Sun, H., Rosli, H. G., Pombo, M. A., Zhang, P., et al. (2016). iTAK: a program for genome-wide prediction and classification of plant transcription factors, transcriptional regulators, and protein kinases. *Mol. Plant* 9, 1667–1670. doi: 10.1016/j.molp.2016.09.014

frontiers | Frontiers in Plant Science

TYPE Original Research
PUBLISHED 23 September 2022
DOI 10.3389/fpls.2022.975356

OPEN ACCESS

EDITED BY
Jose G. Vallarino,
University of Malaga, Spain

REVIEWED BY
Delphine Maya Pott,
University of Tübingen, Germany
Neftali Ochoa-Alejo,
Centro de Investigación y de Estudios Avanzados del Instituto Politécnico Nacional, Mexico

*CORRESPONDENCE
Jiancheng Zhang
zjcnd001@163.com
Peitao Lü
ptlv@fafu.edu.cn

†These authors have contributed equally to this work

SPECIALTY SECTION
This article was submitted to Plant Systems and Synthetic Biology, a section of the journal Frontiers in Plant Science

RECEIVED 22 June 2022
ACCEPTED 09 September 2022
PUBLISHED 23 September 2022

CITATION
Cheng C, Guo Z, Li H, Mu X, Wang P, Zhang S, Yang T, Cai H, Wang Q, Lü P and Zhang J (2022) Integrated metabolic, transcriptomic and chromatin accessibility analyses provide novel insights into the competition for anthocyanins and flavonols biosynthesis during fruit ripening in red apple.
Front. Plant Sci. 13:975356.
doi: 10.3389/fpls.2022.975356

Integrated metabolic, transcriptomic and chromatin accessibility analyses provide novel insights into the competition for anthocyanins and flavonols biosynthesis during fruit ripening in red apple

Chunzhen Cheng[1†], Ziwei Guo[1†], Hua Li[2†], Xiaopeng Mu[1], Pengfei Wang[1], Shuai Zhang[1], Tingzhen Yang[3], Huacheng Cai[3], Qian Wang[3], Peitao Lü[2*] and Jiancheng Zhang[1*]

[1]College of Horticulture, Shanxi Agricultural University, Jinzhong, China, [2]College of Horticulture, FAFU-UCR Joint Center for Horticultural Biology and Metabolomics, Haixia Institute of Science and Technology, Fujian Agriculture and Forestry University, Fuzhou, China, [3]Fruit Research Institute, Shanxi Agricultural University, Jinzhong, China

Fruit ripening is accompanied by a wide range of metabolites and global changes in gene expression that are regulated by various factors. In this study, we investigated the molecular differences in red apple 'Hongmantang' fruits at three ripening stages (PS1, PS5 and PS9) through a comprehensive analysis of metabolome, transcriptome and chromatin accessibility. Totally, we identified 341 and 195 differentially accumulated metabolites (DAMs) in comparison I (PS5_vs_PS1) and comparison II (PS9_vs_PS5), including 57 and 23 differentially accumulated flavonoids (DAFs), respectively. Intriguingly, among these DAFs, anthocyanins and flavonols showed opposite patterns of variation, suggesting a possible competition between their biosynthesis. To unveil the underlying mechanisms, RNA-Seq and ATAC-Seq analyses were performed. A total of 852 DEGs significantly enriched in anthocyanin metabolism and 128 differential accessible regions (DARs) significantly enriched by MYB-related motifs were identified as up-regulated in Comparison I but down-regulated in Comparison II. Meanwhile, the 843

DEGs significantly enriched in phenylalanine metabolism and the 364 DARs significantly enriched by bZIP-related motifs showed opposite trends. In addition, four *bZIPs* and 14 *MYBs* were identified as possible hub genes regulating the biosynthesis of flavonols and anthocyanins. Our study will contribute to the understanding of anthocyanins and flavonols biosynthesis competition in red apple fruits during ripening.

KEYWORDS

anthocyanin, flavonol, fruit ripening, expression regulation, omics

Introduction

The old saying 'An apple a day keeps the doctor away' can be explained by the fact that apples can help people to stay healthy and away from the doctor by reducing the risk of numerous chronic diseases due to its high antioxidant content. As a major contributor to the total antioxidant capacity, flavonoids were hence considered as one of the most important phytonutrients that apples nourish people (Lee et al., 2003). Apples are identified as one of the main diet sources of flavanols and flavonols for people (Vrhovsek et al., 2004). Moreover, the anthocyanins accumulation in apples skin and flesh affects greatly the external quality and health care values of apples (Martin, 2013). Therefore, the study of flavonoids, especially anthocyanin biosynthesis, has been an attention hotspot for apple studies.

To date, there are more than 10,000 known flavonoids that have been identified. According to their structures, they can be divided into six groups: dihydroflavones, flavones, isoflavones, flavonols, flavanols and anthocyanidins. The main synthetic pathway of flavonoids are well established, i.e., dihydroflavonoids are first synthesized, and then flavonoids, isoflavones, flavonols, flavanols and anthocyanidins are further synthesized through a series of branching pathways catalyzed by enzymes encoded by structural genes, such as phenylalanine ammonia-lyase (PAL), cinnamic acid 4-hydroxylase (C4H), 4-coumarate-CoA ligase (4CL), chalcone synthase (CHS), chalcone isomerase (CHI), flavanone-3-hydroxylase (F3H), flavonoid-3'-hydroxylase (F3'H), flavonoid-3'-5'-hydroxylase (F3'5'H), flavonol synthase (FLS), dihydroflavonol reductase (DFR), anthocyanidin synthase (ANS), leucocyanidin reductase (LAR), anthocyanidin reductase (ANR), etc. (Gutierrez et al., 2017). In addition to structural genes, the flavonoids biosynthesis is also regulated by many transcription factors (TFs), which are directly or indirectly modulating the spatiotemporal expression of structural genes (Zhang et al., 2021). Among them, MYB has long been considered as one of the most important TFs regulating the flavonoids synthesis in apple (Takos et al., 2006). Some other TFs have also contributed greatly to the regulation of flavonoids biosynthesis, mainly through interacting with various MYB members. For example, EIL3 (EIN3-LIKE1) can bind to the promoter of *MdMYB1* to activate *MdMYB1* gene expression and to induce anthocyanin accumulation and fruit color transformation (An et al., 2018c); MdERF1B interacts with MdMYB9, MdMYB1 and MdMYB11 and can bind to the promoters of their encoded genes to affect anthocyanin biosynthesis (Zhang et al., 2018).

Recently, integrated metabolomic and transcriptomic analyses have been successfully applied in the exploration of the key factors regulating metabolites accumulations in many fruits (Xu H. et al., 2020; Zhang et al., 2020; Fu et al., 2022). However, the two methods can only reflect changes in gene expression and metabolites accumulation at the RNA and metabolite levels, respectively, and the factors influencing gene expression cannot be directly deciphered. Access to open chromatin can reveal the regulation mechanisms of gene expression, which is a hot topic in epigenetic research. ATAC-seq (Assay for Transpoase-accessible Chromatin with High Throughput sequencing), an innovative technology developed by Buenrostro et al. (2013), is an epigenetic research technique for analyzing Tn5 transposase accessibility chromatin region using high-throughput sequencing and is considered as a potential tool for identifying *cis*-regulatory regions such as TF binding sites (Grandi et al., 2022). Based on the ATAC-Seq data, all the open chromatin regions in a specific spatiotemporal condition could be obtained. Through investigating the accessible chromatin regions (ACRs) in root, leaf bud, flower, flower bud, developing seed, and pod of soybean using ATAC-Seq, Huang et al. (2022) reported that the ACRs occupied more than 3% of the soybean genome. By integrating the RNA-seq and TF ChIP-seq results, they found that ACRs were tightly associated with gene expressions and TF binding capacities. In *Vitis vinifera* leaves, more than 16,000 ACRs were identified, with nearly 5,000 distal enhancer candidates located in intergenic regions > 2 kb from the nearest transcription start site (TSS), which were found to be enriched in TCP family

binding sites by motif search, suggesting that these regions may be regulated by TCP (Schwope et al., 2021). Through the combined ATAC-Seq and RNA-Seq analyses, nine TF genes, including *RAV1*, were identified as responsible for high cold hardiness of *V. amurensis* (Ren et al., 2021).

Red-flesh apples, containing anthocyanins in both fruit skin and flesh, are popular for their anthocyanin-rich characteristics. The red-flesh apple 'Hongmantang', selected from *Malus pumila* Mill. × *M. baccata* (L.) Borkh hybrids, is of purple-red flower and blood-red flesh. Compared with its parent *M. pumila* Mill., its total anthocyanins and total polyphenols contents in fruits are much higher, suggesting that it can be used as a suitable material for the flavonoids biosynthesis studies of *Malus* species (Yang et al., 2015). In our previous study, through analyzing the changes in total anthocyanins contents during fruit ripening, we found that there were two anthocyanin content peaks (at PS5 and PS9, respectively) throughout fruit ripening stage (Guo et al., 2021) (Figure S1). In this study, to reveal the mechanisms underlying the bioactive compounds changes during fruit ripening, we investigated the metabolome, transcriptome and chromatin accessibility changes in 'Hongmantang' fruits at three ripening stages, PS1 (at about 7 weeks post flowering with the lowest anthocyanin content), PS5 (at about 15 weeks post flowering with the highest anthocyanins content) and PS9 (at about 23 weeks post flowering, the second anthocyanins accumulation peak), by using the ultra-performance liquid chromatography-tandem mass spectrometry (UPLC-MS/MS)-based widely targeted metabolome, RNA-Seq and ATAC-Seq technologies, respectively. The results obtained in this study could provide a basis for the comprehensive understanding of the metabolites changes during fruit ripening in red apple.

Materials and methods

Plant materials

The red apple 'Hongmantang' used in this study is an ornamental red apple with purple-red flower and blood-red flesh, and was selected from *M. pumila* Mill. × *M. baccata* (L.) Borkh interspecific hybrids by Shanxi Academy of Agricultural Sciences. In this study, the 'Hongmantang' fruits were harvested at three key developmental stages (PS1: at about 7 weeks post flowering; PS5: at about 15 weeks post flowering; PS9: at about 23 weeks post flowering) and stored in a -80°C freezer for further use.

Metabolites extraction and determination

Briefly, 50 mg of red apple fruit samples were added to 1 mL of 70% methanol solution, homogenized at 30 Hz for 3 min, vortexed for 1 min, placed on ice for 15 min, centrifuged at 12,000 rpm at 4°C for 10 min, and then the supernatant was collected for subsequent LC-MS/MS analysis at Wuhan MetWare Biotechnology Co., Ltd. (Wuhan, China). The analysis was performed using a liquid chromatography-electrospray ionization-mass spectrometry (LC-ESI-MS/MS) system according to the method described by Chen et al. (2013). The column of Agilent SB-C18 (1.8 μm, 2.1 mm * 100 mm) and the mobile phase consisted of solvent A (ultrapure water with 0.04% acetic acid) and solvent B (acetonitrile with 0.04% acetic acid) were used in the analysis. The gradient program was set as follows: 95% solvent A and 5% solvent B at 0 min; a liner gradient to 5% solvent A and 95% solvent B within 9 min and kept for 1 min; and adjustment to 95% solvent A and 5% solvent B within 1.1 min and kept for 2.9 min (Li et al., 2022). The flow rate was 0.35 mL/min with injection volume of 4 μL, and the column temperature was 40°C. The effluent was connected to an ESI-triple quadrupole-linear ion trap (QTRAP)-MS (AB4500 Q TRAP UPLC/MS/MS System) equipped with an ESI Turbo Ion-Spray interface. Analyst 1.6.3 software (AB Sciex) was used for controlling the positive and negative ion modes. The MetWare database (MWDB) together with several public databases were used for metabolites annotation (Li et al., 2022). And metabolites were quantified using the multiple reaction monitoring method. Three biological replicates were performed on fruits at each selected stage (PS1, PS5 and PS9). The OPLS-DA (Orthogonal Projection to Latent Structures Discriminant Analysis) model was established using multiple supervision methods and examined using the Variable Importance in Projection (VIP) parameter. For the identification of differentially accumulated metabolites (DAMs) in fruits of the three ripening stages, VIP ≥ 1 and fold change ≥ 2 or ≤ 0.5 were used as criteria (Yuan et al., 2018; Zhang et al., 2020).

RNA extraction, quantification and transcriptome sequencing

Total RNA of red apple fruits was extracted using Trizol (Invitrogen, CA, USA). After digestion of DNA contamination with DNase I, the RNA quality and quantity were detected using NanoDrop 2000 spectrophotometer (NanoDrop Technologies, Wilmington, DE, USA) and a Bioanalyzer 2100 system (Agilent Technologies, CA, USA). High-quality total RNA was used for RNA-Seq on a MGI-SEQ 2000 platform to generate 150 bp paired-end reads at Wuhan Frasergen Bioinformatics Co., Ltd. (Wuhan, China). The raw clean reads were mapped to the *M. baccata* (L.) Borkh. genome [downloaded from https://www.ncbi.nlm.nih.gov/genome/?term=Malus_baccata_v1.0] for gene transcriptional level studies using hisat2 software. For each stage, three biological replicates were performed, with at least ten fruits being mixed in each replicate. Differentially expressed genes

(DEGs) were identified using DESeq2 with criteria of log2(fold change) > 1 or < -1 and corrected *q*-value < 0.05. The RNA-Seq raw data has been deposited at NCBI under the BioProject number PRJNA861071 (https://www.ncbi.nlm.nih.gov/sra/PRJNA861071).

ATAC-Seq library construction and analysis

ATAC-Seq libraries were constructed and sequenced according to the methods described by Buenrostro et al. (2013) and Corces et al. (2017). For fruits at each stage, two biological replicates were performed. Briefly, total DNA from Tn5 digestion was purified by phenol/chloroform extraction and precipitation, electrophoresed on a 2% agarose gel, amplified using PCR, purified and sequenced by Illumina method. clean reads were mapped to the *M. baccata* genome using Bowtie2 (Langmead and Salzberg, 2012), and redundancy was removed from the obtained comparison files using the Picard program, followed by peak detection by MACS2. The distribution of peaks in each sample relative to gene transcription start sites (TSSs) and transcription end sites (TESs) was statistically analyzed and the proportion of peaks at various locations in the genome, including 5'UTR, 3'UTR, 1st exon, other exon, 1st intron, other intron, downstream (≤ 300 bp) and distal intergenic, was calculated. For the identification of differential peaks, DESeq2 was used with a threshold of FDR (false discovery rate) < 0.05 and fold change > 1.5 or < -1.5. The GenomicFeatures (R packages) was used to extract the genes nearby the differential peaks. For the enrichment analysis of genes involved in differential accessible regions (DARs), GO and KEGG enrichment analyses were performed with *P* (classicFisher) ≤ 0.05 and corrected *P*-value < 0.05, respectively. The ATAC-Seq raw data has been deposited at NCBI under BioProject number PRJNA860789 (https://www.ncbi.nlm.nih.gov/sra/PRJNA860789).

Quantitative real time PCR analysis

Complementary DNA (cDNA) of different samples was synthesized separately using the PrimeScript RT Master Mix (Perfect Real Time) kit (Takara, Dalian, China). Gene specific primers for selected genes were designed using Primer 3 (https://bioinfo.ut.ee/primer3-0.4.0/) according to their CDS (coding sequence) sequences (Table S1). qRT-PCR experiment was performed on Efficiency T96 real-time quantitative fluorescent PCR instrument (Beijing Leadaeon Technology Co. Ltd, Beijing, China). The qRT-PCR conditions were set as follows: pre-denaturation at 95°C for 30 s; denaturation at 95°C for 10 s, annealing at 54.8~58.8°C for 20 s, extension at 72°C for 20 s, 50 cycles. qRT-PCR reaction system consisted of 10 μL SYBR Premix ExTaq^{TM} (TaKaRa) fluorescent dye (containing Oligo (dT) and random primers), 7.4 μL ddH_2O, 0.8 μL of each upstream and downstream primer, and 1 μL cDNA template. Their relative expression levels in different samples were calculated using the $2^{-\Delta\Delta Ct}$ method with *actin* as internal reference gene (Jiang et al., 2019).

Results

UPLC-MS/MS analysis of metabolic profiles in red apple fruits during ripening

The UPLC-MS/MS-based untargeted metabolome approach enables the detection of many primary and secondary metabolic compounds from red apple fruit samples. Totally, we identified 753 metabolites from red apple fruits at three ripening stages, including 399 primary metabolites and 354 secondary metabolites (Table S2). These metabolites could be further classified into 11 groups, including phenolic acids, flavonoids, lipids, amino acids and derivatives, organic acids, nucleotides and derivatives, alkaloids, terpenoids, tannins, lignans and coumarins, and others (Figure S2). Metabolites belonging to amino acids and derivatives, flavonoids, alkaloids, phenolic acids, nucleotides and derivatives, lignans and coumarins, and tannins mostly showed high accumulation at PS1 but low accumulation at PS5. However, many terpenoids and some lipids and phenolic acids accumulated highly at PS9. Moreover, some metabolites, such as saccharides and alcohols, vitamin and stilbene, were classified into 'others' group and showed very low or even no accumulation at PS1, but their contents increased with fruit ripening.

PCA analysis of the metabolites among red apple fruits at three different ripening stages revealed that their metabolomes were clearly different (Figure 1A). A total of 341 differentially accumulated metabolites (DAMs) were identified, including 69 increased and 272 decreased DAMs in comparison PS5_vs_PS1 (Comparison I) (Table S3; Figure 1B). There were much less increased metabolites than decreased metabolites for DAMs belonging to phenolic acids (16 increased and 54 decreased), flavonoids (5 increased and 52 decreased), lipids (7 increased and 41 decreased), amino acids and derivatives (4 increased and 37 decreased), organic acids (9 increased and 16 decreased), alkaloids (3 increased and 16 decreased), terpenoids (1 increased and 13 decreased), nucleotides and derivatives (2 increased and 9 decreased), tannins (only 9 decreased) and lignans and coumarins (2 increased and 5 decreased). However, for the saccharides and alcohols related DAMs, a larger proportion of increased metabolites (17 increased and 14 decreased) was observed. Notably, among the 57 different accumulated flavonoids (DAFs) (Table S4; Figure 1B), two anthocyanins, cyanidin-3-*O*-galactoside and cyanidin-3-*O*-glucoside

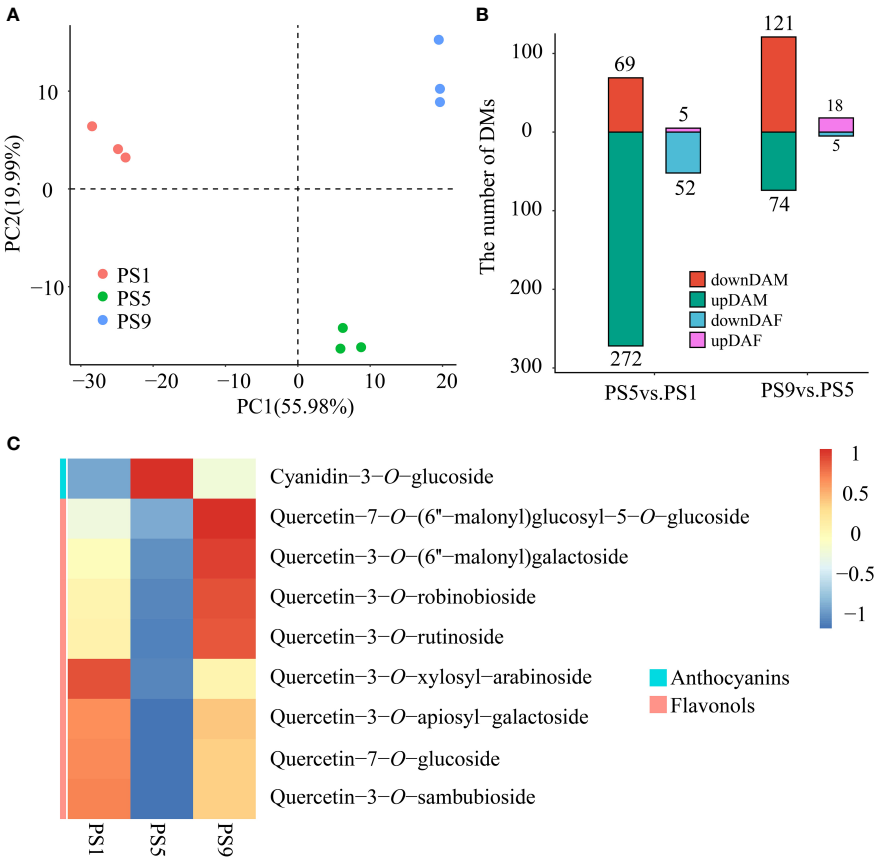

FIGURE 1
Metabolome differences in red apple fruits at three different ripening stages. **(A)** PCA analysis of red apple fruit metabolome data at PS1, PS5 and PS9; **(B)** The numbers of differentially accumulated metabolites and flavonoids in two comparisons. DAM, differentially accumulated metabolites; DAF, differentially accumulated flavonoids; **(C)** Differential accumulation was commonly identified in comparisons of PS5_vs_PS1 and PS9_vs_PS5 of anthocyanins and flavonols.

(Kuromanin), increased in PS5 for 1.57- and 2.31-fold, respectively.

A total of 195 DAMs were identified in PS9_vs_PS5 (Comparison II), including 121 increased and 74 decreased (Table S5). There were more increased than decreased metabolites for DAMs belonging to phenolic acids (24 increased and 6 decreased), flavonoids (18 increased and 5 decreased), lipids (23 increased and 8 decreased), terpenoids (24 increased and 2 decreased) and lignans and coumarins (5 increased and 2 decreased). However, more metabolites were decreased than increased for DAMs belonging to amino acids and derivatives (6 increased and 19 decreased), organic acids (8 increased and 9 decreased), alkaloids (1 increased and 6 decreased), nucleotides and derivatives (4 increased and 7 decreased) and tannins (only 1 decreased).

For the DAMs belonging to amino acids and derivatives, organic acids, alkaloids, nucleotides and derivatives and tannins, the number of decreased DAMs was higher than that of the increased ones in both comparisons, suggesting that the accumulations of these kinds of metabolites mostly reduced as fruit ripened. In contrast, the number of the increased saccharides and alcohols related metabolites was both higher than that of the decreased ones, which is in consistent with the sugar accumulation during fruit ripening. Moreover, the numbers of increased DAMs belonging to phenolic acids, flavonoids, lipids, terpenoids, and lignans and coumarins were much lower than the that of the decreased ones in Comparison I, but much higher than the numbers of decreased ones in Comparison II, suggesting that the accumulation of these kinds of metabolites reduced in the early fruit development stages but increased in the late fruit ripening stages.

Interestingly, we found that in Comparison I, all differentially accumulated anthocyanins increased, while all differentially accumulated quercetins decreased (Table S4). In Comparison II, we found a decrease in all differentially accumulated anthocyanins (Table S6), and an increase in all quercetins except quercetin-3-*O*-rhamnosyl (1→2) arabinoside (Table S6). In both comparisons, Cyanidin-3-*O*-glucoside and

the eight quercetins were found to be DAMs, and showed completely opposite expression trends (Figure 1C). Therefore, we conclude that there is dynamic competition between anthocyanins and flavonols biosynthesis during red apple fruit development and ripening.

Comparative transcriptome analysis results

To further explore the molecular mechanisms regulating the dynamic of anthocyanins and flavonols, especially quercetins, during red apple fruit ripening, we performed RNA-seq analysis on red apple fruits at PS1, PS5 and PS9 stages. PCA analysis of transcriptome data showed that red apple fruits at the three ripening stages were well distinguished from each other (Figure 2A). The mapping ratios of all transcriptome data from the nine cDNA libraries against the reference genome were all above 79% (Table S7). By using |log2 (Fold change)| ≥ 1 and *q*-value ≤ 0.05 as criteria, we identified 8,089 differentially expressed genes (DEGs, 2,579 up-regulated and 5,510 down-regulated) in PS5_vs_PS1, and 11,681 DEGs (4,345 up-regulated and 7,336 down-regulated) in PS9_vs_PS5 (Figure 2B). Among them, 852 DEGs were up-regulated in PS5_vs_PS1 but down-regulated in PS9_vs_PS5 (Figure 2C; Table S8), which showed the same dynamic patterns as anthocyanins accumulation during fruit ripening. KEGG enrichment analysis showed that these 852 common DEGs were involved in phenylpropanoid biosynthesis, phenylalanine metabolism, flavonoid biosynthesis, flavone and flavonol biosynthesis and anthocyanin biosynthesis pathways (Figure 2D). Moreover, we identified 843 DEGs up-regulated in PS9_vs_PS5 but down-regulated in PS5_vs_PS1

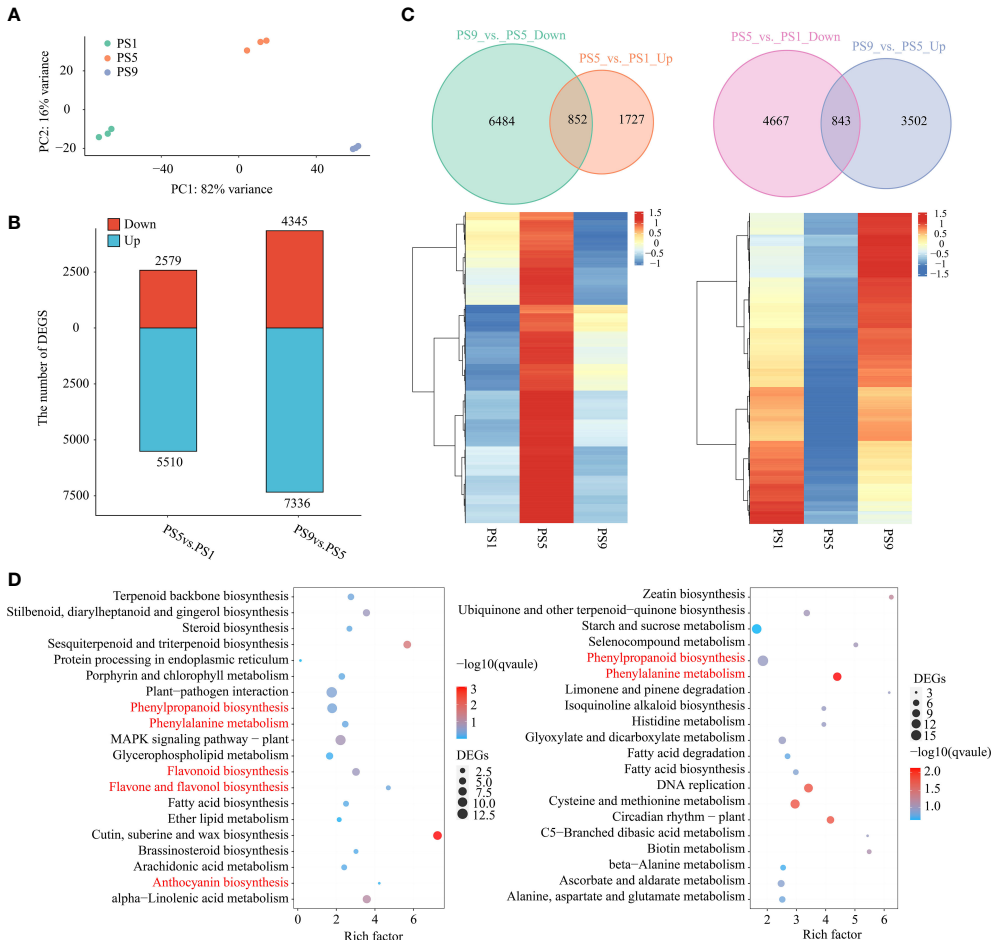

FIGURE 2
Comparative transcriptome analysis of red apple fruits at three different ripening stages. **(A)** PCA analysis result of red apple transcriptome data for PS1, PS5 and PS9; **(B)** Number of differentially expressed genes; **(C)** Venn diagram and heatmap of DEGs up-regulated in PS5_vs_PS1 but down-regulated in PS9_vs_PS5 (left) and DEGs down-regulated in PS5_vs_PS1 but up-regulated in PS9_vs_PS5 (right); **(D)** KEGG enrichment analysis of DEGs showing the same pattern of changes in anthocyanins (left) and flavonols (right) accumulations during fruit ripening.

(showing the same dynamic patterns as most flavonols, especially quercetins) (Figure 2C; Table S9). KEGG enrichment analysis showed that these genes were significantly enriched in phenylalanine metabolism, phenylpropanoid biosynthesis, etc. (Figure 2D). Among the 852 DEGs that were found to be up-regulated in PS5_vs_PS1 but down-regulated in PS9_vs_PS5 and the 843 DEGs up-regulated in PS9_vs_PS5 but down-regulated in PS5_vs_PS1, there were many flavonoid biosynthesis structural genes, including seven *PALs*, fifteen *4CLs*, two *CHSs*, four *CHIs*, three *F3Hs*, three *F3'5'Hs*, five *F3'Hs*, four *FLSs*, two *DFRs*, one *ANS*, three *LARs*, four *ANRs*, and two *UFGTs* (Figure S3). Interestingly, almost all the DEGs encoding enzymes catalyzing the reactions from dihydroflavonols to anthocyanidins, such as *F3'5'H*, *F3'H*, *DFR* and *ANS*, showed the lowest expression at PS9, whereas the two genes encoding FLS enzyme catalyzing the conversion of dihydroflavonols to flavonols showed the highest expression at PS9.

Quantitative real time PCR (qRT-PCR) results showed that all the expression patterns of our selected flavonoids biosynthetic structural genes were identical to our transcriptome data, suggesting that our transcriptome data are reliable. The lowest expression of *DFR* was also found at PS9, indicating that its low expression might be closely related to the anthocyanins reduction at this stage. The *FLS* gene, however, showed the lowest expression at PS5 but the highest expression at PS9 according to our transcriptome and qRT-PCR results, which was the same pattern as the change in flavonols content (Figure S4).

Chromatin accessibility dynamics in red apple fruits during ripening

ATAC-Seq was applied to investigate the chromatin accessibility changes during ripening in red apple (Table S10). PCA analysis of the ATAC-Seq data showed a clear distinction in chromatin accessibility among the three ripening stages in red apple fruits (Figure 3A). We identified 41,292 to 58,869 peaks in each ATAC-Seq library (Table S11; Figure S5). Relative location analysis of peaks showed that they were mainly distributed in distal intergenic region (75.78%), promoter (≤ 1 kb) region (12.83%) and promoter (1-2 kb) region (5.11%) (Figure 3B), with their distributions peaked around the TSSs (Figure 3C). By using FDR < 0.05 and FC > 1.5 or FC < -1.5 as criteria, we identified 908 up-regulated differential accessible regions (DARs) and 662 down-regulated DARs in PS5_vs_PS1, and 3,347 up-regulated and 816 down-regulated DARs in PS9_vs_PS5 (Figure 3D, Table S12).

To show the possible regulation of chromatin accessibility on the expression of genes related to anthocyanins and flavonols biosynthesis, we further focused on DARs showing opposite patterns of change between PS5_vs_PS1 and PS9_vs_PS5. In total, we identified 128 DARs up-regulated in the former comparison but down-regulated in the latter one (consistent with the pattern of change for differentially accumulated anthocyanins) (Figure 3E, Table S13), and 364 DARs up-regulated in the later comparison but down-regulated in the former one (consistent with the pattern of change for differentially accumulated quercetins) (Figure 3E, Table S14). The MYB-bHLH-WD40 (MBW) regulatory complex has been frequently discovered to function in regulating flavonoids biosynthesis (Zhao et al., 2019). Among the DARs up-regulated in PS5_vs_PS1 and down-regulated in PS9_vs_PS5, we identified two *MYB* genes (C1H46_025763 and C1H46_027060) and one *bHLH* gene (C1H46_000912) (Figure S6A). Moreover, ten *MYB* genes, eleven *bHLH* genes and one *WD40* gene were found to be down-regulated in the DARs of PS5_vs_PS1 and up-regulated in PS9_vs_PS5 (Figure S6B). Interestingly, two *bHLH* genes (C1H46_035986 and C1H46_021331) are identified in the common DARs. A motif enrichment analysis using HOMER showed that MYB-related motifs were significantly enriched in the DARs with the same change pattern as the differentially accumulated anthocyanins (Figure 3F, Table S15), while bZIP-related motifs were significantly enriched in the DARs with the same change pattern as differentially accumulated flavonols (Figure 3F, Table S16).

To further reveal the potential regulatory roles of TFs on the expression of genes related to anthocyanins and flavonols biosynthesis, PlantTFDB was applied to predict the genes encoding TFs in the above common DEGs. The results showed that among the 852 common DEGs that were up-regulated in PS5_vs_PS1 but down-regulated in PS9_vs_PS5, genes encoding MYB, ERF, WRKY, bHLH and NAC accounted for more than 10% of all TF genes, with the percentages of 14.29%, 14.29%, 14.29%, 13.27% and 12.24%, respectively (Figure 4A; Table S17). In contrast, among the 843 common DEGs up-regulated in PS9_vs_PS5 but down-regulated in PS5_vs_PS1, genes encoding TF family proteins such as MYB, ERF, TCP, bZIP, Dof, bHLH and ZF-LD accounted for a larger proportion of all TF-encoding DEGs, accounting for 15.38%, 9.62%, 9.62%, 7.69%, 7.69%, 5.77% and 5.77%, respectively (Figure 4A; Table S18).

By integrating the results of metabolome and motif enrichment analysis, it was predicted that TF MYBs have many functions and different MYB members play various roles in regulating both anthocyanins and flavonols biosynthesis, while bZIP transcription factors might play important roles in regulating flavonols biosynthesis during fruit ripening in red apple. Among these *MYB* and *bZIP* genes, four *bZIPs* and 14 *MYBs* showed significant positive correlations with anthocyanins and quercetins contents, respectively (Figure 4B; Table 1), and they could be considered as hub genes regulating the dynamics of anthocyanins and quercetins, respectively. Among these *bZIP* and *MYB* genes, some of their homologous

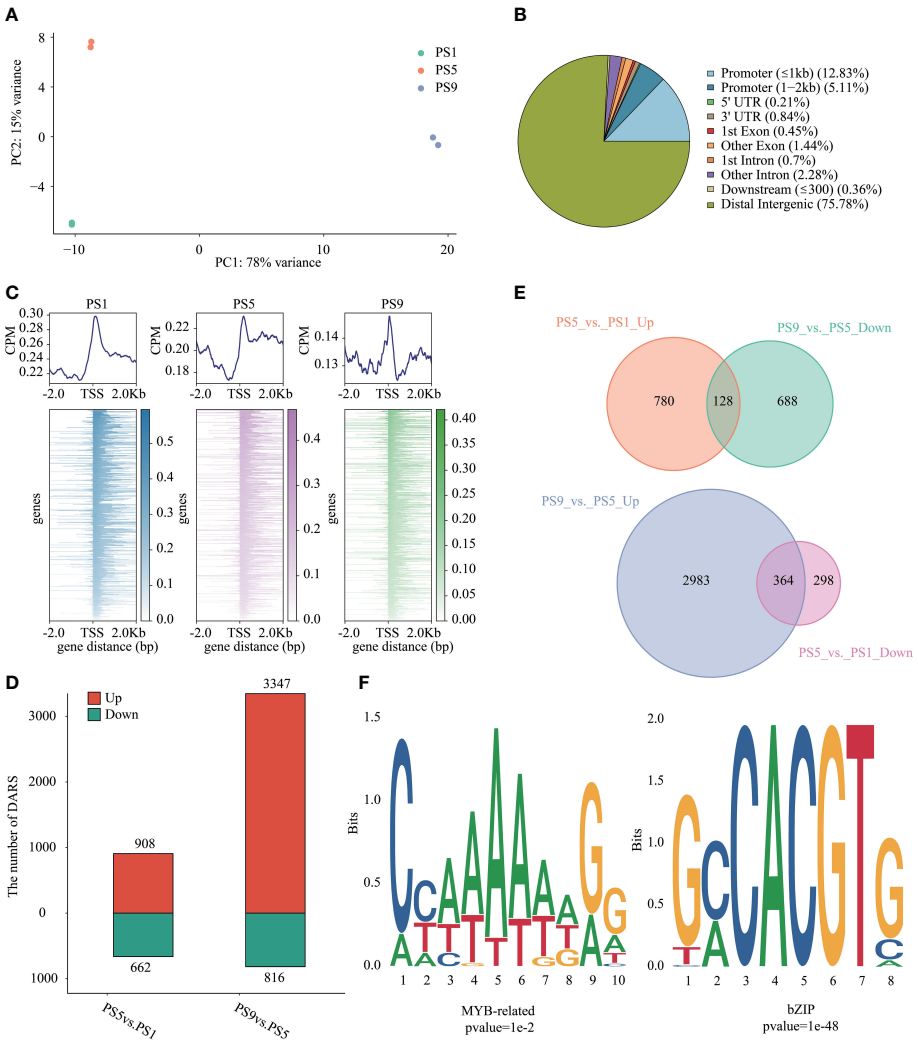

FIGURE 3
Chromatin accessibility features of red apple fruit during ripening. **(A)** PCA analysis result of red apple ATAC-Seq data at PS1, PS5 and PS9; **(B)** Relative location of the identified peaks in different gene regions; **(C)** Relative location of peaks to red apple genes in the upstream of 2 Kb and downstream of 2 Kb in the TSSs region; **(D)** Numbers of DARs in different comparisons; **(E)** Venn diagrams of DARs up-regulated in PS5_vs_PS1 but down-regulated in PS9_vs_PS5 (top) and DARs down-regulated in PS5_vs_PS1 but up-regulated in PS9_vs_PS5 (bottom); **(F)** Motif enrichment analysis results of MYB related motifs in DARs up-regulated in PS5_vs_PS1 but down-regulated in PS9_vs_PS5 and bZIP motifs in DARs up-regulated in PS9_vs_PS5 but down-regulated in PS5_vs_PS1.

genes, including Arabidopsis *vip1*, pear *MYB10*, apple *MYB24-like* and *MYB11* have been reported to be associated with anthocyanin biosynthesis (Stracke et al., 2001; Sun et al., 2019; Wang et al., 2019a; Li et al., 2020b; Land et al., 2021). Notably, the chromatin accessibility in the promoter region of one *bZIP* gene (C1H46_010137) was found to be positively correlated with its gene expression level at the three stages (Figure 4C; Tables S19, S20), and its function in the competition for anthocyanins and flavonols biosynthesis needs to be further explored in future studies. Moreover, our qRT-PCR results showed that the expression patterns of the two selected *MYB* and three *bZIP* genes were identical to our transcriptome data (Figure S4), which well supported our transcriptome data and indicated that these TFs might contribute greatly to the competition between anthocyanins and flavonols biosynthesis.

Discussion

Fruit ripening is a complex process accompanied by extensive metabolites and global changes in gene expression controlled by a variety of factors, including developmental and environmental factors. These changes varied greatly in different plant species and different cultivars of the same plant species.

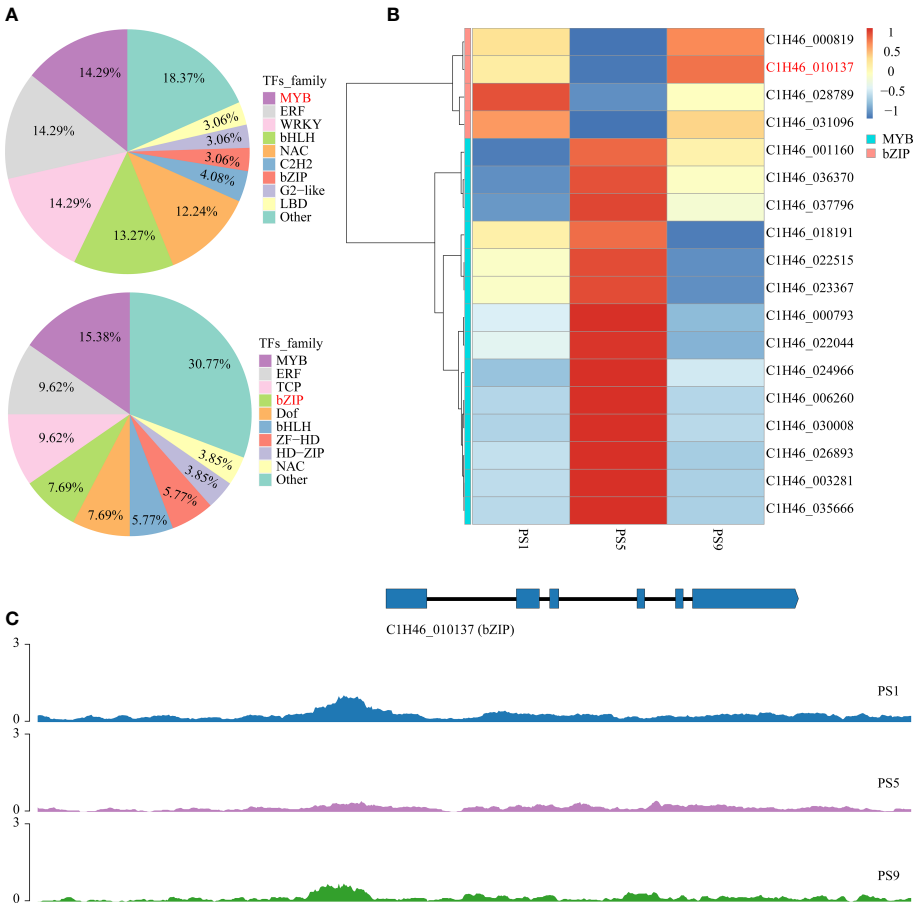

FIGURE 4
Candidate TF genes that play roles in the competition for anthocyanins and quercetins biosynthesis. **(A)** Frequencies of the transcription factor gene families in all the differentially expressed transcription factor genes; **(B)** Heatmap of differentially expressed *MYB* and *bZIP* genes that showed adverse change patterns in comparison PS5_vs_PS1 and comparison PS9_vs_PS5. **(C)** Chromatin accessibilities of a *bZIP* gene (C1H46_010137) at three different ripening stages.

Malus spp. is rich in flavonoids, especially in their flowers and fruits. In this study, we investigated the metabolome, transcriptome and chromatin accessibility changes of apple 'Hongmantang' with purple-red flower and blood-red flesh during fruit ripening, through integrative analyses of the datasets of UPLC-MS/MS-based widely targeted metabolome, RNA-Seq and ATAC-Seq from three ripening stages (PS1, PS5 and PS9).

Changes in the accumulation of different kinds of metabolites varied markedly during red apple fruit ripening

In the study by Xu et al. (2020), more than half of the metabolites identified in apple (*M. domestica*) fruits showed high accumulation at early ripening stages. In our present study, we found that most metabolites belonging to amino acids and derivatives, organic acids, nucleotides and derivatives and tannins accumulated the highest in red apple fruits at PS1, and the numbers of decreased DAMs were both higher than that of the increased DAMs in the two comparisons, suggesting that the accumulations of these kinds of metabolites mostly reduced as fruit ripened. However, the numbers of the increased saccharides and alcohols related metabolites were both higher than the decreased ones, which is in consistent with the sugar accumulation during fruit ripening (Xu et al., 2020). Moreover, the numbers of increased DAMs belonging to phenolic acids, flavonoids, lipids, terpenoids, lignans and coumarins were much lower than the decreased ones in the comparison PS5_vs_PS1, but were much higher than the increased ones in the comparison PS9_vs_PS5, suggesting that the accumulations of these kinds of metabolites are associated with the red apple ripening process.

Given that they share the same biosynthesis substrates, competition occurred between anthocyanins and flavonols biosynthesis pathways in many plants (Luo et al., 2016; Zhong et al., 2020; Wong et al., 2022). For example, a comparison of anthocyanins and flavonols contents in the petals of ten *Rhododendron* species revealed that species with low anthocyanin contents had high flavonols (Liu et al., 2016); in *Malus*, competition between anthocyanins and kaempferol glycosides was found to be related to pollen tube growth and seed set (Chen et al., 2021); in bilberry, procyanidins and quercetins were identified as the major flavonoids in the early fruit ripening stage, but anthocyanins accounted for the largest fraction in the later ripening stages (Jaakola et al., 2002). In our present study, we found that many flavonoids were identified as DAMs during red apple fruit ripening. Moreover, in both PS5_vs_PS1 and PS9_vs_PS5 comparisons, cyanidin-3-*O*-glucoside and eight quercetins were found to be DAMs, but showed completely opposite accumulation trends. Therefore, it is hypothesized that there is a dynamic competition between anthocyanins and flavonols biosynthesis in red apple fruits during fruit development and ripening.

The differential expression of structural genes for flavonoids biosynthesis contributed greatly to the accumulations of different kinds of flavonoids

The accumulations of anthocyanins and flavonols largely contribute to the color changes during fruit ripening (Jaakola et al., 2002). Dihydroflavonols, the intermediates and branch point of the anthocyanins and flavonols biosynthetic pathways, are required for anthocyanins and flavonols productions and as substrates for their competition (Davies et al., 2003). This competitive process is controlled by many biosynthetic genes, especially *DFRs* and *FLSs* (Chen et al., 2021). In tomato, the *anthocyanin without* mutant, harboring a defect in *DFR*, displayed elevated flavonols and anthocyanins deficiency, and another mutant, *anthocyanin reduced* (*are*) has been reported to be caused by the mutation in a *FLS*, a gene encoding an enzyme catalyzing the first step of flavonol biosynthesis (Maloney et al., 2014). By using the white-flowered, flavonol accumulating Mitchell line of petunia as material, Davies et al. (2003) found that overexpression both of 35SCaMV-*DFR* sense and/or *FLS* antisense transgene led to the anthocyanins production and resulted in a pink-flowered phenotype. Constitutive overexpression of *FLS* genes from *Rosa rugosa*, *Prunus persica*, and *Petunia hybrida* in tobacco all resulted in white flowers, while the heterologous overexpression of *DFR* genes resulted in increased anthocyanins accumulations and redder flowers (Luo et al., 2016; Wong et al., 2022). Liu et al. (2019b) reported that heterologous expression of the *Muscari aucheri MaFLS* gene in tobacco increased *NtFLS* expression, but inhibited the expression of tobacco anthocyanins biosynthesis genes, such as *NtDFR*, *NtANS* and *NtAN2*, and reduced the pigmentation of tobacco petals. Similarly, Park et al. (2020) reported that the overexpression of the onion *FLS* gene (*AcFLS-HRB*) increased the flavonols contents in tobacco petals but decreased the anthocyanins accumulation and produced lighter-pink flowers. In our study, almost all the DEGs encoding enzymes that catalyze the reactions from dihydroflavonols to anthocyanidins were least expressed at PS9, which is in consistent with the relatively low accumulation of anthocyanins in red apple fruits at this stage. Moreover, two red apple *FLS* genes had the highest expression at PS9, which well explains the high accumulation of flavonols in red apple fruit at the late stage. It is therefore concluded that the differential expression of these structural genes contributes greatly to the accumulations of different kinds of flavonoids, and that altering their expression by genetic methods may have great potential for balancing anthocyanins and flavonols production (Davies et al., 2003).

MYB and bZIP transcription factors played dominant regulatory roles in balancing the biosynthesis of anthocyanins and flavonols

In addition to structural genes, the biosynthesis of flavonoids is also controlled by many TFs (Martins et al., 2013; Zhang et al., 2021). The regulatory roles of MBW complex (consisted of MYB, bHLH and WD40 TFs) in flavonoid biosynthesis are well known (Zhao et al., 2019). Consistently, we identified many *MBW* genes, especially *MYB* and *bHLH* genes, as DEGs during ripening in red apple, indicating that these TFs play important roles in flavonoid biosynthesis in red apple. Moreover, we identified more than twenty *MBW* genes in the DARs that showed opposite change patterns between PS5_vs_PS1 and PS9_vs_PS5 comparisons. For example, the mutant of Arabidopsis *vip1*, a homologous gene of the *bZIP* (C1H46_000819), showed much less anthocyanin accumulation under phosphate-limiting conditions (Land et al., 2021); the pear *MYB10*, a homologous gene of the red apple *MYB* (C1H46_023367) has been proved to play roles in regulating anthocyanin biosynthesis and transport in red-skinned pears (Li et al., 2020); and the apple *MYB24-like* (homologous to red apple *MYB* (C1H46_030008)) and *MYB11* (homologous to red apple *MYB* (C1H46_01819)) genes, were both proved to be involved in flavonoids biosynthesis (Sun et al., 2019; Wang et al., 2019a). As one of the most important TFs regulating the flavonoids synthesis, the regulatory roles of MYBs in both flavonols and anthocyanins biosynthesis have been continuously demonstrated in many fruit trees, such as apple (Takos et al., 2006; An et al., 2018a; An et al., 2018b; Wang et al., 2019a; Wang et al., 2019b; Jia et al., 2020; Xu H. et al., 2020), pear (Li et al., 2020a; Li et al., 2020), grape (Deluc et al., 2006), kiwifruit (Wang

TABLE 1 The identified differentially expressed *bZIP* and *MYB* genes that showed opposite change patterns between PS5_vs_PS1 and PS9_vs_PS5 comparisons.

TF family	Gene ID	Tophit homologous genes/similarity	Homologous Arabidopsis gene/ similarity	References
bZIP	C1H46_000819	apple VIP1-like (XM_008340896)/55.17%	AT1G43700 (SUE3,VIP1)/43.81%	Land et al., 2021
	C1H46_010137	apple transcriptional activator hacA-like (XM_008369083.3)/66.95%	AT1G19490 (bZIP62)/49.27%	
	C1H46_028789	apple basic leucine zipper 43-like (XM_008395159)/ 66.88%	AT5G60830 (bZIP70)/46.73%	
	C1H46_031096	apple transcriptional activator hacA-like (XM_017331100)/54.57%	AT1G19490 (bZIP62)/45.14%	
MYB	C1H46_000793	apple MYB30-like (XM_008366038.3)/71.03%	AT2G31180 (MYB14)/56.61%	
	C1H46_001160	apple MYB55 (MG099798)/86.61%	AT5G57620 (MYB36)/53.73%	
	C1H46_003281	apple MYB93-like (XM_008347508)/81.80%	AT1G34670 (MYB93)/57.22%	
	C1H46_022044	apple MYB25 (NM_001293983.1)/67.28%	AT2G31180 (MYB14)/51.8%	
	C1H46_023367	pear MYB10 (KT601121.1)/96.33%	AT1G56650 (MYB7)/52.62%	Li X. et al., 2020
	C1H46_024966	apple MYB93-like (XM_008385715.3)/76.39%	AT1G34670 (MYB93)/58.06%	
	C1H46_026893	apple MYB24-like (XM_029096516.1)/55.08%	AT4G13480 (MYB79)/51.7%	Wang et al., 2019a
	C1H46_030008	apple MYBR24 (MG099810.1)/89.46%	AT2G38090/61.65%	
	C1H46_036370	apple WER-like (XM_008341803.3)/69.74%	AT5G40330 (MYB23)/54.46%	
	C1H46_037796	apple MYB8-like (XM_008347850.3)/84.64%	AT3G12720 (MYB67,ATY53)/49.31%	
	C1H46_018191	apple MYB11 (NM_001294029.1)/50.48%	AT5G35550 (MYB123)/36.27%	Stracke et al., 2001; Sun set al., 2019
	C1H46_022515	apple ETC1 (XM_008347609.3)/31.30%	AT4G01060 (ETC3)/51.01%	
	C1H46_006260	apple MYB42 (MG099785.1)/64.68%	AT4G21440 (MYB102)/40.23%	
	C1H46_035666	apple MYB42 (MG099785.1)/60.09%	AT3G12720 (MYB67,ATY53)/26.7%	

et al., 2019; Li et al., 2020a) and blueberry (Han et al., 2021) and so on. These reports showed that MYBs can be extensively involved in regulating flavonoids biosynthesis by interacting with some other TFs and with structural genes of flavonoids biosynthesis, thus affecting the color formation and development of plant organs such as leaves, petals and fruits.

Moreover, there are evidences that MYBs paly diverse roles in regulating flavonols and anthocyanins biosynthesis. For example, overexpression of apple *MdMYB10* gene increased the anthocyanins accumulation but decreased the kaempferol 3-*O*-glycosides contents in flowers (Chen et al., 2021). Overexpression of a *Gerbera hybrida* R2R3-MYB transcription factor gene (*GhMYB1a*) resulted in decreased anthocyanins but increased flavonols accumulations in both gerbera and tobacco (Zhong et al., 2020). In our study, genes encoding MYB transcription factors were found to account for the largest fraction of differentially expressed *TFs*, which showed positive or negative expression patterns with the accumulations of anthocyanins and flavonols. Furthermore, ATAC-Seq analysis revealed that MYB-related motifs were significantly enriched in DARs, with the same change pattern as anthocyanins, which again indicates that MYBs contributed greatly to the regulation of both anthocyanins and flavonols biosynthesis in red apple.

Some other TFs also contribute greatly to the biosynthesis of flavonoids in plant, mainly through interacting with MYBs. Similarly, in our study, we also identified many other *TF* genes that showed positive or negative expression patterns with anthocyanins and flavonols accumulations, such as *ERFs*, *bHLHs*, *WRKYs*, *NACs*, *bZIPs*, *TCPs* and so on. And there were many evidences for the roles of these TFs in flavonoids biosynthesis (An et al., 2018c; An et al., 2020; Li C. et al., 2020; Li et al., 2020b; Ma et al., 2021; Zhang et al., 2021; Tu et al., 2022). Notably, bZIP-related motifs were identified to be significantly enriched in DARs that showed the same change pattern with differentially accumulated anthocyanins, suggesting that such TFs also play a major role in regulating flavonoids biosynthesis in red apple. In consistent with our study, numerous evidences demonstrate that the combinatorial action of bZIP and MYB in controlling the flavonoids biosynthesis in many plants (Stracke et al., 2010; Shin et al., 2013; Zhao et al., 2021). In Arabidopsis, bZIP TFs were shown to be functional in promoting anthocyanins accumulation by interacting with MYBL2 (Nguyen et al., 2015), PFG1/MYB12 (Stracke et al., 2010) and MYB75 (Shin et al., 2013) TFs and anthocyanin biosynthetic genes. In soybean, GmMYB and GmbZIP5 interact synergistically in controlling flavonoids biosynthesis. In tea plants, the CsbZIP1-CsMYB12 interaction mediates flavonols production *via* a coordinated activator-repressor network (Zhao et al., 2021).

Notably, most of the *bZIP* family genes reported to be involved in the regulation of anthocyanins biosynthesis were

identified as positive regulators of anthocyanins biosynthesis (Han et al., 2021; Tu et al., 2022), which is also consistent with our results. Arabidopsis HY5 promotes anthocyanin accumulation by upregulating the expression of the *DFR* gene (Zhang et al., 2011). Tomato HY5 has been reported to be functional in mediating the CRY1a-induced anthocyanins biosynthesis (Liu et al., 2018; Qiu et al., 2019), and *SlHY5* frameshift mutation showed decreased anthocyanin accumulation (Qiu et al., 2019). Soybean bZIP TF G/HBF-1 plays a key role in increasing phytoalexin accumulation by binding to the promoter of *CHS* gene (Dröge-Laser et al., 1997). The pear bZIP transcription factor PybZIPa has the ability to bind to the promoter of *PyUFGT* and functions in promoting the light-induced anthocyanin accumulation (Liu et al., 2019a). Grapevine VvHY5 promotes flavonol biosynthesis by activating the expression of *FLS* (Loyola et al., 2016); another grapevine bZIP, VvibZIPC22, can promote the accumulation of several kinds of flavonoids by regulating the expression of the *CHS* and *FLS* genes; and VvHY5 promotes flavonol biosynthesis by activating the expression of an *FLS* gene (Malacarne et al., 2016). In the study by Wang et al. (2022), two pomegranate *bZIP* genes, *PgbZIP16* and *PgbZIP34*, which are associated with anthocyanin biosynthesis, were expressed at much higher levels in red petals than in white petals, and their heterologous transient overexpression in tobacco leaves both resulted in increased anthocyanin accumulation. In apple, An et al. (2018d) reported that the ABA inducible MdbZIP44 functioned in the ABA-induced anthocyanin accumulation by enhancing the binding activity of MdMYB1 to the promoters of anthocyanin biosynthetic genes. All these reports suggest that the *bZIP* TFs identified in our present study might play important roles in regulating the biosynthesis of flavonoids in red apple.

Conclusions

In summary, through combined analyses of metabolome, transcriptome and chromatin accessibility datasets, we investigated the molecular changes in red apple 'Hongmantang' fruits at three ripening stages (PS1, PS5 and PS9) (Figure 5). Metabolic analysis showed that most of the metabolites belonging to amino acids and derivatives, organic acids, nucleotides and their derivatives, and tannins decreased, while most metabolites belonging to saccharides and alcohols, vitamins and stilbene increased with fruit ripening. Notably, a dynamic competition between anthocyanins and flavonols biosynthesis was found. The differential expression of

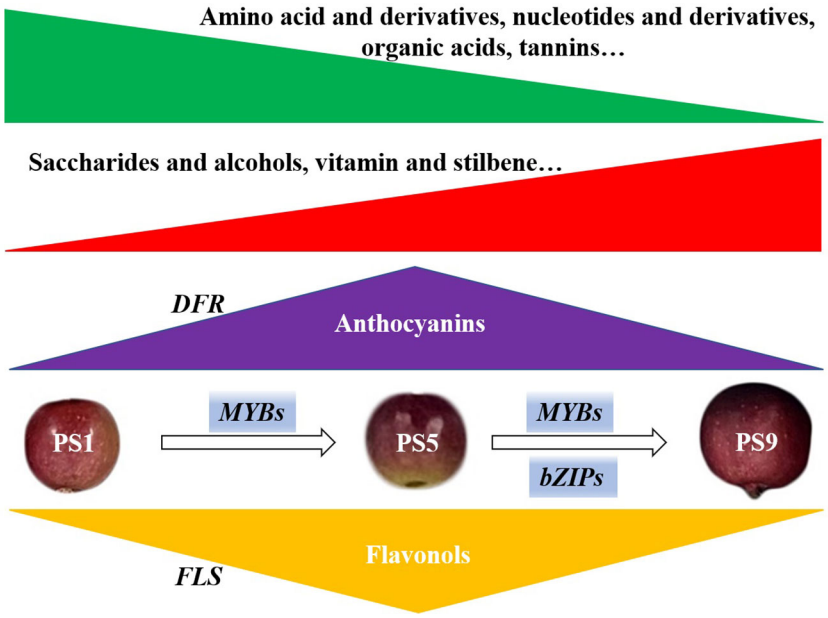

FIGURE 5
Schematic diagram of the molecular changes in red apple fruits during ripening. The green and red triangle represent the decreased and increased change pattern of metabolites. The accumulations of metabolites mostly belonging to amino acids and derivatives, organic acids, nucleotides and derivatives, and tannins reduced with fruit ripening, while the accumulations of metabolites mostly belonging to saccharides and alcohols, vitamins and stilbene increased with fruit ripening. The accumulation of anthocyanins peaked at PS5 and decreased at PS9. However, the flavonols accumulated least at PS5 but increased at PS9. The differential expression of *DFRs* and *FLSs*, functioned greatly to the accumulations of anthocyanins and flavonols, respectively. Changes in chromatin accessibility and expression of *MYBs* and *bZIPs* suggest that they play dominant regulatory roles in the competition for anthocyanins and flavonols biosynthesis.

structural genes for flavonoids biosynthesis, such as *FLSs* and *DFRs*, played a major role in the accumulations of the two kinds of flavonoids. Moreover, chromatin accessibility and changes in gene expression of *MYB* and *bZIP* genes were predicted to play dominant regulatory roles in balancing the anthocyanins and flavonols biosynthesis.

Data availability statement

The original contributions presented in the study are publicly available. This data can be found here: NCBI, PRJNA860789 & PRJNA861071.

Author contributions

JZ, PL and CC conceived and designed the experiments. CC, ZG, HL, JZ and PL wrote the original draft. CC, ZG, HL, XM, PW, SZ, TY, HC and QW performed the experiments. CC, ZG, HL and PL analyzed the results. CC, HL, XM, PL and JZ reviewed and edited the manuscript. All authors read and approved the final manuscript. The authors have no conflict of interest to declare.

Funding

This work was supported by the National Key Research and Development Program of China (2018YFD1000200), the earmarked fund for Modern Agro-industry Technology Research System of Shanxi Province, the Reward Fund for PhDs and Postdoctors of Shanxi Province (SXBYKY2022004), the Fund for High-level Talents of Shanxi Agricultural University (2021XG010).

Conflict of interest

The authors declare that the research was conducted in the absence of any commercial or financial relationships that could be construed as a potential conflict of interest.

Publisher's note

Supplementary material

The Supplementary Material for this article can be found online at: https://www.frontiersin.org/articles/10.3389/fpls.2022.975356/full#supplementary-material

SUPPLEMENTARY FIGURE 1
Changes in phenotype **(A)** and anthocyanin accumulation **(B)** of red apple during fruit ripening. PS1 to P10 represent fruits collected at 7, 9, 11, 13, 15, 17, 19, 21, 23 and 25 weeks post flowering, respectively. There were two anthocyanins accumulation peaks in red apple fruits during ripening, i.e., at PS5 (15 weeks post flowering) and PS9 (23 weeks post flowering), respectively.

SUPPLEMENTARY FIGURE 2
Heatmap of clustering of metabolites in red apple fruits at three ripening stages. PS1, PS5 and P9 represent fruits collected at 7, 15 and 23 weeks post flowering, respectively. For each stage, three replicates were performed. Red and green colors represent high and low accumulations, respectively.

SUPPLEMENTARY FIGURE 3
Differentially expressed flavonoids biosynthesis-related genes in red apple fruits at different ripening stages. PAL, phenylalanine ammonia-lyase; 4CL, 4-coumarate-CoA ligase; CHS, chalcone synthase; CHI, Chalcone isomerase; F3H, flavonone-3-hydroxylase; F3'H, flavonoid-3'-hydroxylase; F3'5'H, flavonoid-3'-5'-hydroxylase; FLS, flavonol synthase; DFR, dihydroflavonol reductase; ANS, anthocyanidin synthase; LAR, leucocyanidin reductase; ANR, anthocyanidin reductase; UFGT, anthocyanidin 3-*O*-glucosyltransferase; PA, proanthocyanidins. Red and blue colors represent high expression levels of genes.

SUPPLEMENTARY FIGURE 4
Quantitative real time PCR (qRT-PCR) analysis of some differentially expressed flavonoids biosynthetic structural genes and transcription factor genes. C1H46_001201: PAL (phenylalanine ammonia-lyase); C1H46_013998: 4CL (4-coumarate-CoA ligase); C1H46_010805: CHS (chalcone synthase); C1H46_009496: CHI (Chalcone isomerase); C1H46_033494: F3H (flavonone-3-hydroxylase); C1H46_012818: F3'H (flavonoid-3'-5'-hydroxylase); C1H46_020507: DFR (dihydroflavonol reductase); C1H46_005520: FLS (flavonol synthase); C1H46_043502: UFGT (anthocyanidin 3-O-glucosyltransferase); C1H46_023367 and C1H46_018191: MYB genes; C1H46_000819, C1H46_010137 and C1H46_028789: bZIP genes. The bar plots represent the relative expression levels of genes according to qRT-PCR analysis. The triangles with dashed lines represent the average FPKM values of the genes.

SUPPLEMENTARY FIGURE 5
Insert size distribution, euclidean distance and venn diagrams of the ATAC-Seq data for fruits at three different ripening stages. For each stage of fruits, two biological replicates were performed.

SUPPLEMENTARY FIGURE 6
Heatmap of the *MBW* genes identified in differential accessible regions (DARs) showing opposite change pattern in the comparisons of PS5_vs_PS1 and PS9_vs_PS5. A: The *MBW* genes identified in DARs up-regulated in PS5_vs_PS1 and down-regulated in PS9_vs_PS5. B: The *MBW* genes identified in DARs down-regulated in PS5_vs_PS1 and up-regulated in PS9_vs_PS5, the two *bHLH* genes in red were identified in the common DARs.

References

An, J. P., An, X. H., Yao, J. F., Wang, X. N., You, C. X., Wang, X. F., et al. (2018a). BTB protein MdBT2 inhibits anthocyanin and proanthocyanidin biosynthesis by triggering MdMYB9 degradation in apple. *Tree Physiol.* 38 (10), 1578–1587. doi: 10.1093/treephys/tpy063

An, J. P., Li, R., Qu, F. J., You, C. X., Wang, X. F., and Hao, Y. J. (2018b). R2R3-MYB transcription factor MdMYB23 is involved in the cold tolerance and proanthocyanidin accumulation in apple. *Plant J.* 96 (3), 562–577. doi: 10.1111/tpj.14050

An, J. P., Wang, X. F., Li, Y. Y., Song, L. Q., Zhao, L. L., You, C. X., et al. (2018c). EIN3-LIKE1, MYB1, and ethylene response factor 3 act in a regulatory loop that synergistically modulates ethylene biosynthesis and anthocyanin accumulation. *Plant Physiol.* 178 (2), 808–823. doi: 10.1104/PP.18.00068

An, J. P., Yao, J. F., Xu, R. R., You, C. X., Wang, X. F., and Hao, Y. J. (2018d). Apple bZIP transcription factor MdbZIP44 regulates abscisic acid-promoted anthocyanin accumulation. *Plant Cell Environ.* 41 (11), 2678–2692. doi: 10.1111/pce.13393

An, J. P., Zhang, X. W., Bi, S. Q., You, C. X., Wang, X. F., and Hao, Y. J. (2020). The ERF transcription factor MdERF38 promotes drought stress-induced anthocyanin biosynthesis in apple. *Plant J.* 101 (3), 573–589. doi: 10.1111/tpj.14555

Buenrostro, J. D., Giresi, P. G., Zaba, L. C., Chang, H. Y., and Greenleaf, W. J. (2013). Transposition of native chromatin for fast and sensitive epigenomic profiling of open chromatin, DNA-binding proteins and nucleosome position. *Nat. Methods*. 10 (12), 1213–1218. doi: 10.1038/nmeth.2688

Chen, W., Gong, L., Guo, Z., Wang, W., Zhang, H., Liu, X., et al. (2013). A novel integrated method for large-scale detection, identification, and quantification of widely targeted metabolites: Application in the study of rice metabolomics. *Mol. Plant*. 6 (6), 1769–1780. doi: 10.1093/mp/sst080

Chen, W., Xiao, Z., Wang, Y., Wang, J., Zhai, R., Lin-Wang, K., et al. (2021). Competition between anthocyanin and kaempferol glycosides biosynthesis affects pollen tube growth and seed set of *Malus*. *Horticult. Res.* 8 (1), 173. doi: 10.1038/s41438-021-00609-9

Corces, M. R., Trevino, A. E., Hamilton, E. G., Greenside, P. G., Sinnott-Armstrong, N. A., Vesuna, S., et al. (2017). An improved ATAC-seq protocol reduces background and enables interrogation of frozen tissues. *Nat. Methods*. 14 (10), 959–962. doi: 10.1038/nmeth.4396

Davies, K. M., Schwinn, K. E., Deroles, S. C., Manson, D. G., Lewis, D. H., Bloor, S. J., et al. (2003). Enhancing anthocyanin production by altering competition for substrate between flavonol synthase and dihydroflavonol 4-reductase. *Euphytica*. 131 (3), 259–268. doi: 10.1023/A:1024018729349

Deluc, L., Barrieu, F., Marchive, C., Lauvergeat, V., Decendit, A., Richard, T., et al. (2006). Characterization of a grapevine R2R3-MYB transcription factor that regulates the phenylpropanoid pathway. *Plant Physiol.* 140 (2), 499–511. doi: 10.1104/pp.105.067231

Dröge-Laser, W., Kaiser, A., Lindsay, W. P., Halkier, B. A., Loake, G. J., Doerner, P., et al. (1997). Rapid stimulation of a soybean protein-serine kinase that phosphorylates a novel bZIP DNA-binding protein, G/HBF-1, during the induction of early transcription-dependent defenses. *EMBO J.* 16 (4), 726–738. doi: 10.1093/emboj/16.4.726

Fu, L., Ding, Z., Tie, W., Yang, J., Yan, Y., and Hu, W. (2022). Integrated metabolomic and transcriptomic analyses reveal novel insights of anthocyanin biosynthesis on color formation in *Cassava tuberous* roots. *Front. Nutr.* 9. doi: 10.3389/fnut.2022.842693

Grandi, F. C., Modi, H., Kampman, L., and Corces, M. R. (2022). Chromatin accessibility profiling by ATAC-seq. *Nat. Protoc.* 17 (6), 1518–1552. doi: 10.1038/s41596-022-00692-9

Guo, Z., Hou, W., Fu, H., Zhang, J., Wang, P., Mu, X., et al. (2021). Changes of phenolic substances and antioxidant capacity during fruit development of different apple varieties. *Shandong Agric. Sci.* 53 (11), 35–44. doi: 10.14083/j.issn.1001-4942.2021.11.006

Gutierrez, E., Velasco, A. G., Antonio Lucas, J., Gutierrez-Mañero, F. J., and Ramos-Solano, B. (2017). The flavonol-anthocyanin pathway in blackberry and arabidopsis: State of the art. *Flavonoids From Biosynthesis to Hum. Health*. doi: 10.5772/67902

Han, T., Wu, W., and Li, W. (2021). Transcriptome analysis revealed the mechanism by which exogenous ABA increases anthocyanins in blueberry fruit during veraison. *Front. Plant Sci.* 12. doi: 10.3389/fpls.2021.758215

Han, H., Xu, F., Li, Y., Yu, L., Fu, M., Liao, Y., et al. (2021). Genome-wide characterization of *bZIP* gene family identifies potential members involved in flavonoids biosynthesis in *Ginkgo biloba* l. *Sci. Rep.* 11 (1), 23420. doi: 10.1038/s41598-021-02839-2

Huang, M., Zhang, L., Zhou, L., Yung, W. S., Wang, Z., Xiao, Z., et al. (2022). Identification of the accessible chromatin regions in six tissues in the soybean. *Genomics*. 114 (3), 110364. doi: 10.1016/j.ygeno.2022.110364

Jaakola, L., Määttä, K., Pirttilä, A. M., Törrönen, R., Kärenlampi, S., and Hohtola, A. (2002). Expression of genes involved in anthocyanin biosynthesis in relation to anthocyanin, proanthocyanidin, and flavonol levels during bilberry fruit development. *Plant Physiol.* 130 (2), 729–739. doi: 10.1104/pp.006957

Jia, D., Li, Z., Dang, Q., Shang, L., Shen, J., Leng, X., et al. (2020). Anthocyanin biosynthesis and methylation of the *MdMYB10* promoter are associated with the red blushed-skin mutant in the red striped-skin "changfu 2" apple. *J. Agric. Food Chem.* 68 (15), 4292–4304. doi: 10.1021/acs.jafc.9b07098

Jiang, S., Chen, M., He, N., Chen, X., Wang, N., Sun, Q., et al. (2019). MdGSTF6, activated by MdMYB1, plays an essential role in anthocyanin accumulation in apple. *Horticult. Res.* 6 (1), 40. doi: 10.1038/s41438-019-0118-6

Land, E. S., Cridland, C. A., Craige, B., Dye, A., Hildreth, S. B., Helm, R. F., et al. (2021). A role for inositol pyrophosphates in the metabolic adaptations to low phosphate in arabidopsis. *Metabolites*. 11, 601. doi: 10.3390/metabo11090601

Langmead, B., and Salzberg, S. L. (2012). Fast gapped-read alignment with bowtie 2. *Nat. Methods*. 9 (4), 357–359. doi: 10.1038/nmeth.1923

Lee, K. W., Kim, Y. J., Kim, D. O., Lee, H. J., and Lee, C. Y. (2003). Major phenolics in apple and their contribution to the total antioxidant capacity. *J. Agric. Food Chem.* 51 (22), 6516–6520. doi: 10.1021/jf034475w

Li, Y., Cui, W., Qi, X., Lin, M., Qiao, C., Zhong, Y., et al. (2020a). MicroRNA858 negatively regulates anthocyanin biosynthesis by repressing *AaMYBC1* expression in kiwifruit (*Actinidia arguta*). *Plant Sci.* 296, 110476. doi: 10.1016/j.plantsci.2020.110476

Li, H., Lv, Q., Liu, A., Wang, J., Sun, X., Deng, J., et al. (2022). Comparative metabolomics study of tartary (Fagopyrum tataricum (L.) gaertn) and common (Fagopyrum esculentum moench) buckwheat seeds. *Food Chem.* 371, 131125. doi: 10.1016/j.foodchem.2021.131125

Liu, C. C., Chi, C., Jin, L. J., Zhu, J., Yu, J. Q., and Zhou, Y. H. (2018). The bZIP transcription factor HY5 mediates CRY1a-induced anthocyanin biosynthesis in tomato. *Plant Cell Environ.* 41 (8), 1762–1775. doi: 10.1111/pce.13171

Liu, H., Su, B., Zhang, H., Gong, J., Zhang, B., Liu, Y., et al. (2019b). Identification and functional analysis of a *flavonol synthase* gene from grape hyacinth. *Molecules*. 24 (8), 1579. doi: 10.3390/molecules24081579

Liu, H., Su, J., Zhu, Y., Yao, G., Allan, A. C., Ampomah-Dwamena, C., et al. (2019a). The involvement of PybZIPa in light-induced anthocyanin accumulation *via* the activation of *PyUFGT* through binding to tandem G-boxes in its promoter. *Horticult. Res.* 6 (1), 134. doi: 10.1038/s41438-019-0217-4

Liu, L., Zhang, L. Y., Wang, S. L., and Niu, X. Y. (2016). Analysis of anthocyanins and flavonols in petals of 10 *Rhododendron* species from the sygera mountains in southeast Tibet. *Plant Physiol. Biochem.* 104, 250–256. doi: 10.1016/j.plaphy.2016.03.036

Li, C., Wu, J., Hu, K., Wei, S. W., Sun, H. Y., Hu, L. Y., et al. (2020). PyWRKY26 and PybHLH3 cotargeted the *PyMYB114* promoter to regulate anthocyanin biosynthesis and transport in red-skinned pears. *Horticult. Res.* 7 (1), 37. doi: 10.1038/s41438-020-0254-z

Li, X., Wu, T., Liu, H., Zhai, R., Wen, Y., Shi, Q., et al. (2020). REVEILLE transcription factors contribute to the nighttime accumulation of anthocyanins in 'red zaosu' (*Pyrus bretschneideri* rehd.) pear fruit skin. *Int. J. Mol. Sci.* 21 (5), 1634. doi: 10.3390/ijms21051634

Li, Y., Xu, P., Chen, G., Wu, J., Liu, Z., and Lian, H. (2020b). FvbHLH9 functions as a positive regulator of anthocyanin biosynthesis by forming a HY5-bHLH9 transcription complex in strawberry fruits. *Plant Cell Physiol.* 61 (4), 826–837. doi: 10.1093/pcp/pcaa010

Loyola, R., Herrera, D., Mas, A., Wong, D. C. J., Höll, J., Cavallini, E., et al. (2016). The photomorphogenic factors UV-b RECEPTOR 1, ELONGATED HYPOCOTYL 5, and HY5 HOMOLOGUE are part of the UV-b signalling pathway in grapevine and mediate flavonol accumulation in response to the environment. *J. Exp. Bot.* 67 (18), 5429–5445. doi: 10.1093/jxb/erw307

Luo, P., Ning, G., Wang, Z., Shen, Y., Jin, H., Li, P., et al. (2016). Disequilibrium of flavonol synthase and dihydroflavonol-4-reductase expression associated tightly to white vs. red color flower formation in plants. *Front. Plant Sci.* 6. doi: 10.3389/fpls.2015.01257

Malacarne, G., Coller, E., Czemmel, S., Vrhovsek, U., Engelen, K., Goremykin, V., et al (2016). The grapevine VvibZIPC22 transcription factor is involved in the regulation of flavonoid biosynthesis. *Journal of Experimental Botany*, 67(11):3509–3522. doi: 10.1093/jxb/erw181

Maloney, G. S., DiNapoli, K. T., and Muday, G. K. (2014). The anthocyanin reduced tomato mutant demonstrates the role of flavonols in tomato lateral root and root hair development. *Plant Physiol.* 166 (2), 614–631. doi: 10.1104/pp.114.240507

Martin, C. (2013). The interface between plant metabolic engineering and human health. *In Curr. Opin. Biotechnol.* 24 (2), 344–353. doi: 10.1016/j.copbio.2012.11.005

Martins, T. R., Berg, J. J., Blinka, S., Rausher, M. D., and Baum, D. A. (2013). Precise spatio-temporal regulation of the anthocyanin biosynthetic pathway leads to petal spot formation in *Clarkia gracilis* (Onagraceae). *New Phytol.* 197 (3), 958–969. doi: 10.1111/nph.12062

Ma, H., Yang, T., Li, Y., Zhang, J., Wu, T., Song, T., et al. (2021). The long noncoding RNA MdLNC499 bridges MdWRKY1 and MdERF109 function to regulate early-stage light-induced anthocyanin accumulation in apple fruit. *Plant Cell*. 33 (10), 3309–3330. doi: 10.1093/plcell/koab188

Nguyen, N. H., Jeong, C. Y., Kang, G. H., Yoo, S. D., Hong, S. W., and Lee, H. (2015). MYBD employed by HY5 increases anthocyanin accumulation *via* repression of MYBL2 in arabidopsis. *Plant J.* 84 (6), 1192–1205. doi: 10.1111/tpj.13077

Park, S., Kim, D. H., Yang, J. H., Lee, J. Y., and Lim, S. H. (2020). Increased flavonol levels in tobacco expressing *AcFLS* affect flower color and root growth. *Int. J. Mol. Sci.* 21 (3), 1011. doi: 10.3390/ijms21031011

Qiu, Z., Wang, H., Li, D., Yu, B., Hui, Q., Yan, S., et al. (2019). Identification of candidate HY5-dependent and -independent regulators of anthocyanin biosynthesis in tomato. *Plant Cell Physiol.* 60 (3), 643–656. doi: 10.1093/pcp/pcy236

Ren, C., Li, H., Wang, Z., Dai, Z., Lecourieux, F., Xin, H., et al. (2021). Characterization of chromatin accessibility and gene expression upon cold stress reveals that the RAV1 transcription factor functions in cold response in *Vitis amurensis*. *Plant Cell Physiol.* 62 (10), 1615–1629. doi: 10.1093/pcp/pcab115

Schwope, R., Magris, G., Miculan, M., Paparelli, E., Celii, M., Tocci, A., et al. (2021). Open chromatin in grapevine marks candidate CREs and with other chromatin features correlates with gene expression. *Plant J.* 107 (6), 1631–1647. doi: 10.1111/tpj.15404

Shin, D. H., Choi, M., Kim, K., Bang, G., Cho, M., Choi, S. B., et al. (2013). HY5 regulates anthocyanin biosynthesis by inducing the transcriptional activation of the MYB75/PAP1 transcription factor in arabidopsis. *FEBS Lett.* 587 (10), 1543–1547. doi: 10.1016/j.febslet.2013.03.037

Stracke, R., Favory, J. J., Gruber, H., Bartelniewoehner, L., Bartels, S., Binkert, M., et al. (2010). The arabidopsis bZIP transcription factor HY5 regulates expression of the *PFG1/MYB12* gene in response to light and ultraviolet-b radiation. *Plant Cell Environ.* 33 (1), 88–103. doi: 10.1111/j.1365-3040.2009.02061.x

Stracke, R., Werber, M., and Weisshaar, B. (2001). The R2R3-MYB gene family in *Arabidopsis thaliana*. *Curr. Opin. Plant Biol.* 4 (5), 447–456. doi: 10.1016/s1369-5266(00)00199-0

Sun, Q., Jiang, S., Zhang, T., Xu, H., Fang, H., Zhang, J., et al. (2019). Apple NAC transcription factor MdNAC52 regulates biosynthesis of anthocyanin and proanthocyanidin through MdMYB9 and MdMYB11. *Plant Sci.* 289, 110286. doi: 10.1016/j.plantsci.2019.110286

Takos, A. M., Jaffé, F. W., Jacob, S. R., Bogs, J., Robinson, S. P., and Walker, A. R. (2006). Light-induced expression of a *MYB* gene regulates anthocyanin biosynthesis in red apples. *Plant Physiol.* 142 (3), 1216–1232. doi: 10.1104/pp.106.088104

Tu, M., Fang, J., Zhao, R., Liu, X., Yin, W., Wang, Y., et al. (2022). CRISPR/Cas9-mediated mutagenesis of *VvbZIP36* promotes anthocyanin accumulation in grapevine (*Vitis vinifera*). *Horticult. Res.* 9, uhac022. doi: 10.1093/hr/uhac022

Vrhovsek, U., Rigo, A., Tonon, D., and Mattivi, F. (2004). Quantitation of polyphenols in different apple varieties. *J. Agric. Food Chem.* 52 (21), 6532–6538. doi: 10.1021/jf049317z

Wang, Y., Liu, W., Jiang, H., Mao, Z., Wang, N., Jiang, S., et al. (2019a). The R2R3-MYB transcription factor MdMYB24-like is involved in methyl jasmonate-induced anthocyanin biosynthesis in apple. *Plant Physiol. Biochem.* 139, 273–282. doi: 10.1016/j.plaphy.2019.03.031

Wang, Y., Sun, J., Wang, N., Xu, H., Qu, C., Jiang, S., et al. (2019b). MdMYBL2 helps regulate cytokinin-induced anthocyanin biosynthesis in red-fleshed apple (*Malus sieversii* f. Niedzwetzkyana) callus. *Funct. Plant Biol.* 46 (2), 187–196. doi: 10.1071/FP17216

Wang, L., Tang, W., Hu, Y., Zhang, Y., Sun, J., Guo, X., et al. (2019). A MYB/bHLH complex regulates tissue-specific anthocyanin biosynthesis in the inner pericarp of red-centered kiwifruit *Actinidia chinensis* cv. *Hongyang Plant J.* 99 (2), 359–378. doi: 10.1111/tpj.14330

Wang, S., Zhang, X., Li, B., Zhao, X., Shen, Y., and Yuan, Z. (2022). Genome-wide identification and characterization of *bZIP* gene family and cloning of candidate genes for anthocyanin biosynthesis in pomegranate (*Punica granatum*). *BMC Plant Biol.* 22 (1), 170. doi: 10.1186/s12870-022-03560-6

Wong, D. C. J., Perkins, J., and Peakall, R. (2022). Anthocyanin and flavonol glycoside metabolic pathways underpin floral color mimicry and contrast in a sexually deceptive orchid. *Front. Plant Sci.* 13. doi: 10.3389/fpls.2022.860997

Xu, J., Yan, J., Li, W., Wang, Q., Wang, C., Guo, J., et al. (2020). Integrative analyses of widely targeted metabolic profiling and transcriptome data reveals molecular insight into metabolomic variations during apple (*Malus domestica*) fruit development and ripening. *Int. J. Mol. Sci.* 21 (13), 4797. doi: 10.3390/ijms21134797

Xu, H., Zou, Q., Yang, G., Jiang, S., Fang, H., Wang, Y., et al. (2020). MdMYB6 regulates anthocyanin formation in apple both through direct inhibition of the biosynthesis pathway and through substrate removal. *Horticult. Res.* 7 (1), 72. doi: 10.1038/s41438-020-0294-4

Yang, T., Gao, J., Wang, Q., Cai, H., Li, C., Du, X., et al. (2015). A new *Malus* ornamental variety 'Hongmantang'. *J. Fruit Sci.* 32 (4), 727–729. doi: 10.13925/j.cnki.gsxb.20150130

Yuan, H., Zeng, X., Shi, J., Xu, Q., Wang, Y., Jabu, D., et al. (2018). Time-course comparative metabolite profiling under osmotic stress in tolerant and sensitive tibetian hulless barley. *BioMed. Res. Int.* 2018, 9415409. doi: 10.1155/2018/9415409

Zhang, J., Xu, H., Wang, N., Jiang, S., Fang, H., Zhang, Z., et al. (2018). The ethylene response factor MdERF1B regulates anthocyanin and proanthocyanidin biosynthesis in apple. *Plant Mol. Biol.* 98 (3), 205–218. doi: 10.1007/s11103-018-0770-5

Zhang, Q., Wang, L., Liu, Z., Zhao, Z., Zhao, J., Wang, Z., et al. (2020). Transcriptome and metabolome profiling unveil the mechanisms of *Ziziphus jujuba* mill. peel coloration. *Food Chem.* 312, 125903. doi: 10.1016/j.foodchem.2019.125903

Zhang, Y., Liu, F., Wang, B., Wu, H., Wu, J., Liu, J., et al. (2021). Identification, characterization and expression analysis of anthocyanin biosynthesis-related *bHLH* genes in blueberry (*Vaccinium corymbosum* l.). *Int. J. Mol. Sci.* 22 (24), 13274. doi: 10.3390/ijms222413274

Zhang, Y., Zheng, S., Liu, Z., Wang, L. , and Bi, Y.(2011). Both HY5 and HYH are necessary regulators for low temperature-induced anthocyanin accumulation in Arabidopsis seedlings. *Journal of Plant Physiology*, 168(4):367–374. doi: 10.1016/j.jplph.2010.07.025

Zhao, M., Li, J., Zhu, L., Chang, P., Li, L., and Zhang, L. (2019). Identification and characterization of MYB-bHLH-WD40 regulatory complex members controlling anthocyanidin biosynthesis in blueberry fruits development. *Genes*. 10 (7), 496. doi: 10.3390/genes10070496

Zhao, X., Zeng, X., Lin, N., Yu, S., Fernie, A. R., and Zhao, J. (2021). CsbZIP1-CsMYB12 mediates the production of bitter-tasting flavonols in tea plants (*Camellia sinensis*) through a coordinated activator–repressor network. *Horticult. Res.* 8 (1), 110. doi: 10.1038/s41438-021-00545-8

Zhong, C., Tang, Y., Pang, B., Li, X., Yang, Y., Deng, J., et al. (2020). The R2R3-MYB transcription factor GhMYB1a regulates flavonol and anthocyanin accumulation in *Gerbera hybrida*. *Horticult. Res.* 7 (1), 78. doi: 10.1038/s41438-020-0296-2

frontiers | Frontiers in Plant Science

TYPE Original Research
PUBLISHED 13 October 2022
DOI 10.3389/fpls.2022.1021088

OPEN ACCESS

EDITED BY
Peitao Lü,
Fujian Agriculture and Forestry University, China

REVIEWED BY
Yuanyuan Liu,
Fujian Agriculture and Forestry University, China
Fangyuan Zhang,
Southwest University, China

*CORRESPONDENCE
Weiqiang Chen
wqchen@icmm.ac.cn
Huihua Wan
hhwan@icmm.ac.cn

†These authors have contributed equally to this work

SPECIALTY SECTION
This article was submitted to Plant Systems and Synthetic Biology, a section of the journal Frontiers in Plant Science

RECEIVED 17 August 2022
ACCEPTED 29 September 2022
PUBLISHED 13 October 2022

CITATION
Wang S, Cao X, Meng X, Aili M, Dou Q, Wang Y, Wahab AT, Chen S, Sun W, Wan H and Chen W (2022) Characterization and expression analysis of MATEs in *Cannabis sativa* L. reveals genes involving in cannabinoid synthesis. *Front. Plant Sci.* 13:1021088. doi: 10.3389/fpls.2022.1021088

Characterization and expression analysis of MATEs in *Cannabis sativa* L. reveals genes involving in cannabinoid synthesis

Sifan Wang[1†], Xue Cao[1†], Xiangxiao Meng[1†], Maimaiti Aili[2], Qin Dou[2], Yan Wang[3], Atia Tul Wahab[4], Shilin Chen[1], Wei Sun[1], Huihua Wan[1*] and Weiqiang Chen[1,2*]

[1]Key Laboratory of Beijing for Identification and Safety Evaluation of Chinese Medicine, Institute of Chinese Materia Medica, China Academy of Chinese Medical Sciences, Beijing, China, [2]Xinjiang Institute of Traditional Uyghur Medicine, Urumqi, China, [3]Hussain Ebrahim Jamal Research Institute of Chemistry, International Center for Chemical and Biological Sciences, University of Karachi, Karachi, Pakistan, [4]Panjwani Center for Molecular Medicine and Drug Research, International Center for Chemical and Biological Sciences, University of Karachi, Karachi, Pakistan

The medicinal plant *Cannabis sativa* L. (*C. sativa*) accumulates plant cytotoxic but medicinally important cannabinoids in glandular trichomes and flowers of female plants. Although the major biosynthetic pathway of cannabinoids has been revealed, their transportation mechanism is still unknown. Multidrug and toxic compound extrusion proteins (MATEs) can transport plant metabolites, ions and phytohormones intra and inter-cellularly. MATEs could have the potential to translocate cannabinoids or their synthetic intermediates to cellular compartment, thus protecting them from unwanted modifications and cytotoxicity. In this study, we performed a genome-wide identification and expression analysis of *Cannabis sativa* MATEs (CsMATEs) and revealed 42 CsMATEs that were classified phylogenetically into four conserved subfamilies. Forty-two *CsMATEs* were unevenly distributed on 10 chromosomes, with 50% *CsMATEs* were physically adjacent to at least one another *CsMATEs* and 83% CsMATEs localized on plasma membrane. Tandem duplication is the major evolutionary driving force for *CsMATEs* expansion. Real-time quantitative PCR revealed *CsMATE23*, *CsMATE28* and *CsMATE34* mainly expressed in flower, whereas *CsMATE17* and *CsMATE27* showed strong transcription in root. Light responsive *cis*-acting element was most abundant in promoters of *CsMATE23*, *CsMATE28* and *CsMATE34*. Finally, the contents of cannabinoids and corresponding biosynthetic intermediates as well as expressions of *CsMATE28* and *CsMATE34* were determined under UV-B treatment, among which strong correlation was found. Our results indicates that CsMATEs might involve in biosynthesis of cannabinoids and has the potential to be used in heterologous production of cannabinoids.

KEYWORDS

***Cannabis sativa*, cannabinoids, transporter, MATEs, genome-wide, heterologous biosynthesis**

Introduction

The annual dioecious herb *Cannabis sativa* L. (*C. sativa*) from *Cannabis* family accumulates terpenophenolic cannabinoids in glandular trichomes and flowers of female plants (Andre et al., 2016). Till now, over 113 cannabinoids have been isolated from *C. sativa* and many are derived from non-enzymatic decarboxylaion of their acidic forms by heat or UV irradiation (Güllck and Moller, 2020). The well-studied cannabinoids cannabigerol (CBG), Δ9-tetrahydrocannabinol (THC), cannabidiol (CBD) and cannabichromene (CBC) share the same biosynthetic precursors of olivetolic acid (OA) and geranyl diphosphate (GPP) (Güllck and Moller, 2020). Phenolic OA is condensed from one molecule of hexanoyl-CoA and three molecules of malonyl-CoA by coordinated work of olivetol synthase (OLS) (Taura et al., 2009) and olivetolic acid synthase (OAC) (Gagne et al., 2012) in cytosol. The acyl-activating enzyme 1 (AAE1) provides hexanoyl-CoA by converting C6-hexanoic acid which is derived from fatty acid pathway (Stout et al., 2012), while C10-isoprenoid GPP is synthesized by 2-C-methyl-D-erythritol 4-phosphate (MEP) pathway in plastid (Fellermeier et al., 2001). Aromatic prenyltransferase 4 (aPT4) from UbiA protein superfamily subsequently prenylates OA by GPP to produce cannabichromenic acid (CBGA) (Luo et al., 2019; Güllck et al., 2020), which is further oxidized to CBG. CBGA could be converted to Δ9-tetrahydrocannabinolic acid (THCA) or cannabidiolic acid (CBDA) by flavoproteins Δ9-tetrahydrocannabinolic acid synthase (THCAS) (Sirikantaramas et al., 2005) or cannabidiolic acid synthase (CBDAS) (Taura et al., 2007), respectively, and subsequently decarboxylated to THC or CBD by light or heat.

Low abundance in *C. sativa* and important pharmaceutical use evokes tremendous interests for heterologous biosynthesis of cannabinoids. A notable example is the *de novo* production of THCA and CBDA in yeast *Saccharomyces cerevisiae* system (Luo et al., 2019). Co-expression of OA synthetic pathway (*CsAAE1*, *CsOAC* and *CsOLS*) along with plastid-localization-signal-free *CsaPT4*, secretory-signal-free *CsTHCAS* or *CsCBDAS* in a GPP-overproducing yeast strain yielded THCA or CBDA, respectively. When those genes were transiently expressed in tobacco (*Nicotiana benthamiana*) cells, however, either OA, CBGA or THCA was severely glucosylated (Güllck et al., 2020). In addition to been easily glucosylated, CBGA and THCA are cytotoxic (Morimoto et al., 2007). Therefore, mechanisms might exist in *C. sativa* cells that protect cannabinoids from glucosylation and inhibit their cytotoxicity.

Multidrug and toxic compound extrusion proteins (MATEs) are known to translocate second metabolites, ions, and phytohormones intra and intercellularly, and are associated with exnobiotic efflux, aluminum detoxification and disease resistance (Upadhyay et al., 2019). Moreover, MATEs are widely distributed in prokaryotes and eukaryotes, including plants. YdhE was the first isolated MATE from *E.coli* as a multidrug efflux protein that confers bacteria drug resistance (Morita et al., 1998). Soon after, ALF, the first plant MATE from *Arabidopsis thaliana* (*A. thaliana*) (Diener et al., 2001) and many other plant MATEs were sequentially discovered (Wang et al., 2016; Santos et al., 2017; Wang et al., 2017; Huang et al., 2021). Most MATEs consist of about 400-700 amino acids with 12 transmembrane helices and a common MatE domain (pfam 01554), but no consensus sequence thus far has been found in all MATEs (Kusakizako et al., 2020). MATEs transport second metabolites into and out of the membranes through the employment of either Na^+ or H^+ electrochemical gradient (Hvorup et al., 2003). For instance, NtMATE1 and NtMATE2 that localize on the vacuolar membrane of tobacco root cells are believed to sequestrate alkaloid nicotine within the vacuole of the roots, then nicotine is transported to the above-ground organs of the plant in response to plant biotic stresses (Shoji et al., 2009). Similar function in alkaloid transportation is also found for tobacco MATEs Nt-JAT1 and Nt-JAT2, which localize on the vacuolar membrane of leaf cells (Morita et al., 2009). GhTT2, GhMATE12, GhMATE16 and GhMATE38 from *Gossypium hirsutum* L. localized on the tonoplast are proposed to translocate phenolic pro-anthocyanidins (Gao et al., 2016; Xu et al., 2019). VvAM1 and VvAM2 expressed in berry skins of *Vitis vinifera* and subcellularly localized on tonoplast are responsible of translocating flavonoid anthocyanins (Perez-Diaz et al., 2014). Thus, we hypothesis that MATEs from *C. sativa* might have the ability to bind and translocate terpenophenolic cannabinoids or corresponding biosynthetic intermediates, protecting them from glucosylation and inhibiting their cytotoxicity in *C. sativa* cells.

In this study, we identified 42 MATEs in *C. sativa* genome and characterized their physical-chemical properties, gene structure, motif composition and gene expression patterns. Furthermore, qRT-PCR verification and *cis*-acting elements analysis of *CsMATEs* that predominantly expressed in cannabinoids accumulation tissues were conducted. In addition, effects of UV-B on accumulation of cannabinoids and corresponding biosynthetic substrates as well as the expression of *CsMATE23*, *CsMATE28* and *CsMATE34* were studied. Together, our result indicates that CsMATE28 and CsMATE34 might be involved in biosynthesis of cannabinoids or its biosynthetic intermediates.

Materials and methods

Plant material and growing conditions

In this study, we used the *C. sativa* variety Dinamed Kush (DK) for transcriptome sequencing (Yang et al., 2021). DK were grown in the experimental field of the Institute of Chinese Materia Medica of the Chinese Academy of Chinese Medical

Sciences, China. Three-weeks-old *C. sativa* grown in green house at 65% humidity and light wavelength of 380-780 nm (520-860 uM m^{-2} s^{-1}) was used for UV-B light treatment.

Date source

Genome of female *C. sativa* CRBRx (GCA_900626175.1) and transcriptional data of other nine *C. sativa* varieties (Zager et al., 2019) were obtained from the NCBI database (https://www.ncbi.nlm.nih.gov). *Arabidopsis thaliana* MATE gene family members were obtained from the Uniprot database (www.uniprot.org).

Identification and basic information of CsMATEs

CDS sequences and protein sequences of CRBRx were extracted using TBtools (Chen et al., 2020). Protein sequences of *A. thaliana* MATEs were used as queries to perform homology search by BLASTp method (score value of ≥100, e-value ≤ e^{-10}). Duplicated proteins were manually removed. Recognizable domains were initially retrieved using BLAST-based NCBI conserved domain searches (https://www.ncbi.nlm.nih.gov/Structure/cdd/wrpsb.cgi). Molecular weights and isoelectric points were predicted using ExPASy (Duvaud et al., 2021). Subcellular localizations were predicted by WOLF PSORT (Horton et al., 2007).

Chromosomal location, gene structure, phylogenic tree, conserved motifs and *cis*-acting elements analysis of CsMATEs

Visualization of *CsMATEs* structures and chromosome locations were conducted using TBtools (Chen et al., 2020). The amino acid sequences were aligned using MEGA 7.0 software (Kumar et al., 2016). Phylogenetic trees of *C. sativa* and *A. thaliana* were constructed using the neighborjoining (NJ) method with 1000 bootstrap replicates. Conserved motif information of CsMATEs was analyzed using MEME (Bailey et al., 2006). *Cis*-acting elements in 2000 bp upstream of the start codon of each *CsMATEs* were analyzed using PlantCARE (Lescot et al., 2002).

Transcriptomic data analysis, alternative splicing and qRT-PCR

mRNA from five different tissues or organs of female *C. sativa* Dinamed Kush were sequenced. TBtools (Chen et al., 2020) was used to analyze and visualize the differential expression data of *CsMATEs*. RNA was extracted using a kit (Tiangen Biotech, Beijing, China) according to manufacturer's instructions. Three biological replicates of each sample were performed. Extracted RNA was examined by agarose gel electrophoresis and concentrations were determined using Nanodrop (Thermo fisher scientific, Beijing, China). cDNA synthesis was performed using the Reverse Transcription Kit (TransGen, Beijing, China) as described in instruction. qRT-PCR was designed using NCBI-Primer blast (Supplementary Table 1) with *EF1-α* as the reference gene. qRT-PCR reaction included StarLighter SYBR green qPCR mix (Qi Heng Xing, Beijing, China) 10 μL, cDNA template 1 μL, 0.4 μL of each primer and ddH2O 8.2 μL. The CFX96™ real-time system (Roter-Gene Q MDx, QIAGENBio-Rad, Germany) was used for qRT-PCR. The reaction conditions were: 95°C for 5 min, 35 cycles of 95°C for 30 s, 55°C for 30 s, and 72°C for 90 s. Data were processed using $2^{-\Delta\Delta CT}$ (Livak and Schmittgen, 2001).

QQQ-MS/MS conditions

Cannabinoid content was determined using an Agilent UPLC 1290II-G6400 triple quadrupole mass spectrometer (QQQ; Agilent Technologies, Santa Clara, CA). The autosampler was set to 4°C and a 3-μl sample volume was injected. The chromatographic column was a (2.1 * 100 mm, 1.8 μm) C18 column. Mobile phase A contained water with 0.1% formic acid; phase B was 100% methanol. Elution was performed at 0.3 mL/min.

Statistical analysis

All the data were analyzed using Prism 8 Statistics programs. One-way analysis of variance (ANOVA) followed by Tukey's multiple range test was used both for metabolic data and gene expression data.

Results

Identification, characterization and phylogenic analysis of the *MATE* genes in *C. sativa*

We performed the homology search against the Arabidopsis MATE sequences and finally 42 CsMATE candidates were identified and named for their position on the chromosomes (Table 1). Forty-two *CsMATEs* are unevenly scattered on ten chromosomes, with chromosome four contains the highest number of *CsMATEs* and chromosome six contains the least (Table 1 and Figure 1). It's worth noting that twenty-one *CsMATEs* genes are physically adjacent to at least one another

10.3389/fpls.2022.1021088

TABLE 1 Detail information of CsMATEs.

Gene Name[a]	Gene ID[b]	Length[c]	pI[d]	MW[e]	SL[f]
CsMATE01	gene-LOC115702550	603	9.56	64111.87	Plas
CsMATE02	gene-LOC115705200	510	6.16	55448.57	Plas
CsMATE03	gene-LOC115711014	600	5.57	66053.91	Plas
CsMATE04	gene-LOC115712910	478	8.32	52682.78	Plas
CsMATE05	gene-LOC115704231	543	6.25	58847.88	Plas
CsMATE06	gene-LOC115705064	498	8.02	53766.41	Plas
CsMATE07	gene-LOC115704998	480	7.01	52855.52	Plas
CsMATE08	gene-LOC115704386	442	5.91	48420.02	Plas
CsMATE09	gene-LOC115703842	481	6.45	53039.56	Plas
CsMATE10	gene-LOC115704479	621	5.29	68007.98	Vacu
CsMATE11	gene-LOC115704728	501	6.59	54416.21	Vacu
CsMATE12	gene-LOC115707979	524	5.31	56805.39	Plas
CsMATE13	gene-LOC115708894	540	8.7	58085.01	Plas
CsMATE14	gene-LOC115708868	491	8.22	53432.55	Plas
CsMATE15	gene-LOC115710056	507	7.05	54875.91	Plas
CsMATE16	gene-LOC115708683	319	5.94	35375.83	Plas
CsMATE17	gene-LOC115714727	485	8.19	53346.36	Plas
CsMATE18	gene-LOC115714726	495	6.11	54439.4	Plas
CsMATE19	gene-LOC115714655	492	6.47	53938.45	Plas
CsMATE20	gene-LOC115712477	488	6.54	53419.89	Plas
CsMATE21	gene-LOC115714241	490	8.66	53946.72	Plas
CsMATE22	gene-LOC115714240	491	8.68	54434.61	Plas
CsMATE23	gene-LOC115714995	511	6.1	55863.48	Plas
CsMATE24	gene-LOC115712321	500	6.94	54840.62	Plas
CsMATE25	gene-LOC115714210	497	7.53	54268.94	Plas
CsMATE26	gene-LOC115713744	502	8.82	54664.57	Vacu
CsMATE27	gene-LOC115715674	497	5.12	54424.38	Vacu
CsMATE28	gene-LOC115715639	497	5.12	54388.58	Plas
CsMATE29	gene-LOC115715820	553	6	60358.2	Plas
CsMATE30	gene-LOC115717372	483	6.95	52314.4	Plas
CsMATE31	gene-LOC115719395	505	6.1	55712.17	Plas
CsMATE32	gene-LOC115723139	516	7.95	57018.9	Vacu
CsMATE33	gene-LOC115723617	484	8.94	52901.07	Plas
CsMATE34	gene-LOC115724138	473	6.81	51277.63	Plas
CsMATE35	gene-LOC115723312	500	6.41	54589.43	Plas
CsMATE36	gene-LOC115723477	490	5.76	54286.35	Plas
CsMATE37	gene-LOC115695936	502	7.01	53538.67	Vacu
CsMATE38	gene-LOC115697672	536	8.99	58082.75	Plas
CsMATE39	gene-LOC115698206	551	5.73	58931.1	Chlo
CsMATE40	gene-LOC115700595	513	5.97	55800.43	Plas
CsMATE41	gene-LOC115699384	506	6.98	54837.94	Plas
CsMATE42	gene-LOC115701322	526	6.53	57241.14	Plas

[a]Gene named for their position on the chromosomes.
[b]Accession number of *C. sativa* locus ID.
[c]Protein length in amino acid.
[d]Isoelectric points.
[e]Molecular weight in Dalton.
[f]Subcellular localization, plas: plasm membrane, Chol: chloroplast, Vacu: vacuole.

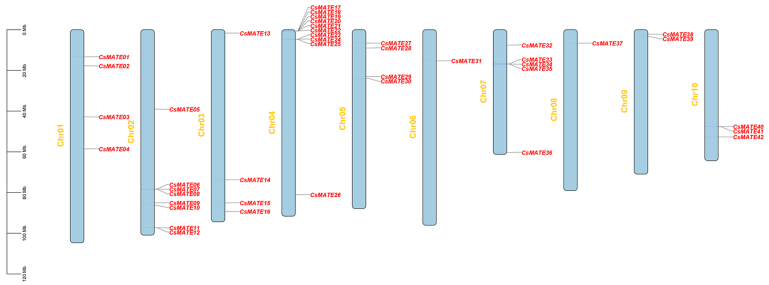

FIGURE 1
Distribution of *CsMATEs* on chromosomes of *C. sativa*. The y-axis indicates the length of chromosome in megabase (Mb).

CsMATEs, such as *CsMATE6–CsMATE8*, *CsMATE11–CsMATE12*, *CsMATE17–CsMATE22*, *CsMATE23–CsMATE25*, *CsMATE29–CsMATE30*, *CsMATE33–CsMATE35*, and *CsMATE40–CsMATE41* (Figure 1). Those *CsMATEs* account for ~50% of the total *CsMATE* genes. Moreover, near half of the *CsMATEs* are located in the proximal region of chromosome telomere (Figure 1).

We also predicted the physical-chemical properties and subcellular localization of the CsMATEs and found that the longest MATE is CsMATE10, consisting of 621 amino acids, while the shortest CsMATE16 is comprised of 319 amino acids (Table 1). The isoelectric points (pI) and molecular weights (MW) of CsMATEs range from 5.12–9.56 and 35.38–68 kilodalton (kDa), respectively (Table 1). Thirty-five CsMATEs were localized in the plasma membrane, six in the vacuole, and only CsMATE39 localized in the chloroplast (Table 1).

To investigate of the evolutionary relationship of the CsMATEs, we constructed an interspecifc phylogenic tree using *C. sativa* and *A. thaliana* MATEs sequences with phylogenetic inference of neighbor-joining (Figure 2). The topology of the phylogenic tree divides CsMATEs into four major subfamilies. Subfamily I contains 14 CsMATEs, subfamily

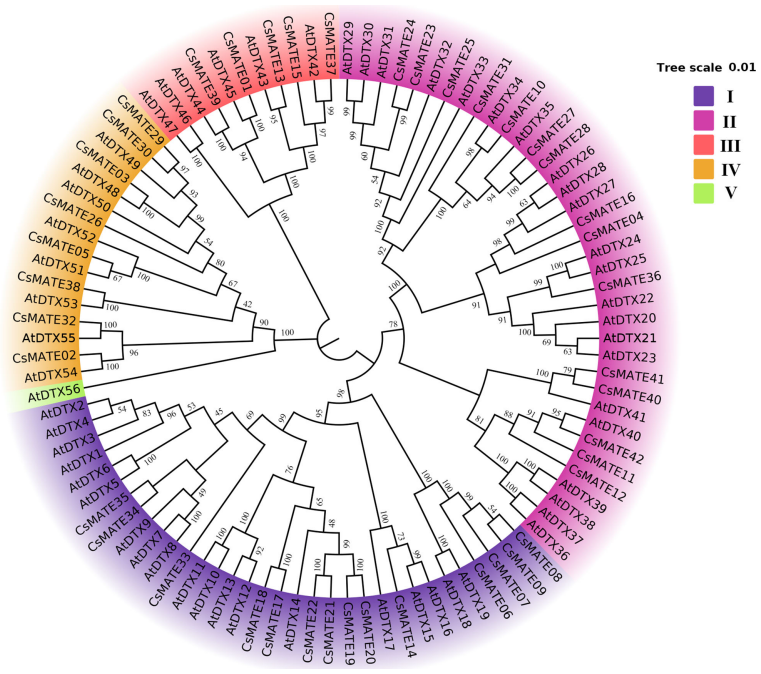

FIGURE 2
Phylogenic tree of MATE proteins in *Cannabis sativa* (CsMATEs) and *Arabidopsis thaliana* (AtDTXs). Phylogenic tree was built using MEGA 7.0 software neighbor-joining method (Kumar et al., 2016) with a bootstrap analysis of 1000 replicates.

II has 15 CsMATEs, subfamily III possesses five CsMATES, and subfamily IV owns eight CsMATEs (Figure 2). Importantly, physically adjacent *CsMATEs* were all clustered in the same subfamily (Figure 1 and Figure 2), which indicates tandem duplication is the major evolutionary driving force for *CsMATEs* expansion (Wang et al., 2019).

Conserved motifs of CsMATEs and gene structure of *CsMATEs*

Conserved protein motifs are associated with gene function and protein subcellular localizations. We isolated 10 predicted conserved motifs (Supplementary Figure S1) using MEME (Bailey et al., 2006) and studied their distributions within CsMATEs. Phylogenetic analysis grouped CsAMTEs into four subfamilies, which is consistent with the interspecific phylogenetic tree in Figure 2 (Figure 3A). We found that 32 CsMATEs (76% of total identified) from subfamily I, II and IV included all 10 motifs and those motifs shared the same order. CsMATE6, 7 and 9 were lack of motif 8; CsMATE8 is without of moitf6 and motif8. CsMATEs from subfamily III had motifs less than six, with CsMATE15 and CsMATE17 only containing motifs 7, 9 and 10 (Figure 3A).

To further examine the evolutionary lineages of *CsMATEs*, we compared the gene structure of *CsMATEs*. The results showed that phylogenetically close *CsAMTEs* shared the same exon number, length and composition (Figure 3B). For instance, *CsMATEs* from subfamily IV had no intron except for *CsMATE2* and *CsMATE38* that contained one and two introns, respectively. *CsMATEs* from subfamily III owned most exons of at least 10. A longest intron that over 20 kb was found in *CsMATE35* from subfamily I (Figure 3B). In addition, as tandem duplication is the main force of *CsMATEs* expansion, physically adjacent *CsMATEs* also showed same exon/intron pattern, such as *CsMATE6*–*CsMATE8* and *CsMATE23*–*CsMATE25* (Figure 1 and Figure 3B). Although gene structures between different subfamilies were divergent, we found two crucial domains that closed to 5' end of the gene bodies (Figure 3B).

Expression pattern of *CsMATEs* in deferent tissues

Gene expression pattern is to some extent indicative for its potential function, especially for transporter proteins that mostly interact with substrates in tissues where metabolites are synthesized (Nogia and Pati, 2021). We visualized the *CsMATEs* expressions from different tissues of hemp variety Dinamed Kush, a species with high cannabinoids content, using FPKM (Fragments Per Kilobase of exon model per Million mapped fragments) and cluster analysis, and indeed found the divergent expression patterns (Figure 4A). Specifically, only *CsMATE1* showed higher expression in seed compared with other tissues, *CsMATE7*, *CsMATE13*, *CsMATE21*, *CsMATE24*, *CsMATE25*, *CsMATE29* and *CsMATE30* exhibit relatively strong expression in root, *CsMATE22* and *CsMATE36* have the moderate stronger expression in stem, transcripts of *CsMATE4*, *CsMATE9*, *CsMATE11*, *CsMATE14*, *CsMATE37*, *CsMATE39* and *CsMATE42* are abundantly detected in leaf, and *CsMATE03*, *CsMATE05 CsMATE17*, *CsMATE23*, *CsMATE28*, *CsMATE31*, *CsMATE34* and *CsMATE40* are the genes that expressed mainly in flowers (Figure 4A).

As we are interested in CsMATEs that involved in transportation of cannabinoids, and to further verify the accuracy of the transcriptomic data, we analyzed the expressions of representative MATE genes by qRT-PCR (real-time quantitative reverse transcription PCR) including *CsMATE17*, *CsMATE23*, *CsMATE28* and *CsMATE34* which

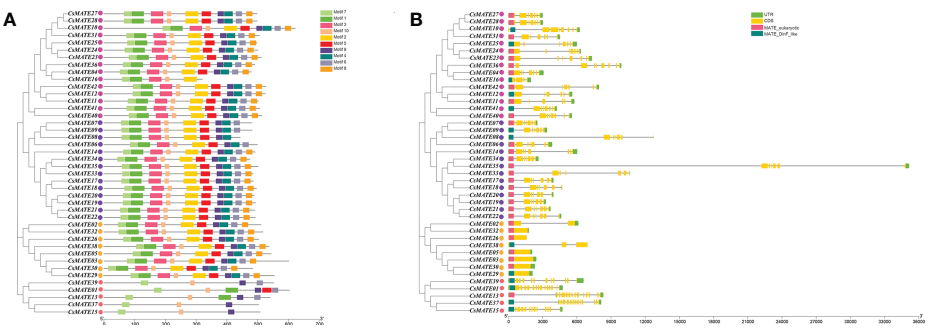

FIGURE 3
Conserved motifs and gene structure of CsMATEs. **(A)** CsMATEs Phylogenic tree and motifs distributions. Motifs are indicated as top right. **(B)** Gene structure and domain distribution. UTR, untranslated region; CDS, coding region; yellow boxes, exons; gray lines, introns; pink boxes, MATE eukaryotic domains; dark green boxes, DinF like domain. Purple dots indicates CsMATE from subfamily I; rose red dots, Subfamily II; pink dots, subfamily III; yellow dots, subfamily IV.

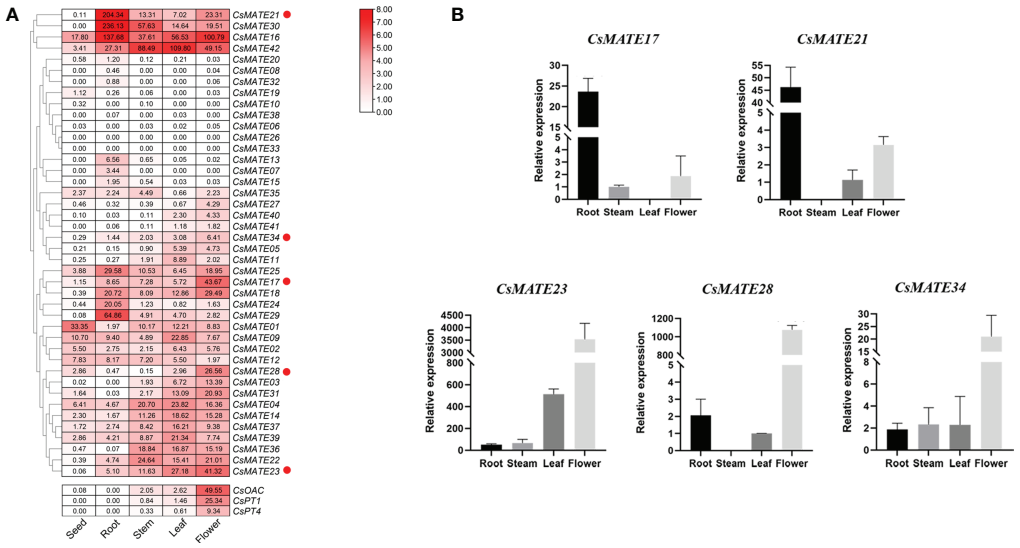

FIGURE 4
Expression of *CsAMTEs* and cannabinoid biosynthetic genes. **(A)** Expression profile of *CsMATEs* in seed, root, stem, leaf and flower. PFKM values were used to configure the heatmap. Red dots, genes selected for expression verification. *CsOAC*, *olivetolic acid synthase*; *CsPT1* and *CsPT4*, *prenyltransferase 1* and *4* gene, repectively. **(B)** quantitative reverse transcription PCR verification. y-axis, relative gene expression normalized to *CsEF1-alpha*. x-axis, different tissues. Data, mean ± SD.

had a highest expression in flower but also expressed moderately in stem and leaf according to transcriptome data, as well as *CsMATE21* that showed strong root specificity in transcriptomic heatmap (Figure 4A). *CsMATE17*, unexpectedly, was predominantly expressed in root, inconsistent with the RNA-seq data, while the other four gene showed the same expression pattern as in RNA-seq (Figure 4B). Additionally, we also examined the expression patterns of cannabinoid biosynthetic pathway genes including *CsOAC*, *CsPT1 and CsPT4* (Figure 4A). The result showed that *CsMATE23*, *CsMATE28* and *CsMATE34* exhibited similar expression patterns with cannabinoids synthetic genes, suggesting those genes might involve in cannabinoids synthesis (Figure 4A).

Expression of alternative splicing isoforms of C*sMATEs* and *cis*-elements in *CsMATE23*, *CsMATE28* and *CsMATE34*

Alternative splicing is widespread in plants as a transcriptional regulatory mechanism that allows a single gene to encode a variety of different transcripts and protein products (Roy et al., 2013). To further understand the transcriptional mechanisms of *CsMATEs*, we performed alternative splicing analysis. We observed 15 *CsMATEs* have alternative splicing events, accounting for about 1/3 of *CsMATEs*, with a total of 43 alternative splicing isoforms. Numbers of alternative splicing isoforms of a single *CsMATE* range from one to seven, and most of the alternative splicing isoforms form the same pre-mRNA were differentially expressed in the same tissues. Of note, although *CsMATE23* and *CsMATE34* both have an alternative splicing isoform, the alternative splicing isoforms barely express in the tissues we examined (Figure 5A).

Light is known to affect the content of cannabinoids (Eichhorn et al., 2019). The *cis*-acting elements in the promoter region (2 kb upstream of ATG codon) of *CsMATE23*, *CsMATE28* and *CsMATE34* were analyzed using plantCARE software (Lescot et al., 2002). We found that the most abundant *cis*-acting element is the light responsive element, and at least six light responsive *cis*-acting elements are found in each of the *CsMATE23*, *CsMATE28* and *CsMATE34* promoter regions (Figure 5B). Phytohormones responsive *cis*-acting elements are the second abundant found in their promoter regions (Figure 5B). We also revealed one and two defense and stress responsive *cis*-acting elements in *CsMATE17* and *CsMATE28* promoters, respectively, and one low temperature-responsive *cis*-element in *CsMATE23* promoter (Figure 5B).

Cannabinoids contents, transcription of *CsMATE23*, *CsMATE28* and *CsMATE34* were affected under UV-B light

As we found numerous light responsive *cis*-acting elements in the promoters of *CsMATE23*, *CsMATE28* and *CsMATE34*

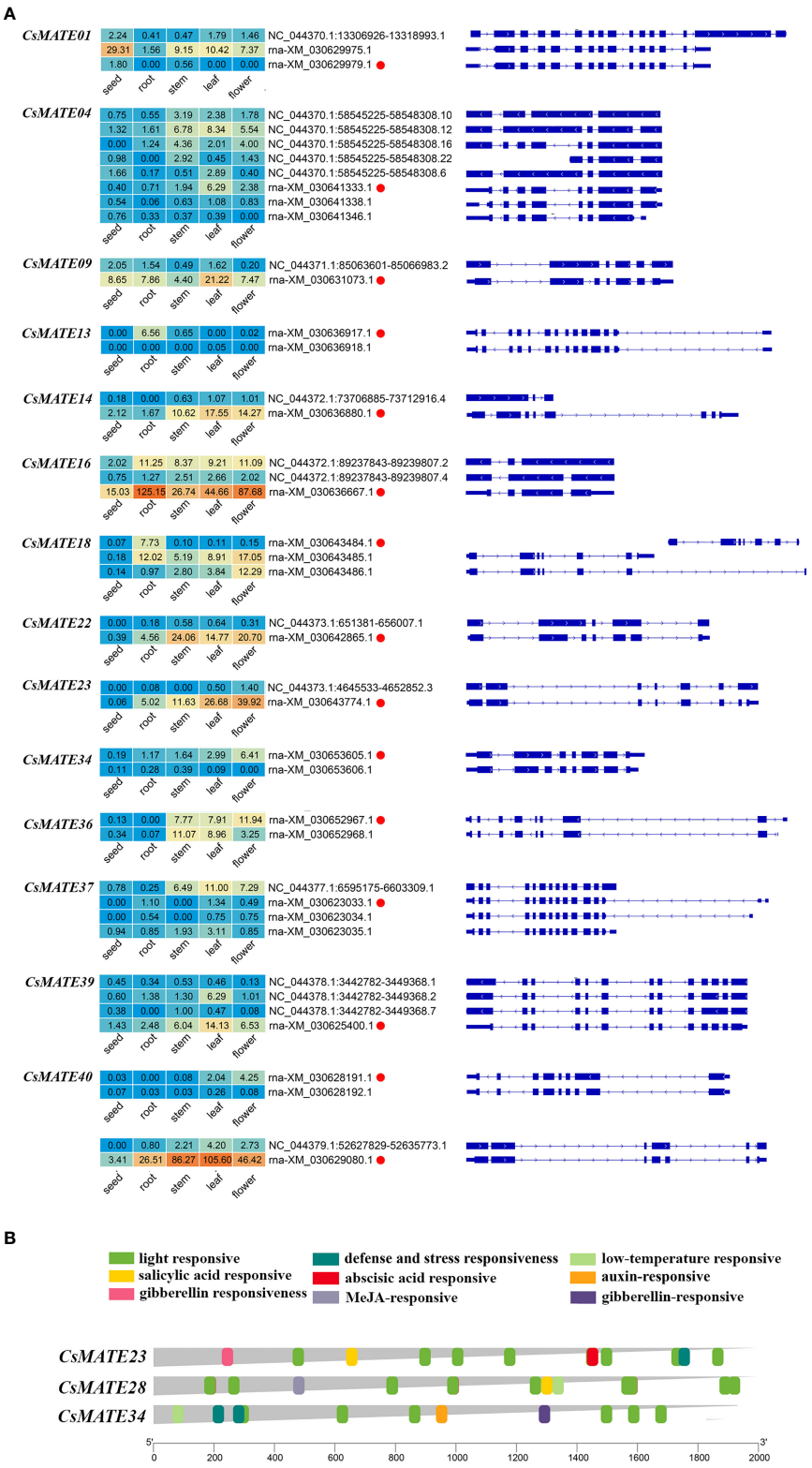

FIGURE 5
Expression of alternative splicing isoforms **(A)** and *cis*-acting elements in *CsMATEs* **(B)**. Red dots, alternative splicing isoform used for analysis in this study. Heatmap was configured using PFKM value. Length of gene promoters in bp.

(Figure 5B) and lights are known to affect accumulation of cannabinoids (Eichhorn et al., 2019), we then studied the content of cannabinoids, cannabinoids biosynthetic intermediates and the expressions of *CsMATE23*, *CsMATE28* and *CsMATE34* under UV-B light treatment.

Three-weeks-old cannabis seedlings were subjected to UV-B light treatment, and quantitative analysis of cannabinoid contents from leaves was performed by QQQ-MS/MS. In summary, content of OA decreased significantly after two hours or six hours UV-B treatment and reached highest at 12 hours, whereas we only observed a decrease of GPP at 12 hours (Figure 6A). Except for CBD that showed a decrease at two hours treatment and an increase after 12 hours UV-B treatment, the contents of CBGA, CBG, THCA, THC and CBDA increased after two hours, then decreased at six hours, reached the highest at 12 hours (Figure 6A).

Correspondingly, expressions of *CsMATE23*, *CsMATE28* and *CsMATE34* also exhibited significant changes under UV-B treatment (Figure 6B). *CsMATE23* was greatly reduced after two hours UV-B treatment and restored its expression at 12 hours. The expression of *CsMATE28 and CsMATE34* displayed no significant change during the first six hours treatment, but significantly increased at 12 hours. (Figure 6B).

Discussion

MATEs have been identified in a variety of plant species, including 56 MATEs in Arabidopsis, 55 in rice (Wang et al., 2016). 67 in tomato (Santos et al., 2017), 64 in potato (Huang et al., 2021), 70 in *Medicago truncatula* (Wang et al., 2017), 72 in cotton (Xu et al., 2019) and 117 in soybean (Liu et al., 2016). In the present study, we identified 42 CsMATEs and investigated their physical-chemical properties, gene distribution, evolutionary relationships, conserved motifs, gene structures and gene expressions. CsMATEs contains only 42 members (Table 1) and is the fewest when compared with other plant species, which suggests CsMATEs may have undergone contraction during evolution. Those 42 CsMATEs were divided into four subfamilies and distributed on 10 chromosomes, with ~50% *CsMATEs* adjacent to at least one another *CsMATEs* (Figure 1), thus the expansion of *CsMATEs* might be largely due to tandem duplication (Wang et al., 2019).

Although cannabinoids synthetic pathways have already been illustrated, the translocation of the cannabinoids and biosynthetic intermediates are not known (Güllck and Moller, 2020). This inevitably hinders cannabinoids heterologous biosynthesis (Güllck et al., 2020). Cannabinoids are

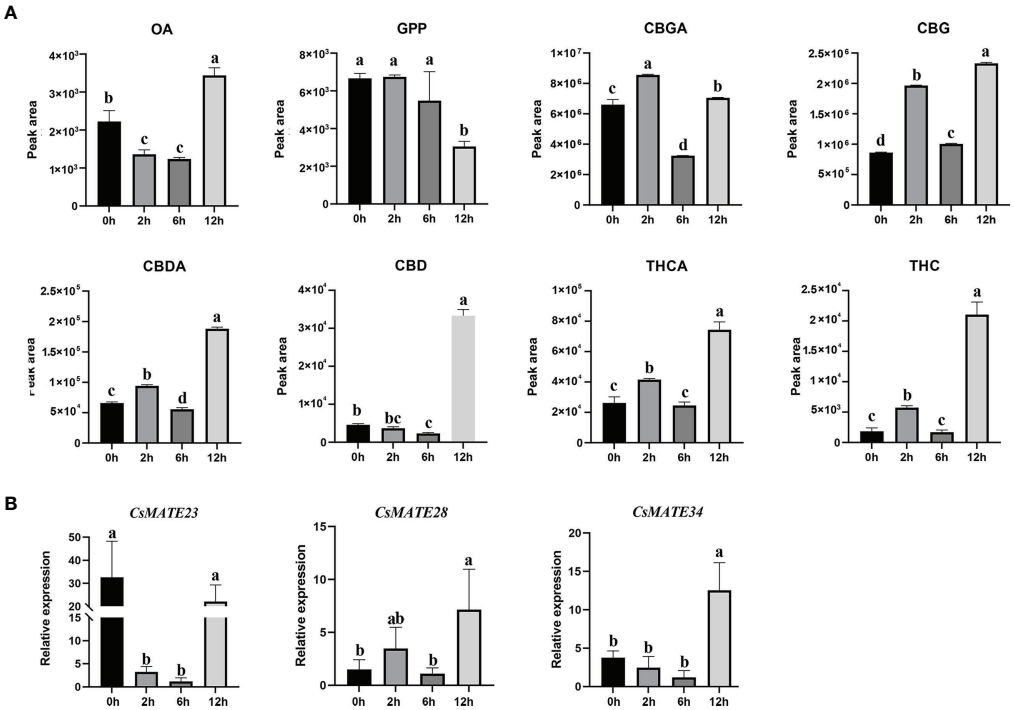

FIGURE 6
Cannabinoids contents **(A)** and expression of *CsMATE23*, *CsMATE38* and *CsMATE34* under UV-B light **(B)**. Leaves from UV-B treated three-weeks-old *C. sativa* seedlings were collected at 0, 2, 6 and 12 hours. Cannabinoids contents were measured using QQQ MS/MS. gene expressions were detected by qRT-PCR with *CsEF1-alpha* as internal reference. Three biological repeats were performed. Different letters above the bars indicate significantly different values ($p < 0.05$) calculated using one-way analysis of variance (ANOVA) followed by Tukey's multiple range test.

synthesized in glandular trichomes and flowers of female *C. sative* and their biosynthetic processes undergo cellular compartmentalization (Güllck and Moller, 2020). For instance, plastid localized CsaPT4 prenylates cytosolic synthesized OA in chloroplast to yield CBGA (Taura et al., 2009; Gagne et al., 2012; Luo et al., 2019; Güllck et al., 2020). Metabolite transporter proteins that could shuttle from cytosol to chloroplast should exist in *C sativa* cells. However, subcellular localization prediction indicates that vast majority of CsMATEs locate in vacuole or plasma membrane (Table 1). Although CsMATE39 contains putative chloroplast localization signal (Table 1), it expresses mainly in leaf (Figure 4A), the tissue that is not the most abundant cannabinoids accumulate. We assume that transporters from other families might be involved in translocating phenolic OA such as ATP binding cassette transporters which could translocate plant phenolic metabolites (Hwang et al., 2016). THCAS is secreted to apoplastic space of the glandular trichome to carry out oxidative cyclization of CBGA (Sirikantaramas et al., 2005). The plastid produced CBGA thus should be translocated across the plasm membrane. Thirty-five CsMATEs are predicted to localized on plasm membrane (Table 1). Of them, *CsMATE03*, *CsMATE05*, *CsMATE23*, *CsMATE28*, *CsMATE31*, *CsMATE34* and *CsMATE40* had a highest expression in flower but also expressed moderately in stem and leaf (the tissues that have glandular trichomes) according to transcriptome data (Figure 4A) and qRT-PCR (Figure 4B). Although we don't have the trichome-specific transcriptional data of those seven genes in variety DK, they uniformly expressed in the trichomes of the other nine *C. sativa* varieties (Zager et al., 2019, Supplementary Figure S2). Moreover, the seven genes exhibited similar expression pattern in different tissues as that of cannabinoid synthetic genes (Figure 4A), which further indicates the involvement CsMATEs in biosynthesis of cannabinoids.

Within the seven genes, except for *CsMATE23*, *CsMATE28*, *CsMATE34* and *CsMATE40* all have an unexpressed alternative spliceform in tissues we studied (Figure 5A). Light responsive *cis*-acting elements were abundantly detected in promoters of the representative *CsMATEs* (*CsMATE23*, *CsMATE28* and *CsMATE34*), reflects those genes could be regulated by lights. UV-B is known to affect accumulation of cannabinoids (Lydon et al., 1987). In accordance with this, the contents of cannabinoids and corresponding intermediates were changed under UV-B treatment (Figure 6A). As expected, the variation trend of CBGA was analogous to its direct downstream THCA, CBDA and CBG (Figure 6A), reflects the precursor nature of the CBGA (Güllck et al., 2020). Notably, although overall variation of OA is similar to CBGA, accumulation of OA is opposed to CBGA at two hours treatment where OA content was decreased but CBGA contents was increased compared to zero hours treatment (Figure 6A). Meanwhile, GPP did not show any change at two hours treatment (Figure 6A). Therefore, increase of CBGA after two hours UV-B treatment could be largely caused by over-usage of OA for synthesizing CBGA either due to enhanced CBGAS activity or more efficient translocation of OA form cytosol to plastid. Unfortunately, none of the *CsMATEs* we tested was up-regulated after two hours treatment (Figure 6B). We reasoned that plastid located ATP binding cassette transporters that translocate phenolic metabolites might responsible for OA transportation (Hwang et al., 2016). Moreover, Although the transcriptional variation of *CsMATE23* is analogous to the content of OA (Figure 6B), OA is synthesized in cytosol and CsMATE23 is localized in plasma membrane (Table 1). Meanwhile, *CsMATE23* is barely transcribed in *C sativa* root, however its Arabidopsis ortholog AtRHS2 (AtDTX31) located in plasma membrane of root is required for hairy root elongation (Won et al., 2009). Hence, we may also exclude participation of CsMATE23 in transporting OA precursors.

The most interesting finding we observed is the correlation between transcriptional alterations of *CsMATEs* with the accumulation of CBGA, THCA and CBDA (Figure 6). As the precursor of THCA and CBDA, CBGA content did not show much alteration at 12 hours treatment compared to the control zero hour (Figure 6A). However, the contents of THCA, THC, CBDA and CBD were all increased at least more than four times at 12 hours compared to zero hours and transcriptions of *CsMATE28* and *CsMATE34* were also significantly enhanced at 12 hours (Figure 6B). This could be explained by that increased CsMATE28 or CsMATE34 more inefficiently transport CBGA to the apoplastic space to enable its subsequent conversions (Sirikantaramas et al., 2005).

Conclusion

We identified 42 CsMATEs and analyzed their structural features, evolutionary relationships and expression patterns. We found number of CsMATEs was subjected to contraction and its expansion within the family was mainly due to tandem duplication. Though RNA-seq and qRT-PCR analysis, we found two root-specifically transcribed *CsMATEs* (*CsMATE17* and *CsMATE27*) and three *CsMATEs* (*CsMATE23*, *CsMATE28* and *CsMATE34*) whose transcription pattern were correlated with transcriptions of cannabinoids biosynthetic genes. In addition, although CBGA content was not much affected under UV-B treatment at 12 hours, accumulations of THCA, CBDA and CBG were increased. This could be due to the increased expression of *CsMATE28* or *CsMATE34*. Although multiple evidences suggest that CsMATEs may play an important role in the synthesis and transport of cannabinoids, the transport of cannabinoids is a complex process. Therefore. The functions of candidate genes (CsMATE28 and CsMATE34) in cannabinoid transportations should be investigated in depth in the future.

Data availability statement

The original contributions presented in the study are included in the article/Supplementary Material. Further inquiries can be directed to the corresponding authors.

Author contributions

WC and HW designed the study. WC, HW, SW, XC and XM wrote the manuscript. SW, XC, XM, YW, AW, MA and QD conducted the bioinformatic analysis. XC and XM performed the qRT-PCR and UV-B treatment. All authors contributed to the article and approved the submitted version.

Funding

This work is supported by Scientific and technological innovation project of China Academy of Chinese Medical Sciences (CI2021A04113).

Conflict of interest

The authors declare that the research was conducted in the absence of any commercial or financial relationships that could be construed as a potential conflict of interest.

Publisher's note

All claims expressed in this article are solely those of the authors and do not necessarily represent those of their affiliated organizations, or those of the publisher, the editors and the reviewers. Any product that may be evaluated in this article, or claim that may be made by its manufacturer, is not guaranteed or endorsed by the publisher.

Supplementary material

The Supplementary Material for this article can be found online at: https://www.frontiersin.org/articles/10.3389/fpls.2022.1021088/full#supplementary-material

References

Andre, C. M., Hausman, J.-F., and Guerriero, G. (2016). *Cannabis sativa*: The plant of the thousand and one molecules. *Front. Plant Sci.* 7. doi: 10.3389/fpls.2016.00019

Bailey, T. L., Williams, N., and Misleh C.and Li, W. W. (2006). MEME: discovering and analyzing DNA and protein sequence motifs. *Nucleic Acids Res.* 34, W369–W373. doi: 10.1093/nar/gkl198

Chen, C., Chen, H., Zhang, Y., Thomas, H. R., Frank, M. H., He, Y., et al. (2020). TBtools: An integrative toolkit developed for interactive analyses of big biological data. *Mol. Plant* 13 (8), 1194–1202. doi: 10.1016/j.molp.2020.06.009

Diener, A. C., Gaxiola, R. A., and Fink, G. R. (2001). Arabidopsis ALF5, a multidrug efflux transporter gene family member, confers resistance to toxins. *Plant Cell.* 13 (7), 1625–1638. doi: 10.1105/tpc.010035

Duvaud, S., Gabella, C., Lisacek, F., Stockinger, H., and Ioannidis V.and Durinx, C. (2021). Expasy, the Swiss bioinformatics resource portal, as designed by its users. *Nucleic Acids Res.* 49 (W1), W216–W227. doi: 10.1093/nar/gkab225

Eichhorn, B. S., Wu, B. S., Rufyikiri, A. S., MacPherson, S., and Lefsrud, M. (2019). An update on plant photobiology and implications for cannabis production. *Front. Plant Sci.* 10. doi: 10.3389/fpls.2019.00296

Fellermeier, M., Eisenreich W., A., Bacher A.,, and Zenk, M. H. (2001). Biosynthesis of cannabinoids. incorporation experiments with (13)C-labeled glucoses. *Eur. J. Biochem.* 268 (6), 1596–1604. doi: 10.1046/j.1432-1033.2001.02030

Gagne, S. J., Stout, J. M., Liu, E., Boubakir, Z., Clark, S. M., Page,, et al. (2012). Identification of olivetolic acid cyclase from cannabis sativa reveals a unique catalytic route to plant polyketides. *Proc. Natl. Acad. Sci. U. S. A.* 109 (31), 12811–12816. doi: 10.1073/pnas.1200330109

Gao, J. S., Wu, N., Shen, Z. L., Lv, K., Qian, S. H., Guo, N., et al. (2016). Molecular cloning, expression analysis and subcellular localization of a transparent testa 12 ortholog in brown cotton (Gossypium hirsutum l.). *Gene* 576 (2 Pt 2), 763–769. doi: 10.1016/j.gene.2015.11.002

Güllck, T., Booth, J. K., Carvalho, A., Khakimov, B., Crocoll, C., Motawia, M. S., et al. (2020). Synthetic biology of cannabinoids and cannabinoid glucosides in nicotiana benthamiana and saccharomyces cerevisiae. *J. Nat. Prod.* 83 (10), 2877–2893. doi: 10.1021/acs.jnatprod.0c00241

Güllck, T., and Moller, B. L. (2020). Phytocannabinoids: Origins and biosynthesis. *Trends Plant Sci.* 25 (10), 985–1004. doi: 10.1016/j.tplants.2020.05.005

Horton, P., Park, K. J., Obayashi, T., Fujita, N., Harada, H., Adams-Collier, C. J., et al. (2007). WoLF PSORT: protein localization predictor. *Nucleic Acids Res.* 35, W585–W587. doi: 10.1093/nar/gkm259

Huang, Y., He, G., Tian, W., Li, D., Meng, L., Wu, D., et al. (2021). Genome-wide identification of MATE gene family in potato (Solanum tuberosum l.) and expression analysis in heavy metal stress. *Front. Genet.* 12. doi: 10.3389/fgene.2021.650500

Hvorup, R. N., Winnen, B., Chang, A. B., Jiang, Y., Zhou, X. F., and Saier, M. H.Jr. (2003). The multidrug/oligosaccharidyl-lipid/polysaccharide (MOP) exporter superfamily. *Eur. J. Biochem.* 270 (5), 799–813. doi: 10.1046/j.1432-1033.2003.03418.x

Hwang, J.-U., Song, W.-Y., Hong, D., Ko, D., Yamaoka, Y., Jang, S., et al. (2016). Plant ABC transporters enable many unique aspects of a terrestrial plant's lifestyle. *Mol. Plant* 9, 338–355. doi: 10.1016/j.molp.2016.02.003

Kumar, S., Stecher, G., and Tamura, K. (2016). MEGA7: Molecular evolutionary genetics analysis version 7.0 for bigger datasets. *Mol. Biol. Evol.* 33 (7), 1870–1874. doi: 10.1093/molbev/msw054

Kusakizako, T., Miyauchi, H., and Ishitani R.and Nureki, O. (2020). Structural biology of the multidrug and toxic compound extrusion superfamily transporters. *Biochim. Biophys. Acta Biomembr.* 1862 (12), 183154. doi: 10.1016/j.bbamem.2019.183154

Lescot, M., Dehais, P., Thijs, G., Marchal, K., Moreau, Y., Van de Peer, Y., et al. (2002). PlantCARE, a database of plant cis-acting regulatory elements and a portal to tools for in silico analysis of promoter sequences. *Nucleic Acids Res.* 30 (1), 325–327. doi: 10.1093/nar/30.1.325

Liu, J., Li, Y., Wang, W., Gai, J., and Li, Y. (2016). Genome-wide analysis of MATE transporters and expression patterns of a subgroup of MATE genes in response to aluminum toxicity in soybean. *BMC Genomics* 17, 223. doi: 10.1186/s12864-016-2559-8

Livak, K. J., and Schmittgen, T. D. (2001). Analysis of relative gene expression data using real-time quantitative PCR and the 2(-delta delta C(T)) method. *Methods* 25 (4), 402–408. doi: 10.1006/meth.2001.1262

Luo, X., Reiter, M. A., d'Espaux, L., Wong, J., Denby, C. M., Lechner, A., et al. (2019). Complete biosynthesis of cannabinoids and their unnatural analogues in yeast. *Nature* 567 (7746), 123–126. doi: 10.1038/s41586-019-0978-9

Lydon, J., Teramura, A. H., and Coffman, C. B. (1987). UV-B radiation effects on photosynthesis, growth and cannabinoid production of two cannabis sativa chemotypes. *Photochem. Photobiol.* 46 (2), 201–206. doi: 10.1111/j.1751-1097.1987.tb04757.x

Morimoto, S., Tanaka, Y., Sasaki, K., Tanaka, H., Fukamizu, T., Shoyama, Y., et al. (2007). Identification and characterization of cannabinoids that induce cell death through mitochondrial permeability transition in cannabis leaf cells. *J. Biol. Chem.* 282 (28), 20739–20751. doi: 10.1074/jbc.M700133200

Morita, Y., Kodama, K., Shiota, S., Mine, T., Kataoka, A., Mizushima, T., et al. (1998). NorM, a putative multidrug efflux protein, of vibrio parahaemolyticus and its homolog in escherichia coli. *Antimicrob. Agents Chemother.* 42 (7), 1778–1782. doi: 10.1128/AAC.42.7.1778

Morita, M., Shitan, N., Sawada, K., Van Montagu, M. C., Inze, D., Rischer, H., et al. (2009). Vacuolar transport of nicotine is mediated by a multidrug and toxic compound extrusion (MATE) transporter in nicotiana tabacum. *Proc. Natl. Acad. Sci. U. S. A.* 106 (7), 2447–2452. doi: 10.1073/pnas.0812512106

Nogia, P., and Pati, P. K. (2021). Plant secondary metabolite transporters: Diversity, functionality, and their modulation. *Front. Plant Sci.* 12. doi: 10.3389/fpls.2021.758202

Perez-Diaz, R., Ryngajllo, M., Perez-Diaz, J., Pena-Cortes, H., Casaretto, J. A., Gonzalez-Villanueva, E., et al. (2014). VvMATE1 and VvMATE2 encode putative proanthocyanidin transporters expressed during berry development in vitis vinifera l. *Plant Cell Rep.* 33 (7), 1147–1159. doi: 10.1007/s00299-014-1604-9

Roy, B., Haupt, L. M., and Griffiths, L. R. (2013). Review: Alternative splicing (AS) of genes as an approach for generating protein complexity. *Curr. Genomics* 14 (3), 182–194. doi: 10.2174/1389202911314030004

Santos, A. L. D., Chaves-Silva, S., Yang, L., Maia, L. G. S., Chalfun-Junior, A., Sinharoy, S., et al. (2017). Global analysis of the MATE gene family of metabolite transporters in tomato. *BMC Plant Biol.* 17 (1), 185. doi: 10.1186/s12870-017-1115-2

Shoji, T., Inai, K., Yazaki, Y., Sato, Y., Takase, H., Shitan, N., et al. (2009). Multidrug and toxic compound extrusion-type transporters implicated in vacuolar sequestration of nicotine in tobacco roots. *Plant Physiol.* 149 (2), 708–718. doi: 10.1104/pp.108.132811

Sirikantaramas, S., Taura, F., Tanaka, Y., Ishikawa, Y., Morimoto, S., and Shoyama, Y. (2005). Tetrahydrocannabinolic acid synthase, the enzyme controlling marijuana psychoactivity, is secreted into the storage cavity of the glandular trichomes. *Plant Cell Physiol.* 46 (9), 1578–1582. doi: 10.1093/pcp/pci166

Stout, J. M., Boubakir, Z., Ambrose, S. J., Purves, R. W., and Page, J. E. (2012). The hexanoyl-CoA precursor for cannabinoid biosynthesis is formed by an acyl-activating enzyme in cannabis sativa trichomes. *Plant J.* 71 (3), 353–365. doi: 10.1111/j.1365-313X.2012.04949.x

Taura, F., Sirikantaramas, S., Shoyama, Y., Yoshikai, K., Shoyama, Y., and Morimoto, S. (2007). Cannabidiolic-acid synthase, the chemotype-determining enzyme in the fiber-type cannabis sativa. *FEBS Lett.* 581 (16), 2929–2934. doi: 10.1016/j.febslet.2007.05.043

Taura, F., Tanaka, S., Taguchi, C., Fukamizu, T., Tanaka, H., Shoyama, Y., et al. (2009). Characterization of olivetol synthase, a polyketide synthase putatively involved in cannabinoid biosynthetic pathway. *FEBS Lett.* 583 (12), 2061–2066. doi: 10.1016/j.febslet.2009.05.024

Upadhyay, N., Kar, D., Deepak Mahajan, B., Nanda, S., Rahiman, R., Panchakshari, N., et al. (2019). The multitasking abilities of MATE transporters in plants. *J. Exp. Bot.* 70 (18), 4643–4656. doi: 10.1093/jxb/erz246

Wang, L., Bei, X., Gao, J., Li, Y., Yan, Y., and Hu, Y. (2016). The similar and different evolutionary trends of MATE family occurred between rice and arabidopsis thaliana. *BMC Plant Biol.* 16 (1), 207. doi: 10.1186/s12870-016-0895-0

Wang, J., Hou, Q., Li, P., Yang, L., Sun, X., Benedito, V. A., et al. (2017). Diverse functions of multidrug and toxin extrusion (MATE) transporters in citric acid efflux and metal homeostasis in medicago truncatula. *Plant J.* 90 (1), 79–95. doi: 10.1111/tpj.13471

Wang, X., Lin, S., Liu, D., Wang, Q., McAvoy, R., Ding, J., et al. (2019). Characterization and expression analysis of ERF genes in fragaria vesca suggest different divergences of tandem ERF duplicates. *Front. Genet.* 10. doi: 10.3389/fgene.2019.00805

Won, S. K., Lee, Y. J., Lee, H. Y., Heo, Y. K., Cho, M., and Cho, H. T. (2009). Cis-element- and transcriptome-based screening of root hair-specific genes and their functional characterization in arabidopsis. *Plant Physiol.* 150 (3), 1459–1473. doi: 10.1104/pp.109.140905

Xu, L., Shen, Z. L., Chen, W., Si, G. Y., Meng, Y., Guo, N., et al. (2019). Phylogenetic analysis of upland cotton MATE gene family reveals a conserved subfamily involved in transport of proanthocyanidins. *Mol. Biol. Rep.* 46 (1), 161–175. doi: 10.1007/s11033-018-4457-4

Yang, L., Meng, X., Chen, S., Li, J., Sun, W., Chen, W., et al. (2021). Identification of the histone deacetylases gene family in hemp reveals genes regulating cannabinoids synthesis. *Front. Plant Sci.* 12. doi: 10.3389/fpls.2021.755494

Zager, J. J., Lange, I., Srividya, N., Smith, A., and Lange, B. M. (2019). Gene networks underlying cannabinoid and terpenoid accumulation in cannabis. *Plant Physiol.* 180 (4), 1877–1897. doi: 10.1104/pp.18.01506

frontiers | Frontiers in Plant Science

TYPE Hypothesis and Theory
PUBLISHED 18 October 2022
DOI 10.3389/fpls.2022.1035119

OPEN ACCESS

EDITED BY
Ji Tian,
Beijing University of Agriculture, China

REVIEWED BY
Xinghui Li,
Nanjing Agricultural University, China
Yahui Huang,
South China Agricultural University, China

*CORRESPONDENCE
Zhidan Chen
asbulletdan@163.com
Weijiang Sun
sunweijiang@hotmail.com

SPECIALTY SECTION
This article was submitted to Plant Systems and Synthetic Biology, a section of the journal Frontiers in Plant Science

RECEIVED 02 September 2022
ACCEPTED 27 September 2022
PUBLISHED 18 October 2022

CITATION
Zhou Z, Chen M, Wu Q, Zeng W, Chen Z and Sun W (2022) Combined analysis of lipidomics and transcriptomics revealed the key pathways and genes of lipids in light-sensitive albino tea plant (*Camellia sinensis* cv. *Baijiguan*). *Front. Plant Sci.* 13:1035119. doi: 10.3389/fpls.2022.1035119

Combined analysis of lipidomics and transcriptomics revealed the key pathways and genes of lipids in light-sensitive albino tea plant (*Camellia sinensis* cv. *Baijiguan*)

Zhe Zhou[1,2], Mingjie Chen[3], Quanjin Wu[4], Wen Zeng[1,2], Zhidan Chen[2,5]* and Weijiang Sun[1,2]*

[1]College of Horticulture, Fujian Agriculture and Forestry University, Fuzhou, China, [2]Ministerial and Provincial Joint Innovation Centre for Safety Production of Cross-Strait Crops, Fujian Agriculture and Forestry University, Fuzhou, China, [3]College of Life Science, Xinyang Normal University, Xinyang, China, [4]Department of Finance and Management, The Open University of Fujian, Fuzhou, China, [5]Anxi College of Tea Science, Fujian Agriculture and Forestry University, Quanzhou, China

Currently, the mechanism by which light-sensitive albino tea plants respond to light to regulate pigment synthesis has been only partially elucidated. However, few studies have focused on the role of lipid metabolism in the whitening of tea leaves. Therefore, in our study, the leaves of the *Baijiguan* (BJG) tea tree under shade and light restoration conditions were analyzed by a combination of lipidomics and transcriptomics. The leaf color of BJG was regulated by light intensity and responded to light changes in light by altering the contents and proportions of lipids. According to the correlation analysis, we found three key lipid components that were significantly associated with the chlorophyll SPAD value, namely, MGDG (36:6), DGDG (36:6) and DGDG (34:3). Further weighted gene coexpression network analysis (WGCNA) showed that *HY5* TF and *GLIP* genes may be hub genes involved lipid regulation in albino tea leaves. Our results lay a foundation for further exploration of the color changes in albino tea leaves.

KEYWORDS

***Camellia sinensis*, albino tea plant, light, lipidomics, transcriptomics, WGCNA**

Introduction

The tea plant (*Camellia sinensis*) is a perennial evergreen woody plant, of which its shoots are often processed into various tea products, such as green tea, black tea, and oolong tea (Li et al., 2019). To date, tea cultivars and their products in China show a 'colorful' trend (Wang et al., 2015). Albino tea cultivars are special mutants of the tea plants with white or yellow leaves under certain environmental conditions, such as low temperature or high light intensity (Du et al., 2006; Peng et al., 2012; Feng et al., 2014). Compared to normal green cultivars, albino cultivars are deficient in chlorophyll. The albino tea germplasm is valuable because of its special flavor, distinct leaf color and scarcity (Du et al., 2006). Sunlight is one of the necessary conditions for photosynthesis and plays an important role in the chlorophyll synthesis (Fan et al., 2019). BJG, a light-sensitive albino tea cultivar, the new shoots display a white color under high light intensity, and turn green under low light intensity (Wu et al., 2016). Currently, the research on the formation of albino leaves is mainly focused on the metabolism of chlorophyll and carotenoids (Wang et al., 2014; Wang et al., 2016; Liu et al., 2017a; Lu et al., 2019). Under sunlight, the chlorophyll synthesis in *Huangjinya* is blocked and its degradation is accelerated. The contents of the antenna protein and-PSII-and PSI-related proteins were significantly reduced, resulting in arrest of photosynthetic electron transport and a reduction in photosynthetic efficiency (Fan et al., 2019). Transcriptomic analysis found that the affected genes were enriched in the fatty acid metabolic pathway and unsaturated fatty acid metabolic pathway (Wu, 2015).

Lipids are the structural materials of cell membranes that play a number of key roles in plant growth, development, and responses to environmental factors (Welti and Wang, 2004; Liu et al., 2017b). The comprehensive classification system organizes lipids into eight well-defined categories: Fatty acyls, Glycerolipids, Glycerophospholipids, Sphingolipids, Sterol Lipids, Prenol Lipids, Saccharolipids and Polyketides (Fahy et al., 2009). The membranes of plant cells containing 5% to 10% lipids (dry weight) are able to distinguish the cells and compartments where many key processes occur, including the light harvesting and electron transport reactions of photosynthesis (Ohlrogge and Browse, 1995). The chloroplast thylakoid membrane is the place where plants perform photosynthesis. The lipid bilayer of the thylakoid membrane is mainly composed of monogalactosyldiacylglycerol (MGDG) and digalactosyldiacylglycerol (DGDG), which account for a large proportion, as well as sulfoquinovosyldiacylglycerol (SQDG) and phosphatidylglycerol (PG). The synthesis of fatty acids in chloroplast intermediates is the first step in the production of chloroplast lipids and is catalyzed by chloroplast FA synthase (FAS) and acetyl CoA carboxylase (ACC), while phosphatidylic acid (PA) can be produced in the chloroplast and endoplasmic reticulum (ER), depending on the plant species (Benning, 2009; Troncoso-Ponce et al., 2016; Li et al., 2020). Fatty acids must be transported from the plastids to the endoplasmic reticulum, where most of the *de novo* synthesized fatty acids assemble into phospholipids and neutral lipids in the endoplasmic reticulum (Li-Beisson et al., 2013). Fatty acids are synthesized by the condensation, dehydration and reduction of acyl carrier proteins, mainly through prokaryotic and eukaryotic pathways (Boudière et al., 2014; Li et al., 2016; Troncoso-Ponce et al., 2016; Hölzl and Dörmann, 2019). Fatty acids enter the ER and bind through two pathways, one of which is the Kennedy pathway. Fatty acids in the form of fatty acyl-CoA are catalyzed by glycerol-3-phosphate acyltransferase (GPAT) to produce lysophosphatidic acid (LPA). LPA is catalyzed by 1-acyl-sn-glycerol-3-phosphate acyltransferase (plsC) to generate phosphatidic acid (PA). Then, PA is phosphorylated by phosphatidylic acid phosphatase (PLPP) to generate diacylglycerols (DAG). DAG binds to various lipids to generate other lipids such as phosphatidylcholine (PC) (Chapman and Ohlrogge, 2012; LaBrant et al., 2018). The second pathway is "acyl editing". In this pathway, fatty acids are directly added to lysophosphatidylcholine (LPC) to regenerate PC, which is recycled back into LPC. MGDG transfers galactose from uridine diphosphate galactose (UDP-Gal) to DAG backbone under the catalysis of MGDG synthetase (MGD). The second galactose is then transferred from UDP-Gal to MGDG by DGDG synthase (DGD) to form DGDG (Gigon et al., 2004; Lin et al., 2016). The photosynthetic protein complex in chloroplasts is embedded in polar lipids, which are regularly arranged and play a critical role in photosynthesis. The plasma membrane is considered as the main barrier between the organism and the external environment, and it is a material that can overcome pressure damage (Janik et al., 2013).

Changes in lipid content and proportion often alter the thylakoid membrane structure, which has been studied in other plants. Under low temperature, the thylakoid membrane structure becomes unstable, its development is not perfect or it even disintegrates, the stacking of basal grains is reduced, the lamellar structure is unclear, and the contents of starch grains increases. The contents of MGDG, DGDG, PG and other species of lipids, the MGDG to DGDG ratio, the contents of unsaturated fatty acids, and the membrane fluidity all are decreased, which ultimately affects the photosynthetic efficiency (Ling, 2001). Therefore, the changes in lipid composition and structure in the plasma membrane under environmental pressure play an important role in maintaining membrane stability and function. Tea plants can store triacylglycerol (TAG) in low nitrogen environments to maintain the C/N balance, which is helpful to improve the quality of tea. Under normal nitrogen treatment, TAG can ensure the transformation of the unique aroma of tea plants. However, after high nitrogen treatment, the increases of MGDG (36:6) and DGDG (36:6) will lead to an increase in aroma synthesis precursors and produce a large amount of grass gas, which is not conducive to improving of tea quality (Liu et al., 2017b). Under drought stress, the MGDG/DGDG ratio in tobacco was found to be increased, but the relative contents of C18:3 fatty

acids in MGDG and DGDG decreased, which was not conducive to the stability of the thylakoid membrane (Wang et al., 2022). The lower photosynthetic rate of wheat under high temperature stress is the result of the interaction between thylakoid membrane damage, membrane lipid composition and organelle oxidative damage. High temperature stress during flowering significantly decrease the total amounts of MGDG, PG, PC and PA (Narayanan et al., 2016; Djanaguiraman et al., 2018; Djanaguiraman et al., 2020). Such an increase in unsaturated fatty acids in PG reduces the formation of ROS and the damage to photosynthetic complexes, thus improving the low temperature tolerance of tomato plants (Sun et al., 2011). In conclusion, abiotic stress can cause changes in the contents and proportions of chloroplast membrane lipids.

The issue of tea whitening has been widely studied. Among these studies, the gene expression profile, genetic structure, some specific base mutation sites and differential accumulation of secondary metabolites of photosensitive albino teas have been gradually clarified. Currently, we know that albino tea plants are mainly affected by the changes in photosensitive pigments in response to light signals, which induce the differential accumulation of tea pigment compounds. Especially in different light environments, the synthesis and regulation of these pigment compounds have been the focus of attention. Based on the clear response of tea plants to light stress, we understand that light management is a key regulator of albino tea plant leaf color phenotype. However, at the level of lipid metabolism, we know little about the photosensitive albino tea plants, and the correlation between its leaf color and lipid changes needs to be explored (Yue et al., 2021).

In this study, we analyzed the composition of lipids in the albino leaves of BJG and their changes in response to light through lipidomics in combination with transcriptomics to determine the key pathways and genes of that are involved. This work will help us to understand the discoloration mechanism of light-sensitive albino tea plants and allow us to make full use of the characteristics of albino tea plants to select excellent tea varieties.

Materials and methods

Plant materials and experiment

BJG was planted in the Wuyi Star Tea Germplasm Resources Garden at Wuyi Star Tea Co. LTD., Wuyi Mountain, China (27° 55′ 15″ N, 118° 02′ 50″ E). In the middle of September 2018, the second leaves of BJG with a similar growth and development status were taken for treatment. There were three treatments in the experiment: normal light (BS0), shading (BS) and shading for 3 days followed by the resuming of light treatment (BRL). The second leaf was covered with aluminum foil for shading treatment. After 3 days of shading, part of the aluminum foil was removed to restore the light to the blade. The total processing time was 6 days. The samples were named BS0, BS1, BS2, BS4, BS6, BRL1, and BRL3. Before plucking, the chlorophyll SPAD value was measured in the leaf. All samples were frozen with liquid nitrogen and stored at −80°C for lipidomics analysis. Among them, samples BS0, BS1 and BRL3 were also used for transcriptome sequencing.

Determination of chlorophyll content

A SPAD-502PLUS Chl meter (Spectrum Technologies, Konica Minolta, Japan) was used to determine the chlorophyll SPAD value from the leaves (Uddling et al., 2007). We tested each leaf, avoiding the main vein, and repeated the test five times.

Lipid isolation from tea leaves

Glass tubes or vials with Teflon-lined caps were used for all experiments. All solvents, including water, were HPLC-grade. Lipids were extracted from samples of BS0, BS1, BS4, BS6 and BRL3 according to the method of Shiva (Shiva et al., 2018). A total of 2.0 mL isopropanol/0.01% butylated hydroxytoluene was added into 8 mL glass tube with a screw cap (the exact weight of each empty tube exact weight was recorded), and the lid was closed snugly. Then, the mixture was heated to 75 °C. Six to eight tea leaves were rapidly harvested and put into hot isopropanol very quickly into hot isopropanol to avoid lipolytic activity. The lid was placed on snugly to prevent evaporation. The samples were heated for more than 15 minutes, and removed from the heating block and allowed to cool to room temperature. Next, 6.0 mL of chloroform/methanol/water (30/41.5/3.5, v/v/v) was added and the lid was closed snugly. The samples were shaken at room temperature for 24 h (50-100 rpm on shaker) until the green leaves became pale white, which indicated that the lipids had been completely extracted. The extracted tea leaves were transferred to a new vial using forceps, dried overnight at 105 °C, equilibrated to room temperature, and weighed in grams to 6 decimal places. Additionally, using a glass, gass-tight syringe (or a glass pipette), the solvent and lipids were transferred to a 2.0 ml GC vial (clear glass, Teflon lined screw cap lid) and dried down under a nitrogen stream before being taken to the Kansas Lipidomics Research Center (KLRC, USA) for lipid testing.

Analysis of lipids by ESI-triple quadrupole MS in multiple reaction monitoring mode for the analysis of tea plants

These experiments were carried out referencing the methods of Shiva (Shiva et al., 2018) and Vu (Vu et al., 2014). An ESI-triple quadrupole mass spectrometry multiple reactions monitoring

analysis method was used to detect lipids in tea plants. The data were processed using Lipidome DB Data Calculation Environment (http://129.237.137.125:8080/Lipidomics).

Construction of a gene coexpression network module and determination of the enriched functions and pathways

Based on the transcriptome data of three samples, we screened genes with an average FPKM value greater than or equal to 1, and used the WGCNA R program to analyze the WGCNA (Langfelder and Horvath, 2008). First, it was assumed that the gene network obeys the scale-free distribution, and the correlation matrix of gene coexpression and the adjacency function formed by the gene network were defined. The optimal soft threshold in this investigation was power $\beta = 20$, and the resulting adjacency matrix was utilized to determine the topological overlap (TO). Then, the hierarchical clustering tree was constructed by using the dynamic hybrid tree cutting technology. We set the minimum module size to 30 and the minimum height of the combined module to 0.25. Naming genomes with different colors was found to be convenient for distinguishing different gene modules in the subsequent gene function recognition and visual analysis. According to the p value, GeneRatio and the number of differentially expressed genes annotated in the pathway, the KEGG pathway enrichment analysis of the key modules was carried out. Finally, the topological overlap measure from the WGCNA was displayed using Cytoscape 3.9.1 to illustrate the network.

Statistical analysis

The mean and standard deviation of the chlorophyll SPAD value and lipid data were calculated using Microsoft Excel 2019. One-way analysis of variance (ANOVA) with Duncan's test was performed using SPSS 22.0. Differential lipids were analyzed by MetaboAnalyst 5.0 (https://www.metaboanalyst.ca/). Principal component analysis (PCA), partial least-squares discriminant analysis (PLS-DA) were performed using SIMCA14.0. Heatmaps were generated using TBtools software. Correlation analysis was performed using Hiplot software (https://hiplot.com.cn). The correlation data network diagrams and coexpression network diagrams were generated using Cytoscape 3.8.2 software.

Results

Phenotypic characterization of BJG

We observed the second leaf of the BJG after different shading durations. Under normal conditions, the second leaf of BJG remained yellow. After shading treatment, the BJG leaf turned into green within one day, and this process could be reverted by again subjecting the leaves again to strong light (Figure 1A). Moreover, the chlorophyll SPAD value of the leaves under shading increased gradually and was significantly higher than that under light ($P<0.05$). However, the SPAD value after light restoration showed little change compared with that before shading (Figure 1B). The results showed that the shading treatment turned the leaves of BJG into green and increased the chlorophyll content.

Overall lipidomics analysis of BJG after different shading duration

According to the significant difference in chlorophyll SPAD values, we examined 5 samples for lipidomics detection and analysis. First, we conducted multivariate statistical analysis, which can provide preliminary insights into the overall differences between samples as well as variation between samples within groups. Clear differentiation in the samples was observed in the PCA score plot (Figure 2A). The cumulative contribution rates of the first (PC1) and second principal components (PC2) reached 96.58%, which indicated that the fit of the model was high and that the multidimensional statistical analysis results were reliable. Moreover, the cross-validation with 200 permutation tests indicated that the PLS-DA model was reliable and was not overfit (Figure 2B).

Glycerolipids, including phospholipids, glycolipids and neutral lipids, are the most abundant lipids in plants. In this study, 156 lipid molecules were detected, including 16 DGDG, 16 MGDG, 13 PG, 5 lyso phosphatidylglycerols (LPG), 6 LPC, 5 lysophosphatidylethanolamine (LPE),20 PC, 23 phosphatidylethanolaines (PE), 14 phosphatidylinositols (PI), 26 phosphatidylserines (PS) and 12 PA (Figure 3A). As shown in Figure 3B, lipids were classified into 3 lipid categories. The proportions of the different molecules and lipid classes in BJG were analyzed according to their relative contents. Among the lipid subclasses, PC and MGDG accounted for the largest proportion, and the lipids that showed large changes included PA, PE and PC. In BS1, the proportion of PC and PE decreased, while the proportions of PA increased (Figure 3B). Overall, glycerophospholipids accounted for the largest proportion, ranging from 58% to 68.3%, and the proportion after shading and light restoration was lower than that before shading (Figure 3C). Additionally, we calculated the content of total polar lipid content and found that it decreased after shading. Moreover, the content was the highest in BS0 and the lowest in BRL3 (Figure 3D).

Glycolipid changes in BJG after shading and recovery light treatments

MGDG and DGDG are the main components of the thylakoid membrane in plants. The changes in the contents

10.3389/fpls.2022.1035119

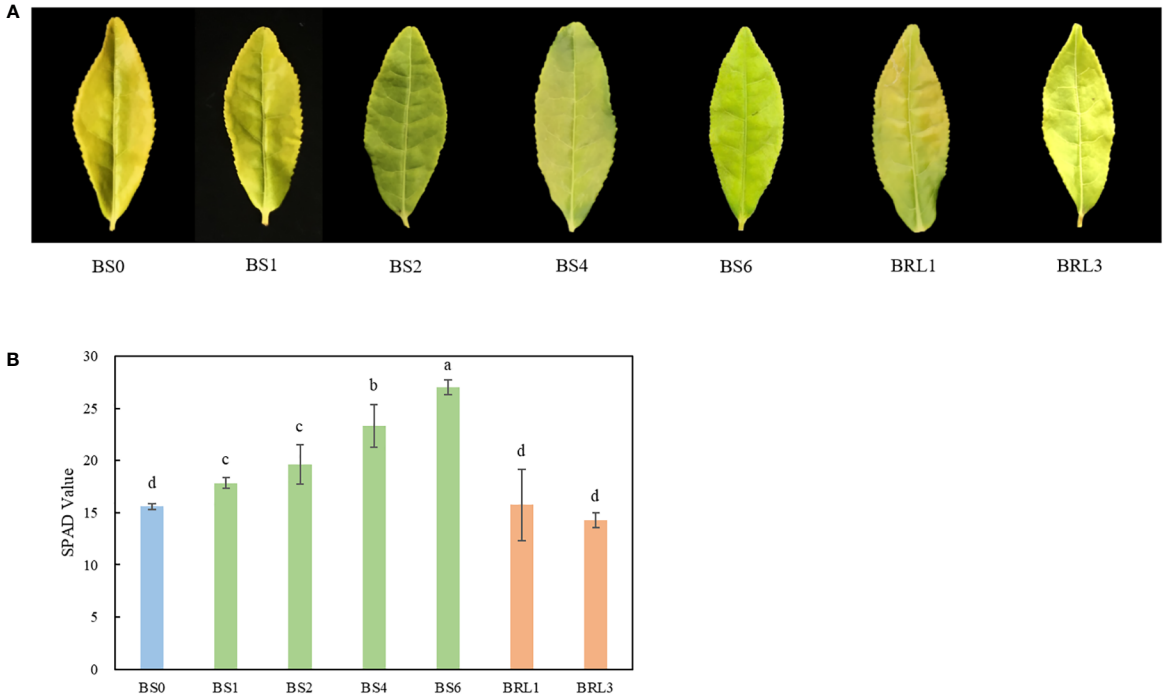

FIGURE 1
Leaf color phenotype and the SPAD value of BJG after shading and recovery light treatments. **(A)** Phenotypic expression and **(B)** the SPAD value of BJG under natural light (BS0), shading for 1 day (BS1), shading for 2 days (BS2), shading for 4 days (BS4), shading for 3 days then light recovery for 1day (BRL1), and shading for 3 days then light recovery for 3 days (BRL3). Data and error bars are the mean ± SD (n = 5). Different lowercase letters indicate a significant difference between the means at $P<0.05$.

of MGDG and DGDG in BJG showed the same trends as those of total lipids. Both lipids decreased sharply in BS1, then increased significantly in BS4, and decreased again in BS6. These lipids also showed a downward trend after returning to light exposure for 3 days (Figures 4A, E). MGDG and DGDG accounted for approximately 1/5 and 1/8 of the total lipids in BJG, respectively. As an important lipid molecule in tea, MGDG (36:6) accounted for the largest proportion in leaves. In BS0, its content was the highest, which reached 19.56 nmol/mg dw, and in BRL3, its content was the lowest at

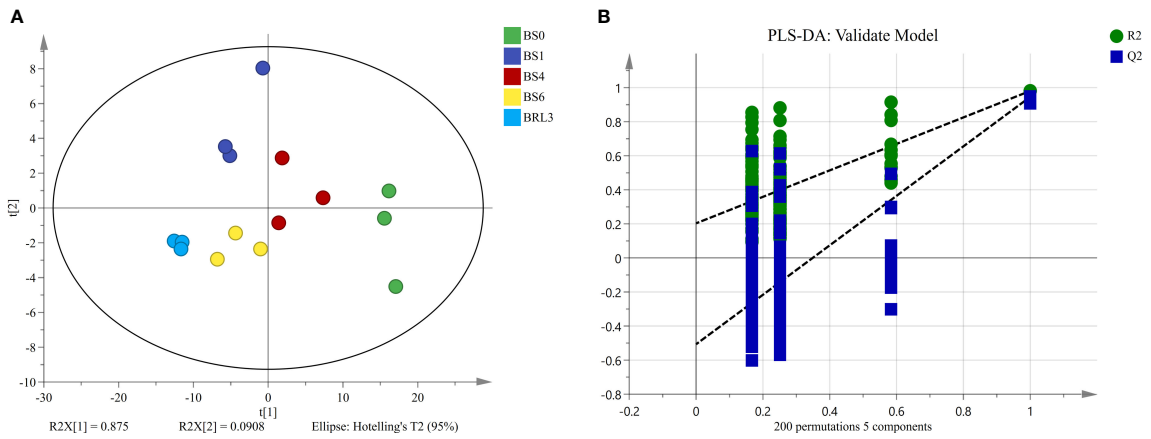

FIGURE 2
Unsupervised and supervised multivariate analysis of the detected lipids in BJG. **(A)** PCA score plot. **(B)** PLS-DA cross-validation plot.

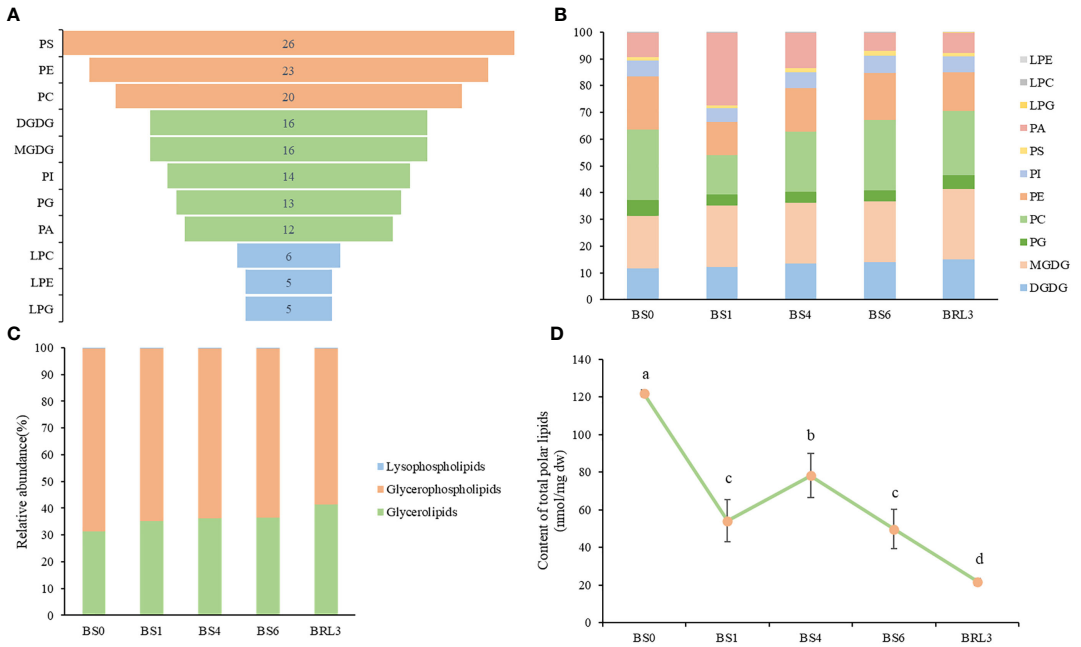

FIGURE 3
Overall lipidomics analysis of in BJG. **(A)** Distribution of each lipid subclass identified. **(B)** Changes of lipid subclasses in BJG after shading and light recovery treatments. **(C)** Lipid categories identified in BJG after shading and light recovery treatments. **(D)** Changes in the content of total polar lipids after shading and light recovery treatments. Data and error bars are the mean ± SD (n = 3). Different lowercase letters indicate a significant difference between the means at $P<0.05$.

4.47 nmol/mg dw. Similarly, among the DGDG species, DGDG (34:3) and DGDG (36:6), which are the main DGDG lipid molecules, have displayed their highest contents in BS0, which were 5.23 nmol/mg dw and 5.71 nmol/mg dw respectively. In BRL3, the lowest values were 1.27 nmol/mg dw and 1.25 nmol/mg dw, respectively (Table S1). By analyzing the ratios of MGDG (36:6)/MGDG and DGDG (36:6)/DGDG, we found that these ratios gradually decreased after shading and reached their lowest in BS6; These ratios then increased under light, and were highest in BS0 (Figure 4B).

The MGDG/DGDG ratio plays an important role in maintaining the structure and function of photosynthetic organs, which affects the permeability of the chloroplast membrane and the stability of the membrane bilayer (Block et al., 1983). The ratios of MGDG/DGDG in BS1 and BRL3 were higher than those in the other samples (Figure 4C). The membrane lipid/chlorophyll ratio is an indicator of the density of thylakoid assembly proteins. The higher the ratio is, the lower the density of the assembly protein is, which reflects the destruction of the fluidity, structure and function of the membrane (Haferkamp and Kirchhoff, 2008; Kirchhoff et al., 2013). The ratios of MGDG/chlorophyll and DGDG/chlorophyll decreased significantly as the number of treatment days increased (Figure 4D).

Glycerophospholipid and lysophospholipid changes in BJG after shading and recovery light treatments

Glycerophospholipids are also plant lipid components. A total of 108 glycerophospholipids were detected, which were mainly including PG, PC, PE, PI, PS and PA. As shown in Figure 5, comparing the overall glycerophospholipid type and contents comparison, after shading and light restoration, their changes in content were significantly different. Most phospholipids were higher in BS0, decreasing significantly after one day of shading, and the difference was the most significant after three days of light restoration. Lysophospholipids, which can be used as signaling molecules, are produced by the partial hydrolysis of phospholipids. The contents of LPC, LPG and LPE in BJG decreased dramatically to approximatlly after shading for one day.

Analysis of significantly different lipids in BJG after shading and recovery light treatments

After descriptive statistics of the lipids, we used VIP in the PLS-DA model to analyze the difference in BJG after shading

10.3389/fpls.2022.1035119

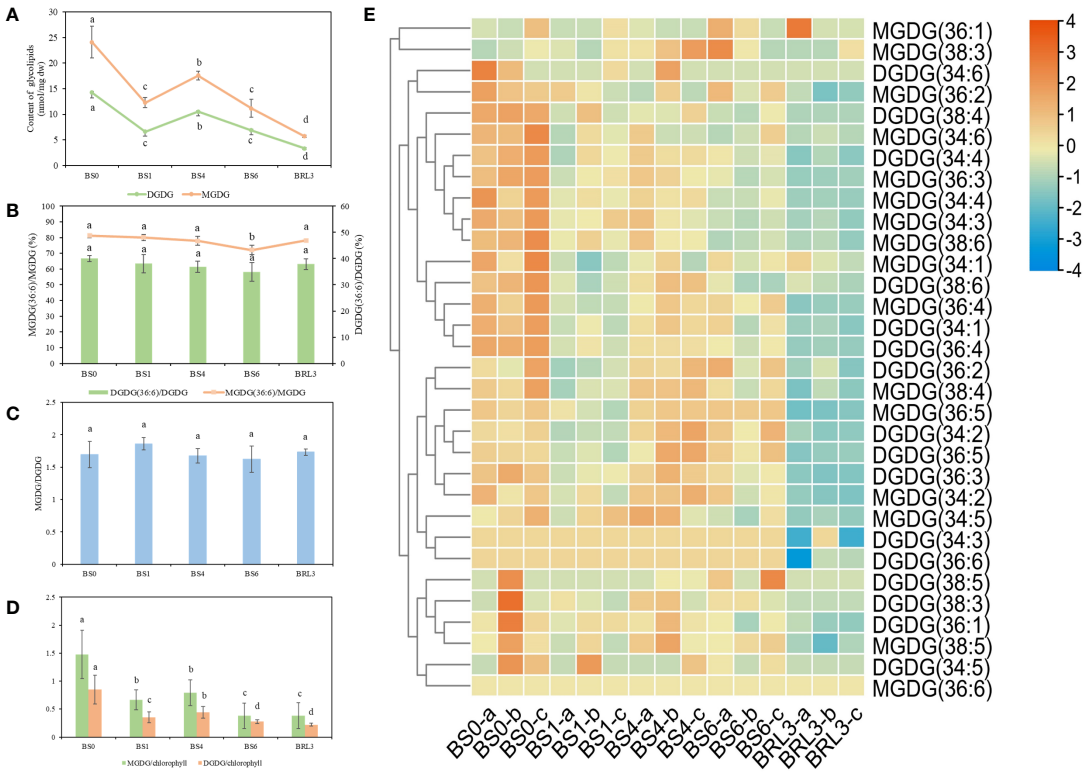

FIGURE 4
Changes in glycolipids in BJG after shading and light recovery treatments. **(A)** Changes in MGDG and DGDG contents in BJG after shading and light recovery treatments. **(B)** The ratio changes in the MGDG (36:6)/MGDG and DGDG (36:6)/DGDG ratios after shading and light recovery treatments. **(C)** The changes in the MGDG/DGDG ratio after shading and light recovery treatments. **(D)** The changes in the MGDG/chlorophyll and DGDG/chlorophyll ratios after shading and light recovery treatments. **(E)** Heatmap of glycolipid changes. Data and error bars are the mean ± SD (n = 3). Different lowercase letters indicate a significant difference between the means at $P<0.05$. Each colored cell on the map corresponds to the content of different lipid species. Orange color indicates a high content, and blue color indicates a low content.

and light recovery treatments. This value represents the contribution of each variable to the model. When VIP ≥1.0 and $P < 0.05$, lipids were considered to be significantly different. Overall, a total of 37 kinds of lipids were identified, including 6 MGDG, 8 DGDG, 2 PI, 6 PS, 4 PC, 6 PE and 5 PA (Figure 6A). Notably, MGDG (36:5), PC (34:3), DGDG (36:5) and DGDG (34:2) gave relatively high VIP scores. Hence, these four substances play a crucial role in BJG after shading and light recovery treatments. After constructing the heatmap, all differential lipids in BRL3 showed a significant negative correlation with the other treatments. In BS0, approximately 24 differential lipids showed a positive correlation with the other treatments, among a significant positive correlation was observed with BS1 and BRL3. We also found that in BS6 and BRL3, PA (34:1), PA (36:6), PA (34:2), PA (34:3) and PA (36:5) showed a significant negative correlation compared with BS0, BS1 and BS4 (Figure 6B).

Chloroplasts are not only the site of plant photosynthesis, but also the major site for fatty acid synthesis. Therefore, we mapped the correlation networks between the chlorophyll SPAD values and 37 different lipids under shading and light conditions, respectively. It can be seen from Figure 6C and Figure S1A show that under shading conditions, most differential lipids were negatively correlated with the chlorophyll SPAD value, among which PA (34:2), MGDG (36:6), DGDG (34:3) and DGDG (36:6) were significantly negatively correlated with the chlorophyll SPAD value (more blue lines). On the contrary, 24 kinds of lipids showed a significant positive correlation with chlorophyll under light conditions (more red lines). They were 5 MGDG, 5 DGDG, 2 PS, 4 PC, 2 PI and 6 PE, including MGDG (36:6), DGDG (34:3) and DGDG (36:6) (Figure 6D and Figure S1B).

Expression patterns of key genes in lipid metabolism pathways

Based on the changes in polar lipids observed during BJG shading, we focused on the expression patterns of key genes related to the lipid biosynthesis pathway. Among them, we

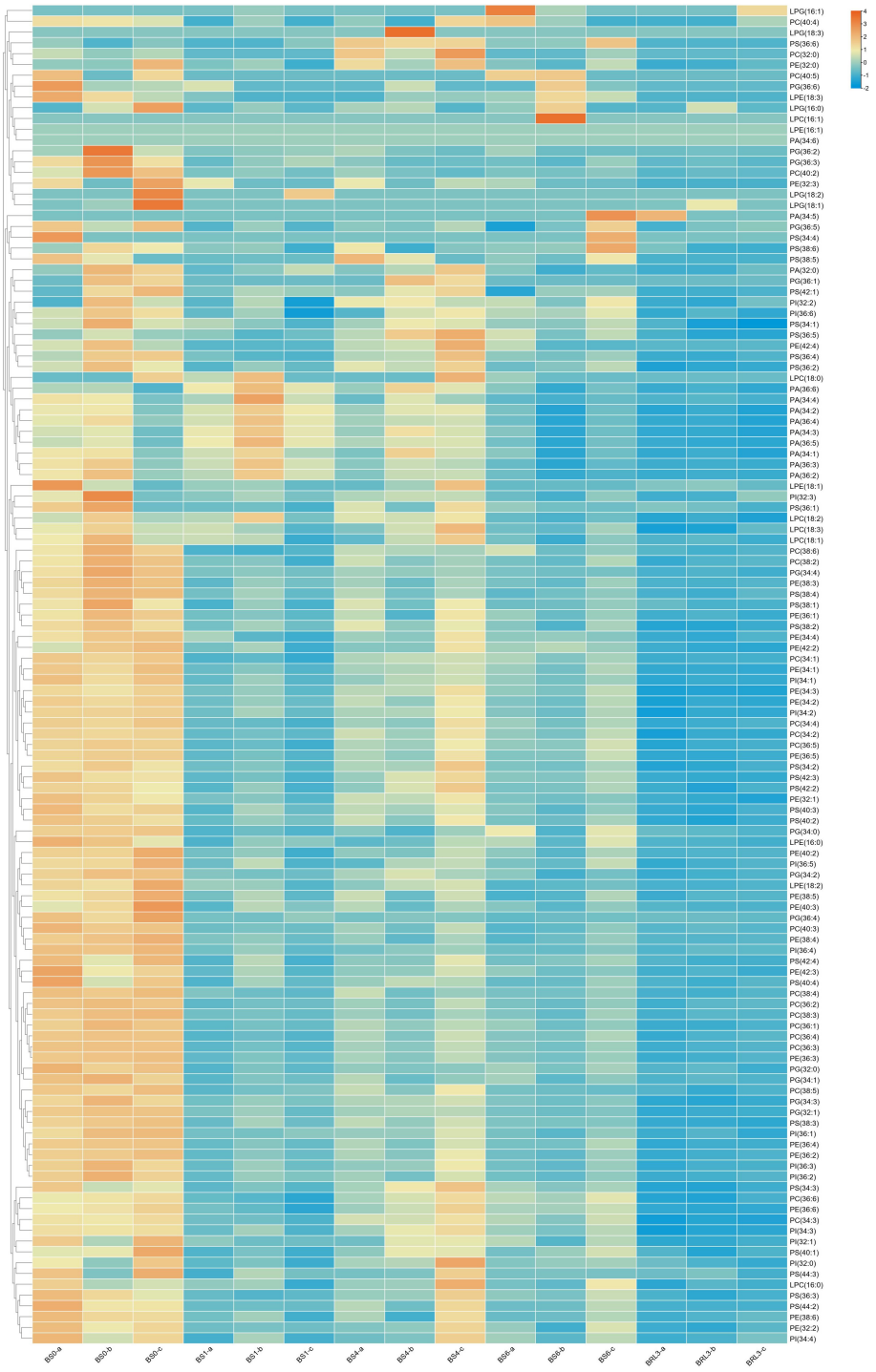

FIGURE 5
Heatmap of the changes in glycerophospholipid and lysophospholipid contents in BJG after shading and light recovery treatments. Each colored cell on the map corresponds to the content of a different lipid species. Orange color indicates a high content, and blue color indicates a low content.

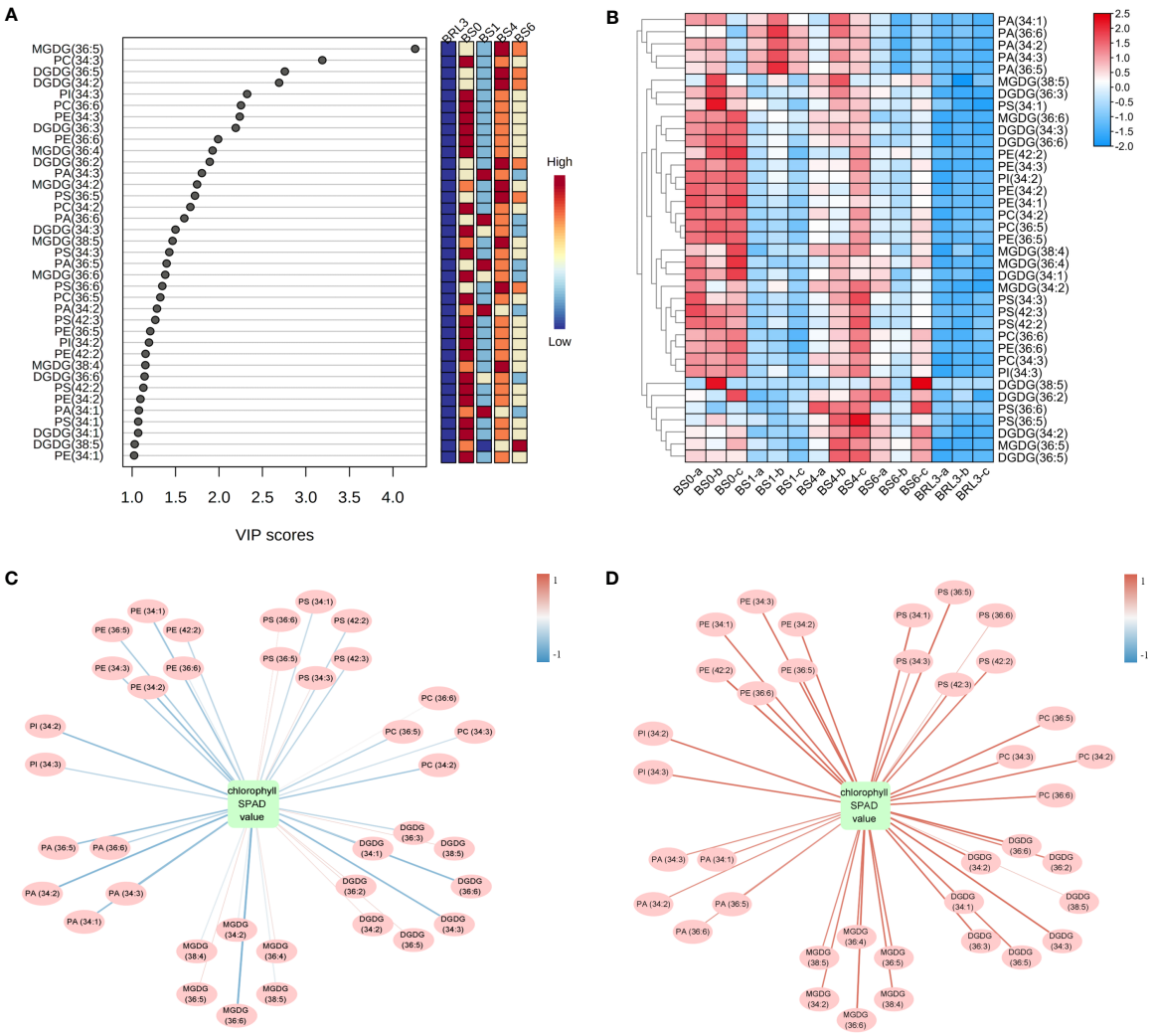

FIGURE 6
Statistical analysis of the differential lipid molecules. **(A)** Scores (VIP ≥1.0) of lipid species by PLS-DA in BJG. **(B)** Heatmap of the differential lipid changes in BJG after shading and light recovery treatments. Each colored cell on the map corresponds to the content of different lipid species. Red color indicates high, and blue color indicates low. **(C)** Correlation network between differential lipid molecules and chlorophyll SPAD value in BJG after shading. **(D)** Correlation network between differential lipid molecules and chlorophyll SPAD values in BS0 and BRL3. The red line indicates a positive correlation, the blue line indicates a negative correlation, and the darker the color is, the stronger the correlation.

focused on the key genes in glycerolipid metabolism and glycerophospholipid metabolism. As shown in Figure 7A, the genes involved in the synthesis of PA and MGDG (*GPAT*, *plsC*, *MGD*, *GLA*) were downregulated after shading and upregulated after light recovery. Genes involved in *DGD* also showed the same trend.

The metabolic pathway of glycerophospholipid is mainly involved in the synthesis of polar lipids such as PC, PE and PG. The genes involved in PG synthesis, *cdsA*, *PGS1* and *GEP4*, were downregulated in BS1 and upregulated after light recovery. *LPGAT* showed the opposite trend. The synthesis of PE is mainly involves by *ENTK*, *PCYT2*, *EPT1*, *psd* and *LPCAT4*. Except for *LPCAT4*, these genes were up-regulated under light and downregulated after shading. The same was true for the synthesis of PS, which PI was just the opposite. PC is mainly synthesized from choline and PE. Among these genes, *CPT1* showed the same trend as the other phospholipid synthetases and was downregulated after shading. However, *CKI1*, *PCYT1* and *plc* had no obvious trend. In summary, we found that the contents of polar lipids and gene expression were consistent in BS0 and BS1, and the expression of synthetic genes increased, and the lipid content also increased. However, in BRL3, the content of polar lipids was inconsistent gene expression (Figure 7B).

10.3389/fpls.2022.1035119

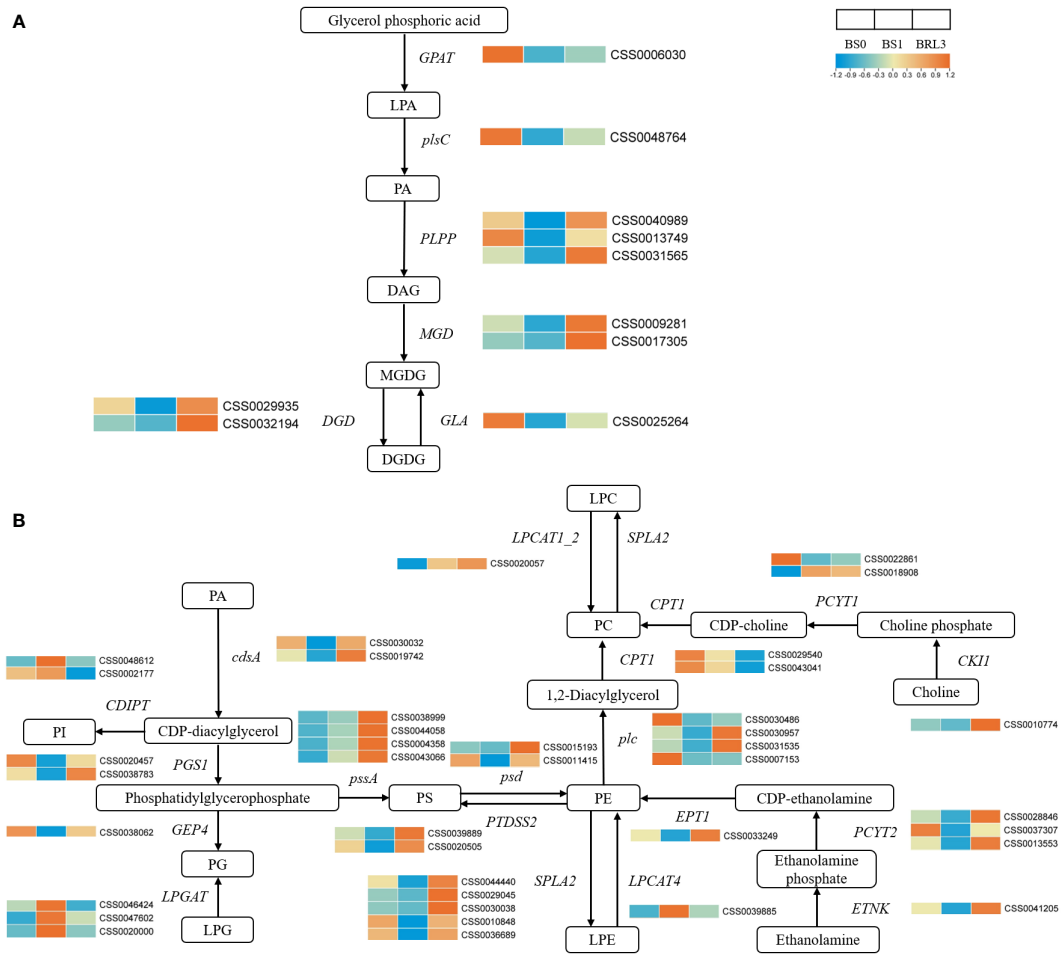

FIGURE 7
Effects of shading and light restoration on the expression of key genes in the pathway of Glycerolipid metabolism and Glycerophospholipid metabolism in BJG. **(A)** The expression of key genes in the pathway of glycerolipid metabolism. *GPAT*, glycerol-3-phosphate O-acyltransferase; *plsC*, 1-acyl-sn-glycerol-3-phosphate acyltransferase; *PLPP*, phosphatidate phosphatase; *MGD*, 1, 2-diacylglycerol 3-beta-galactosyltransferase; *DGD*, DGDG synthase; *GLA*, alpha-galactosidase. **(B)** The expression of key genes in the pathway of glycerophospholipid metabolism. *cdsA*, phosphatidate cytidylyltransferase; *PGS1*, CDP-diacylglycerol-glycerol-3-phosphate 3-phosphatidyltransferase; *GEP4*, phosphatidylglycerophosphatase; *LPGAT*, lysophosphatidylcholine acyltransferase; *pssA*, CDP-diacylglycerol-serine O-phosphatidyltransferase; *psd*, phosphatidylserine decarboxylase; *PTDSS2*, phosphatidylserine synthase 2; *SPLA2*, secretory phospholipase A2; *LPCAT4*, lysophospholipid acyltransferase; *plc*, phospholipase C; *LPCAT1_2*, lysophosphatidylcholine acyltransferase/lyso-PAF acetyltransferase; *CPT1*, diacylglycerol cholinephosphotransferase; *PCYT1*, choline-phosphate cytidylyltransferase; *CKI1*, choline kinase; *ETNK*, thanolamine kinase; *PCYT2*, ethanolamine-phosphate cytidylyltransferase; *EPT1*, ethanolaminephosphotransferase; *CDIPT*, CDP-diacylglycerol-inositol 3-phosphatidyltransferase. Orange color indicates high, and blue color indicates low.

WGCNA analysis

To further study the change in the pattern of membrane lipid content after BJG shading treatment, we selected DGDG (36:6), MGDG (36:6) and DGDG (34:3), which were significantly related to the chlorophyll SPAD value as phenotypic traits, and used WGCNA to search for coexpressed genes. A total of 5 modules (distinguished by different colors) were obtained, and the number of genes included in the different modules ranged from 502 to 2665. Figures 8A, B showed that the Memagenta module and Meblue module displayed the most significant positive correlation with the contents of these key lipids, so we conducted further analysis on these two modules.

Functional and pathway enrichment analysis

The genes in the Memagenta and Meblue modules were analyzed for function and pathway enrichment. As shown in Figure S2A, pathways such as phenylpropanoid biosynthesis and glycerophospholipid metabolism are enriched in the Memagenta

module. “protein processing in endoplasmic reticulum”, “phenylpropanoid biosynthesis”, “biosynthesis amino acid”, “carbon metabolism” and “flavonoid biosynthesis” were enriched in the Meblue module (Figure S2B).

Lipid-related coexpressed gene networks

The top 100 unigenes (kME > 0.7) in the Memagenta module and Meblue module were used to construct the coexpression network, and transcription factors and lipid-related genes were selected as key hub genes in combination with KEGG enrichment. As shown in the Figure 8C, we identified 13 key hub genes in the Memagenta module, including one *Dof* TF (CSS0004951), one *ERF* TF (CSS0017764), one *ACE* gene (CSS0029035), one *GPAT* (CSS0016066), one *VPS18* (CSS0039624), 1 *OSBP* (CSS0049488) and 7 *GLIP* genes (CSS0012159, CSS0034282, CSS0014773, CSS0032332, CSS0034252, CSS0025222, CSS0034819). Similarly, in the Meblue module, we also identified 13 key hub genes. These genes included six TFs and seven lipid- related genes: one *bHLH* TF (CSS0038310), three MYB-related TFs (CSS0005060, CSS0018453, CSS0032956), one *MYB 12* TF (CSS0021675) and one *HY5* TF (CSS0048476), one *fabI* gene (CSS0044108), one *GCP6* gene (CSS0018280), one *ACE* gene (CSS0014865), one *ACS* gene (CSS0005240), one *PATL6* gene (CSS0027961), one *CXE* gene (CSS0037283) and one *ACC1* gene (CSS0020243) (Figure 8D). These results

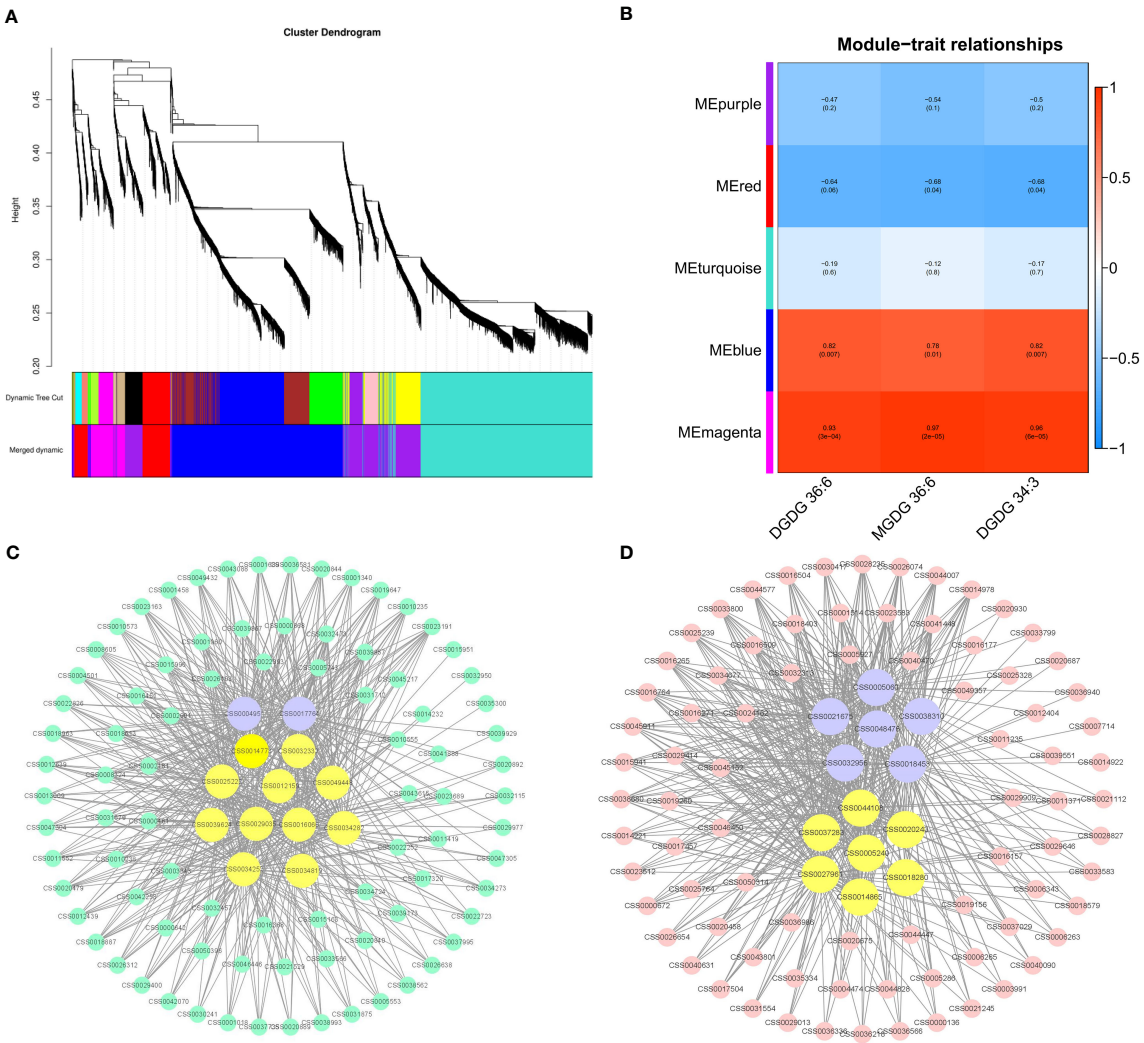

FIGURE 8
Coexpression analysis networks of lipids related to albino leaf color in BJG. **(A)** Cluster dendrogram and gene modules after WGCNA analysis. **(B)** Correlation between five gene modules and the contents of three important lipid contents. **(C)** Coexpression network of candidate genes in the Memagenta module. **(D)** Coexpression network of candidate genes in the Meblue module.

indicate that the lipid metabolism in BJG involves a complex molecular regulation process.

Discussion

To date, many studies have focused on the regulatory mechanism of chlorophyll metabolism in albino tea plants, and multiomics analysis is an excellent tool for such research (Xu et al., 2020; Liu et al., 2022; Zhang et al., 2022a; Zhang et al., 2022b). However, there has been no comprehensive study on the response of lipid metabolism to light in albino tea plants. Therefore, the purpose of our research was to understand the changes in the lipid response to light in albino tea plants, and to try to determine the key pathways and genes involved in these lipid changes to make good use of the advantages of albino tea plants in tea cultivation and breeding.

The leaf color of BJG was regulated by light intensity

The mechanism of plant leaf albinism may involve multiple regulatory pathways and metabolic processes, and may be affected by the interactions with internal and external factors (Costa et al., 2006). In higher plants, the occurrence of white or yellow leaves mainly depends on the biosynthesis and transportation of chlorophyll. Chlorophyll absorbs light energy and transfers it to other molecules in the photosynthetic electron transport chain (Liu et al., 2009). Therefore, the leaf phenotype of albino teas is closely related to chlorophyll content and is regulated by light intensity. BJG is more sensitive to high light intensity; its chloroplast development is retarded, and its chlorophyll content is lower than that of other green-leaf varieties at the same developmental stage (Wu et al., 2016). Moreover, the chlorophyll accumulation in plants is dynamic (Tian et al., 2011; Ding et al., 2016) and is a comprehensive process of synthesis and decomposition. Our studies have shown that the SPAD value of BJG leaves basically did not change in the natural environment, while increased linearly with shading treatment. The leaves notably turned green after shading treatment, while they returned to yellow if light treatment is resumed. *Huangjinya* is one of the most widely studied albino tea varieties, and shading treatment significantly increases its chlorophyll content (Fan et al., 2019). Similarly, the yellow or pale leaves of *Yujinxiang* also turned green under weak light intensity after shading, and the green leaves induced by shading recovered their yellow or pale color again by re-exposure to natural sunlight (Xu et al., 2020). This revealed that light plays a key role in regulating leaf color.

BJG responds to light changes by changing the lipid contents and proportions

The effect of membrane lipids on the photosystem is multifaceted. When subjected to environmental stress, plants protect themselves from damage by changing the composition of membrane lipids to maintain normal growth. Under normal light, the polar lipids in BJG are generally maintained at a high level. The most important unsaturated fatty acids in DGDG and MGDG, account for a large proportion, so that albino leaves can adapt to normal light and grow to be healthy. The contents of MGDG and DGDG in cold-tolerant pepper varieties were higher than those in low-temperature-sensitive varieties, which could better maintain the membrane homeostasis (Xu et al., 2021). Plants maintain a balance between the physical state of the membrane and the normal function of membrane proteins by adjusting the ratio of MGDG/DGDG (Narasimhan et al., 2013). When the ratio is high, the membrane stability is better and the thylakoid membrane integrity is higher; when the ratio is low, the thylakoid membrane structure is unstable. The ratio of MGDG/DGDG in albino leaves was low, and the thylakoid membrane structure was unstable. After shading, the leaf color gradually turned green, and the ratio suddenly rose. The thylakoid membrane tends to be complete at first, and then its structure becomes structure is unstable after the light is removed. This means that BJG can respond quickly to changes in light. After the restoration of light, the ratio was similar to that under normal light conditions, indicating that the thylakoid membrane structure remained a relatively stable state at this time. However, the ratios of membrane lipid/chlorophyll (MGDG/chlorophyll and DGDG/chlorophyll), which are indicators of thylakoid assembly protein density, decreased with increasing treatment time, indicating that the thylakoid assembly protein density increased from low to high, and the membrane structure gradually stablized. This is consistent with a study in peppers (Xu et al., 2021). This stability may represent an adaptive strategy that enables plants to tolerate stress by maintaining cell membranes in a physical state that supports the normal functions of membrane proteins. According to the correlation analysis, we discovered three key lipid components that are significantly related to the chlorophyll SPAD value, which are MGDG (36:6), DGDG (36:6) and DGDG (34:3), which are found that they are thylakoid membrane lipids with high contents. This further suggested that membrane lipids can respond to light and promote the color changes in light-sensitive albino tea leaves.

The genes *HY5* and *GLIP* can participate in the lipid regulation of albino tea leaves

Changes in the composition, contents and proportions of membrane lipids will lead to changes in the integrity of the

thylakoid membrane, and genes in the lipid metabolism pathway can respond over time. To explore the mechanism of the lipid response to leaf color changes in light-sensitive albino tea plants, we performed transcriptome sequencing of BJG leaves exposed to different light treatments. Lipid metabolism is regulated by many genes and TFs (Afitlhile et al., 2015; Afitlhile et al., 2021). An increase in membrane lipid synthesis gene expression can promote membrane lipid synthesis, thus allowing the thylakoid membrane structure to be intact. Genes involved in the synthesis of PA, MDGD and DGDG (*GPAT*, *PLSC*, *MGD*, *DGD*, *GLA*) were downregulated after shading and upregulated after light recovery, which indicated that light could promote the synthesis of lipids in albino leaves, while shading had the opposite effect. This also explains why the lipid content in BS0 was higher but significantly decreased after shading. Similar results have been confirmed in Arabidopsis. *MGD1* can be upregulated by light, and the expression of *MGD1* in etiolated seedlings of wild-type Arabidopsis thaliana increased twofold after 6 hours of light exposure. The expression of *DGD1* in wild-type seedlings increased after illumination, while the expression of *DGD2* remained unchanged (Kobayashi et al., 2014). However, the expression of synthetic genes is not consistent with their contents after light recovery, so we speculate that lipid degradation genes may be involved. The genes involved in PG synthesis, *cdsA*, *PGS1* and *GEP4*, were downregulated in BS1 and upregulated after light recovery. *LPGAT* displayed the opposite trend. Therefore, we speculate that change in PG content after shading is mainly caused by the degradation of LPG.

In this study, we found 8 TFs and 18 hub genes based on WGCNA, which may be related to lipid metabolism. The TFs were one *Dof* (CSS0004951), one *ERF* (CSS0017764), one *bHLH* TF (CSS0038310), three *MYB-related* TFs (CSS0005060, CSS0018453, CSS0032956), one *MYB 12* TF (CSS0021675) and one *HY5* TF (CSS0048476). *Dof* TFs are a family of plant-specific transcription factors (Yanagisawa, 2002). It has been reported that proteins containing the Dof domain are involved in many different plant-specific physiological processes, including light-dependent gene regulation in maize (Yanagisawa and Sheen, 1998). *HY5*, a transcription factor of the *bZIP* class, is located downstream of photoreceptors and transmits light signals to downstream acting-elements. Under light and dark changes, the dynamic processes of *HY5*, *COP1* and *ABI4* in the nucleus and cytoplasm regulate the key genes of many tetrapyrrole synthetases, such as *PORA*, *HEMA2* and *FC2* (Burko et al., 2020; Hand and Shabek, 2022). Therefore, this will affect the chlorophyll biosynthesis process. In addition, *HY5* also targets many genes involved in lipid biosynthesis, such as *DGD1*, *FAD3*, and *FAD6*. Genome-wide analysis has identified that *DGD1* and *CHLH* are direct targets of *HY5* (Lee et al., 2007). Similar studies have also found that during the process of photomorphogenesis, light signals through *HY5* and cytokinin signals through *AHK2* and *AHK3* were involved in the up regulation of *MGD1* and *DGD1* (Kobayashi et al., 2014). In our research, the expression of *HY5* was significantly downregulated after shading and upregulated after light recovery (Figure S3), showing the same expression trend as lipid-related genes such as *DGD*, which further confirmed that *HY5* was closely related to lipid biosynthesis.

GPAT was identified among the 18 hub genes. This is an important group of enzymes that catalyzes the acylation of sn-glycerol-3-phosphate at sn-1 or sn-2 to produce lysophosphatidic acid. This reaction is the first step in the assembly of stored lipids and is also important in polar and extracellular lipid biosynthesis (Jayawardhane et al., 2018). For example, overexpression of *SsGPAT* in the halophyte *Suaeda salsa* in Arabidopsis leads to enhanced salt tolerance, which may be to alleviate the photoinhibition of PSII and PSI under salt stress by increasing the content of unsaturated fatty acids (Sui et al., 2017). Similarly, in this study, the expression of *GPAT* under natural light was higher than that under shading, which could also confirm its contribution to alleviating photoinhibition.

In particular, we found 7 *GLIP* genes (CSS0012159, CSS0034282, CSS0014773, CSS0032332, CSS0034252, CSS0025222, CSS0034819), which are the members of a subfamily of lipolytic enzymes with broad substrate specificity that have been widely identified in plants (Gao et al., 2017). Physiologically, the GDSL esterase/lipase found is mainly involved in the regulation of plant development, morphogenesis, secondary metabolite synthesis and defense response (Oh et al., 2005; Kwon et al., 2009; Agee et al., 2010). The comprehensive lipid profiling analysis of rice by some researchers showed that the *OsGLIP* gene negatively controls rice defense by regulating lipid metabolism. Changes in *OsGLIP* expression is related to the significant changes in lipid species (including MGDG and DGDG), which are most likely to be inhibitors of the immune response in rice. Exogenous addition of MGDG and DGDG can reduce disease resistance (Gao et al., 2017). In our study, the expression of *GLIP* genes in BS0 was significantly higher than that in BS1 and BRL3, and the contents of MGDG and DGDG were also maintained at a high level (Figure S3). Therefore, this result can also explain why the stress resistance in albino leaves is poor, and provide a new idea for tea breeding.

Conclusion

Our study compared the effects of light intensity on the lipid metabolites and transcripts in albino tea plants, and found that the leaf color of BJG was regulated by light intensity and responded to light changes by changing the lipid contents and proportions. Three lipids that were significantly related to the chlorophyll SPAD value were found among the differential lipids: MGDG (36:6), DGDG (36:6) and DGDG (34:3). The results of WGCNA analysis indicated that the *HY5* and *GLIP* genes may be hub genes involved in lipid regulation in albino

leaves. These results can further explain the changes in tea leaf color in response to light. Therefore, the future research can focus on explaining the interaction between these hub genes and TFs, with an aim to provide a reference for genetic breeding and research on albinism mechanisms.

Data availability statement

The data presented in the study are deposited in the OMIX, China National Center for Bioinformation/Beijing Institute of Genomics, Chinese Academy of Sciences, accession number OMIX002015.

Author contributions

WS, MC, ZC, and QW conceived and designed the experiments; ZZ performed the experiments; ZZ analyzed the data; ZZ wrote the manuscript; and MC, QW, and WZ revised the manuscript critically. WS and ZC oversaw the project. All the authors read and approved the final manuscript.

Funding

This work was financially supported by the Fujian Agriculture and Forestry University Construction Project for Technological Innovation and Service System of Tea Industry Chain (K1520005A01/K1520005A04), the National Natural Science Foundation of China (31770732), the cooperative project of production and study in universities of Fujian Province (2019N5007), Special Fund for Science and TechnologyInnovation of Fujian Zhang Tianfu Tea Development Foundation (FJZTF01).

Acknowledgments

Thanks are extended to Shixian Cao and Shuntian Yu for support in sample gathering, and the Kansas Lipidomics Research Center for lipid analysis.

Conflict of interest

The authors declare that the research was conducted in the absence of any commercial or financial relationships that could be construed as a potential conflict of interest.

Publisher's note

All claims expressed in this article are solely those of the authors and do not necessarily represent those of their affiliated organizations, or those of the publisher, the editors and the reviewers. Any product that may be evaluated in this article, or claim that may be made by its manufacturer, is not guaranteed or endorsed by the publisher.

Supplementary material

The Supplementary Material for this article can be found online at: https://www.frontiersin.org/articles/10.3389/fpls.2022.1035119/full#supplementary-material

References

Afitlhile, M., Fry, M., and Workman, S. (2015). The TOC159 mutant of arabidopsis thaliana accumulates altered levels of saturated and polyunsaturated fatty acids. *Plant Physiol. Biochem.* 87, 61–72. doi: 10.1016/j.plaphy.2014.12.018

Afitlhile, M., Worthington, R., Heda, G., and Brown, L. (2021). The TOC159 null mutant of arabidopsis thaliana is impaired in the accumulation of plastid lipids and phosphatidylcholine. *Plant Physiol. Biochem.* 159, 148–159. doi: 10.1016/j.plaphy.2020.12.011

Agee, A. E., Surpin, M., Sohn, E. J., Girke, T., Rosado, A., Kram, B. W., et al. (2010). MODIFIED VACUOLE PHENOTYPE1 is an arabidopsis myrosinase-associated protein involved in endomembrane protein trafficking. *Plant Physiol.* 152 (1), 120–132. doi: 10.1104/pp.109.145078

Benning, C. (2009). Mechanisms of lipid transport involved in organelle biogenesis in plant cells. *Annu. Rev. Cell Dev. Biol.* 25 (1), 71–91. doi: 10.1146/annurev.cellbio.042308.113414

Block, M. A., Dorne, A.-J., Joyard, J., and Douce, R. (1983). Preparation and characterization of membrane fractions enriched in outer and inner envelope membranes from spinach chloroplasts. II. biochemical characterization. *J. Biol. Chem.* 258 (21), 13281–13286. doi: 10.1016/S0021-9258(17)44113-5

Boudière, L., Michaud, M., Petroutsos, D., Rébeillé, F., Falconet, D., Bastien, O., et al. (2014). Glycerolipids in photosynthesis: composition, synthesis and trafficking. *Biochim. Biophys. Acta (BBA)-Bioenerg.* 1837 (4), 470–480. doi: 10.1016/j.bbabio.2013.09.007

Burko, Y., Seluzicki, A., Zander, M., Pedmale, U. V., Ecker, J. R., and Chory, J. (2020). Chimeric activators and repressors define HY5 activity and reveal a light-regulated feedback mechanism. *Plant Cell* 32 (4), 967–983. doi: 10.1105/tpc.19.00772

Chapman, K. D., and Ohlrogge, J. B. (2012). Compartmentation of triacylglycerol accumulation in plants. *J. Biol. Chem.* 287 (4), 2288–2294. doi: 10.1074/jbc.R111.290072

Costa, L., Vicente, A. R., Civello, P. M., Chaves, A. R., and Martínez, G. A. (2006). UV-C treatment delays postharvest senescence in broccoli florets. *Postharvest Biol. Technol.* 39 (2), 204–210. doi: 10.1016/j.postharvbio.2005.10.012

Ding, Y., Wu, G., and Guo, C.-k. (2016). Research advance on chlorophyll degradation in plants. *Biotechnol. Bull.* 32 (11), 1. doi: 10.13560/j.cnki.biotech.bull.1985.2016.11.001

Djanaguiraman, M., Boyle, D., Welti, R., Jagadish, S., and Prasad, P. (2018). Decreased photosynthetic rate under high temperature in wheat is due to lipid desaturation, oxidation, acylation, and damage of organelles. *BMC Plant Biol.* 18 (1), 1–17. doi: 10.1186/s12870-018-1263-z

Djanaguiraman, M., Narayanan, S., Erdayani, E., and Prasad, P. V. (2020). Effects of high temperature stress during anthesis and grain filling periods on photosynthesis, lipids and grain yield in wheat. *BMC Plant Biol.* 20 (1), 1–12. doi: 10.1186/s12870-020-02479-0

Du, Y., Liang, Y., Wang, H., Wang, K., Lu, J., Zhang, G., et al. (2006). A study on the chemical composition of albino tea cultivars. *J. Hortic. Sci. Biotechnol.* 81 (5), 809–812. doi: 10.1080/14620316.2006.11512142

Fahy, E., Subramaniam, S., Murphy, R. C., Nishijima, M., Raetz, C. R., Shimizu, T., et al. (2009). Update of the LIPID MAPS comprehensive classification system for lipids1. *J. Lipid Res.* 50, S9–S14. doi: 10.1194/jlr.R800095-JLR200

Fan, Y., Zhao, X., Wang, H., Tian, Y., and Zhang, L. (2019). Effects of light intensity on metabolism of light-harvesting pigment and photosynthetic system in camellia sinensis l. cultivar 'Huangjinya'. *Environ. Exp. Bot.* 166, 103796. doi: 10.1016/j.envexpbot.2019.06.009

Feng, L., Gao, M.-J., Hou, R.-Y., Hu, X.-Y., Zhang, L., Wan, X.-C., et al. (2014). Determination of quality constituents in the young leaves of albino tea cultivars. *Food Chem.* 155, 98–104. doi: 10.1016/j.foodchem.2014.01.044

Gao, M., Yin, X., Yang, W., Lam, S. M., Tong, X., Liu, J., et al. (2017). GDSL lipases modulate immunity through lipid homeostasis in rice. *PloS Pathog.* 13 (11), e1006724. doi: 10.1371/journal.ppat.1006724

Gigon, A., Matos, A.-R., Laffray, D., Zuily-Fodil, Y., and Pham-Thi, A.-T. (2004). Effect of drought stress on lipid metabolism in the leaves of arabidopsis thaliana (ecotype Columbia). *Ann. Bot.* 94 (3), 345–351. doi: 10.1093/aob/mch150

Haferkamp, S., and Kirchhoff, H. (2008). Significance of molecular crowding in grana membranes of higher plants for light harvesting by photosystem II. *Photosyn. Res.* 95 (2), 129–134. doi: 10.1007/s11120-007-9253-2

Hand, K. A., and Shabek, N. (2022). The role of E3 ubiquitin ligases in chloroplast function. *Int. J. Mol. Sci.* 23 (17), 9613. doi: 10.3390/ijms23179613

Hölzl, G., and Dörmann, P. (2019). Chloroplast lipids and their biosynthesis. *Annu. Rev. Plant Biol.* 70, 51–81. doi: 10.1146/annurev-arplant-050718-100202

Janik, E., Bednarska, J., Zubik, M., Puzio, M., Luchowski, R., Grudzinski, W., et al. (2013). Molecular architecture of plant thylakoids under physiological and light stress conditions: A study of lipid–light-harvesting complex II model membranes. *Plant Cell* 25 (6), 2155–2170. doi: 10.1105/tpc.113.113076

Jayawardhane, K. N., Singer, S. D., Weselake, R. J., and Chen, G. (2018). Plant sn-glycerol-3-phosphate acyltransferases: Biocatalysts involved in the biosynthesis of intracellular and extracellular lipids. *Lipids* 53 (5), 469–480. doi: 10.1002/lipd.12049

Kirchhoff, H., Sharpe, R. M., Herbstova, M., Yarbrough, R., and Edwards, G. E. (2013). Differential mobility of pigment-protein complexes in granal and agranal thylakoid membranes of C3 and C4 plants. *Plant Physiol.* 161 (1), 497–507. doi: 10.1104/pp.112.207548

Kobayashi, K., Fujii, S., Sasaki, D., Baba, S., Ohta, H., Masuda, T., et al. (2014). Transcriptional regulation of thylakoid galactolipid biosynthesis coordinated with chlorophyll biosynthesis during the development of chloroplasts in arabidopsis. *Front. Plant Sci.* 5, 272. doi: 10.3389/fpls.2014.00272

Kwon, S. J., Jin, H. C., Lee, S., Nam, M. H., Chung, J. H., Kwon, S. I., et al. (2009). GDSL lipase-like 1 regulates systemic resistance associated with ethylene signaling in arabidopsis. *Plant J.* 58 (2), 235–245. doi: 10.1111/j.1365-313X.2008.03772.x

LaBrant, E., Barnes, A. C., and Roston, R. L. (2018). Lipid transport required to make lipids of photosynthetic membranes. *Photosyn. Res.* 138 (3), 345–360. doi: 10.1007/s11120-018-0545-5

Langfelder, P., and Horvath, S. (2008). WGCNA: An r package for weighted correlation network analysis. *BMC Bioinf.* 9 (1), 1–13. doi: 10.1186/1471-2105-9-559

Lee, J., He, K., Stolc, V., Lee, H., Figueroa, P., Gao, Y., et al. (2007). Analysis of transcription factor HY5 genomic binding sites revealed its hierarchical role in light regulation of development. *Plant Cell* 19 (3), 731–749. doi: 10.1105/tpc.106.047688

Li-Beisson, Y., Shorrosh, B., Beisson, F., Andersson, M. X., Arondel, V., Bates, P. D., et al. (2013). Acyl-lipid metabolism. *Arabidopsis book/American Soc. Plant Biol.* 11, 1–70. doi: 10.1199/tab.0161

Li, J., Liu, L.-N., Meng, Q., Fan, H., and Sui, N. (2020). The roles of chloroplast membrane lipids in abiotic stress responses. *Plant Signaling Behav.* 15 (11), 1807152. doi: 10.1080/15592324.2020.1807152

Li, N.-N., Lu, J.-L., Li, Q.-S., Zheng, X.-Q., Wang, X.-C., Wang, L., et al. (2019). Dissection of chemical composition and associated gene expression in the pigment-deficient tea cultivar 'Xiaoxueya'reveals an albino phenotype and metabolite formation. *Front. Plant Sci.* 10, 1543. doi: 10.3389/fpls.2019.01543

Lin, Y.-T., Chen, L.-J., Herrfurth, C., Feussner, I., and Li, H.-m. (2016). Reduced biosynthesis of digalactosyldiacylglycerol, a major chloroplast membrane lipid, leads to oxylipin overproduction and phloem cap lignification in arabidopsis. *Plant Cell* 28 (1), 219–232. doi: 10.1105/tpc.15.01002

Ling, Y. (2001). Effects of different low temperature treatments on compositions of polar lipids in cucumber cotyledons. *Acta Hortic. Sin.* 28 (1), 36. https://www.ahs.ac.cn/EN/Y2001/V28/I1/36

Liu, M.-Y., Burgos, A., Ma, L., Zhang, Q., Tang, D., and Ruan, J. (2017b). Lipidomics analysis unravels the effect of nitrogen fertilization on lipid metabolism in tea plant (Camellia sinensis l.). *BMC Plant Biol.* 17 (1), 1–10. doi: 10.1186/s12870-017-1111-6

Liu, G.-F., Han, Z.-X., Feng, L., Gao, L.-P., Gao, M.-J., Gruber, M. Y., et al. (2017a). Metabolic flux redirection and transcriptomic reprogramming in the albino tea cultivar 'Yu-Jin-Xiang'with an emphasis on catechin production. *Sci. Rep.* 7 (1), 1–15. doi: 10.1038/srep45062

Liu, N., Lin, Z.-F., Van Devender, A., Lin, G.-Z., Peng, C.-L., Pan, X.-P., et al. (2009). Spectral reflectance indices and pigment functions during leaf ontogenesis in six subtropical landscape plants. *Plant Growth Regul.* 58 (1), 73–84. doi: 10.1007/s10725-008-9353-9

Liu, Y., Pang, D., Jiang, H., Chen, C., Sun, Y., Tian, Y., et al. (2022). Identifying key genes involved in yellow leaf variation in 'Menghai huangye'based on biochemical and transcriptomic analysis. *Funct. Integr. Genomics* 22 (2), 251–260. doi: 10.1007/s10142-022-00829-9

Li, N., Xu, C., Li-Beisson, Y., and Philippar, K. (2016). Fatty acid and lipid transport in plant cells. *Trends Plant Sci.* 21 (2), 145–158. doi: 10.1016/j.tplants.2015.10.011

Lu, M., Han, J., Zhu, B., Jia, H., Yang, T., Wang, R., et al. (2019). Significantly increased amino acid accumulation in a novel albino branch of the tea plant (Camellia sinensis). *Planta* 249 (2), 363–376. doi: 10.1007/s00425-018-3007-6

Narasimhan, R., Wang, G., Li, M., Roth, M., Welti, R., and Wang, X. (2013). Differential changes in galactolipid and phospholipid species in soybean leaves and roots under nitrogen deficiency and after nodulation. *Phytochemistry* 96, 81–91. doi: 10.1016/j.phytochem.2013.09.026

Narayanan, S., Tamura, P. J., Roth, M. R., Prasad, P. V., and Welti, R. (2016). Wheat leaf lipids during heat stress: I. high day and night temperatures result in major lipid alterations. *Plant Cell Environ.* 39 (4), 787–803. doi: 10.1111/pce.12649

Ohlrogge, J., and Browse, J. (1995). Lipid biosynthesis. *Plant Cell* 7 (7), 957. doi: 10.1105/tpc.7.7.957

Oh, I. S., Park, A. R., Bae, M. S., Kwon, S. J., Kim, Y. S., Lee, J. E., et al. (2005). Secretome analysis reveals an arabidopsis lipase involved in defense against alternaria brassicicola. *Plant Cell* 17 (10), 2832–2847. doi: 10.1105/tpc.105.034819

Peng, Y., Zhang, Y., Lv, J., Zhang, J., Li, P., Shi, X., et al. (2012). Characterization and fine mapping of a novel rice albino mutant low temperature albino 1. *J. Genet. Genomics* 39 (8), 385–396. doi: 10.1016/j.jgg.2012.05.001

Shiva, S., Enninful, R., Roth, M. R., Tamura, P., Jagadish, K., and Welti, R. (2018). An efficient modified method for plant leaf lipid extraction results in improved recovery of phosphatidic acid. *Plant Methods* 14 (1), 1–8. doi: 10.1186/s13007-018-0282-y

Sui, N., Tian, S., Wang, W., Wang, M., and Fan, H. (2017). Overexpression of glycerol-3-phosphate acyltransferase from suaeda salsa improves salt tolerance in arabidopsis. *Front. Plant Sci.* 8, 1337. doi: 10.3389/fpls.2017.01337

Sun, X.-l., Yang, S., Wang, L.-Y., Zhang, Q.-Y., Zhao, S.-J., and Meng, Q.-W. (2011). The unsaturation of phosphatidylglycerol in thylakoid membrane alleviates PSII photoinhibition under chilling stress. *Plant Cell Rep.* 30 (10), 1939–1947. doi: 10.1007/s00299-011-1102-2

Tian, M., Song, M., Fan, S., Pang, C., and Yu, S. (2011). Advance in research of molecular mechanism of chlorophyll-deficient mutants in plants. *Acta Botanica Boreali-Occidentalia Sin.* 31 (9), 1900–1907. doi: 10.1631/jzus.B1000171

Troncoso-Ponce, M. A., Nikovics, K., Marchive, C., Lepiniec, L., and Baud, S. (2016). New insights on the organization and regulation of the fatty acid biosynthetic network in the model higher plant arabidopsis thaliana. *Biochimie* 120, 3–8. doi: 10.1016/j.biochi.2015.05.013

Uddling, J., Gelang-Alfredsson, J., Piikki, K., and Pleijel, H. (2007). Evaluating the relationship between leaf chlorophyll concentration and SPAD-502 chlorophyll meter readings. *Photosyn. Res.* 91 (1), 37–46. doi: 10.1007/s11120-006-9077-5

Vu, H. S., Shiva, S., Roth, M. R., Tamura, P., Zheng, L., Li, M., et al. (2014). Lipid changes after leaf wounding in arabidopsis thaliana: Expanded lipidomic data form the basis for lipid co-occurrence analysis. *Plant J.* 80 (4), 728–743. doi: 10.1111/tpj.12659

Wang, L., Cao, H., Chen, C., Yue, C., Hao, X., Yang, Y., et al. (2016). Complementary transcriptomic and proteomic analyses of a chlorophyll-deficient tea plant cultivar reveal multiple metabolic pathway changes. *J. Proteomics* 130, 160–169. doi: 10.1016/j.jprot.2015.08.019

Wang, K. R., Liang, Y. R., Ming, L. I., and Zhang, L. J. (2015). Progress in the development of germplasm resources for albino and purple tea cultivars. *China Tea Process.* 03, 5–8. doi: 10.15905/j.cnki.33-1157/ts.2015.03.001

Wang, G.-P., Xue, X.-M., Yang, X.-h., Chen, R., and Han, X.-P. (2022). The genetic engineering of glycine betaine synthesis in tobacco improves the resistance of the photosynthetic apparatus to drought stress. *Plant Biotechnol. Rep.* 16 (2), 229–242. doi: 10.1007/s11816-022-00747-z

Wang, L., Yue, C., Cao, H., Zhou, Y., Zeng, J., Yang, Y., et al. (2014). Biochemical and transcriptome analyses of a novel chlorophyll-deficient chlorina tea plant cultivar. *BMC Plant Biol.* 14 (1), 1–13. doi: 10.1186/s12870-014-0352-x

Welti, R., and Wang, X. (2004). Lipid species profiling: a high-throughput approach to identify lipid compositional changes and determine the function of genes involved in lipid metabolism and signaling. *Curr. Opin. Plant Biol.* 7 (3), 337–344. doi: 10.1016/j.pbi.2004.03.011

Wu, Q. (2015) Gene differential analysis and physicochemical characteristics of camellia sinensis cv. baijiguan in response to light. *PhD Fujian Agric. For. Univ. Fujian Province thesis.* 36–57

Wu, Q., Chen, Z., Sun, W., Deng, T., and Chen, M. (2016). *De novo* sequencing of the leaf transcriptome reveals complex light-responsive regulatory networks in camellia sinensis cv. baijiguan. *Front. Plant Sci.* 7, 332. doi: 10.3389/fpls.2016.00332

Xu, D., Lam, S. M., Zuo, J., Yuan, S., Lv, J., Shi, J., et al. (2021). Lipidomics reveals the difference of membrane lipid catabolism between chilling injury sensitive and non-sensitive green bell pepper in response to chilling. *Postharvest Biol. Technol.* 182, 111714. doi: 10.1016/j.postharvbio.2021.111714

Xu, P., Su, H., Jin, R., Mao, Y., Xu, A., Cheng, H., et al. (2020). Shading effects on leaf color conversion and biosynthesis of the major secondary metabolites in the albino tea cultivar "Yujinxiang". *J. Agric. Food Chem.* 68 (8), 2528–2538. doi: 10.1021/acs.jafc.9b08212

Yanagisawa, S. (2002). The dof family of plant transcription factors. *Trends Plant Sci.* 7 (12), 555–560. doi: 10.1016/S1360-1385(02)02362-2

Yanagisawa, S., and Sheen, J. (1998). Involvement of maize dof zinc finger proteins in tissue-specific and light-regulated gene expression. *Plant Cell* 10 (1), 75–89. doi: 10.1105/tpc.10.1.75

Yue, C., Wang, Z., and Yang, P. (2021). The effect of light on the key pigment compounds of photosensitive etiolated tea plant. *Bot. Stud.* 62 (1), 1–15. doi: 10.1186/s40529-021-00329-2

Zhang, C., Liu, G., Chen, J., Xie, N., Huang, J., and Shen, C. (2022a). Translational landscape and metabolic characteristics of the etiolated tea plant (Camellia sinensis). *Sci. Hortic.* 303, 111193. doi: 10.1016/j.scienta.2022.111193

Zhang, X., Wen, B., Zhang, Y., Li, Y., Yu, C., Peng, Z., et al. (2022b). Transcriptomic and biochemical analysis reveal differential regulatory mechanisms of photosynthetic pigment and characteristic secondary metabolites between high amino acids green-leaf and albino tea cultivars. *Sci. Hortic.* 295, 110823. doi: 10.1016/j.scienta.2021.110823

frontiers | Frontiers in Plant Science

TYPE Original Research
PUBLISHED 19 October 2022
DOI 10.3389/fpls.2022.1041141

OPEN ACCESS

EDITED BY
Peitao Lü,
Fujian Agriculture and Forestry University, China

REVIEWED BY
Liangsheng Zhang,
Zhejiang University, China
Fan Zhang,
Huazhong Agricultural University, China

*CORRESPONDENCE
Yuerong Gao
Gaoyr86@outlook.com

†These authors have contributed equally to this work

SPECIALTY SECTION
This article was submitted to Plant Systems and Synthetic Biology, a section of the journal Frontiers in Plant Science

RECEIVED 10 September 2022
ACCEPTED 04 October 2022
PUBLISHED 19 October 2022

CITATION
Jiang C, Jiang T, Deng S, Yuan C, Liang Y, Li S, Ma C and Gao Y (2022) Integrative analysis of transcriptome, proteome, and ubiquitome changes during rose petal abscission. *Front. Plant Sci.* 13:1041141. doi: 10.3389/fpls.2022.1041141

Integrative analysis of transcriptome, proteome, and ubiquitome changes during rose petal abscission

Chuyan Jiang[1†], Tianhua Jiang[1†], Shuning Deng[1], Chaoli Yuan[2], Yue Liang[1], Susu Li[1], Chao Ma[1] and Yuerong Gao[2*]

[1]Beijing Key Laboratory of Development and Quality Control of Ornamental Crops, Department of Ornamental Horticulture, China Agricultural University, Beijing, China, [2]Beijing Key Laboratory for Agricultural Application and New Technique, College of Plant Science and Technology, Beijing University of Agriculture, Beijing, China

Plant organ abscission is regulated by multiple physiological and biochemical processes. However, the transcriptional, translational, and post-translational modifications occurring during organ abscission have not been systematically investigated. In this study, we report transcriptome, proteome, and ubiquitome data for the abscission zone (AZ) of rose petals collected during petal shedding. We quantified 40,506 genes, 6,595 proteins, and 2,720 ubiquitinated proteins in rose petal AZ. Our results showed that during petal abscission, 1,496 genes were upregulated and 2,199 were downregulated; 271 proteins were upregulated and 444 were downregulated; and 139 ubiquitination sites in 100 proteins were upregulated and 55 ubiquitination sites in 48 proteins were downregulated. Extracellular levels of cell component proteins were significantly increased, while levels within protoplasts were significantly decreased. During petal abscission, transcript levels of genes involved in defense response, transport, and metabolism changed significantly. Levels of proteins involved in the starch and sucrose metabolism and phenylpropanoid biosynthesis pathways were significantly altered at both the transcript and protein levels. The transcriptional and translational upregulation of peroxidase (POD), in the phenylpropanoid biosynthesis, pathway may be associated with deposition of lignin, which forms a protective layer during petal abscission. Overall, our data provide a comprehensive assessment of the translational and post-translational changes that occur during rose petal abscission.

KEYWORDS

petal abscission, transcriptome, proteome, ubiquitome, rose

Introduction

Rose (*Rosa* spp.) is one of the most important ornamental crops worldwide. The timing of petal shedding is a major factor in determining the longevity of the rose flower and is thus important for its economic value. Petal abscission, leading to petal shedding, in response to endogenous and exogenous cues is the terminal stage of petal development (Taylor and Whitelaw, 2001; Tucker and Kim, 2015). The cell separation process preceding shedding occurs in a region of functionally specialized cells known as the abscission zone (AZ) (Taylor and Whitelaw, 2001). Previous genetic and mutational studies have identified many molecular components involved in the transcriptional regulation of petal abscission (Estornell et al., 2013; Kim, 2014; Tucker and Kim, 2015; Ma et al., 2021). Global transcriptional regulation of floral organ abscission has been studied in several plant species, including Arabidopsis (Cai and Lashbrook, 2008), tomato (Meir et al., 2006; Meir et al., 2010), and rose (Gao et al., 2016). These studies have highlighted the critical roles of auxin and ethylene pathway genes during abscission (Meir et al., 2006; Gao et al., 2016). However, little is known about the translational and post-translational regulation of this process.

A decrease in protein levels is a hallmark of senescence and can occur through transcriptional downregulation or through post-translational protein degradation, such as proteosome-mediated degradation triggered by the ubiquitination post-translational modification (Shahri and Tahir, 2014). In petunia and rose, proteome and ubiquitome analyses have demonstrated that ubiquitination participates in protein degradation during petal senescence (Guo et al., 2017; Lu et al., 2019). Further investigation of changes in the ubiquitination profile of proteins during petal abscission could thus deepen our understanding of the molecular regulation of abscission.

A previous study has shown that in an abscission-prone rose (*Rosa hybrida* cv Golden Shower), flower opening stages 3 and 5 are marker stages before and after the initiation of abscission, respectively (Liang et al., 2020). In this study, we analyzed petal AZs of 'Golden Shower' at stages 3 and 5 for transcriptome changes by RNA-seq, and changes of proteome and ubiquitome using a label-free quantitative strategy involving antibody-based affinity enrichment and high-resolution liquid chromatography-tandem mass spectrometry (LC-MS/MS). In total, we identified 40,506 transcripts including 3,695 differentially expressed genes (DEGs); 6,595 proteins including 715 differentially expressed proteins (DEPs); and 2,720 ubiquitinated proteins including 148 differentially ubiquitinated proteins (Figure 1). Our transcriptome, proteome, and ubiquitome data provide a comprehensive analysis of petal abscission at the translational and post-translational levels in rose.

Results and discussion

Transcriptome changes in AZ during petal abscission

We obtained transcriptome data sets for stage 3 and stage 5 petal AZ using RNA-seq. In total, we obtained 44.88 GB of clean data and assembled 41,232 transcripts using the Trinity software package. We identified DEGs using a cutoff ratio of >2 or <0.5 (p-value <0.05) through a pairwise comparison of expression levels between stage 3 and stage 5 (S5 vs S3) (Supplementary Table 1). This yielded 1,496 upregulated and 2,199 downregulated genes (Supplementary Figure 1A; Supplementary Table 1).

To evaluate the putative functions of DEGs during petal abscission, we determined clusters of orthologous groups of proteins (COG) amongst these genes. DEGs were enriched in pathways related to signal transduction, defense mechanism, and the transport and metabolism of biomolecules such as carbohydrates, lipids, nucleotides, amino acids, and secondary metabolites (Supplementary Figure 1B). A previous transcriptome study in the cultivar 'Gold Medal' (Gao et al., 2016) had also showed that defense response, transport, and metabolism were enriched during rose petal abscission.

An analysis of DEGs for Kyoto Encyclopedia of Genes and Genomes (KEGG) enrichment showed that the DEGs were enriched in the pathways of starch and sucrose metabolism, plant hormone signal transduction, carbon metabolism, and phenylpropanoid biosynthesis (Supplementary Figure 1C). This is consistent with previous transcriptome data for genes involved in petal abscission in the cultivar 'Gold Medal' (Gao et al., 2016), which showed that 52 DEGs were enriched in the auxin pathway and 38 DEGs were enriched in the ethylene pathway. Here, we found 46 and 33 DEGs related to auxin and ethylene signaling, respectively (Supplementary Table 2), confirming their important roles in rose petal abscission. Previous studies have identified several genes with functions in rose petal abscission whose expression is responsive to petal abscission. The expression profiles of these genes, including *RhERF1* (ethylene response factor1; RchiOBHmChr2g0135921), *RhSUC2* (sucrose carrier2; RchiOBHmChr6g0272341), and *RhARF7* (auxin response factor7; RchiOBHmChr2g0095551), were generally in agreement with

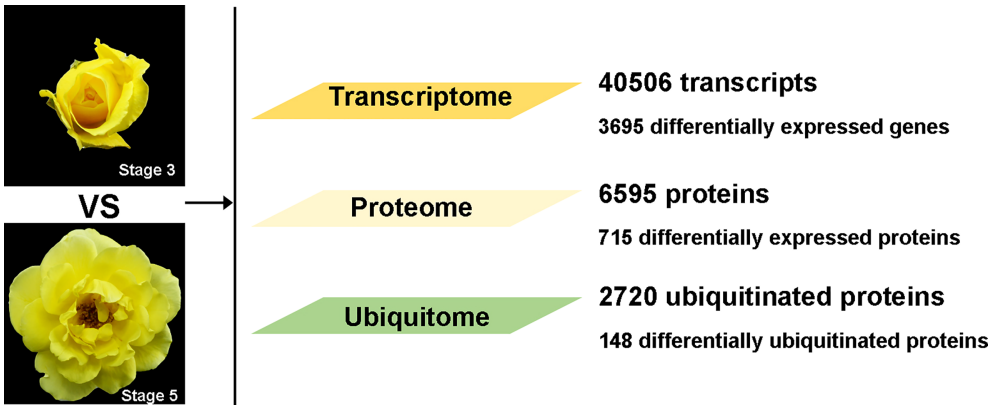

FIGURE 1
Overall data for transcriptome, proteome, and ubiquitome in petal AZ at flower opening stages 3 and 5.

the expression profiles that we observed in our RNA-seq date (Supplementary Table 1) (Gao et al., 2019; Liang et al., 2020).

Proteome changes in AZ during petal abscission

Our investigation of proteome changes between stage 3 and 5 petal AZs revealed 715 DEPs with significant changes in abundance, using a threshold of a 1.5-fold difference in abundance (p-value <0.05) in stage 5 compared with stage 3. Among these DEPs, 271 proteins were significantly upregulated and 444 proteins were significantly downregulated at stage 5 compared with stage 3 (Supplementary Table 3).

To elucidate the potential functions of these DEPs, we first divided them into four categories according to their ratio of stage 5 to stage 3 abundance, with Q1 representing ratios <0.5, Q2 representing ratios of 0.5–0.667, Q3 representing ratios of 1.5–2, and Q4 representing ratios >2 (Figure 2A; Supplementary Table 3). Next, we performed Gene Ontology (GO) enrichment assays for DEPs based on clustering analysis. In the cellular component category, upregulated proteins were enriched in the extracellular component category, including extracellular regions, apoplasts, cell periphery, cell wall, and external encapsulating structure. In contrast, downregulated proteins were enriched in the intracellular component category, including the nucleus, membrane-bounded organelles, endoplasmic reticulum, and endomembrane system (Supplementary Figure 2A). These results suggest that during petal abscission, external cellular components of the protoplasm are metabolically active, whereas metabolism within the protoplast slows down. Execution of organ abscission occurs mainly in the middle lamella regions of AZ, and due to the breakdown of the primary cell wall and degradation of pectic polysaccharides (Patterson, 2001; Ogawa et al., 2009; Swain et al., 2011). We also found that a large proportion of upregulated proteins were highly enriched in the metabolic processing of monosaccharides such as hexose, polysaccharides, DNA, and cell wall macromolecules. Downregulated proteins were enriched in the biosynthetic processes of carbohydrates, polysaccharides, membrane lipids, lipoproteins, and glycerolipids (Supplementary Figure 2B). These results suggest that cell wall degradation is an important part of petal abscission and that the biosynthesis of organic molecules is reduced during rose petal abscission.

To further delineate the metabolic pathways involved in petal abscission, we mapped the DEPs against the KEGG database (Figure 2D). We found that the upregulated proteins were significantly enriched in the metabolism of glyoxylate, dicarboxylate, galactose, and tryptophan, as well as in phenylpropanoid biosynthesis. Downregulated proteins were significantly enriched in starch and sucrose metabolism; protein processing in endoplasmic reticulum, spliceosome; and cutin, suberine and wax biosynthesis (Figure 2D).

Ubiquitination changes in AZ during petal abscission

Next, we examined dynamic protein ubiquitination based on the proteome. The ubiquitome dataset was defined by imputing missing values and normalization of 6,844 ubiquitin-modified peptides and 7,026 lysine ubiquitination (K^{ub}) sites in 2,720 proteins, of which 3,718 K^{ub} sites in 1,379 proteins were quantified. Among these quantified K^{ub} sites and proteins, 139 sites in 100 proteins were identified as upregulated ubiquitination sites, and 55 sites in 48 proteins were identified as downregulated ubiquitination sites (Figure 2B; Supplementary Tables 4). These results suggest that AZ ubiquitination levels are increased during rose petal abscission.

10.3389/fpls.2022.1041141

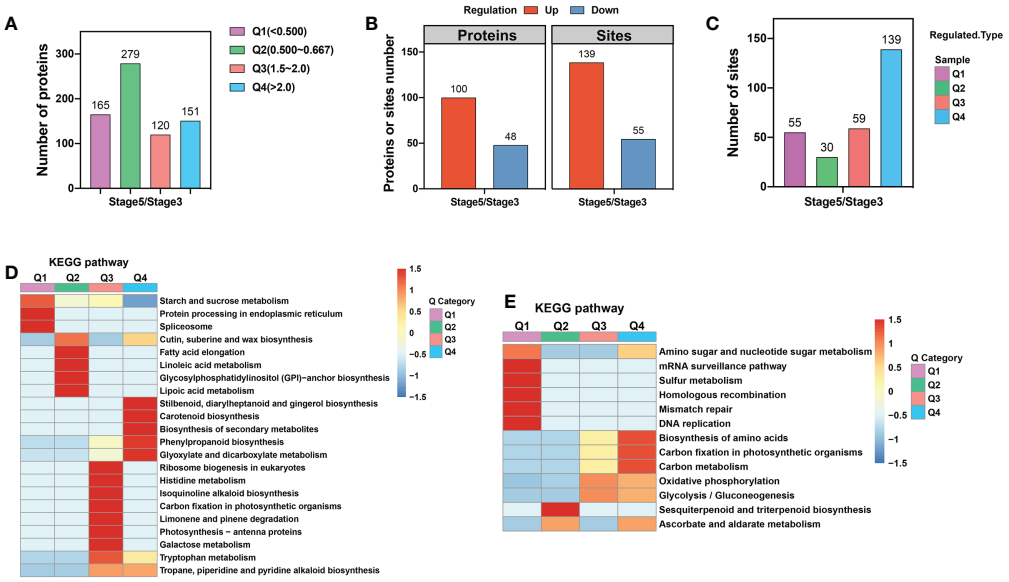

FIGURE 2
KEGG enrichment analysis of proteome and ubiquitome changes in petal AZ identified through comparison of stages 3 and 5. **(A)** Numbers of differentially expressed proteins (DEPs). **(B)** Numbers of proteins or sites showing significant changes in ubiquitination. **(C)** The four categories of ubiquitination sites defined based on the ratio of stage 5 to stage 3. Q1 represents ratios of <0.667, Q2 represents ratios of 0.667–0.769, Q3 represents ratios of 1.3–1.5, and Q4 represents ratios >1.5. **(D)** KEGG enrichment analysis of proteins with significantly altered abundance. **(E)** KEGG enrichment analysis of sites showing significant changes in ubiquitination.

To explore the functional differences between proteins with upregulated and downregulated ubiquitination, we first divided proteins with changed K^{ub} sites into four categories according to their stage 5/stage 3 ratio, with Q1 representing ratios <0.667, Q2 representing ratios of 0.667–0.769, Q3 representing ratios of 1.3–1.5, and Q4 representing ratios >1.5 (Figure 2C; Supplementary Table 4). GO enrichment analysis showed that, in the cellular component category, proteins with upregulated K^{ub} sites were enriched in proton transport of the vacuolar-type ATPase complex, while proteins with downregulated K^{ub} sites were enriched in membrane proteins (Supplementary Figure 2C). In the biological process category, up- and downregulated K^{ub} proteins were enriched in 19 processes. Among them, upregulated K^{ub} proteins were enriched in *S*-adenosylmethionine metabolic and biosynthetic process, ribose phosphate and single-organism carbohydrate catabolic biosynthetic process, and nucleoside and ribose phosphate metabolic process. Downregulated K^{ub} proteins were enriched in hydrogen and monovalent inorganic cation transport and ATP-hydrolysis-coupled transmembrane ion transport (Supplementary Figure 2D).

To further delineate the metabolic pathways of proteins with changed K^{ub} sites, we preformed KEGG analysis, and found enrichment in oxidative phosphorylation, nucleotide excision repair, amino sugar and nucleotide sugar metabolism, and glycolysis/gluconeogenesis (Figure 2E). Among these, proteins with upregulated K^{ub} sites were enriched in amino acid biosynthesis, carbon metabolism, oxidative phosphorylation, and glycolysis/gluconeogenesis. Proteins with downregulated K^{ub} sites were enriched in amino sugar and nucleotide sugar metabolism, homologous recombination, mismatch repair, DNA replication, and biosynthesis of sesquiterpenoids and triterpenoids (Figure 2E).

Next, we investigated the position-specific frequencies of amino acid residues surrounding K^{ub} sites identified in petal AZ using the program Motif-X (Supplementary Table 4). Among the 7,026 K^{ub} sites, 5,025 unique sites were assigned to 13 conserved motifs (Supplementary Figure 3A), which accounted for approximately 71.5% of the sites identified. Nine of these 13 motifs have been reported previously (Xie et al., 2015; Guo et al., 2017; Lu et al., 2019; Fan et al., 2021), while the other 4 motifs are novel: $K^{ub}Q$, DNK^{ub}, $DNNK^{ub}$, and $ENNNNNNK^{ub}$ (where N indicates any amino acid). In addition, we observed that 4 distinct residues were enriched around K^{ub}, including alanine (A), glutamate (E), aspartate (D), and glutamine (Q). (Supplementary Figure 3B).

Integrative analysis of AZ transcriptome and proteome

Comparing the quantitative correlation between transcriptome and proteome data could reveal potential

regulatory relationships between proteins and transcripts. Therefore, we performed a correlation analysis between the DEGs and DEPs and divided them into 8 different expression clusters (Figure 3A; Supplementary Table 5). The results showed that the expression of 67 members was downregulated at both the transcript and protein levels (cluster 1), whereas the expression of 55 members was upregulated at the transcript and protein levels (cluster 8, Figure 3A). GO enrichment analysis showed that DEGs/DEPs of cluster 1 were enriched in steroid biosynthetic process, alcohol biosynthetic process, energy reserve metabolic process, and cell wall modification process (Figure 3B). KEGG analysis showed that DEGs/DEPs of cluster 8 were enriched in photosynthesis, tryptophan metabolism, and carbon metabolism (Figure 3C).

Although not exhibiting changes at the transcript level, at the protein level, 359 and 181 further members were downregulated (cluster 2) and upregulated (cluster 7), respectively (Figure 3A). GO enrichment analysis showed that DEGs and DEPs of cluster 2 were enriched in protein modification and metabolic process, macromolecule biosynthetic process, and cellular or protein metabolic processes. DEGs/DEPs of cluster 7 were enriched in DNA metabolic process and cell wall organization (Figure 3B). Clusters 4 and 5 contain the largest sets of members (408 and 475, respectively) and exhibited altered expression at the transcriptional level, but not at the protein level (Figure 3A).

Integrative analysis of AZ proteome and ubiquitome

To test whether ubiquitination plays an important role in protein abundance and function during rose petal abscission, we compared DEPs with changes in protein ubiquitination (Figure 4; Supplementary Table 6). We found that the abundance of 18 upregulated and ubiquitinated proteins was decreased, including heat shock protein HSP90, phosphoinositide phospholipase C, and oligopeptide transporter (Figure 4B; Supplementary Table 6). The abundance of 6 downregulated and ubiquitinated proteins was increased, including pyridoxal 5'-phosphate synthase, ribosome biogenesis factor NIP7, START-like domain, and Bet v I type allergen (Figure 4D; Supplementary Table 6). Although the technology used in our study may not detect protein abundance or degradation regulated by the 26S proteasome,

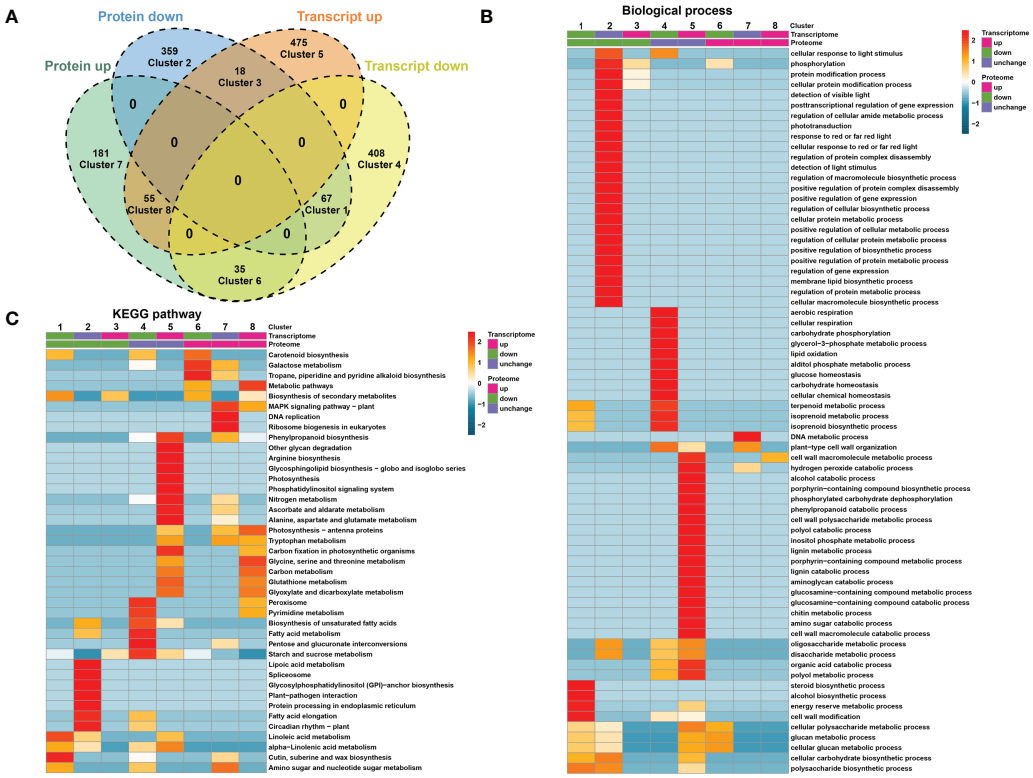

FIGURE 3
Correlation analysis between DEGs and DEPs. **(A)** Venn diagram showing that DEGs and DEPs are divided into 8 differential expression clusters. **(B)** Gene Ontology (GO)-based enrichment analysis of differential expression clusters in biological process class. **(C)** KEGG enrichment analysis of differential expression clusters.

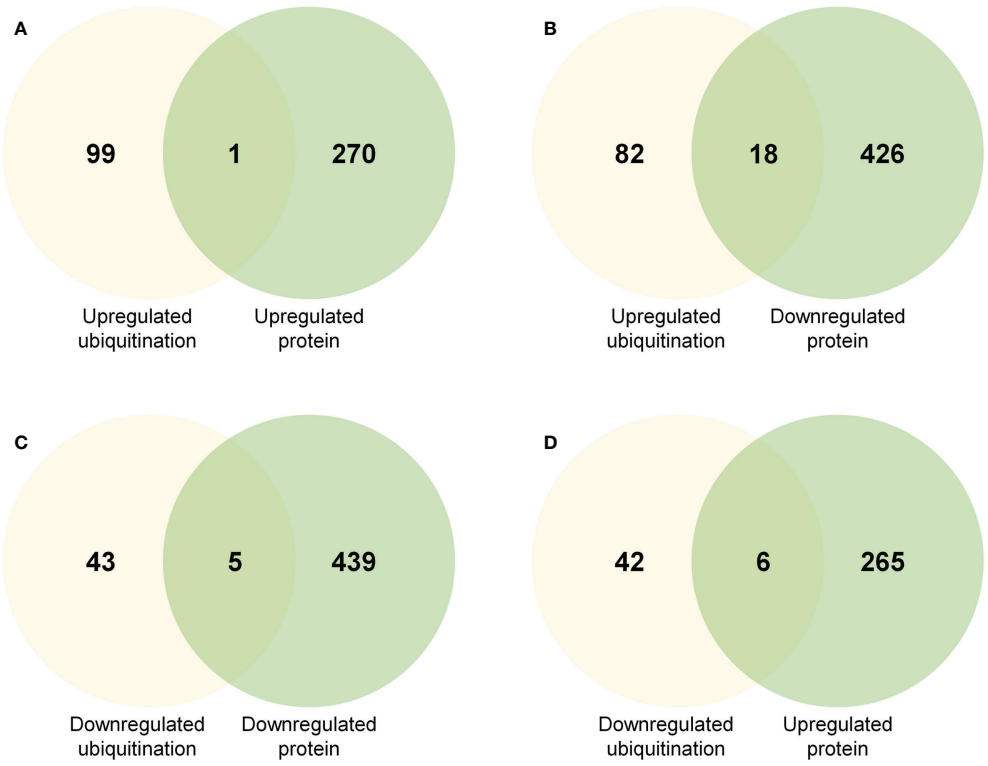

FIGURE 4
Venn diagrams showing common proteins significantly up- or downregulated in regard to protein abundance and ubiquitination level **(A)** Common proteins in regard to upregulated protein abundance and upregulated ubiquitination level. **(B)** Common proteins in regard to downregulated protein abundance and upregulated ubiquitination level. **(C)** Common proteins in regard to downregulated protein abundance and downregulated ubiquitination level. **(D)** Common proteins in regard to upregulated protein abundance and downregulated ubiquitination level.

our results revealed only a few non-regulatory proteins (Figures 4B, D), suggesting that the ubiquitination degradation pathway may not play a critical role in rose petal abscission.

Involvement of phenylpropanoid biosynthesis pathway in petal abscission

While cell separation occurs during abscission, the AZ on the mother plant develops a primary protective layer against pests and pathogens, consisting of suberin and lignin deposits (Addicott, 1982). Suberin and lignin are phenylpropanoid-based polymers, and the regulation of the phenylpropanoid biosynthesis pathway has been demonstrated at multiple levels (Vogt, 2010). Our KEGG enrichment analyses showed that the phenylpropanoid biosynthesis pathway was enriched in both its transcriptome (Supplementary Figure 1C) and proteome (Figure 2D). We observed that among the genes related to phenylpropanoid biosynthesis, the abundance of multiple peroxidase (POD) members was increased at the transcript and protein levels (Figure 5B; Supplementary Table 7). We validated the expression of genes related to phenylpropanoid biosynthesis in RNA-seq data by RT-qPCR. The results of RT-qPCR were generally in agreement with expression profiles obtained by RNA-seq data (Supplementary Figure 4). PODs are involved in the polymerization of monolignols (coniferyl-alcohol) into lignin (Figure 5A) (Zhao et al., 2013; Liu et al., 2018). Overexpression of sweet potato POD in tobacco has been reported to cause an increase in the content of phenol and lignin, and enhanced stress tolerance (Kim et al., 2008), and ectopic expression of FaPOD in strawberry (*Fragaria* × *ananassa*) fruit significantly affects lignin biosynthesis and fruit firmness (Yeh et al., 2014). However, the specific role of PODs in organ abscission are yet to be determined.

Abscission-responsive transcription factors

Transcription factors (TFs) act critical regulators of transcriptional reprogramming. We identified a large number of TFs in petal abscission transcriptome (208 DEGs) and

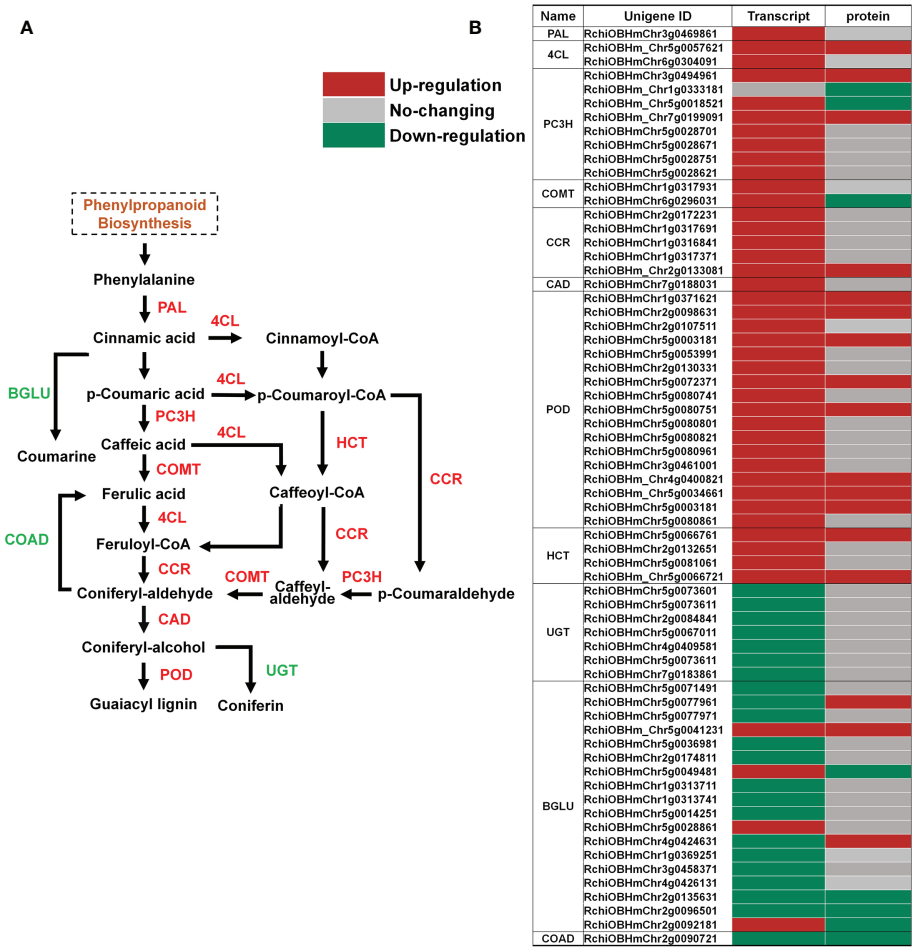

Name	Unigene ID	Transcript	protein
PAL	RchiOBHmChr3g0469861		
4CL	RchiOBHm_Chr5g0057621		
	RchiOBHmChr6g0304091		
PC3H	RchiOBHmChr3g0494961		
	RchiOBHm_Chr1g0333181		
	RchiOBHm_Chr5g0018521		
	RchiOBHm_Chr7g0199091		
	RchiOBHmChr5g0028701		
	RchiOBHmChr5g0028671		
	RchiOBHmChr5g0028751		
	RchiOBHmChr5g0028621		
COMT	RchiOBHmChr1g0317931		
	RchiOBHmChr6g0296031		
CCR	RchiOBHmChr2g0172231		
	RchiOBHmChr1g0317691		
	RchiOBHmChr1g0316841		
	RchiOBHmChr1g0317371		
	RchiOBHm_Chr2g0133081		
CAD	RchiOBHmChr7g0188031		
POD	RchiOBHmChr1g0371621		
	RchiOBHmChr2g0098631		
	RchiOBHmChr2g0107511		
	RchiOBHmChr5g0003181		
	RchiOBHmChr5g0053991		
	RchiOBHmChr2g0130331		
	RchiOBHmChr5g0072371		
	RchiOBHmChr5g0080741		
	RchiOBHmChr5g0080751		
	RchiOBHmChr5g0080801		
	RchiOBHmChr5g0080821		
	RchiOBHmChr5g0080961		
	RchiOBHmChr3g0461001		
	RchiOBHm_Chr4g0400821		
	RchiOBHm_Chr5g0034661		
	RchiOBHmChr5g0003181		
	RchiOBHmChr5g0080861		
HCT	RchiOBHmChr5g0066761		
	RchiOBHmChr2g0132651		
	RchiOBHmChr5g0081061		
	RchiOBHm_Chr5g0066721		
UGT	RchiOBHmChr5g0073601		
	RchiOBHmChr5g0073611		
	RchiOBHmChr2g0084841		
	RchiOBHmChr5g0067011		
	RchiOBHmChr4g0409581		
	RchiOBHmChr5g0073611		
	RchiOBHmChr7g0183861		
BGLU	RchiOBHmChr5g0071491		
	RchiOBHmChr5g0077961		
	RchiOBHmChr5g0077971		
	RchiOBHm_Chr5g0041231		
	RchiOBHmChr5g0036981		
	RchiOBHmChr2g0174811		
	RchiOBHmChr2g0049481		
	RchiOBHmChr1g0313711		
	RchiOBHmChr1g0313741		
	RchiOBHmChr5g0014251		
	RchiOBHmChr5g0028861		
	RchiOBHmChr4g0424631		
	RchiOBHmChr1g0369251		
	RchiOBHmChr3g0458371		
	RchiOBHmChr4g0426131		
	RchiOBHmChr2g0135631		
	RchiOBHmChr2g0096501		
	RchiOBHmChr2g0092181		
COAD	RchiOBHmChr2g0090721		

FIGURE 5
Changes in transcript and protein levels of phenylpropanoid biosynthesis pathway members in AZ during petal abscission. **(A)** Schematic of the phenylpropanoid biosynthesis pathway. **(B)** Expression of genes related to phenylpropanoid biosynthesis at transcript and protein levels.

proteome (33 DEPs). Among these TF related DEGs in transcriptome, the top 10 largest TF families included: zinc finger (39 DEGs), bHLH (25 DEGs), MYB (24 DEGs), AP2/ERF (22 DEGs), homeobox (HB) (17 DEGs), WRKY (14 DEGs), BTB/POZ (8 DEGs), Aux/IAA (7 DEGs), bZIP (7 DEGs), heat stress transcription factor (HSF) (6 DEGs) (Figure 6A; Supplementary Table 8). This is relatively consistent with previous transcriptome data for DEGs involved in petal abscission in the cultivar 'Gold Medal', which also showed same top 10 largest TF families during petal abscission except HSF family (Gao et al., 2016). These results indicated that those TF families may play important roles in petal abscission. Among TF related DEPs in proteome, WD40 (13 DEPs), zinc finger (7 DEPs), BTB/POZ (4 DEPs), bZIP (2 DEPs), calmodulin binding transcription activator (CAMTA) (2 DEPs) are the largest TF families (Figure 6B; Supplementary Table 8). In addition, we identified 3 TFs related DEPs with changed ubiquitination including 1 WD40 protein, and 2 ARF proteins (Supplementary Table 8). These results suggested that petal abscission triggers a complex transcriptional reprogramming.

Materials and methods

Plant material

Rose (*Rose hybrida* cv Golden Shower) was used as plant material. The flowers were harvested at opening stage 3 and stage 5 in a greenhouse at the China Agricultural University (Beijing, China). We collected petal AZ samples

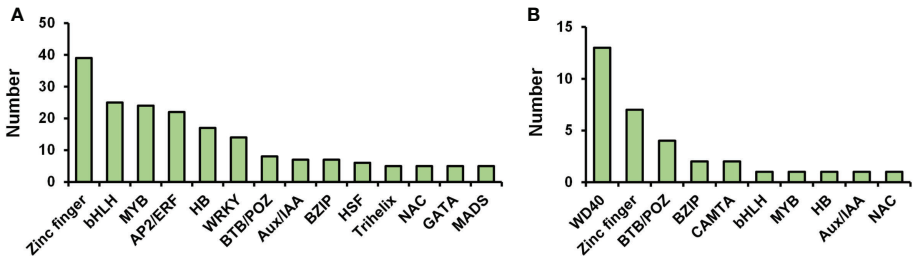

FIGURE 6
Distribution of transcription factors in transcriptome **(A)** and proteome **(B)**.

by excising both sides at the base of petals and receptacles adjacent to the petals as previously described (Liang et al., 2020).

Total RNA extraction, RT-qPCR, and RNA-seq analysis

Total RNA was extracted using the hot borate method and subjected to RNase-free DNase I (Promega) treatment as previously described (Gao et al., 2016).

For RT-qPCR, first-strand cDNA was synthesized from 1 μg RNA using oligo d(T) and random primers. The RT-qPCR reactions (20 μl) containing 1 μl cDNA were performed by Step One Plus real-time PCR system (Thermo Fisher Scientific). *RhUBI2* was used as the internal control (Liang et al., 2020). The primers used in this study are listed in Supplementary Table 9.

For RNA-seq analysis, RNA integrity was analyzed using the Agilent 2100 bioanalyzer (Agilent Technologies). Six RNA samples (three biological replicates for each stage) were sent to Beijing Novogene Bioinformatics Technology Co., Ltd (http://www.novogene.com/) for RNA-seq analysis. The RNA-seq data were processed as described previously (Liu et al., 2022). Clean sequencing reads were aligned using a reference genome sequence (*Rosa chinensis* Old Blush; https://lipm-browsers.toulouse.inra.fr/pub/RchiOBHm-V2/). Genes with at least 2-fold difference and an adjusted *p*-value <0.05 were assigned as DEGs.

Protein extraction

Petal AZ samples were ground in liquid nitrogen and resuspended in lysis buffer (8 M urea, 1% Triton X-100, 10 mM dithiothreitol, 1% protease inhibitor (Calbiochem), deubiquitinase inhibitors PR-619 (Sigma), and 2 mM EDTA). The mixtures were sonicated and centrifuged at 20,000 *g* (4°C, 10 min) to remove remaining debris. A final concentration of 20% (v/v) trichloroacetic acid (TCA) was added to the supernatants, and the mixtures were kept at 4°C for 2 hours. The mixtures were then centrifuged at 12,000 *g* (4°C, 3 min). The precipitates were washed three times with precooled acetone and dissolved in 8 M urea.

Trypsin digestion

For digestion, protein solutions were reduced with dithiothreitol (5 mM) for 30 min at 56°C and then alkylated with 11 mM iodoacetamide in darkness for 15 min at 23°C. The solutions were then diluted with 100 mM TEAB to a urea concentration of <2 M. Finally, the protein samples were digested at a 1:50 trypsin/protein ratio overnight or a 1:100 trypsin/protein ratio for 4 hours.

HPLC fractionation

Tryptic peptides were fractionated by high pH reverse-phase HPLC using an Agilent 300 extend C18 column (5 μm particles, 4.6 mm ID, and 250 mm length) for proteome analysis, and using a Thermo Betasil C18 column (5 μm particles, 10 mm ID, and 250 mm length) for ubiquitome analysis.

LC-MS/MS analysis

LC-MS/MS analysis was carried out by PTM Biolab Co., Ltd (https://www.ptmbiolabs.com/). Briefly, tryptic peptides were dissolved in 0.1% formic acid, and then loaded onto a reverse-phase analytical column (15 cm length and 75 μm ID). An increasing gradient was applied of 0.1% formic acid in 90% acetonitrile from 6% to 23% over 26 min, 23% to 35% in 8 min, and held at 80% in 3 min, all at a constant flow rate of 400 nL/min on an EASY-nLC 1000 UPLC system (Thermo Fisher Scientific).

Peptides were subjected to an NSI source followed by tandem mass spectrometry (MS/MS) in a Q Exactive™ Plus Quadrupole-Orbitrap™ mass spectrometer (Thermo Fisher Scientific) coupled online to the UPLC. The electrospray voltage applied was 2.0 kV. The *m*/*z* scan range was 350–1,800 for a full scan. Intact peptides were detected in the Orbitrap at a resolution of 70,000. Peptides were selected for MS/MS using a normalized collision energy (NCE) setting of 28, and fragments were detected in the Orbitrap at a resolution of 17,500. A data-dependent procedure that alternated between one MS scan and 20 MS/MS scans was applied with 15.0-s dynamic exclusion. Automatic gain control was set at 5E4.

MS/MS data processing and bioinformatic analysis were performed as previously described (Lu et al., 2019).

Data availability statement

The datasets presented in this study can be found in online repositories. The names of the repository/repositories and accession number(s) can be found in the article/Supplementary Material. RNA-seq data can be found in GenBank under accession number: PRJNA876907. Proteome and ubiquitome data can be found in ProteomeXchange (http://www.proteomexchange.org/) under accession numbers: PXD036672 (proteome) and PXD036665 (ubiquitome).

Author contributions

CJ and YG conceived and designed the experiments. CJ and TJ performed most of the experiments, SD and SL contributed to the transcriptome assay, CY and YL contributed to the proteome assay. CM provided technical support and conceptual advice. CJ, TJ, and YG analyzed the data and wrote the article. All authors contributed to the article and approved the submitted version.

Funding

This study was supported by the National Natural Science Foundation of China (32102423), The Construction of Beijing Science and Technology Innovation and Service Capacity in Top Subjects (CEFF-PXM2019_014207_000032), and The improvement plan of scientific research and innovation ability for young teachers of Beijing university agriculture (QJKC2022015), and Science and Technology General Project of Beijing Municipal Education Commission (KM202110020008).

Conflict of interest

The authors declare that the research was conducted in the absence of any commercial or financial relationships that could be construed as a potential conflict of interest.

Publisher's note

All claims expressed in this article are solely those of the authors and do not necessarily represent those of their affiliated organizations, or those of the publisher, the editors and the reviewers. Any product that may be evaluated in this article, or claim that may be made by its manufacturer, is not guaranteed or endorsed by the publisher.

Supplementary material

The Supplementary Material for this article can be found online at: https://www.frontiersin.org/articles/10.3389/fpls.2022.1041141/full#supplementary-material

SUPPLEMENTARY TABLE 4
Changes in ubiquitinated proteins and ubiquitination sites.

SUPPLEMENTARY TABLE 5
Correlation between transcriptome and proteome.

SUPPLEMENTARY TABLE 6
Correlation between proteome and ubiquitome.

SUPPLEMENTARY TABLE 7
DEGs and DEPs related to the phenylpropanoid biosynthesis pathway.

SUPPLEMENTARY TABLE 8
Differentially expressed transcription factors in transcriptome, proteome, and ubiquitome.

References

Addicott, F. T. (1982). *Abscission* (Berkeley: University of California Press).

Cai, S., and Lashbrook, C. C. (2008). Stamen abscission zone transcriptome profiling reveals new candidates for abscission control: enhanced retention of floral organs in transgenic plants overexpressing arabidopsis ZINC FINGER PROTEIN2. *Plant Physiol.* 146, 1305–1321. doi: 10.1104/pp.107.110908

Estornell, L. H., Agusti, J., Merelo, P., Talon, M., and Tadeo, F. R. (2013). Elucidating mechanisms underlying organ abscission. *Plant Sci.* 199-200, 48–60. doi: 10.1016/j.plantsci.2012.10.008

Fan, W., Zheng, H., and Wang, G. (2021). Proteomic analysis of ubiquitinated proteins in maize immature kernels. *J. Proteomics* 243, 104261. doi: 10.1016/j.jprot.2021.104261

Gao, Y. R., Liu, Y., Liang, Y., Lu, J. Y., Jiang, C. Y., Fei, Z. J., et al. (2019). Rosa Hybrida RhERF1 and RhERF4 mediate ethylene- and auxin-regulated petal abscission by influencing pectin degradation. *Plant J.* 99, 1159–1171. doi: 10.1111/tpj.14412

Gao, Y., Liu, C., Li, X., Xu, H., Liang, Y., Ma, N., et al. (2016). Transcriptome profiling of petal abscission zone and functional analysis of an Aux/IAA family gene RhIAA16 involved in petal shedding in rose. *Front. Plant Sci.* 7, 1375. doi: 10.3389/fpls.2016.01375

Guo, J., Liu, J., Wei, Q., Wang, R., Yang, W., Ma, Y., et al. (2017). Proteomes and ubiquitylomes analysis reveals the involvement of ubiquitination in protein degradation in petunias. *Plant Physiol.* 173, 668–687. doi: 10.1104/pp.16.00795

Kim, ,. J. (2014). Four shades of detachment: regulation of floral organ abscission. *Plant Signal Behav.* 9, e976154. doi: 10.4161/15592324.2014.976154

Kim, Y. H., Kim, C. Y., Song, W. K., Park, D. S., Kwon, S. Y., Lee, H. S., et al. (2008). Overexpression of sweetpotato swpa4 peroxidase results in increased hydrogen peroxide production and enhances stress tolerance in tobacco. *Planta* 227, 867–881. doi: 10.1007/s00425-007-0663-3

Liang, Y., Jiang, C., Liu, Y., Gao, Y., Lu, J., Aiwaili, P., et al. (2020). Auxin regulates sucrose transport to repress petal abscission in rose (Rosa hybrida). *Plant Cell* 32, 3485–3499. doi: 10.1105/tpc.19.00695

Liu, X., Fang, P., Wang, Z., Cao, X., Yu, Z., Chen, X., et al. (2022). Comparative RNA-seq analysis reveals a critcal role for ethylene in rose (Rosa hybrida) susceptible response to podosphera pannosa. *Front. Plant Sci.* 13, 1018427. doi: 10.3389/fpls.2022.1018427

Liu, Q. Q., Luo, L., and Zheng, L. Q. (2018). Lignins: Biosynthesis and biological functions in plants. *Int. J. Mol. Sci.* 19, 335. doi: 10.3390/ijms19020335

Lu, J., Xu, Y., Fan, Y., Wang, Y., Zhang, G., Liang, Y., et al. (2019). Proteome and ubiquitome changes during rose petal senescence. *Int. J. Mol. Sci.* 20, 6108. doi: 10.3390/ijms20246108

Ma, C., Jiang, C.-Z., and Gao, J. (2021). Regulatory mechanisms underlying activation of organ abscission. *Annu. Plant Rev. Online* 4, 27–56. doi: 10.1002/9781119312994.apr0741

Meir, S., Hunter, D. A., Chen, J.-C. C., Halaly, V., and Reid, M. S. (2006). Molecular changes occurring during acquisition of abscission competence following auxin depletion in mirabilis jalapa. *Plant Physiol.* 141, 1604–1616. doi: 10.1104/pp.106.079277

Meir, S., Philosoph-Hadas, S., Sundaresan, S., Selvaraj, K. S., Burd, S., Ophir, R., et al. (2010). Microarray analysis of the abscission-related transcriptome in the tomato flower abscission zone in response to auxin depletion. *Plant Physiol.* 154, 1929–1956. doi: 10.1104/pp.110.160697

Ogawa, M., Kay, P., Wilson, S., and Swain, S. M. (2009). Arabidopsis dehiscence zone polygalacturonase1 (adpg1), adpg2, and quartet2 are polygalacturonases required for cell separation during reproductive development in arabidopsis. *Plant Cell* 21, 216–233. doi: 10.1105/tpc.108.063768

Patterson, S. E. (2001). Cutting loose. abscission and dehiscence in arabidopsis. *Plant Physiol.* 126, 494–500. doi: 10.1104/pp.126.2.494

Shahri, W., and Tahir, I. (2014). Flower senescence: some molecular aspects. *Planta* 239, 277–297. doi: 10.1007/s00425-013-1984-z

Swain, S., Kay, P., and Ogawa, M. (2011). Preventing unwanted breakups: using polygalacturonases to regulate cell separation. *Plant Signal Behav.* 6, 93–97. doi: 10.4161/psb.6.1.14147

Taylor, J. E., and Whitelaw, C. A. (2001). Signals in abscission. *New Phytol.* 151, 323–339. doi: 10.1046/j.0028-646x.2001.00194.x

Tucker, M. L., and Kim, J. (2015). Abscission research: what we know and what we still need to study. *Stewart Postharvest Rev.* 2, 7. doi: 10.2212/spr.2015.2.1

Vogt, T. (2010). Phenylpropanoid biosynthesis. *Mol. Plant* 3, 2–20. doi: 10.1093/mp/ssp106

Xie, X., Kang, H., Liu, W., and Wang, G. L. (2015). Comprehensive profiling of the rice ubiquitome reveals the significance of lysine ubiquitination in young leaves. *J. Proteome Res.* 14, 2017–2025. doi: 10.1021/pr5009724

Yeh, S. Y., Huang, F. C., Hoffmann, T., Mayershoferand, M., and Schwab, W. (2014). FaPOD27 functions in the metabolism of polyphenols in strawberry fruit (Fragaria sp.). *Front. Plant Sci.* 5, 518. doi: 10.3389/fpls.2014.00518

Zhao, Q., Nakashima, J., Chen, F., Yin, Y. B., Fu, C. X., Yun, J. F., et al. (2013). LACCASE is necessary and nonredundant with PEROXIDASE for lignin polymerization during vascular development in arabidopsis. *Plant Cell* 25, 3976–3987. doi: 10.1105/tpc.113.117770

frontiers | Frontiers in Plant Science

TYPE Review
PUBLISHED 24 October 2022
DOI 10.3389/fpls.2022.1044500

OPEN ACCESS

EDITED BY
Peitao Lü,
Fujian Agriculture and Forestry University, China

REVIEWED BY
Zheng Li,
Northwest A&F University, China
Qiang Li,
Agricultural University of Hebei, China

*CORRESPONDENCE
Huasen Wang
whsych66@163.com
Yong He
heyong@zafu.edu.cn

SPECIALTY SECTION
This article was submitted to Plant Systems and Synthetic Biology, a section of the journal Frontiers in Plant Science

RECEIVED 14 September 2022
ACCEPTED 12 October 2022
PUBLISHED 24 October 2022

CITATION
Zhao W, Zhao H, Wang H and He Y (2022) Research progress on the relationship between leaf senescence and quality, yield and stress resistance in horticultural plants.
Front. Plant Sci. 13:1044500.
doi: 10.3389/fpls.2022.1044500

Research progress on the relationship between leaf senescence and quality, yield and stress resistance in horticultural plants

Wenxue Zhao[1], Huayuan Zhao[2], Huasen Wang[1*] and Yong He[1*]

[1]Collaborative Innovation Center for Efficient and Green Production of Agriculture in Mountainous Areas of Zhejiang Province, College of Horticultural Science, Zhejiang Agriculture and Forest University, Lin'an, Hangzhou, China, [2]Bashan Management Area of the Management Committee for Taishan Historic and Scenic Area in Tai'an City, Tai'an, China

Leaf senescence, the final stage of leaf development, is one of the adaptive mechanisms formed by plants over a long period of evolution. Leaf senescence is accompanied by various changes in cell structure, physiological metabolism, and gene expressions. This process is controlled by a variety of internal and external factors. Meanwhile, the genes and plant hormones involved in leaf aging affect the quality, yield and stress resistance in horticultural plants. Leaf senescence mediated by plant hormones affected plant quality at both pre-harvest and post-harvest stages. Exogenous plant growth regulators or plant hormone inhibitors has been applied to delay leaf senescence. Modification of related gene expression by over-expression or antisense inhibition could delay or accelerate leaf senescence, and thus influence quality. Environmental factors such as light, temperature and water status also trigger or delay leaf senescence. Delaying leaf senescence could increase chloroplast lifespan and photosynthesis and thus improve source strength, leading to enhanced yield. Accelerating leaf senescence promotes nutrient redistribution from old leaves into young leaves, and may raise yield under certain circumstances. Many genes and transcriptional factors involved in leaf senescence are associated with responses to abiotic and biotic stresses. WRKY transcriptional factors play a vital role in this process and they could interact with JA signalling. This review summarized how genes, plant hormones and environmental factors affect the quality, yield. Besides, the regulation of leaf senescence holds great promise to improving the resistance to plant biotic and abiotic stresses.

KEYWORDS

leaf senescence, yield, quality, stress resistance, post-harvest storage

1 Introduction

Leaf senescence is the final stage of leaf development. It is the adaptive mechanism formed by plants in their long-term evolutionary process. The most evident morphological indicator of leaf senescence is the change in leaf color from green to yellow. Accompanied by the decrease of chlorophyll content, the protein content and net photosynthesis rate decline during leaf senescence. In general, leaf senescence is mainly controlled by the developmental age (Song et al., 2014). However, leaf senescence may be triggered by environmental clues. It has been suggested that 'programmed cell death' (PCD) in plants occurs at a specific stage of intrinsic senescence and becomes irreversible after leaf yellowing reaches a "point of no return" (Sobieszczuk et al., 2018). As the last step of leaf development, leaf senescence affects plant productivity and quality, either positively or negatively.

With the improvement of living standard and yield required for the increasing population, more attention is drawn to pre-harvest management and post-harvest management of plant cultivation. Once horticultural plants are harvested, the leaves have certain similarities with the aging caused by development. The plant leaves are like unique windows (Jan et al., 2018), revealing various changes of cells, tissues, and organs during aging. For instance, Reactive oxygen species (ROS) are accumulated during leaf senescence, contributing to the degradation of chlorophyll. On the contrast, increase Carbohydrate-related metabolism Plasma-Activated Water (PAW) enhanced the resistance to "chilling injury" and delayed leaf senescence in spinach, PAW treatment may contribute to the preservation of valuable nutrients (Uhlig et al., 2021). Plants usually redistribute nutrients from senescent leaves to other organs (Woo et al., 2019), and this strategy could be beneficial for the survive of plants under abiotic stresses, indicating low and high temperatures, drought stress. In addition, plant hormones may delay or advance leaf aging, Zhang et al. elaborated the role of salicylate and ROS in leaf senescence and plant immunity (Zhang et al., 2020). Furthermore, some genes are involved in leaf senescence. These genes are related to the degradation of proteins, nucleic acid and chlorophyll degradation and they are identified mainly by using mutants related to the aging process.

In this review, we summarized the relationship between leaf senescence and the quality, productivity, and stress resistance in horticultural plants (Figure 1). We focused on the molecular mechanism of leaf senescence. This review aimed to gain insights into the regulation of leaf senescence in horticultural industry. This provides a basis for maximizing yield and quality and enhancing stress resistance.

2 Leaf senescence and horticultural plant qualities

2.1 Plant hormones regulate leaf senescence and affect the quality of horticultural plants

Plant hormones affect most stages of the plant life cycle, including leaf senescence. Meanwhile, plant hormones are key players in the quality formation of horticultural plants. Thus modification of phytohormones could affect both leaf senescence and product quality (Figure 2).

2.1.1 Plant hormones regulate leaf senescence to affect pre-harvest quality

Exogenous hormones can delay the aging of pre-harvest leaves, increase photosynthesis, promote the accumulation of assimilates, and thus improve quality. For example, 10~80 mg/L 1-Naphthaleneacetic acid (NAA) and Gibberellin A_3 (GA_3) have significant effects on preventing A4 seedless lychee from falling fruit before harvest and improving the quality of fruit. Among them, treatment at 40 mg/L had the best effect on reducing the pre-harvest fruit drop rate. Treatment with GA_3 at a

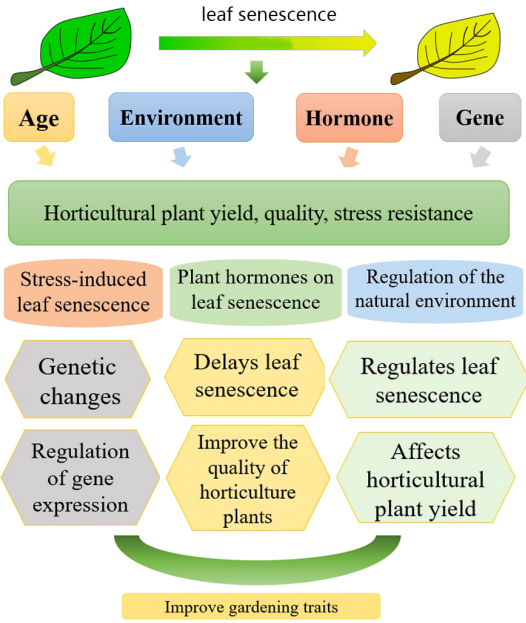

FIGURE 1
Relationship between leaf aging and the yield, quality and stress resistance in horticultural plants (leaf senescence of horticultural plants is subject to the influence of hormones, genes, exogenous hormones, and growth age control; aging has a certain effect on the yield, quality, and stress resistance of horticultural plants.).

concentration of 20 mg/L increased the single fruit weight of lychee (Yang et al., 2015). Cut flower roses sprayed with 1-Methylcyclopropene (1-MCP) before harvest have a storage period of up to 26 days. The 1-MCP treatment significantly extends the life of the bottle insert for 0 or 6 days for refrigerated flowers, extending them by 27.1% and 42.6%, respectively (Huang et al., 2017). During the growth process of thick-skinned melon, the leaves usually appear after fruit setting, and leaf aging causes their yellowing. Thus, photosynthesis rate cannot maintained, resulting in decreased yield and fruit quality. Exogenous 6-BA (Zhu, 2015) and exogenous calcium nitrate (Zhang et al., 2014) affected the aging of thick-skinned melon leaves and thus influenced their quality. Zhu et al. observed the soluble solid content and vitamin C content of T2 treated fruits were 12.3% and 11.3% higher than those of the control. (Zhu, 2015). Comprehensive previous studies have revealed that exogenous hormones slowed down the aging degree of leaves to a certain extent, prolonged photosynthesis, promoted the accumulation of assimilates, and improved the quality of horticultural plants.

2.1.2 Plant hormones regulate leaf senescence to affect post-harvest quality

For foliage plants and leafy vegetables, the status of leaves is an important attribute of product quality. For instance, the leafy vegetables should not be wilt, and have green color (Hassan and Mahfouz, 2012; Miret et al., 2018). Ethylene(ET) are considered to be involved in post-harvest process and leaf senescence (Tomotsugu, 2018). The release of ET during post-harvest promoted the over-accumulation of reactive oxygen species (ROS), leading to the yellowing of cabbage leaves (Yu and Xi, 1997). Low temperatures can inhibit ET production, thereby slowing down the yellowing of leaves and inhibiting chlorophyll degradation (Yu and Xi, 1997). Exogenous ET promoted the leaf yellowing and senescence and degradation of chlorophyll in fresh-cut chrysanthemums (Liu et al., 2022b). Treatment with 1-MCP at a concentration of 0.5 μl/L reduced respiration in the *Glebionis coronaria*, alleviated the decline in protein content, and extended shelf life. However, low concentration of 1-MCP (< 0.5 μl/L) did not affect shelf life of the *Glebionis coronaria*. (Ma, 2006).Gibberellic acid (GA) interacts with ET *via* DELLA proteins (Achard et al., 2006), and thus affect leaf senescence. During the storage process of Chinese cabbage, exogenous GA inhibited the expression of aging-related genes, delayed leaf aging and maintained a high chlorophyll content (Xiao et al., 2019). Pre-harvest spray of 20 $mg{\cdot}L^{-1}GA_3$ significantly reduced the rot rate of fruits during storage period, increased the accumulation of malondialdehyde (MDA), and delayed the degradation of vitamin C, thereby inhibiting the aging of Gongci fruit (Ma et al., 2009). Moreover, GA_3-treated cabbage maintained a high maximum quantum yield (Fv/Fm) and total chlorophyll content (Fan et al., 2018).

Abscisic acid (ABA) is a key player in stomatal closure, and thus influence the water loss during post-harvest. Manipulation of ABA levels has an important effect on postharvest quality of leafy vegetables. Miret observed ABA can inhibit leaf senescence during storage, thereby prolonging the shelf life of vegetables (Miret et al., 2017). ABA reactive protein *MdBT2* interacted with *MdbHLH93* to induce ubiquitination and degradation of *MdbHLH93* protein, thereby delaying leaf senescence in apple

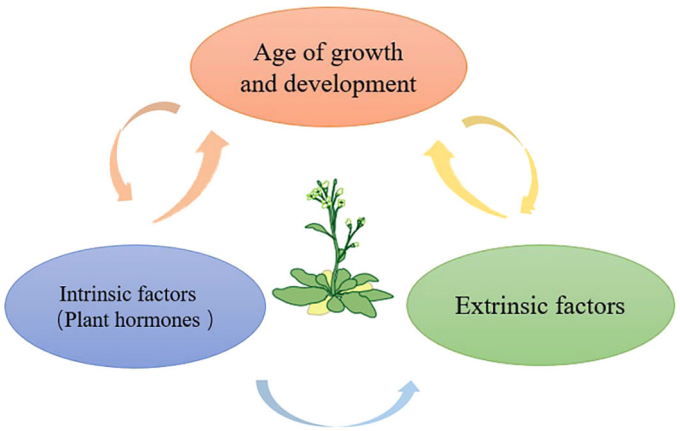

FIGURE 2
Leaf senescence is the final stage of leaf development, and leaf aging is regulated by a variety of factors, such as strict developmental age, exogenous factors and endogenous factors, thereby regulating the whole process of plant growth and development.

(An et al., 2019). The ABA pretreatment significantly reduced the brown detergentilence of the 'Yellow Crown' pear, improved the ability of POD, APX and peel free radical to varying degrees, and reduced the MDA content (Liu et al., 2017). ABA treatment is used to inhibit the aging of leafy vegetables, improve the postharvest quality of storage at room temperature, and delay the loss of sensory metabolites.

Cytokinins bear upon leaf senescence in horticultural plants. An increase in cytokinin level is thought to block the aging process of leaves associated with age and stress, thereby preserving the photosynthetic properties of the leaves (Lira et al., 2017). Chen et al. discovered that after Forchlorfenuron (CPPU) treatment, the degradation rate of soluble proteins after 3 d of storage at room temperature was significantly slower than that of the control cabbage. CPPU can inhibit the activity of cabbage heart protein hydrolases and slow down yellowing, thereby improving the quality of postharvest gardening plants (Chen et al., 2001). 6-BA can delay the aging of yellow flowers of cauliflower (Gao, 1998).

Based on the analysis of previous studies, exogenous hormones can delay leaf aging, thereby improving the photosynthesis of plant leaves, which has an important effect on postharvest storage. This property extends the shelf life and promotes the postharvest quality of horticultural plants, which helps to increase in their market value.

2.2 Leaf senescence under genetic regulation affects the quality of horticultural plants

In modern horticultural production, genetic modification could become a key strategy for improving biomass and nutritional quality. Genes that change in expression levels during leaf senescence are called leaf senescence- associated genes (SGAs). In previous studies, a large number of SAGs have been isolated in rice (Table 1). These senescent genes are involved in macromolecular degradation, nutrient redistribution, transcriptional regulation, stress defense, etc. (Leng et al., 2017; Woo et al., 2019). In tomatoes, promoters SGA12/SGA13 come into play, flowering earlier and increasing chlorophyll content, thereby increasing yield (Swartzberg et al., 2006). Antisense inhibition of *GIGANTEA*(*BoGI*) in kale (*Brassica oleracea* var. *sabellica*)

TABLE 1 Promoter/Transcription factor regulates the effects of leaf senescence on horticultural plants (n.d. = not determined).

Plant	Promoter/Transcription factor	Chlorophyll	Biomass/yield	References
Tomato	AGPaseS1	n.d.	n.d.	Luo et al. (2005)
Tomato	SAG12/SAG13	Advanced flowering	Fruit weight increases	Swartzberg et al. (2006)
Canola	AtMYB32	Chlorophyll levels are high	Production increases	Kant et al. (2015)
eggplant	SAG12	Higher than wild type	Yield increases	Xiao et al. (2017)
Rosa hybrida	RhGA20ox1	n.d.	n.d.	Lü et al. (2014)
Brassica napus L.	SAG12	Decreased chlorophyll content of old leaves and nitrogen deficiency	n.d.	Gombert (2006)
cucumber	SAG12	Chlorophyll increases	Production increased	Liu et al. (2022a)
Camellia oleifera Abel.	SAG12	Delay chlorophyll degradation	Yield increased	Yang et al. (2020)
Tomato	SAG12/SAG13	n.d.	n.d.	Swartzberg et al. (2011)
Gerbera	SAG12/SAG13	n.d.	Extend lifespan	Huang et al. (2021)
Betula platyphylla	BpEIN3.1	n.d.	Yield increased	Song et al. (2022)
Chinese flowering cabbage	BrNAC087	n.d.	n.d.	Fan et al. (2021)
Tomato	SlERF.F5	The accumulation of chlorophyll content is reduced	n.d.	Chen et al. (2022)
Tomato	SlNAP2	Production increases	Production increases	Ma et al. (2018)
Brassica napus L.	*BnaNAM*	n.d.	n.d.	Wang et al. (2022)
Chinese flowering cabbage	*BrNAC041*	n.d.	n.d.	Fan et al. (2020)
Brassica napus L.	*BnaWGR1*	n.d.	n.d.	Yang et al. (2018)
Chinese flowering cabbage	*BrTCP21*	n.d.	n.d.	Xiao et al. (2019)

delayed both leaf senscence and flowering (Thiruvengadam et al., 2015).

Leaf aging affects the quality of apple fruit, Wang et al. cloned the *MhYTP1* and *MhYTP2* genes, and found that their expressions were positively correlated with plant leaf senescence, suggesting that these genes can be indicator of plant senescence (Wang et al., 2017).Tomato transcription factor SlWRKY37 can regulate dark leaf senescence, which can reduce tomato sensitivity to external aging signals, thus providing target genes for delayed leaf yellowing (Wang et al., 2022). Tomato *MYC2*, as a key factor in leaf senescence, transduces jasmonic acid (JA) signaling and induces JA-mediated senescence in tomato leaves by accelerating chlorophyll degradation and inhibiting carbon fixation (Ding et al., 2022). *BnaNTL1* is a membrane-bound NAC (NAM, ATAF and CUC) transcription factor (TF) in rape (Yan et al., 2021) and it is expressed primarily in senescent leaves and can actively regulate ROS production. By regulating key genes, *BnaNTL1* can promote the fruit ripening period and postharvest storage, regulate the ripening time, and extend shelf life. Through the regulation of leaf aging genes, the quality of horticultural plants is improved to a certain extent and the shelf life is extended.

2.3 Leaf senescence and horticultural plant quality under environmental regulation

Environmental stresses such as drought, waterlogging, high-temperature, low-temperature, soil salinity stresses, are important factors restricting plant productivity. Environmental stress regulates leaf aging, affecting both quality and yield in horticultural plants.

2.3.1 Temperature

In general, low temperature during post-harvest inhibits the leaf respiration and delays leaf senescence. Low temperature provides a way for spinach post-harvest preservation storage by delaying the decline of antioxidant enzyme activity and leaf aging (Tian et al., 2014). Under low-temperature storage, especially at 0° conditions, it can maintain the high nutrient content of slow down leaf aging, prolong shelf life, and solve the problem of rapid yellowing of leaves (An et al., 2020). In *Arabidopsis thaliana*, low temperature inhibited the phyB nucleus output, thereby inhibiting the transcriptional activity of ET signaling media and delaying leaf senescence (Lee et al., 2022). On the contrast, high temperature acceleated leaf aging, decreasedthe soluble protein content of strawberries, which directly affected the photosynthetic ability of strawberries (Yang et al., 2012).

2.3.2 Light

Both light intensity and light quality affect the leaf senescence and plant quality in horticultural plants. Extremely low light intensity such as darkness accelerates leaf aging and affects grain and oil yield in sunflower (Dosio et al., 2020). During low light intensity, carbon fixation efficiency determines leaf senescence; however, plant photoreceptor pigment A has a regulatory effect on carbon fixation efficiency (Brower et al., 2012). High light intensity could induce light inhibition and damage. Shading net is a routine measure in horticulture production. Under the color shading net, the quality of the grapes is better than those under black shading nets because the absence of high light intensity causes premature leaf failure, which improves the quality of grapes; the soluble solids are also affected differently under various shade nets, whereas unshashed grapes show thermal damage (Zha et al., 2022). Studies have shown that Supplemental lighting(SL) sources affect the physiology and productivity of plants. Supplemental lighting (SL) within the canopy increases the overall tomato yield and maintains the nutrient content of plants (Gómez and Mitchell, 2016). Besides, light quality has a certain influence on the growth of rhododendrons. Exposure to short period of ultraviolet radiation per day improved water utilization inside plants, thereby delaying the aging of tomato leaves, favoring plants to cope with drought conditions, and playing a key role in water-saving irrigation in agriculture (Mannucci et al., 2022). RBL(red and blue lights) can increase the synthesis of photosynthetic pigments and improve antioxidant enzyme activity. This process delays leaf aging and ensures plant growth. (Wang,Y. et al.,2017)

2.3.3 Moisture

Maximizing leaf lifespan is the key to tea quality; drought and cold have a combined effect on leaf senescence and tea quality (Zheng et al., 2016). Zhao et al. (2016) reported that PYL9 and leaf senescence play an important role in coping with drought stress. PYL9 inhibits drought by limiting water loss during respiration, and the combination of ABA receptor PYL9 and other transcription factors accelerates leaf senescence, thereby improving drought tolerance and survival in plants. The upregulation of SAG12 gene and downregulation of *Cab* gene reflects the transition of sinks/sources in cabbage-type rape leaves, which are accurate physiological indicators of leaf aging and can effectively identify the degree of nitrogen deficiency in leaves (Gombert, 2006).

The environment is essential for the adaptability and productivity of plants. Leaf aging is an important stage of development for productivity and quality. Natural environmental factors such as light, temperature, and moisture all regulate leaf aging, which affects the quality of horticultural plants.

3 Leaf senescence and horticultural plant yield

3.1 Increasing horticultural plant yield by increasing chloroplast lifespan

Leaf senescence is caused by the gradual loss of green pigment and the degradation of chlorophyll (Gan and Hörtensteiner, 2013). Thomas hypothesized that extending the maximum photosynthetic period delays the aging process, thereby increasing yield (Thomas and Stoddart, 1980). Photosynthesis is the basis of plant growth and material accumulation and important for nutrient accumulation, quality formation and sustainable development of production capacity. Manipulating leaf aging-related genes is an effective strategy to improve pulp yield (Lira et al., 2017), that is, by delaying leaf aging to prolong the photosynthetic characteristics of leaves, thereby enhancing source activity. Zhao et al. (2022) revealed the changes in photosynthetic ability of grape leaves during development and aging and analyzed the nutrient absorption of leaves during the growing season; their results showed significance for improving the yield of horticultural plants. ROS has been identified as a dependent signal to mediate leaf aging, analyzed the differences between dark-induced and natural aging, and proposed to increase plant yield by increasing the chloroplast lifespan (Bartoli et al., 2013; Weaver et al., 1998; Buchanan-Wollaston et al., 2005).

The shortage of assimilates in leaves eventually accelerates the maturation process of plants (Gan, 2003), strongly affecting plant productivity. The most evident manifestation of leaf senescence is the breakdown of chlorophyll into non-green derivatives, which causes the yellowing of leaves (Mayta et al., 2019). As the keys to nutrient cycling, chloroplast degradation and Rubisco play important roles, with protein degradation starting in chloroplasts (Feller et al., 2008). Given that chloroplasts contain most of the nutrients, they are the main source during plant carbon and nitrogen cycles. The disintegration of photosynthetic organs is a developmental stage in the aging process. ROS production is likely to be caused by changes in the electronic pathway and photosynthetic organs. Chloroplasts are the most important site of ROS production (Laloi and Havaux, 2015). The subcellular localization of *OsPLS4*, which is found in chloroplasts, chloroplast development and biosynthesis of rice cuticle waxes are affected by *OsPLS4* mutations, decreased photosynthetic rate, and premature leaf aging (Zhou et al., 2020). Cytokinin slows down leaf senescence and prevents chlorophyll degradation and destruction (Talla et al., 2016). Delaying leaf aging and maintaining the green color of leaves has various meanings, including provision of more carbon and promoted root growth; thus, the onset of aging promotes the increase in plant yield.

3.2 Raising yield *via* delaying of leaf senescence

Improving the photosynthetic efficiency is the basis for increasing yields. Delaying the aging of plant leaves, which increases the leaf area to a certain extent, is conducive to plant photosynthesis, thus increasing the accumulation of assimilates (Figure 3).

The study revealed that *pSARK-IPT* transgenic plants can increase CO2 fixation under drought conditions and delay leaf aging, thereby increasing tolerance to extreme drought. Moreover, the yield of genetically modified plants has increased significantly (Blumwald et al., 2009). For the peach

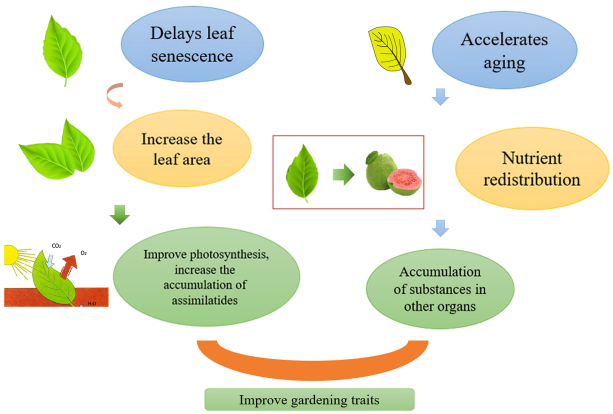

FIGURE 3
Regulation of leaf aging affects horticultural plant yield, delays leaf aging, increases leaf area, thereby improving photosynthesis and increasing the accumulation of assimilates. Accelerates leaf aging, redistributes nutrients, and promotes the accumulation of substances in other organs. Both pathways can increase yields.

tree, the aging of roots and leaves is delayed, and the nutrient storage level is increased, thereby increasing the fruit yield (Zhang et al., 2021). Shading delays the aging of peony leaves, thereby increasing photosynthetic capacity. The development of seeds and accumulation of nutrients are prolonged, thereby increasing the yield (Han et al., 2020). Improving nitrogen utilization can delay the aging of rapeseed leaves. Varieties with high nitrogen use can adapt to low light conditions during flowering. Studies have also shown a positive correlation between nitrogen use and delayed leaf senescence (Schulte auf'm Erley et al., 2007). Precise regulation of leaf aging enables plants to respond quickly to environmental signals. In apples, *MdAB15* inhibits the transcriptional activity of downstream target genes *MdNYE1* and *MdNYC1*. This condition slows down the aging of ABA-induced leaves (An et al., 2021). DCPTA is sprayed on the foliar surface of sugar beet to enhance leaf development and photosynthetic productivity. Rubisco activity is increased to a certain extent, demonstrating an increase in plant net photosynthesis. Delayed leaf aging increases net carbon assimilation of leaves (Keithly et al., 1990). In the late stage of growth and development, especially in the period of yield formation, the delayed leaf aging and maintenance of the leaf area are keys to improving the accumulation of dry matter. In summary, delaying the onset of leaf aging can improve photosynthesis, which in turn increases horticultural plant yields.

3.3 Improving yield through nutrient redistribution mediated by accelerated leaf senescence

As leaves begin to age, the materials they have accumulated during the growth phase are converted into nutrients that can be exported and supplied to other tissues and organs (Woo et al., 2019). Aging is accompanied by the reuse of nutrients, which can increase plant yield to a certain extent (Figure 3). When a plant is subjected to adversity stress, the leaves age early, allowing the plant to adapt better to the environment. For several annual plants, nutrients are transferred to the fruit and grain as the leaves age. A study showed that C2H2-type zinc finger *MdZAT10* can accelerate the aging of apple leaves (Yang et al., 2021). In Arabidopsis, knocking out *HDA15* can accelerate leaf aging and promote plant flowering (Huang et al., 2022). In safflower, *CtCP1* promotes the hydrolysis of the CtbHLH41 protein, accelerating the transcriptional activity of related genes and leaf senescence (Hong et al., 2022). A study revealed that *MdHHO3* promotes early leaf aging under nitrate deficiency, which proves that the lack of nitrates can cause aging of apple leaves (Wen et al., 2022). The sink-source relationship affects leaf aging, and the large source of the sink or the large source of the sink will lead to abnormal leaf maturity. Both the sink and the source are important factors that determine yield. If plant vegetative growth is too vigorous, reproductive growth is restricted, resulting in reduced yield and quality. Therefore, to ensure the coordination of the relationship between the sink and the source, we can obtain high-yield and high-quality horticultural crops. Reproductive growth also promotes leaf senescence to a certain extent. A competition for nutrition exists between vegetative and reproductive organs. In summary, accelerating leaf senescence can increase yield to a certain extent.

3.4 Genes regulate leaf senescence and horticultural plant yield

Genetic modification can delay leaf aging, maintain photosynthesis for a long time, and sustain leaf activity, thereby increasing yield. According to Kant et al., the IPT gene encodes cytokinin synthesis to delay the aging of rapeseed leaves under flooding conditions. During long periods, transgenic rapeseed maintains the high chlorophyll levels, which improves crop yield under water stress conditions (Kant et al., 2015). At the genetic level, plant responses to stresses differ significantly from aging procedures and are associated with accelerated aging process (Guo and Gan, 2011). Leaf senescence caused by environmental stress or intrinsic inheritance can reduce photosynthesis, lead to premature cell death, and cause the supply of anabolites to decrease before flowering, thus negatively regulating the final grain weight (Gregersen et al., 2008). In numerous annual plants, such as monocotyledonous plants, aging is usually controlled by reproductive structures. Mature leaves are regulated by environmental and other organ physiological signals that trigger reversible events, which eventually lead leaves at to a "point of no return", which is a sign of the onset of irreversible aging (Lim et al., 2007). Genes, such as the NAC transcription factor *S1NAP2* that controls the aging of tomato leaves. This prolongs the photosynthesis time of the leaves, which increases the fruit yield and sugar content of tomatoes (Ma et al., 2018). In cucumbers, transient expression of the MT and MT synthetic gene *CsASMT* inhibits leaf senescence under dark conditions. MT delays leaf aging, reduces the rate of decline in chlorophyll, and promotes photosynthesis. This condition speeds up the growth of cucumbers and increases yield (Liu et al., 2022a). In Chinese cabbage leaf senescence, ET reactive factor (ERF) works in conjunction with JA. The transcription factor *BrERF72* is a nucleus-localizing protein that activates the expression of JA biosynthetic genes by directly targeting its promoter (Tan et al., 2018). In summary, leaf senescence is not controlled by a single gene, but by a polygenic regulatory system. Predecessors revealed that the aging gene, which regulates leaf aging at the molecular level, provides a basis for anti-aging breeding of horticultural plants and increasing yields.

4 Leaf senescence and plant stress resistance

4.1 Leaf senescence and disease resistance of horticultural plants

For plants that are frequently exposed to adverse conditions, biological and abiotic stresses are inevitable during the growing season (Gregersen et al., 2013). Leaf senescence is an important component of plant development and an adaptation strategy for plants to cope with stress. It can also reduce pathogen transmission. Zhang et al. observed that powdery mildew and propabenzole (PBZ)-activated ethylene (ET) signal transduction, upregulates the expressions of *CSEIN3* and *CsCCGs* and *CsRBOHs*, leads to leaf senescence, and improves the plant's resistance to powdery. An invading pathogen causes a "suicide" hypersensitivity reaction in leaves, which triggers a cascade of immune responses and a slow green loss phenomenon, which is indicative of the rapid aging process of cells (Zhang et al., 2022). Wang et al. have also shown that cucumber anthrax and downy mildew resistance is directly regulated by NYE1/SGR1 (Wang et al., 2019).

The improvement of leaf disease resistance is an important factor for the increase in plant yield. Plant leaf aging reduces the invasion of pathogens to a certain extent. Numerous genes that control leaf aging are also involved in plant stress resistance. In eggplant, P-SAG12-IPT overexpression plays a role in delayed leaf aging while enhancing tolerance to drought and cold; the activity of ROS-scavenging enzymes is higher than that of wild-type eggplant, and growth rate and yield are relatively improved (Xiao et al., 2018).

WRKY18 works with WRKY40 and WRKY60 and can modulate disease resistance. WRKY18, WRKY40, WRKY60 three mutants and double mutants WRKY18, WRKY40 and WRKY18, WRKY60 are significantly more resistant to lilac. In addition, in terms of resistance to powdery mildew fungi, two mutants, WRKY18, are more resistant to WRKY40 (Xu et al., 2006). WRKY70 expression has a diametrically opposite effect on the resistance of Arabidopsis necrotrophic bacteria and biotrophic bacteria (Li et al., 2006). Mutant *nore1-1*was found in EMS mutagenesis of *Arabidopsis thaliana*; it is associated with leaf senescence, where the mutant activates the defense system, accelerates leaf senescence, and improves the plant's disease resistance (Lee et al., 2016). Salicylic acid (SA) and reactive oxygen species (ROS) can regulate leaf senescence and defend against pathogen invasion. The WRKY55 transcription factor accelerates leaf senescence and improves resistance to Pseudomonas syringum by modulating these two factors (Wang et al., 2020). In rice, the overexpressed *OsNBL1* interacts with the localized protein *OsClpP6*, delays leaf senescence, contains a higher chlorophyll content than wild-type plant leaves, and is critical for salt and disease resistance (Zhao et al., 2021). Leaf aging plays a key role in disease resistance. Regulating leaf aging is conducive to horticultural plants to cope with different diseases, and to a certain extent, the resistance of plants is improved.

4.2 Leaf senescence and stress resistance of horticultural plants

Regulation of the aging process in leaves is a part of the adaptation of plants to different environmental conditions, especially drought stress. Usually, numerous transgenic plants exhibit matching drought resistance and green leaf traits. Darkness can induce leaf senescence, and shading is an important way to improve plant performance (Brower et al., 2012). Field crops will benefit from shady and dark conditions, resulting in nutrient remobilization after leaf aging, which is conducive to the photosynthesis of plants. Under the induction of dark environment and JA, the aging rate of plant leaves significantly improves. Specifically, SlWRKY37 plays a positive role in regulating leaf aging in tomatoes. Wang et al. revealed the function of SlWRKY37 in leaf aging, and delayed leaf yellowing by reducing the sensitivity to external aging signals through a target gene (Wang, Z. et al. 2022). Sucrose phosphatase prevents plant leaf senescence under drought stress conditions (Sami et al., 2016). Cytokinin levels in roots are suppressed due to nutrient deficiencies, causing leaf senescence and allowing nutrient transport (Maillard et al., 2015; Havé et al., 2016). Delays the onset of leaf senescence, improves photosynthesis, and as nutrients are transferred from old leaves to young leaves, the antioxidant capacity of plants increases to resist stress and allow normal growth to return (Jan et al., 2018). WRKY transcription factors have an important influence on leaf senescence and environmental stress. Gu et al. isolated the gene GhWRKY91 from WRKY, and its transgenic plants showed a strong drought tolerance, delayed degree of leaf aging in an arid environment, enhanced gene expression associated with drought stress, and relatively weakened aging gene (Gu et al., 2019). Tea plants generally grow under cold and drought stress conditions, which affect their quality and leaf aging. Zheng et al. discovered that drought induction delays leaf aging, thus enhancing antioxidant capacity, prolonging photosynthesis, and revealing the relationship between quality, stress resistance, and leaf life (Zheng et al., 2016). Lee et al. identified the drought-responsive NAC transcription factor NTL4, which promotes the production of ROS in senescent leaves under drought stress and accelerates leaf aging; however, mutants lacking NTL4 show delayed leaf senescence and improved drought resistance (Lee et al., 2012). Accelerate leaf senescence and improve nutrient reuse, pepper leaves, after inoculation with CMV, accelerate senescence and improve resistance, and the difference between CMV-inoculated resistant peppers and sensitive peppers and changes in their photosynthesis was studied (Stefanov et al., 2011). Hu et al. reviewed the relationship between JA-mediated leaf senescence

and tolerance to cold stress and observed that JA treatment can increase the expression of senescent genes (Hu et al., 2017). The drought tolerance of sorghum after flowering is tightly bound to the greening of leaves, thereby increasing biomass (Harris et al., 2019). Overexpressed *SlERF5* in transgenic tomatoes can maintain leaf moisture status and chlorophyll concentrations, giving plants strong salt stress and drought tolerance; however, studies have shown the minimal influence of these findings on production (Pan et al., 2012). The short period of ultraviolet radiation per day has a certain effect on improving water utilization inside the plant, thereby delaying the aging of Tom tomato leaves, favoring plants to cope with drought conditions, and playing a key role in water-saving irrigation in agriculture (Mannucci et al., 2022). The use of ABA has a slight effect on the yield composition and vegetative growth of grapes, but it can lead to aging, shedding, and dormancy of grape leaves, which increases freezing tolerance (Li and Dami, 2015). Delaying the aging of plant leaves can improve the stress resistance of plants to a certain extent. After the aging of the leaves is slowed down, photosynthesis is enhanced, which is conducive to plants coping with various stressful environments.

5 Conclusions and perspectives

This paper reviews the relationship between leaf aging and horticultural plant quality, yield, and stress resistance. Through the quality analysis of horticultural plants before and after harvest, most of the reports revealed a certain relationship with leaf aging. Delayed leaf aging plays an important role in prolonging the shelf life of vegetable fruits and is conducive to occupying a huge market potential. We summarized the different roles of various plant hormones which are an important part of regulating plant quality, in the storage of horticultural plants. Through the analysis of gene regulation, that of the WRKY family, NAC family, etc., the potential mechanism of regulating leaf aging, which is the key to maintaining optimal productivity and improving the survival of offspring, can be studied to optimize the productivity of horticultural plants. In addition, we analyzed the possible effects of various environmental conditions on the quality of horticultural plants, and concluded that light, temperature, and moisture all played a pivotal role. Through the summary analysis of leaf senescence and plant yield, delaying the onset of leaf senescence and improves photosynthesis, thereby promoting the accumulation of assimilates to increase yield. Meanwhile, accelerating the aging rate of leaves, improves the reuse of nutrients and promotes the accumulation and maturation of fruit nutrients. Although photosynthesis and photoconjugates play important roles in leaf aging, the molecular mechanisms of aging induction need to be further studied. Controlling leaf aging has important implications for agricultural and horticultural production. Screening mutants with missing functions during leaf aging is beneficial to unravel the mystery of the molecular mechanism of leaf senescence. We believe that by delaying leaf aging, coupled with improved photosynthesis and tolerance to stress, it is possible for horticultural plants to achieve stable yields and yield potential. Leaf senescence is an important part of plant development, but also an adaptation strategy for plants to cope with stress, and the regulation of the aging process is an important method for plants to adapt to different environmental conditions. In summary, the relationship between aging and productivity, quality, and stress tolerance is complex. To achieve high yield and quality of horticultural crops, experts in different fields must work together.

Author contributions

YH, WZ and HW conceived and designed the review. WZ wrote the manuscript, and YH proposed revisions to the manuscript. All authors contributed to the article and approved the submitted version.

Funding

This study was supported by Lingyan Project of Science and Technology Department of Zhejiang Province (Grant No.2022C02051), the National Natural Science Foundation of China (Grant Nos.31872105, 31972221, 32002048), Ministry of Agriculture, and the National Key Research and Development Program of China (Nos.2018YFD1000800 and 2019YFD1000300)

Conflict of interest

The authors declare that the research was conducted in the absence of any commercial or financial relationships that could be construed as a potential conflict of interest.

Publisher's note

References

Achard, P., Cheng, H., De Grauwe, L., Decat, J., Schoutteten, H., Moritz, T., et al. (2006). Integration of plant responses to environmentally activated phytohormonal signals. *Science* 311, 91–94. doi: 10.1126/science.1118642

An, R., Chen, W., Hu, H., and Li, P. (2020). Effects of storage temperature on senescence and active ingredients of postharvest shanghai green leaves. *Packaging Eng.* 41 (09), 7–16. doi: 10.19554/j.cnki.1001-3563.2020.09.002

An, J. P., Zhang, X. W., Bi, S. Q., You, C. X., Wang, X. F., and Hao, Y. J. (2019). Mdb HLH 93, an apple activator regulating leaf senescence, is regulated by ABA and md BT 2 in antagonistic ways. *New Phytol.* 222 (2), 735–751. doi: 10.1111/nph.15628

An, J. P., Zhang, X. W., Liu, Y. J., Zhang, J. C., Wang, X. F., You, C. X., et al. (2021). MdABI5 works with its interaction partners to regulate abscisic acid-mediated leaf senescence in apple. *Plant J.* 105 (6), 1566–1581. doi: 10.1111/tpj.15132

Bartoli, C. G., Casalongué, C. A., Simontacchi, M., Marquez-Garcia, B., and Foyer, C. H. (2013). Interactions between hormone and redox signalling pathways in the control of growth and cross tolerance to stress. *Environ. Exp. Bot.* 94, 73–88. doi: 10.1016/j.cbpa.2009.04.414

Blumwald, E., Rivero, R. M., Wadia, H., Peleg, Z., Szczerba, M., Jauregui, R.N., Li, L., et al. (2009). Delayed leaf senescence induces extreme drought tolerance incrop plants. *Comparative Biochemistry and Physiology Part A: Molecular & Integrative Physiology*, 153 (2), S188. doi: 10.1016/j. cbpa.2009.04.414

Brower, B., Ziolkowska, A., Bagard, M., Keech, O., and Gardestrom, P. (2012). The impact of light intensity on shade-induced leaf senescence. *Plant Cell Environ.* 35 (6), 1084–1098. doi: 10.1111/j.1365-3040.2011.02474.x

Buchanan-Wollaston, V., Page, T., Harrison, E., Breeze, E., Lim, P. O., Nam, H. G., et al. (2005). Comparative transcriptome analysis reveals significant differences in gene expression and signalling pathways between developmental and dark/starvation-induced senescence in arabidopsis. *Plant J.* 42 (4), 567–585. doi: 10.1111/j.1365-313x.2005.02399.x

Chen, Y., Feng, P., Tang, B., Hu, Z., Xie, Q., Zhou, S., et al. (2022). The AP2/ERF transcription factor SlERF. F5 functions in leaf senescence in tomato. *Plant Cell Rep.* 41 (5), 1181–1195. doi: 10.1007/s00299-022-02846-1

Chen, Q., Ye, H., Liu, W., LI, Y., and Chen, J. (2001). The role of CPPU in delaying the aging of cabbage leaves. *Northwest Bot. Sin.* 21 (06), 197–200. doi: 10.3321/j.issn:1000-4025.2001.06.032

Ding, F., Wang, C., Xu, N., Zhang, S., and Wang, M. (2022). SlMYC2 mediates jasmonate-induced tomato leaf senescence by promoting chlorophyll degradation and repressing carbon fixation. *Plant Physiol. Biochem.* 180, 27–34. doi: 10.1016/j.jplph.2008.11.002

Dosio, G. A. A., Izquierdo, N. G., Núñez Bordoy, E. I., and Aguirrezábal, L. A. N. (2020). Leaf senescence did not account for variations in grain and oil yield observed in sunflower under radiation limiting conditions. *Agric. For. Meteorology* 291, 108032. doi: 10.1016/j.agrformet.2020.108032

Fan, Z. Q., Tan, X. L., Shan, W., Kuang, J. F., Lu, W. J., and Chen, J. Y. (2018). Characterization of a transcriptional regulator, BrWRKY6, associated with gibberellin-suppressed leaf senescence of Chinese flowering cabbage. *J. Agric. Food Chem.* 66 (8), 1791–1799. doi: 10.1021/acs.jafc.7b06085

Fan, Z. Q., Tan, X. L., Shan, W., Kuang, J. F., Lu, W. J., Lin, H. T., et al. (2020). Involvement of BrNAC041 in ABA-GA antagonism in the leaf senescence of Chinese flowering cabbage. *Postharvest Biol. Technol.* 168, 111254. doi: 10.1016/j.postharvbio.2020.111254

Fan, Z., Wei, W., Tan, X., Shan, W., Kuang, J., Lu, W., et al. (2021). A NAC transcription factor BrNAC087 is involved in gibberellin-delayed leaf senescence in Chinese flowering cabbage. *Postharvest Biol. Technol.* 181, 111673. doi: 10.1016/j.postharvbio.2021.11167

Feller, U., Anders, I., and Mae, T. (2008). Rubiscolytics: Fate of rubisco after its enzymatic function in a cell is terminated. *J. Exp. Bot.* 59, 1615–1624. doi: 10.1093/jxb/erm242

Gan, S. (2003). Mitotic and postmitotic senescence in plants. *Sci. Aging Knowledge Environ.* 2003 (38), re7–re7. doi: 10.1126/sageke.2003.38.re7

Gan, S.-S., and Hörtensteiner, S. (2013). Frontiers in plant senescence research: from bench to bank. *Plant Mol. Biol.* 82 (6), 503–504. doi: 10.1007/s11103-013-0098-0

Gao, X. (1998). Research on broccoli storage technology. *Yangtze River Vegetables* 11, 36–37. Available at: https://kns-cnki-net-443.webvpn.zafu.edu.cn/kcms/detail/detail.aspx?FileName=CJSC199811025&DbName=CJFQ1998.

Gombert, J. (2006). The expression patterns of SAG12/Cab genes reveal the spatial and temporal progression of leaf senescence in brassica napus l. with sensitivity to the environment. *J. Exp. Bot.* 57 (9), 1949–1956. doi: 10.1093/jxb/erj142

Gómez, C., and Mitchell, C. A. (2016). Physiological and productivity responses of high-wire tomato as affected by supplemental light source and distribution within the canopy. *J. Am. Soc. Hortic. Sci.* 141 (2), 196–208. doi: 10.21273/JASHS.141.2.196

Gregersen, P. L., Culetic, A., Boschian, L., and Krupinska, K. (2013). Plant senescence and crop productivity. *Plant Mol. Biol.* 82 (6), 603–622. doi: 10.1007/s11103-013-0013-8

Gregersen, P. L., Holm, P. B., and Krupinska, K. (2008). Leaf senescence and nutrient remobilisation in barley and wheat. *Plant Biol.* 10, 37–49. doi: 10.1111/j.1438-8677.2008.00114.x

Gu, L., Ma, Q., Zhang, C., Wang, C., Wei, H., Wang, H., et al. (2019). The cotton GhWRKY91 transcription factor mediates leaf senescence and responses to drought stress in transgenic arabidopsis thaliana. *Front. Plant Sci.* 10. doi: 10.3389/fpls.2019.01352

Guo, Y., and Gan, S.-S. (2011). Convergence and divergence in gene expression profiles induced by leaf senescence and 27 senescence-promoting hormonal, pathological and environmental stress treatments. *Plant Cell Environ.* 35 (3), 644–655. doi: 10.1111/j.1365-3040.2011.02442.x

Han, C., Yu, M., Wang, Q., Wang, L., Yang, H., Zhao, Y., et al. (2020). Leaf structure and seed histochemistry analyses provided structural insights into the improved yield and quality of tree peony seed under light shading conditions. *Sci. Rep.* 10 (1), 1–9. doi: 10.1038/s41598-020-61366-8

Harris-Shultz, K. R., Hayes, C. M., and Knoll, J. E. (2019). Mapping QTLs and identification of genes associated with drought resistance in sorghum. *Sorghum* 1931, 11–40. doi: 10.1007/978-1-4939-9039-9_2

Hassan, F. A. S., and Mahfouz, S. A. (2012). Effect of 1-methylcyclopropene (1-MCP) on the postharvest senescence of coriander leaves during storage and its relation to antioxidant enzyme activity. *Scientia Hortic.* 141, 69–75. doi: 10.1016/j.scienta.2012.04.021

Havé, M., Marmagne, A., Chardon, F., and Masclaux-Daubresse, C. (2016). Nitrogen remobilisation during leaf senescence: lessons from arabidopsis to crops. *J. Exp. Bot.* 68 (10), erw365. doi: 10.1093/jxb/erw365

Hong, Y., Zhang, J., Lv, Y., Yao, N., and Liu, X. (2022). The safflower bHLH transcription factor CtbHLH41 negatively regulates SA-induced leaf senescence through interaction with CtCP1. *Environ. Exp. Bot.* 199, 104883. doi: 10.1016/j.envexpbot.2022.104883

Huang, S., Gong, B., Wei, F., and Ma, H. (2017). Pre-harvest 1-methylcyclopropene application affects post-harvest physiology and storage life of the cut rose cv. *Carola. Horticulture Environment Biotechnol.* 58 (2), 144–151. doi: 10.1007/s13580-017-0081-9

Huang, D., Lan, W., Ma, W., Huang, R., Lin, W., Li, M., et al. (2022). WHIRLY1 recruits the histone deacetylase HDA15 repressing leaf senescence and flowering in arabidopsis. *J. Integr. Plant Biol* 64 (7), 1411–1429. doi: 10.1111/jipb.13272

Huang, S., Zhu, K., Chen, Y., Wang, X., and Wang, Y. (2021). Gerbera POE1 (GhPOE1) is involved in leaf senescence in arabidopsis. *South Afr. J. Bot.* 143, 33–41. doi: 10.1016/j.sajb.2021.06.039

Hu, Y., Jiang, Y., Han, X., Wang, H., Pan, J., and Yu, D. (2017). Jasmonate regulates leaf senescence and tolerance to cold stress: crosstalk with other phytohormones. *J. Exp. Bot.* 68 (6), 1361–1369. doi: 10.1093/jxb/erx004

Jan, S., Abbas, N., Ashraf, M., and Ahmad, P. (2018). Roles of potential plant hormones and transcription factors in controlling leaf senescence and drought tolerance. *Protoplasma* 256 (2), 313–329. doi: 10.1007/s00709-018-1310-5

Kant, S., Burch, D., Badenhorst, P., Palanisamy, R., Mason, J., and Spangenberg, G. (2015). Regulated expression of a cytokinin biosynthesis gene IPT delays leaf senescence and improves yield under rainfed and irrigated conditions in canola (Brassica napus l.). *PloS One* 10 (1), e0116349. doi: 10.1371/journal.pone.0116349

Keithly, J. H., Yokoyama, H., and Gausman, H. W. (1990). Effect of 2-(3,4-dichlorophenoxy) triethylamine (DCPTA) on the growth and development of sugarbeet. *Plant Science*, 68 (1), 57–64. doi: 10.1016/0168-9452(90)90152-e

Laloi, C., and Havaux, M. (2015). Key players of singlet oxygen-induced cell death in plants. *Front. Plant Sci.* 6. doi: 10.3389/fpls.2015.00039

Lee, I. H., Lee, I. C., Kim, J., Kim, J. H., Chung, E.-H., Kim, H. J., et al. (2016). NORE1/SAUL1 integrates temperature-dependent defense programs involving SGT1b and PAD4 pathways and leaf senescence in arabidopsis. *Physiologia Plantarum* 158 (2), 180–199. doi: 10.1111/ppl.12434

Lee, J. H., Park, Y. J., Kim, J. Y., and Park, C. M. (2022). Phytochrome b conveys low ambient temperature cues to the ethylene-mediated leaf senescence in arabidopsis. *Plant Cell Physiol.* 63 (3), 326–339. doi: 10.1093/pcp/pcab178

Lee, S., Seo, P. J., Lee, H.-J., and Park, C.-M. (2012). A NAC transcription factor NTL4 promotes reactive oxygen species production during drought-induced leaf senescence in arabidopsis. *Plant J.* 70 (5), 831–844. doi: 10.1111/j.1365-313x.2012.04932. X

Leng, Y., Ye, G., and Zeng, D. (2017). Genetic dissection of leaf senescence in rice. *Int. J. Mol. Sci.* 18 (12), 2686. doi: 10.3390/ijms18122686

Li, J., Brader, G., Kariola, T., and Tapio Palva, E. (2006). WRKY70 modulates the selection of signaling pathways in plant defense. *Plant J.* 46 (3), 477–491. doi: 10.1111/j.1365-313x.2006

Li, S., and Dami, I. E. (2015). Responses of vitis vinifera "Pinot gris" grapevines to exogenous abscisic acid (ABA): I. yield, fruit quality, dormancy, and freezing tolerance. *J. Plant Growth Regul.* 35 (1), 245–255. doi: 10.1007/s00344-015-9529-2

Lim, P. O., Kim, H. J., and Gil Nam, H. (2007). Leaf senescence. *Annu. Rev. Plant Biol.* 58, 115–136. doi: 10.1146/annurev.arplant.57.032905.105316

Lira, B. S., Gramegna, G., Trench, B. A., Alves, F. R. R., Silva, E. M., Silva, G. F. F., et al. (2017). Manipulation of a senescence-associated gene improves fleshy fruit yield. *Plant Physiol.* 175 (1), 77–91. doi: 10.1104/pp.17.00452

Liu, K., Jing, T., Wang, Y., Ai, X., and Bi, H. (2022a). Melatonin delays leaf senescence and improves cucumber yield by modulating chlorophyll degradation and photoinhibition of PSII and PSI. *Environ. Exp. Bot.* 200, 104915. doi: 10.1016/j.envexpbot.2022.104915

Liu, R., Zuo, X., Chen, Y., Qian, Z., Xu, C., Wang, L., et al. (2022b). Transcriptional regulation in leaves of cut chrysanthemum (Chrysanthemum morifolium) 'Fen dante' in response to post-harvest ethylene treatment. *Horticulturae* 8 (7), 573. doi: 10.3390/horticulturae8070573

Liu, P., Wang, X., Wang, Q., and Liu Xu, T. X. (2017). Effects of abscisic acid treatment on the quality and browning of the peel of 'yellow crown' pear after harvesting. *Journal of Agriculture* (02), 84–90. Available at: https://kns-cnki-net-443.webvpn.zafu.edu.cn/kcms/detail/detail.aspx?FileName=XKKJ201702018&DbName=CJFQ2017.

Luo, Y. Y., Gianfagna, T. J., Janes, H. W., Huang, B., Wang, Z., and Xing, J. (2005). Expression of the ipt gene with the AGPase S1 promoter in tomato results in unbranched roots and delayed leaf senescence. *Plant Growth Regul.* 47 (1), 47–57. doi: 10.1007/s10725-005-8647-4

Lü, P., Zhang, C., Liu, J., Liu, X., Jiang, G., Jiang, X., et al. (2014). Rh HB 1 mediates the antagonism of gibberellins to ABA and ethylene during rose (Rosa hybrida) petal senescence. *Plant J.* 78 (4), 578–590. doi: 10.1111/tpj.12494

Ma, S. (2006). *Study on the effect of 1-MCP treatment on postharvest aging and storage of leafy vegetables* (Nanjing Agricultural University: MA thesis).

Maillard, A., Diquélou, S., Billard, V., Laîné, P., Garnica, M., Prudent, M., et al. (2015). Leaf mineral nutrient remobilization during leaf senescence and modulation by nutrient deficiency. *Front. Plant Sci.* 6. doi: 10.3389/fpls.2015.00317

Mannucci, A., Scartazza, A., Santaniello, A., Castagna, A., Santin, M., Quartacci, M. F., et al. (2022). Short daily ultraviolet exposure enhances intrinsic water-use efficiency and delays senescence in micro-tom tomato plants. *Funct. Plant Biol.* 49 (9), 810–821. doi: 10.1071/fp22013

Ma, P., Wu, W., Tang, X., Huang, Y., and Wei, Y. (2009). Effects of pre-harvest spraying salicylic acid (SA) and gibberellin (GA3) on the physiology and storage effect of gongci fruit after harvesting. *J. Fruit Trees* 6, 891–894.

Mayta, M. L., Hajirezaei, M.-R., Carrillo, N., and Lodeyro, A. F. (2019). Leaf senescence: The chloroplast connection comes of age. *Plants* 8 (11), 495. doi: 10.3390/plants8110495

Ma, X., Zhang, Y., Turečková, V., Xue, G.-P., Fernie, A. R., Mueller-Roeber, B., et al. (2018). The NAC transcription factor SlNAP2 regulates leaf senescence and fruit yield in tomato. *Plant Physiol.* 177 (3), 1286–1302. doi: 10.1104/pp.18.00292

Miret, J. A., Munné-Bosch, S., and Dijkwel, P. P. (2017). ABA signalling manipulation suppresses senescence of a leafy vegetable stored at room temperature. *Plant Biotechnol. J.* 16 (2), 530–544. doi: 10.1007/s00299-011-1170-3

Miret, J. A., Munné-Bosch, S., and Dijkwel, P. P. (2018). ABA signalling manipulation suppresses senescence of a leafy vegetable stored at room temperature. *Plant Biotechnol. J.* 16 (2), 530–544. doi: 10.1111/pbi.12793

Pan, Y., Seymour, G. B., Lu, C., Hu, Z., Chen, X., and Chen, G. (2012). An ethylene response factor (ERF5) promoting adaptation to drought and salt tolerance in tomato. *Plant cell rep.* 31 (2), 349–360. doi: 10.1007/s00299-011-1170-3

Sami, F., Yusuf, M., Faizan, M., Faraz, A., and Hayat, S. (2016). Role of sugars under abiotic stress. *Plant Physiol. Biochem.* 109, 54–61. doi: 10.1016/j

Schulte auf'm Erley, G., Wijaya, K.-A., Ulas, A., Becker, H., Wiesler, F., and Horst, W. J. (2007). Leaf senescence and n uptake parameters as selection traits for nitrogen efficiency of oilseed rape cultivars. *Physiologia Plantarum* 130 (4), 519–531. doi: 10.1111/j.1399-3054.2007.00921.x

Sobieszczuk-Nowicka, E., Wrzesiński, T., Bagniewska-Zadworna, A., Kubala, S., Rucińska-Sobkowiak, S. R., Polcyn, W., et al. (2018). Physio-Genetic Dissection of Dark-Induced Leaf Senescence and Timing Its Reversal in Barley. *Plant Physiol.* 178 (2), 654–671. doi: 10.1104/pp.18.00516

Song, S., Ge, M., Wang, W., Gu, C., Chen, K., Zhang, Q., et al. (2022). BpEIN3. 1 represses leaf senescence by inhibiting synthesis of ethylene and abscisic acid in betula platyphylla. *Plant Sci.* 321, 111330. doi: 10.1016/j.plantsci.2022.111330

Song, Y., Yang, C., Gao, S., Zhang, W., Li, L., and Kuai, B. (2014). Age-triggered and dark-induced leaf senescence require the bHLH transcription factors PIF3, 4, and 5. *Mol. Plant* 7 (12), 1776–1787. doi: 10.1093/mp/ssu109

Stefanov, D., Stoimenova, E., Marinova, G., Ivanova, B., and Edreva, A. (2011). Accelerated leaf senescence takes part in enhanced resistance in cucumber mosaic virus inoculated pepper leaves. *Acta Physiologiae Plantarum* 34 (1), 181–190. doi: 10.1007/s11738-011-0816-7

Swartzberg, D., Dai, N., Gan, S., Amasino, R., and Granot, D. (2006). Effects of cytokinin production under two SAG promoters on senescence and development of tomato plants. *Plant Biol.* 8 (5), 579–586. doi: 10.1055/s-2006-924240

Swartzberg, D., Hanael, R., and Granot, D. (2011). Relationship between hexokinase and cytokinin in the regulation of leaf senescence and seed germination. *Plant Biol.* 13 (3), 439–444. doi:10.1111/j.1438-8677. 2010.00376.x

Talla, S. K., Panigrahy, M., Kappara, S., Nirosha, P., Neelamraju, S., and Ramanan, R. (2016). Cytokinin delays dark-induced senescence in rice by maintaining the chlorophyll cycle and photosynthetic complexes. *J. Exp. Bot.* 67 (6), 1839–1851. doi: 10.1093/jxb/erv575

Tan, X., Fan, Z., Shan, W., Yin, X., Kuang, J., Lu, W., et al. (2018). Association of BrERF72 with methyl jasmonate-induced leaf senescence of Chinese flowering cabbage through activating JA biosynthesis-related genes. *Hortic. Res.* 5 (1), 22. doi: 10.1038/s41438-018-0028-z

Thomas, H., and Stoddart, J.L. (2018). Leaf senescence. *Annu. Rev. Plant Physiol.* 31 (1), 83–111, doi: 10.1146/annurev.pp.31.060180.000503

Tian, Y., Hou, J., and Li, D. (2014). Effects of water stress on thephysiological physiology of spinach leaves during refrigeration. *Preservation and processing* 14 (4), 10–15. doi: 10.3969/j.issn.1009-6221.2014.04.003

Tomotsugu, K. (2018). A hidden link between leaf development and senescence. *Plant Sci.* 276, 105–110. doi: 10.1016/j.plantsci.2018.08.006

Thiruvengadam, M., Shih, C. F., and Yang, C.H. (2015). Expression of an antisense Brassica oleracea GIGANTEA (BoGI) gene in transgenic broccoli causes delayed flowering, leaf senescence, and post-harvest yellowing retardation. *Plant Mol Biol Rep.* 33 (5), 1499–1509. doi: 10.1007/s11105-015-0852-3

Thomas, H., and Stoddart, J. L. (1980). Leaf senescence. *Annu. Rev. Plant Physiol.* 31 (1), 83–111.

Tian, Y., Hou, J., and Li, D. (2014). "Effects of water stress on spinach leaf senescence during refrigeration," in *Proceedings of the 9th national food refrigeration chain conference and the 6th national annual conference on innovation and development of refrigerated and refrigerated industry.* 64–70.

Tomotsugu, K. (2018). A hidden link between leaf development and senescence. *Plant Science.* doi: 10.1016/j.plantsci.2018.08.006

Uhlig, S., Fæste, C. K., Ivanova, L., Noriega Fernández, E., Sone, I., and Sivertsvik, M. (2021). Impact of plasma-activated water treatment on quality and shelf-life of fresh spinach leaves evaluated by comprehensive metabolomic analysis. *Foods* 10 (12), 3067 doi: 10.3390/foods10123067

Wang, Y., Cui, X., Yang, B., Xu, S., Wei, X., Zhao, P., et al. (2020). WRKY55 transcription factor positively regulates leaf senescence and defense response through modulating the transcription of genes implicated in ROS and SA biosynthesis in arabidopsis. *Development*, 147 (16), dev.189647. doi: 10.1242/dev.189647

Wang, Z., Gao, M., Li, Y., Zhang, J., Su, H., Cao, M., et al. (2022). The transcription factor SlWRKY37 positively regulates jasmonic acid-and dark-induced leaf senescence in tomato. *J. Exp. Botany*. erac258. doi: 10.1093/jxb/erac258

Wang, X., Rehmani, M. S., Chen, Q., Yan, J., Zhao, P., Li, C., et al. (2022). Rapeseed NAM transcription factor positively regulates leaf senescence *via* controlling senescence-associated gene expression. *Plant Sci.* 323, 111373. doi: 10.1016/j.plantsci.2022.111373

Wang, Y., Tan, J., Wu, Z., Vanden Langenberg, K., Wehner, T. C., Wen, C., et al. (2019). STAYGREEN, STAY HEALTHY: a loss-of-susceptibility mutation in the STAYGREEN gene provides durable, broad-spectrum disease resistances for over 50 years of US cucumber production. *New Phytol.* 221 (1), 415–430. doi: 10.1111/nph.15353

Wang, N., Guo, T., Wang, P., Sun, X., Shao, Y., Liang, B., et al (2017). Functional analysis of apple MhYTP1 and MhYTP2 genes in leaf senescence and fruit ripening. *Scientia Horticulturae*. 221, 23–32. doi: 10.1016/j.scienta.2017.04.018

Weaver, L. M., Gan, S., Quirino, B., and Amasino, R. M. (1998). A comparison of the expression patterns of several senescence-associated genes in response to stress and hormone treatment. *Plant Mol. Biol.* 37 (3), 455–469. doi: 10.1023/a:1005934428906

Wen, B., Gong, X., Deng, W., Chen, X., Li, D., Fu, X., et al. (2022). The apple GARP family gene MdHHO3 regulates the nitrate response and leaf senescence. *Front. Plant Sci.* 13. doi: 10.3389/fpls.2022.932767

Woo, H. R., Kim, H. J., Lim, P. O., and Nam, H. G. (2019). Leaf senescence: Systems and dynamics aspects. *Annu. Rev. Plant Biol.* 70 (1), 347–376. doi: 10.1146/annurev-arplant-050718-095859

Xiao, X. M., Xu, Y. M., Zeng, Z. X., Tan, X. L., Liu, Z. L., Chen, J. W., et al. (2019). Activation of the transcription of BrGA20ox3 by a BrTCP21 transcription factor is associated with gibberellin-delayed leaf senescence in chinese flowering cabbage during storage. *Int. J. Mol. Sci.* 20 (16), 3860. doi: 10.3390/ijms20163860

Xiao, F., Yang, Z., Han, W., Li, Y., Qiu, Y., Sun, Q., et al. (2018). Effects of day and night temperature on photosynthesis, antioxidant enzyme activities, and endogenous hormones in tomato leaves during the flowering stage. *J. Hortic. Sci. Biotechnol.* 93 (3), 306–315. doi: 10.1080/14620316.2017.1287529

Xiao, X. O., Zeng, Y. M., Cao, B. H., Lei, J. J., Chen, Q. H., Meng, C. M., et al. (2017). PSAG12-IPT overexpression in eggplant delays leaf senescence and induces abiotic stress tolerance. *J. Hortic. Sci. Biotechnol.* 92 (4), 349–357. doi: 10.1080/14620316.2017.1287529

Xu, X., Chen, C., Fan, B., and Chen, Z. (2006). Physical and functional interactions between pathogen-induced arabidopsis WRKY18, WRKY40, and WRKY60 transcription factors. *Plant Cell* 18 (5), 1310–1326. doi: 10.1105/tpc.105.037523

Yang, K., An, J. P., Li, C. Y., Shen, X. N., Liu, Y. J., Wang, D. R., et al. (2021). The apple C2H2-type zinc finger transcription factor MdZAT10 positively regulates JA-induced leaf senescence by interacting with MdBT2. *Hortic. Res.* 8, 159. doi: 10.1038/s41438-021-00593-0

Yang, M., Hu, F., Lin, Y., and Wang, X. (2015). Effects of NAA and GA3 on fruit drop and quality of A4 seedless lychee before harvesting. *Guangdong Agric. Sci.* 04), 19–22. doi: 10.16768/j

Yang, S., Liang, K., Wang, A., Zhang, M., Qiu, J., and Zhang, L. (2020). Physiological characterization and transcriptome analysis of camellia oleifera abel. during leaf senescence. *Forests* 11 (8), 812. doi: 10.3390/f11080812

Yang, L., Ye, C., Zhao, Y., Cheng, X., Wang, Y., Jiang, Y. Q., et al. (2018). An oilseed rape WRKY-type transcription factor regulates ROS accumulation and leaf senescence in nicotiana benthamiana and arabidopsis through modulating transcription of RbohD and RbohF. *Planta* 247 (6), 1323–1338. doi: 10.1007/s00425-018-2868-z

Yang, Z., Zhu, J., Zhang, B., Gu, L., and Zhang, J. (2012). Effect of high temperature treatment on aging characteristics of strawberry leaves at the fruiting stage. *Chin. Agric. Meteorology* 04), 512–518.

Yan, J., Li, Y., Zhao, P., Mu, B., Chen, Q., Li, X., et al. (2021). Membrane-bound transcriptional activator NTL1 from rapeseed positively modulates leaf senescence through targeting genes involved in reactive oxygen species production and programmed cell death. *J. Agric. Food Chem.* 69 (17), 4968–4980. doi: 10.1021/acs.jafc.1c00182

Yu, T., and Xi, Y. (1997). Effect of temperature on ethylene release and reactive oxygen species metabolism in Chinese cabbage. *Zhejiang J. Agric.* 06), 11–15. Available at: https://kns-cnki-net-443.webvpn.zafu.edu.cn/kcms/detail/detail.aspx?FileName=ZJNB706.002&DbName=CJFQ1997.

Zhang, Li Y., Liu, H. H, Zhang, Y. P., and Zhu, Li B. (2014). Effects of calcium nitrate on leaf senescence and fruit yield and quality of pachyderm melon fruit setting nodes. *Plant Nutr. Fertilizer Sci.* 02), 490–495. doi: 10.13320/j.cnki.jauh.2014.0008

Zhang, Y., Luo, J., Peng, F., Xiao, Y., and Du, A. (2021). Application of bag-controlled release fertilizer facilitated new root formation, delayed leaf, and root senescence in peach trees and improved nitrogen utilization efficiency. *Front. Plant Sci.* 12. doi: 10.3389/fpls.2021.627313

Zhang, Y., Wang, H. L., Li, Z., and Guo, H. (2020). Genetic network between leaf senescence and plant immunity: crucial regulatory nodes and new insights. *Plants* 9 (4), 495. doi: 10.3390/plants9040495

Zhang, D., Wu, S., Li, N., Gao, J., Liu, S., Zhu, S., et al. (2022). Chemical induction of leaf senescence and powdery mildew resistance involves ethylene-mediated chlorophyll degradation and ROS metabolism in cucumber. *Hortic. Res.* 9, uhac101. doi: 10.1093/hr/uhac101

Zhao, Y., Chan, Z., Gao, J., Xing, L., Cao, M., Yu, C., et al. (2016). ABA receptor PYL9 promotes drought resistance and leaf senescence. *Proc. Natl. Acad. Sci.* 113 (7), 1949–1954. doi: 10.1073/pnas.1522840113

Zhao, S., Deng, C., Zeng, Z., Wu, M., Shi, X., Duan, X., et al. (2022). Changes in mineral nutrition and photosynthetic capacity during leaf development and aging of sunshine rose' grapes and related properties. *J. Pomology*. 1–14 doi: 10.13925/j.cnki.gsxb.20220001

Zhao, X., Zhang, T., Feng, H., Qiu, T., Li, Z., Yang, J., et al. (2021). OsNBL1, a multi-organelle localized protein, plays essential roles in rice senescence, disease resistance, and salt tolerance. *Rice* 14 (1), 1–17. doi: 10.1186/s12284-020-00450-z

Zha, Q., Yin, X., Xi, X., and Jiang, A. (2022). Colored shade nets can relieve abnormal fruit softening and premature leaf senescence of "Jumeigui" grapes during ripening under greenhouse conditions. *Plants* 11 (9), 1227. doi: 10.3390/plants11091227

Zheng, C., Wang, Y., Ding, Z., and Zhao, L. (2016). Global transcriptional analysis reveals the complex relationship between tea quality, leaf senescence and the responses to cold-drought combined stress in camellia sinensis. *Front. Plant Sci.* 7. doi: 10.3389/fpls.2016.01858

Zhou, D., Li, T., Yang, Y., Qu, Z., Ouyang, L., Jiang, Z., et al. (2020). OsPLS4 is involved in cuticular wax biosynthesis and affects leaf senescence in rice. *Front. Plant Sci.* 11. doi: 10.3389/fpls.2020.00782

Zhu, Li B. (2015). *Effects of exogenous 6-BA on leaf senescence and fruit yield and quality of pachyderm melon fruit-setting nodals* (Agricultural University of Hebei: MA thesis).

frontiers | Frontiers in Plant Science

TYPE Original Research
PUBLISHED 03 November 2022
DOI 10.3389/fpls.2022.1044029

OPEN ACCESS

EDITED BY
Ji Tian,
Beijing University of Agriculture, China

REVIEWED BY
Yongshun Gao,
South China Agricultural University, China
Mizhen Zhao,
Jiangsu Academy of Agricultural Sciences (JAAS), China

*CORRESPONDENCE
Xiong Liao
liaox7@163.com.cn

†These authors have contributed equally to this work

SPECIALTY SECTION
This article was submitted to Plant Systems and Synthetic Biology, a section of the journal Frontiers in Plant Science

RECEIVED 14 September 2022
ACCEPTED 29 September 2022
PUBLISHED 03 November 2022

CITATION
Huang H, Zhao S, Chen J, Li T, Guo G, Xu M, Liao S, Wang R, Lan J, Su Y and Liao X (2022) Genome-wide identification and functional analysis of *Cellulose synthase* gene superfamily in *Fragaria vesca*. *Front. Plant Sci.* 13:1044029. doi: 10.3389/fpls.2022.1044029

Genome-wide identification and functional analysis of *Cellulose synthase* gene superfamily in *Fragaria vesca*

Hexin Huang[1†], Shuai Zhao[2,3†], Junli Chen[1], Tianxiang Li[1], Ganggang Guo[1], Ming Xu[3], Sufeng Liao[3], Ruoting Wang[1], Jiayi Lan[1], Yangxin Su[1] and Xiong Liao[1*]

[1]College of Horticulture, Fujian Agriculture and Forestry University, Fuzhou, China, [2]College of Life Science, Fujian Agriculture and Forestry University, Fuzhou, China, [3]College of Agriculture, Key Laboratory of Crop Biotechnology in Fujian Province University, Fujian Agriculture and Forestry University, Fuzhou, China

The *Cellulose synthase* (*CesA*) and *Cellulose synthase-like* (*Csl*) gene superfamilies encode key enzymes involved in the synthesis of cellulose and hemicellulose, which are major components of plant cell walls, and play important roles in the regulation of fruit ripening. However, genome-wide identification and functional analysis of the *CesA* and *Csl* gene families in strawberry remain limited. In this study, eight *CesA* genes and 25 *Csl* genes were identified in the genome of diploid woodland strawberry (*Fragaria vesca*). The protein structures, evolutionary relationships, and *cis*-acting elements of the promoter for each gene were investigated. Transcriptome analysis and quantitative real-time PCR (qRT-PCR) results showed that the transcript levels of many *FveCesA* and *FveCsl* genes were significantly decreased during fruit ripening. Moreover, based on the transcriptome analysis, we found that the expression levels of many *FveCesA/Csl* genes were changed after nordihydroguaiaretic acid (NDGA) treatment. Transient overexpression of *FveCesA4* in immature strawberry fruit increased fruit firmness and reduced fresh fruit weight, thereby delaying ripening. In contrast, transient expression of *FveCesA4*-RNAi resulted in the opposite phenotypes. These findings provide fundamental information on strawberry *CesA* and *Csl* genes and may contribute to the elucidation of the molecular mechanism by which *FveCesA*/*Csl*-mediated cell wall synthesis regulates fruit ripening. In addition, these results may be useful in strawberry breeding programs focused on the development of new cultivars with increased fruit shelf-life.

KEYWORDS

***Fragaria vesca*, *CesA/Csl*, cell wall, fruit firmness, fruit ripening**

Introduction

The firmness of strawberry (*Fragaria* spp.) fruit is a crucial agronomic trait that is closely associated with its storage life and commercial value. Fruit development in strawberry is divided into two stages: the early growth stage and the ripening stage (Liao et al., 2018). During the early stage, the fruit enlarges. During the ripening stage, the fruit texture undergoes dramatic changes, which is defined as fruit softening, mainly as a result of alterations in cell wall structure and composition (Moya-León et al., 2019). The *Cellulose synthase* gene superfamily, which belongs to the glycosyltransferase-2 gene superfamily, is presumed to be involved in the synthesis of major components of the primary and secondary cell walls, such as cellulose and hemicellulose polysaccharides (Czaja et al., 2007). Hence, the mining of genes encoding cellulose synthases that function in fruit development may enable manipulation of fruit ripening and thereby enhance fruit storability.

The *Cellulose synthase* gene superfamily comprises the *Cellulose synthase A* (*CesA*) and *Cellulose synthase-like* (*Csl*) families, which can be resolved into the CesA clade and ten Csl clades, i.e., CslA-CslH, CslJ and CslM (McFarlane et al., 2014). Among the Csl clades, the CslA, CslC and CslD lineages are prevalent in all terrestrial plants (Farrokhi et al., 2006). The CslB lineages are considered to be dicotyledons-specific, whereas the CslF and CslH lineages were indicated to be restricted to grasses (Yin et al., 2009). Cellulose catalyzed by CesA plays a central role in cell morphogenesis and cell wall integrity, which predominantly determines plant development and growth (Cosgrove, 2005; Persson et al., 2007; Liu et al., 2016; Hu et al., 2018a; Hu et al., 2018b). In *Arabidopsis* (*Arabidopsis thaliana*), *AtCesA1*, *AtCesA3* and *AtCesA6-like* genes (*AtCesA2*, *AtCesA5*, *AtCesA6*, and *AtCesA9*) are essential for the synthesis of primary cell wall cellulose, whereas *AtCes4*, *AtCes7*, and *AtCes8* are responsible for the synthesis of secondary cell wall cellulose (Taylor et al., 2003; Desprez et al., 2007; Persson et al., 2007; Malinovsky et al., 2014). Overexpression of *AtCesA2*, *AtCesA5*, and *AtCesA6* in *Arabidopsis* causes enhanced cell elongation and divisiona as well as increased secondary cell wall deposition which, consequently, results in greater biomass production (Hu et al., 2018a). In maize (*Zea mays*), the *ENB1* gene encoding cellulose synthase is predominantly expressed in the basal endosperm transfer layer (BETL) of the endosperm during kernel development (Wang et al., 2022). Loss-of-function of *ENB1* causes defective cell wall ingrowths in BETL cells, which, in turn affects nutrient absorption and, ultimately, results in severe degradation of the endosperm (Wang et al., 2022).

Genes in the *Csl* family, which show significant similarity to *CesA* gene family (Richmond and Somerville, 2000; Cantarel et al., 2009), are grouped into ten subfamilies, including the *CslA-H*, *CslJ*, and *CslM* subfamilies (Richmond and Somerville, 2000; Hazen et al., 2002; Farrokhi et al., 2006; Cantarel et al., 2009; Little et al., 2018). Evidence to date indicates that diverse cell wall polysaccharides catalyzed by *Csl* gene family members are crucial for plant development and for biotic or abiotic stress tolerance. Several members of the Arabidopsis *CslA* family function in the synthesis of mannan polysaccharides (Dhugga et al., 2004; Liepman et al., 2005; Goubet et al., 2009; Liepman and Cavalier, 2012). Overexpression of *AtCslA2*, *AtCslA7*, and *AtCslA9* enhances glucomannan biosynthesis and causes defective embryogenesis, resulting in retard development and occasional embryo death (Goubet et al., 2009). The *CslD* gene family considered to be involved in the synthesis of xylan, homogalacturonan, and mannan polysaccharides (Bernal et al., 2007) and is required for the development of tip-growing cells. In *Arabidopsis*, loss-of-function of *AtCslD2* and *AtCslD3* results in a defective root-hair phenotype, and *AtCslD1* and *AtCslD4* mutants exhibit a defective pollen tube phenotype. Intriguingly, constitutive overexpression of the *Csl* gene *Soly07g043390* in tomato (*Solanum lycopersicum*) significantly enhances symptomatic tolerance and further results in improved plant growth, fruit size, and yield in the tomato-*Tomato yellow leaf curl virus*-pathosystem (Park et al., 2011; Verhertbruggen et al., 2011; Yin et al., 2011; Dhugga, 2012; Yang et al., 2020; Choe et al., 2021). Therefore, *Csl* genes may be utilized to potentially strengthen the plant immunity system and maintain crop productivity.

Together with the mining of large-scale plant genomic sequence data, the *Cellulose synthase* gene superfamily has been identified in a variety of plants, such as rice (*Oryza sativa*) (Hazen et al., 2002), maize (Appenzeller et al., 2004; Li et al., 2019), tomato (Song et al., 2019), and *Physcomitrella patens* (Roberts and Bushoven, 2007). However, genome-wide characterization of the genes associated with cellulose synthesis in strawberry remains to be elucidated. In the present study, to mine the potential cellulose synthesis genes that influence fruit ripening in strawberry, eight *CesA* and 25 *Csl* genes were identified in the genome of diploid woodland strawberry. The significantly down-regulated candidate *FveCesA* and *FveCsl* genes were screened by transcriptome analysis and qRT-PCR. In addition, transient overexpression and knock-down experiments were performed to verify the function of candidate genes involved in the regulation of fruit ripening. These results may facilitate analysis of the mechanism by which *FveCesA*/*Csl*-mediated cell wall synthesis regulates fruit ripening, and the discovery of candidate genotypes for improved fruit shelf-life in strawberry.

Materials and methods

Plant materials and growth conditions

Diploid woodland strawberry (*F. vesca*) seedlings were planted in plastic pots (9 cm × 9 cm) containing an equal

mixture of vermiculite and peat soil. The plants were grown in a growth room under a 16 h/8 h (light/dark) photoperiod at 22°C with 60% relative humidity. Once fully open, flowers were pollinated manually every 2 days with a pollination stick.

Identification and characterization of *Cellulose synthase* superfamily members in the strawberry genome

The *F. vesca* v4.0 genome and v4.0.a2 annotation files were downloaded from the GDR database (https://www.rosaceae.org/). The strawberry protein database was searched using the TBtools software (Chen et al., 2020). The amino acid sequences for members of the *Arabidopsis* cellulose synthase family (10 *AtCesA* and 30 *AtCsl* genes) were extracted from the TAIR database (https://www.arabidopsis.org/) and were employed as queries for BLAST searches with a cutoff *E*-value of $1e^{-5}$ in the strawberry protein database. A total of eight *FveCesA* and 25 *FveCsls* genes were identified by a bi-directional BLAST analysis using the TBtools software and the NCBI Blastp tools. The NCBI Conserved Domain Database (http://www.ncbi.nlm.nih.gov/cdd) and Pfam database (http://pfam.xfam.org/) were used to predict the conserved domains in all putative FveCesA and FveCsl proteins. The TBtools software was used to predict the protein molecular weight, isoelectric point, and gene structure. The Plant-mPLoc server (http://www.csbio.sjtu.edu.cn/bioinf/plant-multi/) was used to predict the subcellular localization of the putative proteins.

Phylogenetic relationship, chromosomal location, and synteny analysis

Multiple sequence alignment of the cellulose synthase protein sequences *F. vesca*, *A. thaliana*, and *O. sativa* was performed with MUSCLE software. Maximum likelihood phylogenetic trees were constructed, with topological support assessed with 1000 bootstrap replicates, under the LG+G+I+F substitution model using MEGA7 (Kumar et al., 2016). The chromosomal distribution of the identified *FveCesA* and *FveCsl* genes, and the syntenic relationships between CesA/Csl homologs of *F. vesca* and *Arabidopsis* were analyzed and visualized using TBtools.

Gene structure, conserved domain, and motif composition analysis

The coding sequences (CDSs) and corresponding genome sequences of the *FveCesA* and *FveCsl* genes were extracted from the *F. vesca* genome and used to predict the exon-intron structures. The conserved domains and motifs of FveCesAs and FveCsl proteins were investigated using the NCBI Conserved Domain Database (https://www.ncbi.nlm.nih.gov/Structure/cdd/wrpsb.cgi) and the MEME Suite tools (https://meme-suite.org/meme/), respectively. Aschematic diagram of gene structure, conserved domains, and motif composition was generated and re-edited with TBtools.

Promoter *Cis*-acting element distribution analysis

The 2000 -bp sequences upstream of the start codon of each *FveCesA* and *FveCsl* gene was extracted as the promoter region and submitted to the PlantCARE database (https://bioinformatics.psb.ugent.be/webtools/plantcare/html/) for prediction of the *cis*-acting elements. A heat map of the *cis*-acting elements of each *FveCesA* and *FveCsl* gene was visualized using TBtools.

Transcriptome data analysis

For transcriptome analysis, strawberry fruits at the small white stage [about 17 days after pollination (DAP)], big white stage (about 21 DAP), pre-turning stage (white receptacle with red achenes), pink stage, and red stage (two or three days after the pink stage) were collected for RNAseq analysis. To inhibit endogenous ABA synthesis, the fruits at big green stage (12-14 DAP) were treated with NDGA and harvested five days after treatment. To investigate the expression patterns of *FveCesA* and *FveCsl* genes during fruit development, the raw data for the above diploid woodland strawberry fruit transcriptome (PRJNA522346) at different developmental stages (Gu et al., 2019) were downloaded from the NCBI database using Aspera software. The Bam files were generated by aligning the transcriptome reads to the *F. vesca* genome using HISAT2 software. Read counts aligned to each *FveCesA* and *FveCsl* gene were counted using the featureCounts program. The DESeq2 R package was used to standardize read counts to obtain transcripts per kilobase million (TPM) values. A heat map of the gene expression patterns was visualized using the TBtools.

RNA isolation and qRT- PCR analyses

To verify the expression pattern of *FveCesA*/*Csl* genes during fruit ripening, according to previous reports, the fruit development of "Yellow Wonder" was divided into 12 stages from fully open flower, including S1 (open flower), S2 (2-4 DAP), S3 (5-7 DAP), S4 (8-10 DAP), S5 (11-13 DAP), S6 (14-16 DAP), S7 (17-19 DAP), RS1 (20-22 DAP), RS2 (23-25 DAP), RS3 (26-28 DAP), RS4 (29-31 DAP), and RS5 (32-34 DAP) (Liao et al., 2018). Total RNA of strawberry fruits in the early development stage (S1, S3 and S5) and the ripening stage (RS4) were isolated using the polysaccharide and polyphenolics-rich RNAprep Pure Kit (Tiangen) in accordance

with the manufacturer's instructions. The cDNA was synthesized from total RNA using the HiScript II Q RT SuperMix for qPCR reagent Kit (Vazyme). The RT-qPCR assay was performed on a CFX96 Real-Time PCR system (Bio-Rad) using the AceQ qPCR SYBR Green Master Mix (Vazyme). *FveACTIN* was used as the internal control for normalization. The primers used for qRT-PCR analyses are listed in Supplementary Table S1.

Construction of plasmid DNA

To generate an overexpression vector, the full-length CDS of *FveCesA4* was cloned into the pCAMBIA1305 vector and designated *35S::FveCesA4*. For strawberry fruit RNAi interference (RNAi) analysis, the pTRV1/pTRV2 viral-induced gene silencing (VIGS) system was employed. A 375 -bp CDS fragment (from 152 bp to 527 bp) of *FveCesA4* was amplified and inserted into the pTRV2 vector, and the construct was designated *pTRV2-FveCesA4*. The primers used in vector construction are listed in Supplementary Table S1.

Transient transformation analysis in strawberry fruit

Strawberry fruits were infiltrated with *Agrobacterium* as previously described (Liao et al., 2018). For the RNAi experiment, fruits at the S4 stage were injected with Agrobacterium *tumefaciens* strain GV3101 harboring *pTRV1* in combination with the vector containing either *pTRV2* or *pTRV2-FveCesA4*. For transient overexpression, fruits at the S7 stage were injected with *A. tumefaciens* strain GV3101 harboring *35S::FveCesA4*. Approximately 15 fruits from five individual plants were selected for transient infiltration in each experiment. The fruit phenotype was evaluated 7 days after injection.

Firmness and fruit size analysis

Fruit size was measured with a vernier calipers. Fresh fruit firmness was detected using a texture analyzer (GY-4; Handpi). Each fruit was measured five times in the equatorial region.

Results

Genomic identification and phylogenetic analysis of *Cellulose synthesis* gene in strawberry

To identify candidate cellulose synthesis genes, a bidirectional BLAST search was performed against the *F. vesca* reference genome using the CesA/Csl protein sequences of *Arabidopsis*. Eight *FveCesA* and 25 *FveCsl* genes were obtained. The candidate *CesA* and *Csl* genes were named consistent with their grouping in a phylogenetic analysis (Supplementary Table S2). Overall, the candidate proteins were predicted to range from 518 (*FveCslA1*) to 1138 (*FveCSLD1*) amino acids and from 5.93 KD (*FveCslA1*) to 12.6 KD (*FveCslD1*) in molecular weight. The pI ranged from 6.05 (*FveCslD1*) to 9.19 (*FveCslA1*). The candidate cellulose synthases were predicted to be localized in the cell membrane, chloroplasts and the Golgi apparatus (Supplementary Table S2).

To explore the evolutionary relationships of FveCesA/Csl proteins in strawberry, 117 CesA and Csl homologs from *F. vesca*, *Arabidopsis*, and rice were selected for phylogenetic analysis (Figure 1 and Supplementary Table S3). The cellulose synthase homologs of the three species were grouped into one CesA clade and eight Csl clades (designated CslA-CslH). Eight FveCesA/Csl proteins were grouped in the CesA clade, which constituted the largest clade. With regard to the remaining homologs from strawberry, three FveCesA/Csl proteins were placed in each of the CslA, CslB, and CslG clades, six were grouped in the CslC clade, and five in each of the CslD and CslE clades. No rice CesA/Csl homologs were grouped in the CslB and CslG clades. In contrast, no CesA/Csl homologs of *Arabidopsis* and strawberry were placed in the CslF and CslH clades, which were only present in rice. In addition, CslD and CesA clades were phylogenetically close, suggesting that the CesA/Csl homologs in these two lineages shared a common ancestor.

Chromosomal distribution and synteny analysis of Cellulose synthesis genes in strawberry

The 33 cellulose synthesis genes were unequally distributed on all seven chromosomes of *F. vesca* (Figure 2A). The *FveCesA* genes were located on all chromosomes except Fvb4. By comparison, *FveCsl* genes were present on all chromosomes except Fvb1. Intriguingly, *FveCslB* and *FveCslE* members exhibited tandem or segmental duplication, and were located at the ends of chromosomes Fvb6 and Fvb3, respectively.

To further explore the evolutionary mechanism of the *FveCesA/Csl* gene family, comparative syntenic maps of *F. vesca* and two representative species (*Arabidopsis thaliana* and *Oryza sativa*) were constructed at the genome-wide scale. Fourteen *FveCesA/Csl* genes and five *FveCesA/Csl* genes exhibited collinearity relationships with those of *Arabidopsis* and rice, respectively (Figure 2B). Interestingly, *FveCesA1*, *FveCesA4*, *FveCslD3*, and *FveCslD4* shared collinear relationships with both of these species, suggesting that these orthologous pairs may have predated the monocotyledon-eudicotyledon divergence.

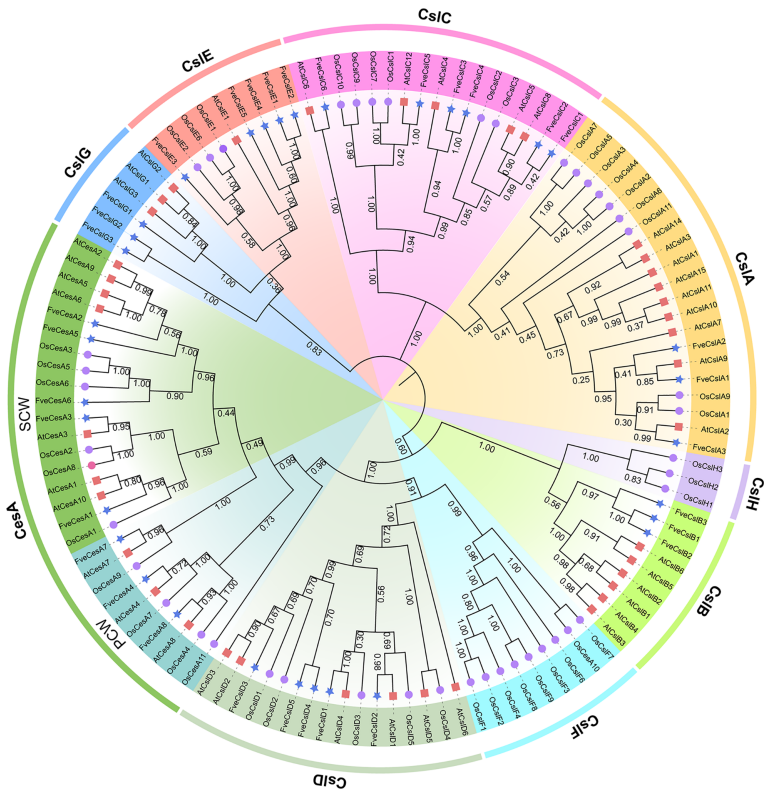

FIGURE 1
Phylogenetic relationships among the *Cellulose synthase* genes from *Arabidopsis* (red square), rice (purple circular) and strawberry (blue star). The selected CesA/Csl proteins are clustered into one CesA subfamily and nine Csl subfamilies and distinguished by different colors.

Sequence analysis of Cellulose synthesis genes in strawberry

To clarify the structural characteristics of the *FveCesA*/*Csl* gene family, the conserved domain, motif composition, and gene structure were analyzed. Two conserved domains in FveCesA/Csl proteins were identified (Figure 3). The 24 proteins of the CesA, CslD, CslB, CslE, and CslG clades contained the cellulose synthase conserved domain (PLN02436, PLN02400, PLN02638, PLN02189, PLN02915, PLN02248 and PLN02893). In comparison, the nine proteins of the CslA and CslC clades contained the glycosyl transferase family 2 domain (CESA_CaSu_A2 and Clyco_tranf_GTA_type) (Figure 3B and Supplementary Table S4). Consistent with the conserved domain analysis, most proteins in the CslD clade shared a similar motif composition with the CesA clade, except for the absent of motif13. Except in rare cases, proteins in the CslB, CslG, and CslE clades, containing the conserved domain PLN02893, shared similar motif orders. In contrast, the CslA and CslC clades contained a similar motif composition, but were distinguished from those of the other clades (Figure 3A). The majority of proteins containing similar motif compositions were grouped in the same clade and may have similar functions.

Analysis of the exon-intron organization of the *FveCesA*/*Csl* genes revealed diverse genetic structures. The number of exons in ranged from four to 14. Among the 33 *FveCesA*/*Csl* genes, the majority (66%) were spliced with more than six exons and five introns (Figure 3C). *FveCesA*/*Csl* genes with similar gene structures were classified together, for example, the CslD and CslC clades harbored five exons and four introns. The number of exons of the CesA clade ranged from 11 to 14, whereas the other clades contained nine (CslB clade), six to eight (CslG clade), eight (CslE clade), and nine (CslA clade). The diversity of gene structure indicated that *FveCesA/Csl* clades had experienced diverse evolutionary scenarios.

To further analyze the conserved domain of the FveCesA/Csl proteins, the amino acid sequence alignment of proteins in each clade was performed (Supplementary Figures S1–S4 and Supplementary Table S4). We found that *Cellulose synthase* domain (cellulose_synt) was ubiquitously present in CesA, CslB, CslD, CslE, CslG subfamily proteins (Supplementary Figures S1, S2, S4). However, CslA and CslC subfamily proteins contained glycosyltransferase family domain (Glyco_trans_2_3), which further confirmed that these two subfamilies may have different evolutionary origination (Supplementary Figure S4). Almost all FveCesA/Csl proteins

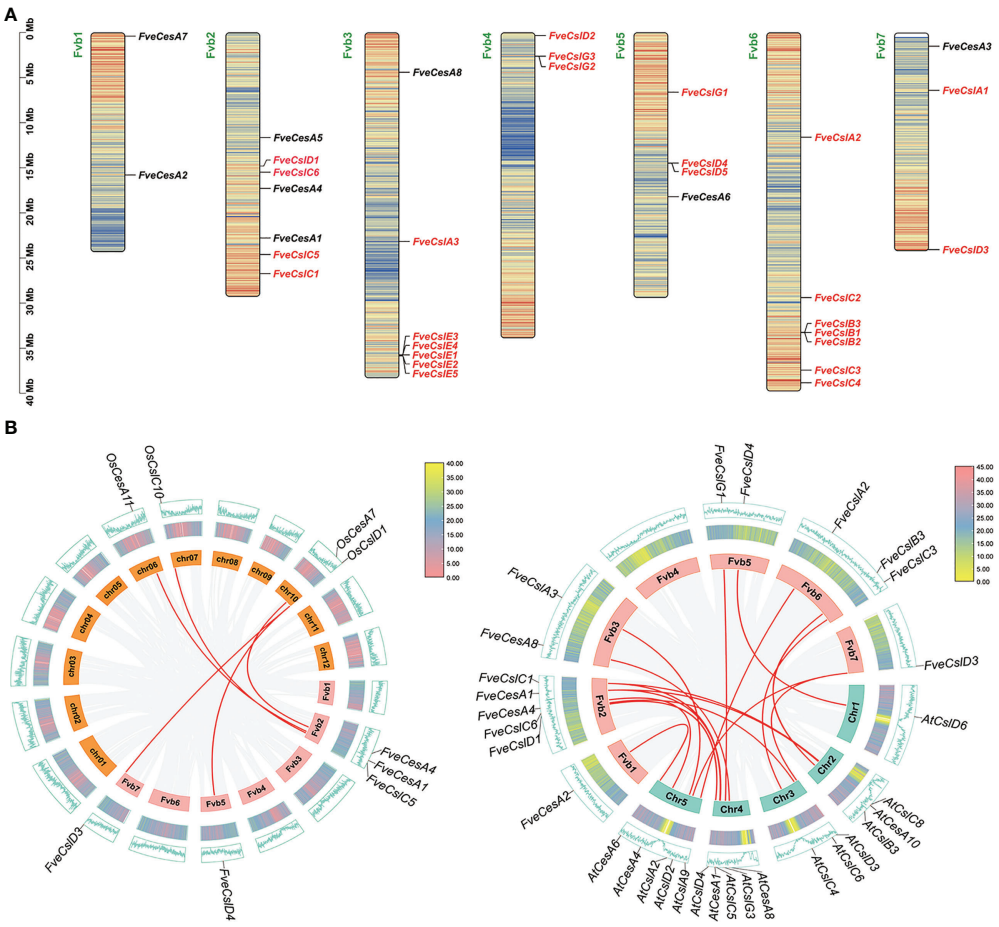

FIGURE 2
Chromosome distribution and synteny analysis of *Cellulose synthase* gene superfamily in strawberry. **(A)** Distribution diagram of *Cellulose synthase* genes in strawberry chromosome. The strawberry chromosomes are denoted as "Fvb", strawberry *CesA* family and *Csl* families are distinguished by black and red letters, respectively; **(B)** Synteny analysis of *Cellulose synthase* genes between strawberry, *Arabidopsis* and rice. Left diagram: analysis between rice and strawberry; right diagram: analysis between *Arabidopsis* and strawberry.

typically contained "D, D, D and QxxRW" active site, suggesting that they have conserved catalytic function. The "Q" amino acid of the "QxxRW" motif was replaced by other amino acids, implying that they may have functional differentiation. Unlike other families, the N- terminals of A and D contain zinc finger structures (Supplementary Figures S1), including conserved cysteine residues, which presumably may contribute to homologous or heteropolymerization.

Analysis of *Cis*-acting elements in *FveCesA/Csl* promoters of strawberry Cellulose synthesis genes

The *cis*-acting elements distributed in the regulatory regions of a promoter principally determine the gene expression pattern. The *cis*-acting elements in the promoter of the identified *FveCesA/Csl* genes were predicted. In total, 18 types of *cis*-acting elements were detected in the promoter of the *FveCesA/Csl* genes (Figure 4A). These elements included a light-responsive element (G-box), defense and stress response elements (TC-rich-repeats, LTR-element, and ARE-element), phytohormone response elements (ABRE, TGACG-motif, CGTCA-motif, and TCA-element), and growth and development-related elements (circadian, CAT-box, and GCNA4-motif). In particular, the G-box, ARE-element, TGACG-motif, and CGTCA-motif were abundant in the promoters of most *FveCesA/Csl* genes, indicating that these genes were required for stress tolerance and the growth and development of strawberry, and were extensively regulated by abscisic acid (ABA) and jasmonic acid (JA) hormone signaling.

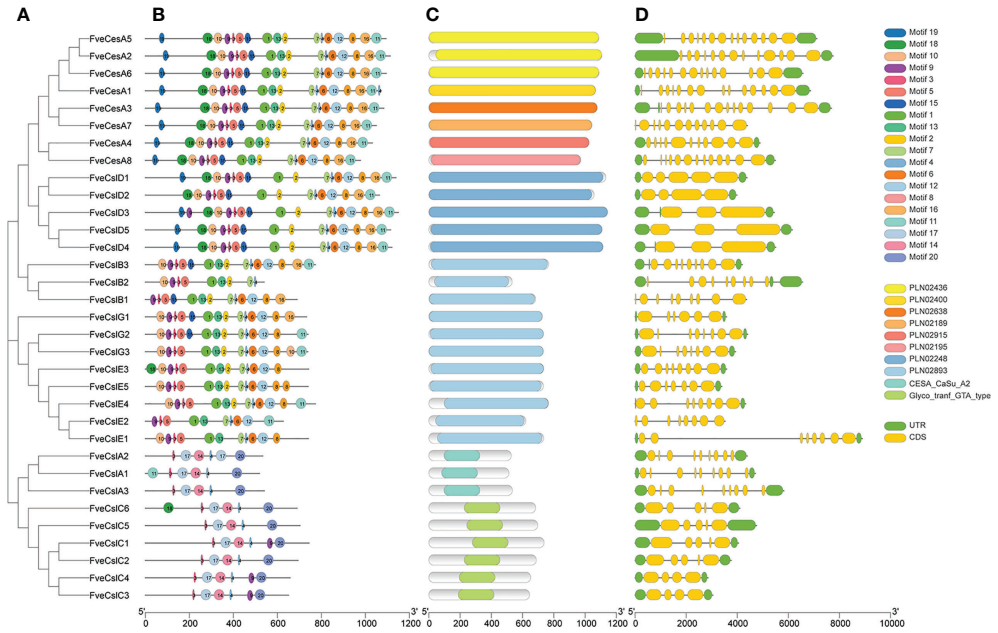

FIGURE 3
Structure characteristic of cellulose synthase gene in strawberry. **(A)** Phylogenetic analysis of FveCesA/Csl proteins. **(B)** Conserved motifs of FveCesA/Csl proteins. **(C)** Conserved domains of FveCesA/Csl proteins. **(D)** Exon-intron structures of *FveCesA/Csl* genes. UTRs are highlighted in green rectangles; exons are highlighted in yellow rectangles; introns are represented by solid lines. The scale bars indicate the length of the corresponding proteins and genes.

Expression profiles of Cellulose synthesis genes during strawberry fruit ripening

To investigate the expression profiles of *FveCesA* and *FveCsl* genes during fruit development, we analyzed RNA-seq data for diploid woodland strawberry fruit at different developmental stages. The expression profiles of *FveCesA* and *FveCsl* genes in the transcriptome data were represented as a heat map (Figure 4B). The transcript levels of the *FveCesA1*, *2*, *4*, *5*, and *6*, *FveCslA2* and *3*, and *FveCslC1*, *2*, and *5* genes were significantly decreased in the late stage of fruit development compared with the early stage. Interestingly, after ABA biosynthesis was inhibited by nordihydroguaiaretic acid (NDGA) treatment, the expression levels of *FveCesA1* and *FveCslC4* were remarkably increased, whereas the expression levels of *FveCesA5* and *6*, *FveCslA2* and *3*, *FveCslC1* and *2*, and *FveCslD3* were significantly decreased. Therefore, the expression of these genes may be regulated by ABA signaling, which is required for strawberry fruit ripening.

To further verify the RNA-seq results, we divided diploid woodland strawberry fruit development, starting from anthesis, into 11 stages as described previously (Liao et al., 2018), comprising seven early stages (S1-S7) and four ripening stage (RS1-RS4). Based on the promoter and RNA-seq data, the transcript levels of 9 *FveCesA*/*Csl* genes were detected by qRT-PCR during the early and ripening stages of fruit development (Figure 5). In the early stages (S1, S3 and S5), the expression of *FveCesA4*, *FveCesA7* and *FveCslG2* was dramatically increased, but the expression of *FveCesA6* was not changed significantly. In the ripening stage (RS4), the expression of the four genes was significantly decreased (Figures 5A–C, I). With regard to *FveCslC2*, *FveCslC3*, *FveCslC5* and *FveCslD5*, the expression levels of were high at the S1 stage, but dramatically decreased with progression of fruit development (Figures 5D–F, H). Interestingly, the expression levels of *FveCslD3* remained low in the early stages, but showed a marked upward trend in the ripening stages (Figure 5G), suggesting that *FveCslD3* may have different function in the regulation of fruit development. These results indicated that *FveCesA* and *FveCsl* genes displayed functional diversity during fruit development.

FveCesA4 negatively regulates strawberry fruit ripening by enhancing fruit firmness

To investigate the function of cellulose synthesis genes in strawberry fruit ripening, *FveCesA4* was transiently overexpressed in the fruit at the S7 stage (Figure 6A). The expression level of *FveCesA4* in *35S::FveCesA4* fruit increased dramatically after injection (Figure 6B), resulting in reduced fruit weight and significantly enhanced fruit firmness compared

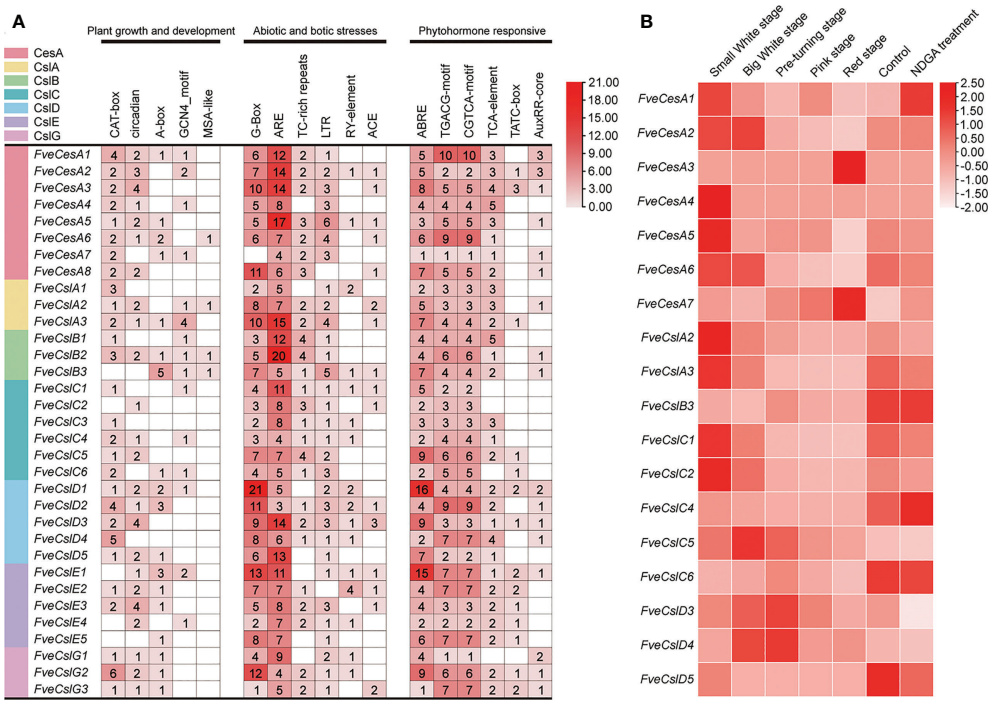

FIGURE 4
Promoter *cis*-acting elements and expression pattern analysis of *FveCesA/Csl* in strawberry. **(A)** Promoter *cis*-acting elements analysis of *FveCesA/Csl* genes. *CesA/Csl* subfamilies are distinguished by different colors. Number and color depth are represented the number of corresponding *cis*-elements. **(B)** Transcriptome analysis reveals the expression level of *FveCesA/Csl* genes during strawberry fruit development.

with the mock control (Figures 6E, F). Next, we deployed RNAi of *FveCesA4* at the S4 stage using the VIGS system. The expression level of *FveCesA4* was greatly suppressed at 7 days after transient silencing (Figures 7A, B). Accompanying the suppression of *FveCesA* expression, significantly increased fruit weight and decreased fruit firmness in *FveCesA4-RNAi* fruit were observed, in comparison with those of the control (Figures 7E, F). In contrast, the fruit size and shape showed no significant change in *FveCesA4-RNAi* and *35S::FveCesA4* fruits (Figures 6C, D, 7C, D). Taken together, these results indicated that FveCesA4 affects fruit ripening and biomass accumulation by regulating fruit firmness.

Discussion

The *CesA* and *Csl* gene families associated with cell wall polysaccharide biosynthesis play important roles in plant growth and development and responses to environmental stress (McFarlane et al., 2014). To date, the *CesA/Csl* gene families have been extensively identified and studied in various species, such as *Arabidopsis* (Persson et al., 2007), rice (Hazen et al., 2002), cotton (Pear et al., 1996) and banana (Yuan et al., 2021), but they have not been reported previously in strawberry. In this study, eight *FveCesA* genes and 25 *FveCsl* genes were identified in diploid woodland strawberry by genome-wide sequence analysis. Further analyses of phylogenic relationships, *cis*-acting elements in promoter, synteny, gene expression patterns, subcellular localization, and transient transformation provide clues for understanding the mechanism of CesA/Csl function in the development and ripening of a non-climacteric fruit.

Previous studies have demonstrated that the cellulose synthase gene superfamily can be resolved into the CesA clade and ten Csl clades, (i.e., CslA-CslH, CslJ and CslM) (McFarlane et al., 2014). Among the Csl clades, the CslA, CslC and CslD lineages are prevalent in all terrestrial plant (Farrokhi et al., 2006). The CslB lineages is considered to be dicotyledons-specific, whereas the CslF and CslH lineages have been indicated to be restricted to grasses (Yin et al., 2009). The present phylogenetic analysis showed that the 33 putative FveCesA/Csl proteins were dividable into seven distinct subfamilies (Figure 1). Eight putative proteins were clustered into the CesA clade, as the largest clade, and the remaining putative proteins were grouped into the CslA, B, C, D, E, and G clades with different abundances, suggesting that the *CesA/Csl* gene family members have undergone extensive expansion and diversification during evolution. The CslD clade was

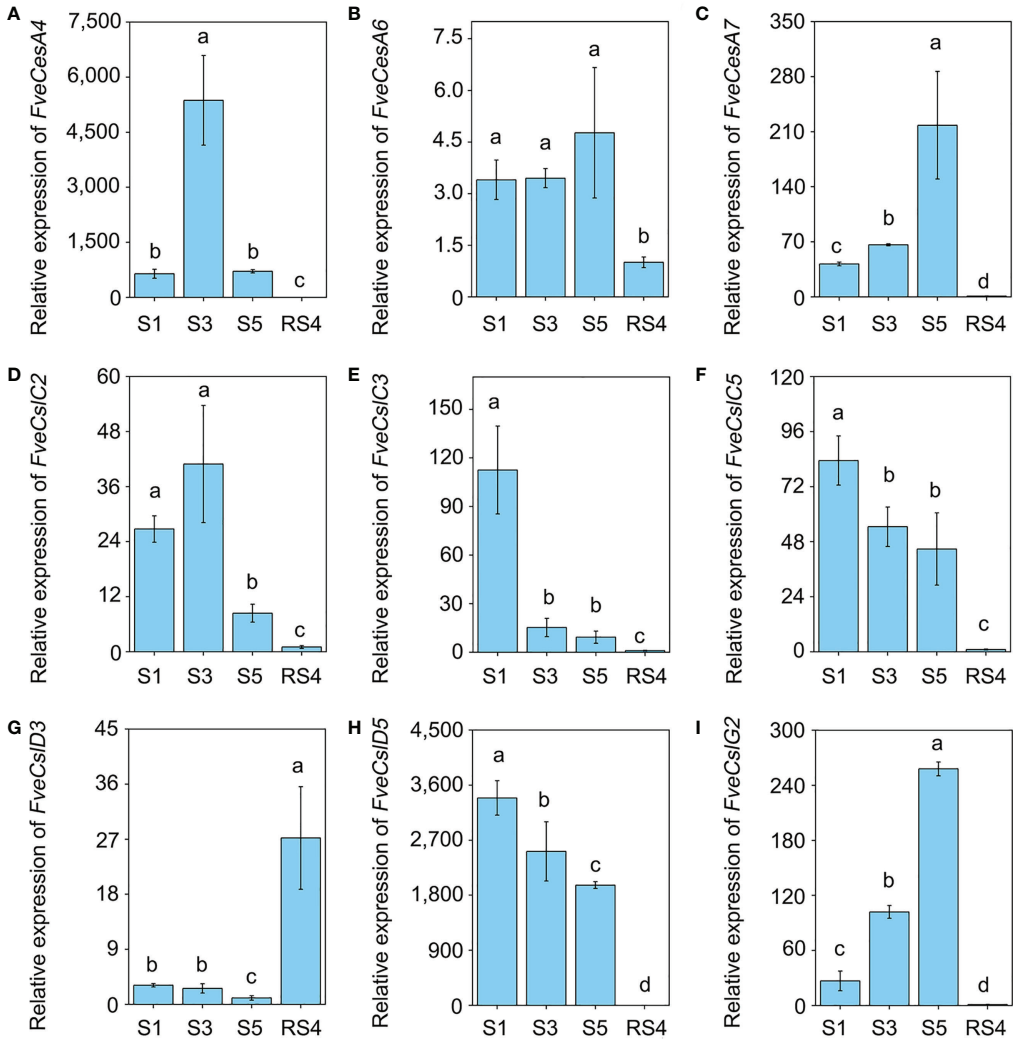

FIGURE 5
The expression pattern of *Cellulose synthase* genes during fruit development. **(A–I)** The relative expression levels of *FveCesA4* **(A)**, *FveCesA6* **(B)**, *FveCesA7* **(C)**, *FveCslC2* **(D)**, *FveCslC3* **(E)**, *FveCsl5* **(F)**, *FveCslD3* **(G)**, *FveCslD5* **(H)**, and *FveCslG2* **(I)** during fruit development were detected by qRT-PCR. Error bars represents SD of three independent replicates (5-10 fruits were used for each replicate). Letter in figure indicates significant differences between stages ($P < 0.05$, one-way ANOVA, Tukey's HSD *post hoc* test).

phylogenetically close to the CesA clade, indicating that these two lineages shared a common ancestor. No *FveCesA/Csl* genes were resolved in the CslF and CslH clades, which was consistent with previous reports (Yin et al., 2009). The CslA and CslC clades are considered to have a distinct evolutionary origins from the remaining Csl clades due to their close relationship with the single-copy homologue found in six green algae species (Yin et al., 2009). The present analysis of structural characteristics demonstrated that the CslA and CslC clades in strawberry contained the glycosyl transferase family 2 domain, whereas the remaining clades contained the cellulose synthase domain (Figure 3C). Similar to the conserved domain analysis, the motif components of strawberry *CesA*, *CslB*, *CslD*, *CslE* and *CslG* genes exhibited high similarity, whereas the *CslA* and *CslC* genes had entirely distinct motif compositions (Figure 3B). These results were consistent with those of previous reports in the other species. Furthermore, the *CslE* genes were distributed in tandem in strawberry Fvb3 chromosome (Figure 2A). It is speculated that *FveCslE* genes may be significantly expanded in strawberry genome possibly through tandem gene replication, which is similar to the conclusions of a study (Yin et al., 2009).

CesA and *Csl* family genes encode GT2-tyoe glycosyltransferases, which is characterized by conserved cytosolic substrate binding and catalytic residues composed of D, D, D, and QxxRW motifs (McFarlane et al., 2014). The first two D residues coordinate UDP, the third D residue promotes the

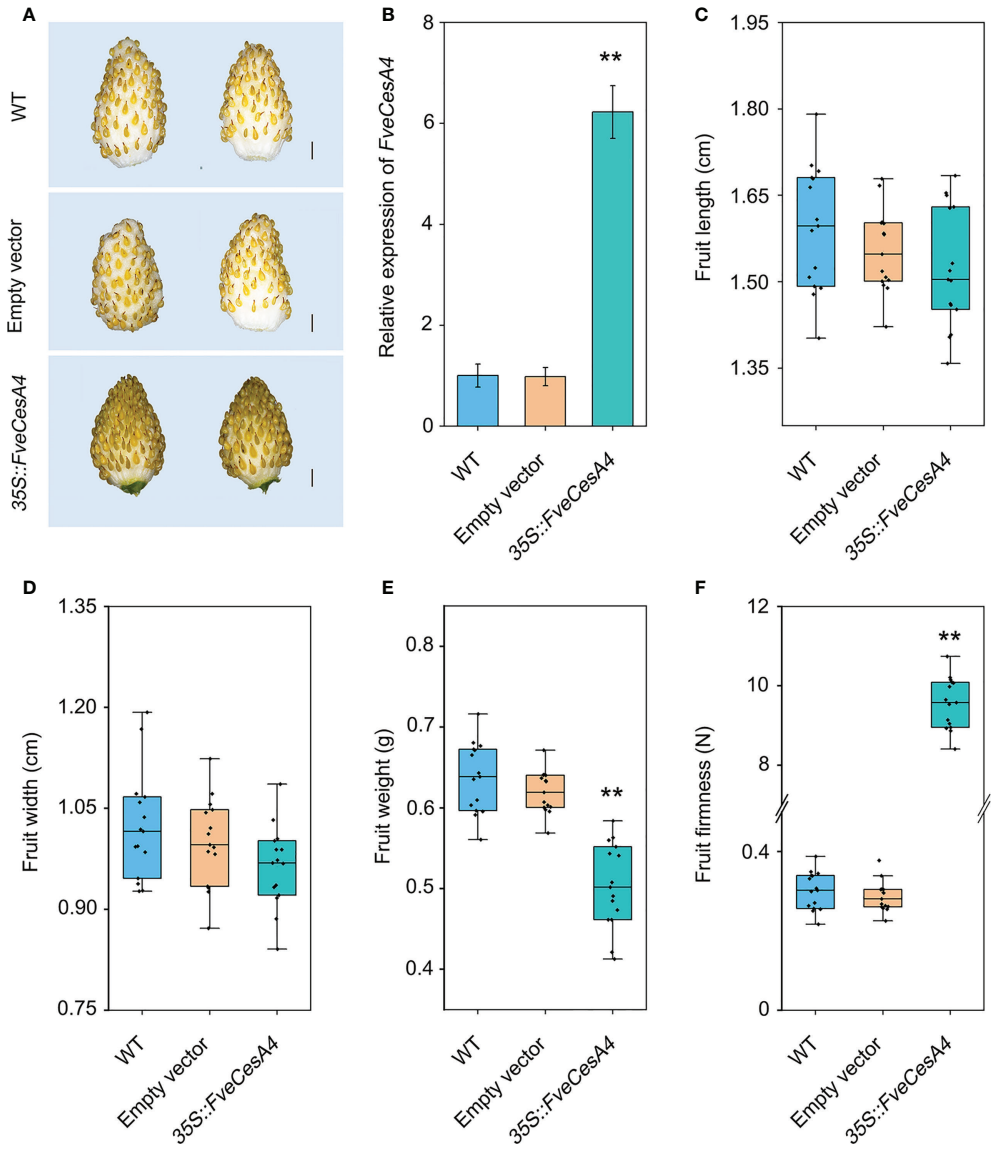

FIGURE 6
Transient overexpression of *FveCesA4* suppressed fruit ripening. *FveCesA4* was transiently overexpressed at S7 stage, and all analyses were performed at 7 days after infiltration. **(A)** Fruit ripening was delayed after overexpression of *FveCesA4*, whereas the control fruits ripened. Scale bar: 10 mm. **(B)** *FveCesA4* transcript levels in *35S::FveCesA4* fruits dramatically increased compared with control. **(C–F)** Fruit length **(C)**, width **(D)**, weight **(E)** and firmness **(F)** analyses of *35S::FveCesA4* fruits. All analyses were performed in three independent replicates with 15 fruits per replicate. ** indicates significant differences between groups ($P < 0.05$, one-way ANOVA, Tukey's HSD *post hoc* test).

glucan extension, and the QxxRW residues are responsible for binding the glycogen residue at the terminus of cellulose chain (Morgan et al., 2013). The present amino acid sequence alignment showed that almost all FveCesA/Csl proteins typically contained D, D, D, and QxxRW motifs (Supplementary Figures S1–S4). The substitution of glutamine residues in the QxxRW motif of FveCslE1, FveCslE2, and FveCslG2 proteins by other residues implies that they may have different functional properties (Supplementary Figure S3), further supporting the hypothesis that the CslE and CslG clade genes have acquired new plant-specific functions through diversification during evolution (Yin et al., 2009). Cellulose synthesis in plants is catalyzed by the rosette-like cellulose synthesis complex localized on the plasma membrane (McFarlane et al., 2014). The present prediction of subcellular localization showed that all the FveCesA/Csl proteins were localized on the membrane (Supplementary Table S2). In addition, proteins in the CesA and Csl clades contained the conserved N-terminal zinc-finger domain (Supplementary Figures S1, S2), which may be involved in CesA functions specific to higher plants, such as the formation of rosette

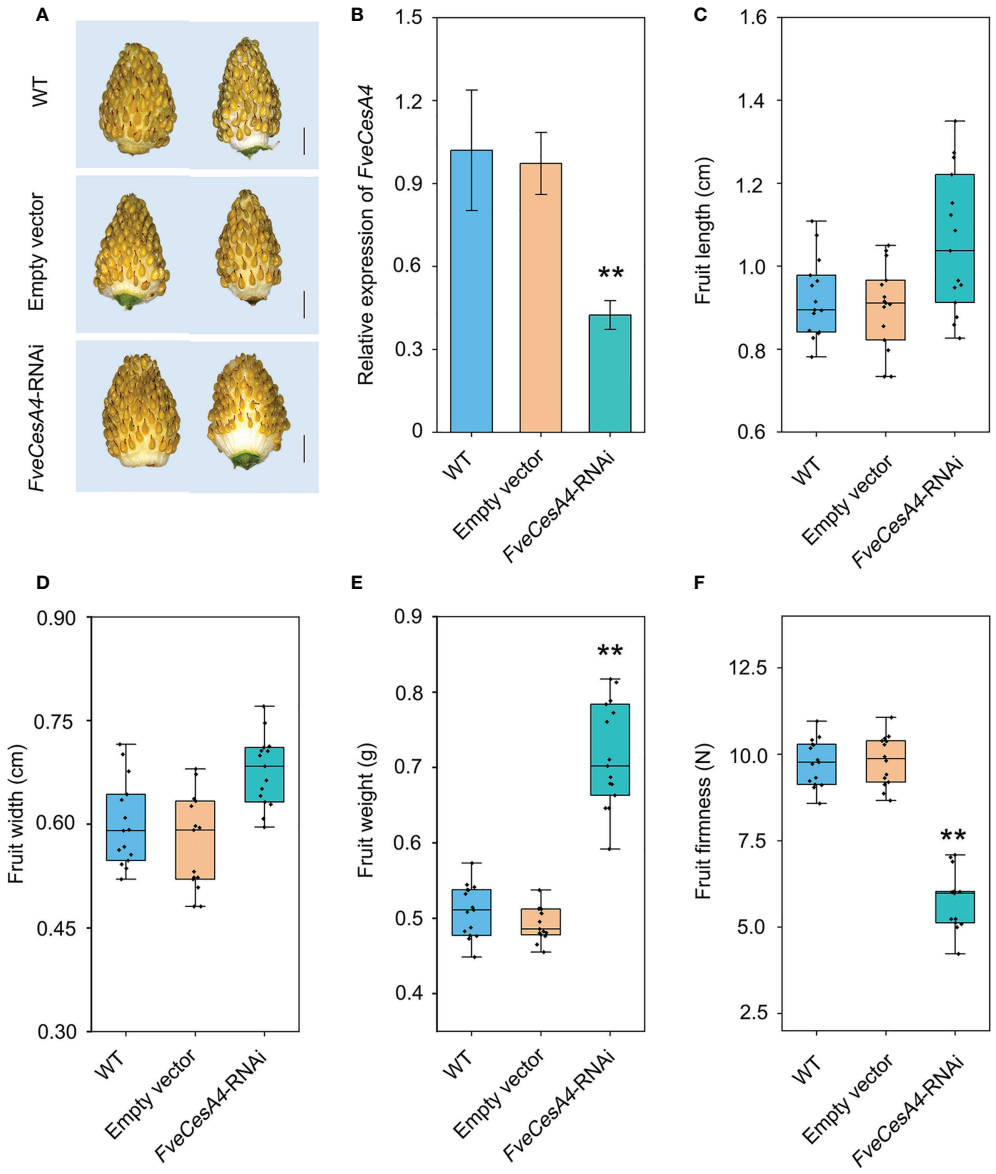

FIGURE 7
Transient silencing of *FveCesA4* accelerated fruit ripening. *FveCesA4* was transiently silenced at S4 stage, and all analyses were performed at 7 days after infiltration. **(A)** *FveCesA4-RNAi* fruits became ripened, while the control fruits remained unripe. Scale bar: 10 mm. **(B)** *FveCesA4* transcript levels in *FveCesA4-RNAi* fruits dramatically suppressed compared with control. **(C–F)** Fruit length **(C)**, width **(D)**, weight **(E)** and firmness **(F)** analyses of *FveCesA4-RNAi* fruits. All analyses were performed in three independent replicates with 15 fruits per replicate. ** indicates significant differences between groups ($P < 0.05$, one-way ANOVA, Tukey's HSD *post hoc* test).

structure through subunit multimerization and the interaction with regulatory factors (McFarlane et al., 2014).

In general, strawberry fruit firmness and texture change dramatically during development and are regulated by ABA signaling (Liao et al., 2018). Endogenous ABA levels in strawberry fruit remain extremely low level during the early fruit development, but increases sharply in the fruit ripening stage, which, in turn triggers fruit ripening events, such as fruit softening and soluble sugars accumulation (Liao et al., 2018). Fruit firmness and texture are closely related to the composition and content of cell wall catalyzed mainly by cellulose synthesis genes. In the present study, we analyzed the promoters of the *FveCesA*/*Csl* superfamily members (Figure 4A). Abundant *cis*-acting elements associated with plant growth and development, stress response, and hormone regulation were detected in the promoters of the *FveCesA*/*Csl* genes. These results suggested that the *FveCesA*/*Csl* gene family may participate in plant growth and development as well as stress tolerance, and the family members are regulated by

plant hormones, especially ABA signaling. Consistent with the present qRT-PCR results (Figure 5), the transcriptome data showed that the expression levels of several *FveCesA*/*Csl* genes decreased to varying extents in the fruit ripening stage (Figure 4B). Furthermore, after spray application of NDGA to reduce the endogenous ABA content in fruit, the transcript abundance of certain *FveCesA/Csl* genes was changed to some extent (Figure 4B). Moreover, the strawberry fruit transiently overexpressing *FveCesA4* resulted in significantly increased fruit texture firmness and delayed fruit ripening (Figures 6A, B, F). The fruit transient silencing of *FveCesA4* in strawberry showed a similar conclusion (Figures 7A, B, F), implying that *FveCesA4* positively regulates fruit firmness and inhibits fruit ripening. In rice, overexpression of *OsCslD4* increases endogenous ABA levels and enhances rice salt-tolerance (Zhao et al., 2022). Whether the transient overexpression of *FveCesA4* in strawberry fruit also affects endogenous ABA abundance, which is required for fruit ripening, through the alteration of cell wall integrity remains to be determined, and the underling mechanism needs to be further examined. Notably, previous reports have shown that cellulose synthesis genes not only function in plant growth and development but also enhance plant biomass (Hu et al., 2018a). Overexpression of *AtCesA2*, *AtCesA5* and *AtCesA6* enhances secondary cell wall deposition and results in increased biomass production in *Arabidopsis* (Hu et al., 2018a). However, the present data showed that overexpression of *FveCesA4* in strawberry fruit contributed to reduced fruit biomass (Figure 6E). The RNAi results indicated a similar conclusion (Figure 7E). One possible explanation could be that overexpression of *FveCesA4* contributed to improved fruit firmness and inhibited fruit ripening, which, in turn suppressed the accumulation of relevant metabolites and then reduced fruit biomass. Auxin and gibberellin (GA) promote strawberry fruit growth in the early phase. The contents of endogenous IAA and GA_{1+3} increased to the highest at S3 stage during fruit development (Liao et al., 2018). In this study, *FveCesA4* exhibited the highest expression level at S3 stage (Figure 5A), and was phylogenetically closed to *AtCesA4* (Figure 1), which was responsible for the synthesis of secondary cell wall cellulose, suggesting that *FveCesA4*- mediated cell wall synthesis may be regulated by auxin and GA signaling and play an important role in regulating fruit early development. Hence, the underlying mechanism of *FveCesA/Csl*-mediated cell wall synthesis in the regulation of strawberry fruit development and ripening requires further exploration.

Conclusion

In this study, we identified eight *FveCesA* genes and 25 *FveCsl* genes in the genome of diploid woodland strawberry. Analyses of the protein structure, phylogenetic relationships, and expression patterns were performed to investigate the characteristics and functions of the *FveCesA*/*Csl* genes. The transient transformation of *FveCesA4* in fruit further confirmed that cell wall synthesis is essential for strawberry fruit development and ripening. The present results provide a foundation for detailed explorations of whether *FveCesA/Csl*-mediated cell wall synthesis regulates fruit ripening in strawberry, and they will assist in strawberry breeding aimed at improving of the shelf-life of strawberry fruits.

Data availability statement

The original contributions presented in the study are included in the article/Supplementary Material. Further inquiries can be directed to the corresponding author.

Author contributions

HH, SZ, and XL designed the research, analyzed the data, and revised the final manuscript. HH and SZ performed the most of the experiments, with assistance from MX, SL, JC, TL, GG, RW, JL, and YS. SZ and XL wrote the manuscript. All authors contributed to the article and approved the submitted version.

Funding

This study was funded by the National Natural Science Foundation of China (No. 31801840).

Conflict of interest

The authors declare that the research was conducted in the absence of any commercial or financial relationships that could be construed as a potential conflict of interest.

Publisher's note

Supplementary material

The Supplementary Material for this article can be found online at: https://www.frontiersin.org/articles/10.3389/fpls.2022.1044029/full#supplementary-material

SUPPLEMENTARY FIGURE 1
Amino acid sequence alignment of CesA subfamily in strawberry. Conserved zinc-binding domain is highlighted by red line. The conserved cysteine residues in zinc-binding domain are marked with red stars. Conserved cellulose_synt domain is highlighted by blue line. The conserved "D, D, D and QXXRW motif" are marked with blue stars.

SUPPLEMENTARY FIGURE 2
Amino acid sequence alignment of CslD subfamily in strawberry. Conserved zinc-binding domain is highlighted by red line. The conserved cysteine residues in zinc-binding domain are marked with red stars. Conserved cellulose_synt domain is highlighted by blue line. The conserved "D, D, D and QXXRW motif" are marked with blue stars.

SUPPLEMENTARY FIGURE 3
Amino acid sequence alignment of CslA and CslC subfamily in strawberry. **(A)** Amino acid sequence alignment of FveCslAs proteins. **(B)** Amino acid sequence alignment of FveCslCs proteins. Conserved Glyco_tranf_2_3 domain is highlighted by blue line. The conserved "D, D, D and QXXRW motif" are marked with blue stars.

SUPPLEMENTARY FIGURE 4
Amino acid sequence alignment of CslB, CslE and CslG subfamily in strawberry. **(A)** Amino acid sequence alignment of FveCslBs proteins. **(B)** Amino acid sequence alignment of FveCslEs proteins. **(C)** Amino acid sequence alignment of FveCslGs proteins. Conserved Glyco_tranf_2_3 domain is highlighted by blue line. The conserved "D, D, D and QXXRW motif" are marked with blue stars.

References

Appenzeller, L., Doblin, M., Barreiro, R., Wang, H., Niu, X., Kollipara, K., et al. (2004). Cellulose synthesis in maize: isolation and expression analysis of the cellulose synthase (CesA) gene family. *Cellulose* 11 (3), 287–299. doi: 10.1023/B:CELL.0000046417.84715.27

Bernal, A. J., Jensen, J. K., Harholt, J., Sørensen, S., Moller, I., Blaukopf, C., et al. (2007). Disruption of ATCSLD5 results in reduced growth, reduced xylan and homogalacturonan synthase activity and altered xylan occurrence in arabidopsis. *Plant J.* 52 (5), 791–802. doi: 10.1111/j.1365-313X.2007.03281.x

Cantarel, B. L., Coutinho, P. M., Rancurel, C., Bernard, T., Lombard, V., and Henrissat, B. (2009). The carbohydrate-active EnZymes database (CAZy): an expert resource for glycogenomics. *Nucleic Acids Res.* 37 (suppl_1), D233–D238. doi: 10.1093/nar/gkn663

Chen, C., Chen, H., Zhang, Y., Thomas, H. R., Frank, M. H., He, Y., et al. (2020). TBtools: an integrative toolkit developed for interactive analyses of big biological data. *Mol. Plant* 13 (8), 1194–1202. doi: 10.1016/j.molp.2020.06.009

Choe, S., Choi, B., Kang, J. H., and Seo, J. K. (2021). Tolerance to tomato yellow leaf curl virus in transgenic tomato overexpressing a cellulose synthase-like gene. *Plant Biotechnol. J.* 19 (4), 657. doi: 10.1111/pbi.13539

Cosgrove, D. J. (2005). Growth of the plant cell wall. *Nat. Rev. Mol. Cell Biol.* 6 (11), 850–861. doi: 10.1038/nrm1746

Czaja, W., Krystynowicz, A., Kawecki, M., Wysota, K., Sakiel, S., Wróblewski, P., et al. (2007). *Cellulose: Molecular and structural biology* (The Netherlands: Springer Dordrecht). doi: 10.1007/978-1-4020-5380-1

Desprez, T., Juraniec, M., Crowell, E. F., Jouy, H., Pochylova, Z., Parcy, F., et al. (2007). Organization of cellulose synthase complexes involved in primary cell wall synthesis in arabidopsis thaliana. *Proc. Natl. Acad. Sci. U.S.A.* 104 (39), 15572–15577. doi: 10.1073/pnas.0706569104

Dhugga, K. S. (2012). Biosynthesis of non-cellulosic polysaccharides of plant cell walls. *Phytochemistry* 74, 8–19. doi: 10.1016/j.phytochem.2011.10.003

Dhugga, K. S., Barreiro, R., Whitten, B., Stecca, K., Hazebroek, J., Randhawa, G. S., et al. (2004). Guar seed ß-mannan synthase is a member of the cellulose synthase super gene family. *Science* 303 (5656), 363–366. doi: 10.1126/science.1090908

Farrokhi, N., Burton, R. A., Brownfield, L., Hrmova, M., Wilson, S. M., Bacic, A., et al. (2006). Plant cell wall biosynthesis: genetic, biochemical and functional genomics approaches to the identification of key genes. *Plant Biotechnol. J.* 4 (2), 145–167. doi: 10.1111/j.1467-7652.2005.00169.x

Goubet, F., Barton, C. J., Mortimer, J. C., Yu, X., Zhang, Z., Miles, G. P., et al. (2009). Cell wall glucomannan in arabidopsis is synthesised by CSLA glycosyltransferases, and influences the progression of embryogenesis. *Plant J.* 60 (3), 527–538. doi: 10.1111/j.1365-313x.2009.03977.x

Gu, T., Jia, S., Huang, X., Wang, L., Fu, W., Huo, G., et al. (2019). Transcriptome and hormone analyses provide insights into hormonal regulation in strawberry ripening. *Planta* 250 (1), 145–162. doi: 10.1007/s00425-019-03155-w

Hazen, S. P., Scott-Craig, J. S., and Walton, J. D. (2002). Cellulose synthase-like genes of rice. *Plant Physiol.* 128 (2), 336–340. doi: 10.1104/pp.010875

Hu, H., Zhang, R., Feng, S., Wang, Y., Wang, Y., Fan, C., et al. (2018a). Three AtCesA6-like members enhance biomass production by distinctively promoting cell growth in arabidopsis. *Plant Biotechnol. J.* 16 (5), 976–988. doi: 10.1111/j.1467-7652.2005.00169.x

Hu, H., Zhang, R., Tao, Z., Li, X., Li, Y., Huang, J., et al. (2018b). Cellulose synthase mutants distinctively affect cell growth and cell wall integrity for plant biomass production in arabidopsis. *Plant Cell Physiol.* 59 (6), 1144–1157. doi: 10.1093/pcp/pcy050

Kumar, S., Stecher, G., and Tamura, K. (2016). MEGA7: molecular evolutionary genetics analysis version 7.0 for bigger datasets. *Mol. Biol. Evol.* 33 (7), 1870–1874. doi: 10.1093/molbev/msw054

Liao, X., Li, M., Liu, B., Yan, M., Yu, X., Zi, H., et al. (2018). Interlinked regulatory loops of ABA catabolism and biosynthesis coordinate fruit growth and ripening in woodland strawberry. *Proc. Natl. Acad. Sci. U.S.A.* 115 (49), E11542–E11550. doi: 10.1073/pnas.1812575115

Li, Y., Cheng, X., Fu, Y., Wu, Q., Guo, Y., Peng, J., et al. (2019). A genome-wide analysis of the cellulose synthase-like (Csl) gene family in maize. *Biol. Plant* 63 (1), 721–732. doi: 10.1186/s12870-017-1142-z

Liepman, A. H., and Cavalier, D. M. (2012). The cellulose synthase-like a and cellulose synthase-like c families: recent advances and future perspectives. *Front. Plant Sci.* 3. doi: 10.3389/fpls.2012.00109

Liepman, A. H., Wilkerson, C. G., and Keegstra, K. (2005). Expression of cellulose synthase-like (Csl) genes in insect cells reveals that CslA family members encode mannan synthases. *Proc. Natl. Acad. Sci. U.S.A.* 102 (6), 2221–2226. doi: 10.1073/pnas.0409179102

Little, A., Schwerdt, J. G., Shirley, N. J., Khor, S. F., Neumann, K., O'Donovan, L. A., et al. (2018). Revised phylogeny of the cellulose synthase gene superfamily: insights into cell wall evolution. *Plant Physiol.* 177 (3), 1124–1141. doi: 10.1104/pp.17.01718

Liu, Z., Schneider, R., Kesten, C., Zhang, Y., Somssich, M., Zhang, Y., et al. (2016). Cellulose-microtubule uncoupling proteins prevent lateral displacement of microtubules during cellulose synthesis in arabidopsis. *Dev. Cell* 38 (3), 305–315. doi: 10.1016/j.devcel.2016.06.032

Malinovsky, F. G., Fangel, J. U., and Willats, W. G. (2014). The role of the cell wall in plant immunity. *Front. Plant Sci.* 5. doi: 10.3389/fpls.2014.00178

McFarlane, H. E., Döring, A., and Persson, S. (2014). The cell biology of cellulose synthesis. *Annu. Rev. Plant Biol.* 65 (1), 69–94. doi: 10.1146/annurev-arplant-050213-040240

Morgan, J. L., Strumillo, J., and Zimmer, J. (2013). Crystallographic snapshot of cellulose synthesis and membrane translocation. *Nature* 493 (7431), 181–186. doi: 10.1038/nature11744

Moya-León, M. A., Mattus-Araya, E., and Herrera, R. (2019). Molecular events occurring during softening of strawberry fruit. *Front. Plant Sci.* 10. doi: 10.3389/fpls.2019.00615

Park, S., Szumlanski, A. L., Gu, F., Guo, F., and Nielsen, E. (2011). A role for CSLD3 during cell-wall synthesis in apical plasma membranes of tip-growing root-hair cells. *Nat. Cell Biol.* 13 (8), 973–980. doi: 10.1038/ncb2294

Pear, J. R., Kawagoe, Y., Schreckengost, W. E., Delmer, D. P., and Stalker, D. M. (1996). Higher plants contain homologs of the bacterial celA genes encoding the

catalytic subunit of cellulose synthase. *Proc. Natl. Acad. Sci. U.S.A.* 93 (22), 12637–12642. doi: 10.1073/pnas.93.22.12637

Persson, S., Paredez, A., Carroll, A., Palsdottir, H., Doblin, M., Poindexter, P., et al. (2007). Genetic evidence for three unique components in primary cell-wall cellulose synthase complexes in arabidopsis. *Proc. Natl. Acad. Sci. U.S.A.* 104 (39), 15566–15571. doi: 10.1073/pnas.0706592104

Richmond, T. A., and Somerville, C. R. (2000). The cellulose synthase superfamily. *Plant Physiol.* 124 (2), 495–498. doi: 10.1104/pp.124.2.495

Roberts, A. W., and Bushoven, J. T. (2007). The cellulose synthase (CESA) gene superfamily of the moss physcomitrella patens. *Plant Mol. Biol.* 63 (2), 207–219. doi: 10.1007/s11103-006-9083-1

Song, X., Xu, L., Yu, J., Tian, P., Hu, X., Wang, Q., et al. (2019). Genome-wide characterization of the cellulose synthase gene superfamily in solanum lycopersicum. *Gene* 688, 71–83. doi: 10.1016/j.gene.2018.11.039

Taylor, N. G., Howells, R. M., Huttly, A. K., Vickers, K., and Turner, S. R. (2003). Interactions among three distinct CesA proteins essential for cellulose synthesis. *Proc. Natl. Acad. Sci. U.S.A.* 100 (3), 1450–1455. doi: 10.1073/pnas.0337628100

Verhertbruggen, Y., Yin, L., Oikawa, A., and Scheller, H. V. (2011). Mannan synthase activity in the CSLD family. *Plant Signal. Behav.* 6 (10), 1620–1623. doi: 10.4161/psb.6.10.17989

Wang, Q., Wang, M., Chen, J., Qi, W., Lai, J., Ma, Z., et al. (2022). ENB1 encodes a cellulose synthase 5 that directs synthesis of cell wall ingrowths in maize basal endosperm transfer cells. *Plant Cell* 34 (3), 1054–1074. doi: 10.1093/plcell/koab312

Yang, J., Bak, G., Burgin, T., Barnes, W. J., Mayes, H. B., Peña, M. J., et al. (2020). Biochemical and genetic analysis identify CSLD3 as a beta-1, 4-glucan synthase that functions during plant cell wall synthesis. *Plant Cell* 32 (5), 1749–1767. doi: 10.1105/tpc.19.00637

Yin, Y., Huang, J., and Xu, Y. (2009). The cellulose synthase superfamily in fully sequenced plants and algae. *BMC Plant Biol.* 9 (1), 1–14. doi: 10.1186/1471-2229-9-99

Yin, L., Verhertbruggen, Y., Oikawa, A., Manisseri, C., Knierim, B., Prak, L., et al. (2011). The cooperative activities of CSLD2, CSLD3, and CSLD5 are required for normal arabidopsis development. *Mol. Plant* 4 (6), 1024–1037. doi: 10.1093/mp/ssr026

Yuan, W., Liu, J., Takáč, T., Chen, H., Li, X., Meng, J., et al. (2021). Genome-wide identification of banana csl gene family and their different responses to low temperature between chilling-sensitive and tolerant cultivars. *Plants* 10 (1), 122. doi: 10.3390/plants10010122

Zhao, H., Li, Z., Wang, Y., Wang, J., Xiao, M., Liu, H., et al. (2022). Cellulose synthase-like protein OsCSLD4 plays an important role in the response of rice to salt stress by mediating abscisic acid biosynthesis to regulate osmotic stress tolerance. *Plant Biotechnol. J.* 20 (3), 468. doi: 10.1111/pbi.13729

frontiers | Frontiers in Plant Science

TYPE Original Research
PUBLISHED 15 November 2022
DOI 10.3389/fpls.2022.1045270

OPEN ACCESS

EDITED BY
Peitao Lü,
Fujian Agriculture and Forestry University, China

REVIEWED BY
Chao Ma,
China Agricultural University, China
Shupeng Gai,
Qingdao Agricultural University, China

*CORRESPONDENCE
Haixia Pei
phx2003@126.com

SPECIALTY SECTION
This article was submitted to Plant Systems and Synthetic Biology, a section of the journal Frontiers in Plant Science

RECEIVED 15 September 2022
ACCEPTED 31 October 2022
PUBLISHED 15 November 2022

CITATION
Zhang J, Zhang Y, He Y, Du T, Shan D, Fan H, Wang W, Qin Z, Xin C and Pei H (2022) Metabolome and transcriptome integration reveals insights into the process of delayed petal abscission in rose by STS. *Front. Plant Sci.* 13:1045270. doi: 10.3389/fpls.2022.1045270

Metabolome and transcriptome integration reveals insights into the process of delayed petal abscission in rose by STS

Jingjing Zhang, Yuyun Zhang, Yongmei He, Tingting Du, Duoxiu Shan, Houdong Fan, Wenyu Wang, Zhe Qin, Cuihua Xin and Haixia Pei*

School of Life Science ang Technology, Inner Mongolia University of Science and Technology, Baotou, China

The abscission of plant organs plays an important role in ensuring the normal life activities. Rose is one of the most important ornamental plants, and its premature abscission of petal has seriously affected the quality and commercial value. Silver Thiosulfate (STS) is an ethylene inhibitor, which is often used preservative to delay the senescence of fresh cut flowers. To understand the regulatory mechanism of petal abscission in rose by STS, integrative analysis of the metabolome and transcriptome profiles was performed in abscission zone (AZ) tissues of rose under different treatments (MOCK, STS, ETH, STS+ETH). The results showed that STS significantly delayed the petal abscission in phenotype and reduced the activity of two enzymes (pectinase and cellulase) associated with cell wall degradation in physiological level. STS affected the contents of five metabolites (shikonin, jasmonic acid, gluconolactone, stachyose and D-Erythrose 4-phosphate), and involved changes in the expression of 39 differentially expressed genes (DEGs) associated with these five metabolites. Five DEGs (*LOC112192149*, *LOC112196726*, *LOC112189737*, *LOC112188495*, and *LOC112188936*) were probably directly associated with the biosynthesis of shikonin, jasmonic acid, and D-Erythrose 4-phosphate. Meanwhile, the effect of STS on the abscission process significantly involved in the pentose phosphate pathway and amino acid biosynthesis pathway. In addition, STS had a greater effect on the transcription factors, phytohormone related DEGs represented by auxin and ethylene, DEGs related to disease resistance and amino acid, etc. Above all, STS negatively influences petal abscission of rose, these results maybe provide a reference for subsequent studies on petal abscission of rose by STS.

KEYWORDS

silver thiosulfate, rose, abscission, metabolome, transcriptome

1 Introduction

The abscission of tissues and organs is important in the normal growth and reproductive development of plants (Kim et al., 2019; Liu et al., 2022). Abscission is the process by which an organ or tissue is separated from the main body of the plant. This process is usually restricted to a localized region of cells termed an abscission zone (AZ). The abscission process comprises four stages: (1) differentiation of the AZ; (2) sensing of the abscission signal in the AZ and initiation of abscission; (3) cell separation leading to abscission of the organ or tissue; and (4) differentiation of the abscission layer and protective layer (Singh et al., 2020). Premature senescence, which includes premature abscission of plant organs such as flowers and fruits, can severely affect agricultural production (Patharkar and Walker, 2018).

Changes in endogenous phytohormone contents are a critical factor in the initiation of abscission (Kim et al., 2019). Among phytohormones, ethylene is considered to be an important regulator of abscission, and many factors involved in ethylene biosynthesis and signal transduction participate in this process (Gao et al., 2016). In Arabidopsis, the abscission of floral organs is inhibited in the ethylene-insensitive mutants *etr1-1* and *ein2* (Patterson and Bleecker, 2004). The abscission of tomato pedicels is accompanied by upregulation of the expression of *1-AMINOCYCLOPROPANE-1-CARBOXYLATE SYNTHASE 1A* (*ACS1A*), *ACS2*, *ACS6*, *ACC OXIDASE 1* (*ACO1*), *ACO5*, and *ETHYLENE RESPONSE FACTOR 52* (*ERF52*) (Meir et al., 2010; Nakano et al., 2014). In lychee, a low expression level of *LcERF2* reduces the rate of fruit abscission (Yi et al., 2021). Experimental treatment with exogenous ethylene in many studies has demonstrated that the onset of abscission is strongly associated with the presence of ethylene. For example, the application of ethephon (which is converted to ethylene in plant tissues) accelerates fruit abscission in sweet cherry and sweet orange, and treatment of rose, geranium, and tulip with exogenous ethylene leads to the early onset of flower organ abscission (John-Karuppiah and Burns, 2010; Smith and Whiting, 2010; Singh et al., 2022). In contrast, inhibitors of ethylene synthesis or action effectively delay abscission, but the effect of ethylene inhibitors on the mechanism of action of ethylene and petal abscission is uncertain.

The silver thiosulfate (STS) complex is commonly used as an inhibitor of ethylene synthesis. Application of STS extends the vase life of many cut flowers, such as lily, sunflower, and carnation, but does not significantly extend the vase life of all cut flower types (Liu et al., 2018; Kılıç et al., 2020; Krause et al., 2021). For example, treatment of gardenia cut flowers with STS has no effect on the vase life, and STS treatment of goldenseal cut flowers slightly promotes flower opening but does not extend the vase life (Çelikel et al., 2020; Kato et al., 2022). In addition, STS impacts on other physiological functions in plants. For example, STS can induce the expression of androgenic-related genes in female cannabis plants to develop male flowers (Adal et al., 2021). Ethephon prevents the bending of goldenseal stems, whereas STS promotes the bending rate of goldenseal stems (Naing et al., 2021). Under a humid environment, STS reduces the emission of carnation fragrance after harvesting, thus prolonging the fragrance of carnations (Kishimoto, 2021). Supplementation of the culture medium with STS significantly increases the number of regenerating shoots per leaf and significantly improves the *in vitro* regeneration frequency of a peach rootstock (Ricci et al., 2020). Although STS solution effectively prolongs the vase life of rose cut flowers (Son et al., 2003), the detailed mechanism by which STS delays petal abscission in rose remains unclear.

Rose is among the most economically important cut flower crops worldwide. Petal senescence is the main factor that affects the rose flower quality and petal abscission is the culmination of the senescence process (Gao et al., 2016). Most previous studies of petal abscission in rose have focused on the regulatory mechanism of endogenous phytohormones, such as auxin, ethylene and jasmonic acid. In rose, silencing of the AUX/IAA gene *RhIAA16* promotes petal abscission (Gao et al., 2016). In petal abscission of rose, the ethylene receptor genes *RhERF1* and *RhERF4* coordinate ethylene and auxin signaling by reducing the expression level of the pectin-metabolizing gene beta-GALACTOSIDASE 1 (*RhBGLA1*), thereby inhibiting abscission (Gao et al., 2019). Synergistic action of the auxin response factor *RhARF7* and the sucrose transporter protein RhSUC2 inhibits ethylene-induced petal abscission (Liang et al., 2019). Ethylene promotes petal abscission of rose and affects gene expression in the AZ (Singh et al., 2020), whereas the jasmonic acid pathway is strongly regulated during abscission, which negatively affects petal abscission in rose (Singh et al., 2022). In summary, petal abscission is a complex physiological process, and the regulatory mechanisms of multiple factors, including STS, on this process require further in-depth investigation.

In this study, we analyzed the effect of STS in four treatment solutions (distilled water, STS, ETH, and STS+ETH) on petal abscission in rose cut flowers at the phenotypic, physiological, transcriptomic, and metabolomic levels. The present study provide some results into the metabolite contents and molecular mechanism of STS-delayed petal abscission of rose flowers.

2 Materials and methods

2.1 Plant materials and treatments

The ethylene-sensitive rose cultivar *R. hybrida* cv. 'Tineke' was as material for the experiments in this study. The fresh rose

flowers at flower opening stage 2 were harvested from a flower plantation in Baotou, Inner Mongolia Autonomous Region, China (Gao et al., 2016). The rose flowers were brought back to the laboratory immediately after harvesting, then they were cut to 25 cm in length under water and placed in deionized water until further processing. The rose flowers were inserted into four different treatment solutions (deionized water, STS, ETH, STS+ETH), the number of flowers under each treatment was 36, and the experiment was repeated three times. The solution of STS was a mixture of 158 mg/L $AgNO_3$ and 924 mg/L anhydrous $Na_2S_2O_3$, the solution of ETH was configured with 25 mg/L ethephon, and the solution of STS and ETH was a 1:1 mixture of the solutions of STS and ETH separately. Rose flowers were treated with the four solutions for 8 h, and the time point at which treatments were finished was recorded as 0 hour. Then the roses were kept on cultivating in the solution of 8-Hydroxyquinoline (8-HQ) with a concentration of 200 mg/L. Here, 8-HQ only acts as a bacterial inhibitor. Meanwhile, the 8-HQ solution was changed daily and the rose flowers were cut a little under water everyday. The rose flowers in 8-HQ were placed in a light incubator at 23 ± 1°C, 60%-80% relative humidity, and a 16/8 h (light/dark) light cycle.

2.2 Collection of AZ samples in rose

The sampling criterion for AZ was to cut the petal base and the petal receptacle less than 1 mm in length respectively in rose petals (Gao et al., 2016), and the sample location was shown in Supplementary Figure 1. The AZ samples at flower opening stage 2 were recorded as untreated samples (UT). After 8 h of treatment with different treatment solutions, the solution was replaced with 8-HQ for 24 h and 48 h. Then we obtained the AZ samples in different treatments, respectively. The samples were recorded as MOCK24h, STS24h, Eth24h, S_E24h and MOCK48h, STS48h, Eth48h, S_E48h. Meanwhile, the AZ samples were immediately frozen in liquid nitrogen and stored at -80°C for subsequent experiments.

2.3 Observation on abscission time of rose petal under different treatments

The abscission time of rose petal in MOCK, STS, ETH and STS+ETH treatments were observed and recorded. Photographs (Canon EOS 6D Mark II) were taken from the top angle of the rose flowers every 24 h to show the phenotype in abscission process. The observations were continued until the petals completely finished abscission or dried up on the branches.

2.4 Determination of pectinase and cellulase activities

The AZ samples from untreated (0 h), 8 h treated with different solutions and 48 h (8 + 48 h) in 8-HQ vase solution were selected to measure pectinase and cellulase activities in rose. Pectinase and cellulase activities were assayed using kits purchased from Nanjing Jiancheng Bioengineering Institute for pectinase (Item No. A140-1-1) and cellulase (Item No. A138).

Cellulase activity was measured according to the following steps: (1) Sample pretreatment: Weigh the samples of AZ in the single rose flower, add buffer to homogenize in ice bath, 4000 rpm, centrifuge at room temperature for 10 min, take one part of the supernatant of the homogenate for testing, and the other part of the supernatant of the homogenate in boiling water bath for 5 min (to inactivate the enzyme), then take it out and cool it to make the boiling supernatant of the homogenate; (2) Enzymatic reaction: Mix the supernatant of homogenate with buffer solution and substrate in proportion, incubate at 37°C for 30 min, take it out immediately and incubate in a boiling water bath for 15 min, take it out to cool, centrifuge at 4000 rpm for 10 min at room temperature, and prepare saccharified supernatant; (3) Color reaction: Mix the saccharified supernatant and color solution in proportion, and measure the OD value at the wave length of 550 nm. Cellulase activity (U/g tissue) = [(OD of assay tube - OD of control tube)/(OD of standard tube - OD of blank tube)) × concentration of standard) (ug/mL) × volume of reaction fluid (mL)] ÷ [(volume of sample taken (mL)/volume of extract added (mL)) × sample mass (g)] ÷ reaction time (min).

Pectinase activity was measured according to the following steps: (1) Extraction of crude enzymes extract: Weigh the samples of AZ in the single rose flower, add 5-10 times the volume of the extract buffer (mL) to homogenize in ice bath; at 4°C, 10000g, centrifuge for 10 min; take the supernatant, and place it on the ice for testing; (2) Mix the supernatant with reagent 2, and react in water bath at 50°C for 30 min. Then add reagent 3, take a boiling water bath for 5 min, cool by the ice bath to stop the reaction; 8000 g, 4°C, centrifuge for 10 min; take the supernatant, and measure the absorbance value A at the wave length of 540 nm, $\triangle A=A_{\text{measuring tube}}-A_{\text{control tube}}$; (3) Then calculate according to the formula. Pectinase activity (U/h/g tissue) = $[(\Delta A+0.008)/3.9642] \times V_{\text{inverse total}} \div (\times W \div V_{\text{sample total}}) \div T = 2.523 \times (\Delta A+0.008) \div W$.

2.5 Metabolites extraction and analysis of UHPLC-MS/MS

At the end of 8 h of different treatments of rose, the vase solutions were uniformly changed to 8-HQ to continue vialing.

The petals of ethylene-treated rose started abscission after 48 h in 8-HQ vase solution, so we made 24 h as the time point for metabolome analysis. At this moment, that did not exhibit abscission phenomenon in each treatment. Metabolomic samples were selected as UT, MOCK24h, STS24h, ETH24h, S_E24h, and six biological replicates were set. Sample preparation was as follows: tissues (100 mg) were individually grounded with liquid nitrogen and the homogenate was resuspended with prechilled 80% methanol by well vortex. The samples were incubated on ice for 5 min and then were centrifuged at 15,000 g, 4°C for 20 min. Some of supernatant was diluted to final concentration containing 53% methanol by LC-MS grade water. The samples were subsequently transferred to a fresh Eppendorf tube and then were centrifuged at 15000 g, 4°C for 20 min. Finally, the supernatant was injected into the LC-MS/MS system analysis (Want et al., 2013). UHPLC-MS/MS analyses were performed using a Vanquish UHPLC system (Thermo Fisher, Germany) coupled with an Orbitrap Q Exactive™ HF mass spectrometer (Thermo Fisher, Germany) in Novogene Co., Ltd. (Beijing, China). Samples were injected onto a Hypesil Goldcolumn (100×2.1 mm, 1.9 μm) using a 17-min linear gradient at a flow rate of 0.2 mL/min. The eluents for the positive polarity mode were eluent A (0.1% FA in Water) and eluent B (Methanol). The eluents for the negative polarity mode were eluent A (5 mM ammonium acetate, pH 9.0) and eluent B (Methanol). The solvent gradient was set as follows: 2% B, 1.5 min; 2-85% B, 3 min; 85-100% B, 10 min; 100-2% B, 10.1 min; 2% B, 12 min. Q Exactive™ HF mass spectrometer was operated in positive/negative polarity mode with spray voltage of 3.5 kV, capillary temperature of 320°C, sheath gas flow rate of 35 psi and aux gas flow rate of 10 L/min, S-lens RF level of 60, Aux gas heater temperature of 350°C.

2.6 Data processing and metabolite identification

The raw data files generated by UHPLC-MS/MS were processed using the Compound Discoverer 3.1 (CD3.1, Thermo Fisher) to perform peak alignment, peak picking, and quantitation for each metabolite. The main parameters were set as follows: retention time tolerance, 0.2 minutes; actual mass tolerance, 5ppm; signal intensity tolerance, 30%; signal/noise ratio, 3; and minimum intensity. After that, peak intensities were normalized to the total spectral intensity. The normalized data was used to predict the molecular formula based on additive ions, molecular ion peaks and fragment ions. And then peaks were matched with the mzCloud (https://www.mzcloud.org/), mzVault and Mass List database to obtain the accurate qualitative and relative quantitative results. Statistical analyses were performed using the statistical software R (R version R-3.4.3), Python (Python 2.7.6 version) and CentOS (CentOS release 6.6), When data were not normally distributed, it was standardized according to the formula: sample raw quantitation value/(The sum of sample metabolite quantitation value/The sum of QC1 sample metabolite quantitation value) to obtain relative peak areas. And compounds whose CVs of relative peak areas in QC samples were greater than 30% were removed, and finally the identification and relative quantification results of metabolites were obtained. The screening criteria for different comparative combinations of differential metabolites were VIP > 1.0, FC > 1.2 or FC < 0.833, p-value < 0.05.

2.7 Samples of transcriptome preparation, library construction and sequencing

Samples were selected as UT, MOCK24h, STS24h, ETH24h, S_E24h, and three biological replicates were set for each AZ sample. Total RNA was extracted using an RNA extraction kit (Tiangen, Beijing, Biotechnology, China) according to the manufacturer's instructions. RNA integrity was assessed using the RNA Nano 6000 Assay Kit of the Bioanalyzer 2100 system (Agilent Technologies, CA, USA). Total RNA was used as input material for the sample preparations of RNA. Firstly, mRNA was purified from total RNA using poly-T oligo-attached magnetic beads. Fragmentation was carried out using divalent cations under elevated temperature in first strand synthesis reaction buffer (5X). First strand cDNA was synthesized using random hexamer primer and M-MuLV Reverse Transcriptase, then RNaseH was used to degrade the RNA. Second strand cDNA synthesis was subsequently performed using DNA Polymerase I and dNTP. Remaining overhangs were converted into blunt ends *via* exonuclease/polymerase activities. After adenylation of 3' ends of DNA fragments, adaptor with hairpin loop structure was ligated to prepare for hybridization. In order to select cDNA fragments of preferentially 370~420 bp in length, the library fragments were purified with AMPure XP system (Beckman Coulter, Beverly, USA). Then PCR was performed with Phusion High-Fidelity DNA polymerase, Universal PCR primers and Index (X) primer. At last, PCR products were purified by AMPure XP system and library quality was assessed on the Agilent Bioanalyzer 2100 system. The clustering of the index-coded samples was performed on a cBot Cluster Generation System using TruSeq PE Cluster Kit v3-cBot-HS (Illumia) according to the manufacturer's instructions. After cluster generation, the library preparations were sequenced on an Illumina Novaseq platform and 150 bp paired-end reads were generated.

2.8 Analysis of transcriptome data

Index of the reference genome was built using Hisat2 v2.0.5. And the paired-end clean reads were aligned to the reference

genome (https://www.ncbi.nlm.nih.gov/genome/11715) using Hisat2 v2.0.5. Feature Count v1.5.0-p3 was used to count the reads numbers mapped to each gene. And then FPKM of each gene was calculated based on the length of the gene and reads count mapped to this gene. FPKM, expected number of Fragments Per Kilobase of transcript sequence per Millions base pairs sequenced. Differential expression analysis of two comparative combinations was performed using the DESeq2 R package (1.20.0). The resulting P-values were adjusted using the Benjamini and Hochberg's approach for controlling the false discovery rate. We used p-value < 0.05 and |log2foldchange| > 0 as thresholds for differential gene screening for different comparative combinations. We used Cluster Profiler R package (3.4.4) to test the statistical enrichment of differential expression genes in KEGG pathways.

2.9 qRT-PCR validation

The samples of AZ (MOCK, STS, ETH, S_E at UT, 24h and 48h) were collected for qRT-PCR validation in rose. Reverse transcription of cDNA was performed using Evo M-MLV RT Mix Kit with gDNA Clean for qPCR (Accurate Biology, Hunan, China). QRT- PCR was performed using SYBR Green Pro HS qPCR kit (Accurate Biology, Hunan, China) and a 7500 Fast Real-Time PCR System (Applied Biosystems, Foster City, USA), using *RhUBI2* as the internal reference gene (Liang et al., 2020). The primers were designed using the NCBI online tool (https://www.ncbi.nlm.nih.gov/). The sequences of primers used in this study were shown in Supplementary Table 1. Three biological replicates were guaranteed for each treatment, and the data was processed using $2^{-\triangle\triangle CT\wedge 2}$ (Livak and Schmittgen, 2001).

2.10 Statistical analysis and image processing

ANOVA analysis of variance was performed using SPSS (version 24.0, Chicago, IL, United States), and graphs were plotted using Origin 2018 (Microcal Software, Northampton, MA). Image processing software was performed using Photoshop CC (Adobe, San Jose, California, United States).

3 Results

3.1 Effects of STS treatments on petal abscission time and physiological indicators in rose

To evaluate the potential role of STS on the process of petal abscission in rose, the phenotype, timing of petal abscission and physiological indicators were recorded and analysed. The timing of petal abscission in each treatment was ranked (from earliest to latest) as ETH > MOCK > STS + ETH > STS (Figure 1A). The petals of ETH-treated flowers started to abscise at 2.4 ± 0.1 d and abscised completely at 3.7 ± 0.1 d. Petal abscission in the MOCK began at 5.0 ± 0.14 d and was completed at 6.6 ± 0.1 d. In the combined STS+ETH treatment, the petals started to abscise at 7.8 ± 0.3 d and abscission was completed at 9.0 ± 0.2 d. In contrast, the petals of STS-treated flowers did not abscise, and were wilted or withered at the end of the experimental period (Figure 1B). Thus, ETH promoted petal abscission, whereas STS significantly inhibited the phenomenon.

The initial activation of the abscission process is usually directly associated with primary cell wall degradation, in which pectinases and cellulases are crucial promotive factors (Lashbrook and Cai, 2008). Therefore, we examined the changes in pectinase and cellulase activities in the AZ of rose petals. The comparative pectinase activity in the AZ for each treatment was ranked as ETH > STS+ETH > MOCK > STS after 8 h of treatment. This ranking remained unchanged at 48 h after the vase solution was changed 8-HQ. The cellulases activity in the treatments showed a similar pattern (Figures 1C, D). According to these results, primary cell wall degradation was associated with petal abscission and STS inhibited degradation of the cell wall.

3.2 Metabolomic analysis of rose AZ under STS treatments

To explore the changes in metabolite accumulation in the STS-treated rose, we performed UHPLC-MS/MS analysis of the AZ. The reproducibility of the metabolite assays was assessed by means of an overlap analysis using total ion chromatograms (TIC). As shown in Supplementary Figure 2, the peak shapes of Quality Control (QC) samples in both positive and negative ion modes were reproducible; i.e., the response intensities and retention times of the peaks were consistent. These results indicated that variation caused by instrumental errors was negligible and the mass spectrometry signals tended to be stable throughout the experiment, thus supporting the reproducibility and reliability of the metabolomics data. A total of 1120 metabolites were detected among all samples (Supplementary Table 2). Principal component analysis (PCA) of all metabolites detected revealed a degree of variation between samples, but little variation between samples within groups (Supplementary Figure 3A). The 1120 metabolites were compared against the KEGG Orthology (KO) database, which yielded 351 metabolites with annotations (Supplementary Table 3). These metabolites were classified into three major categories among level 1 KO pathways, namely Environmental information processing, Genetic information processing, and Metabolism. Fourteen categories were annotated among level 2 KO pathways, of which the categories annotated with a high number of

10.3389/fpls.2022.1045270

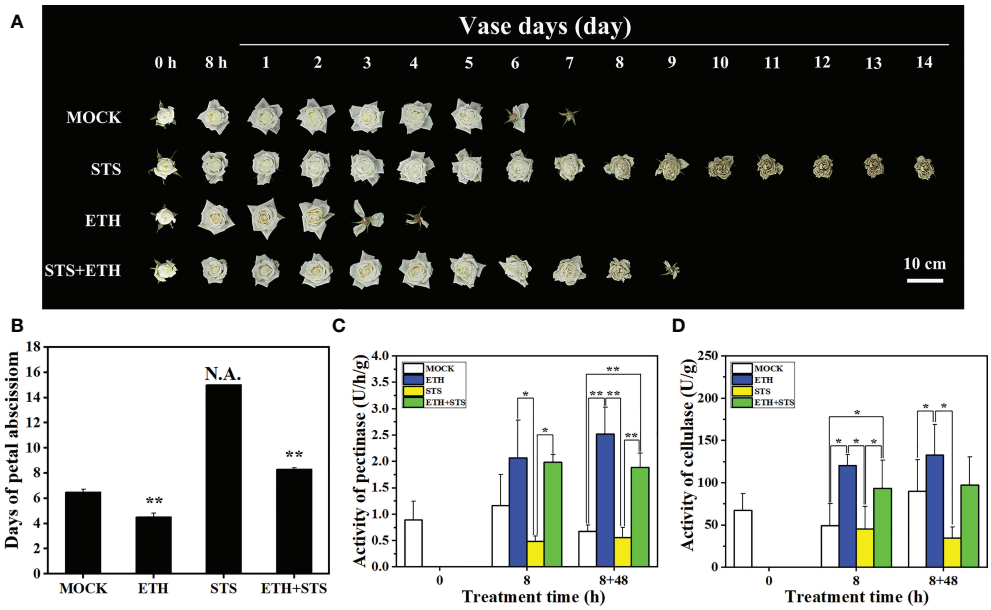

FIGURE 1
Analysis of phenotype, abscission time and enzyme activity in petal abscission process of rose. **(A, B)** Abscission phenotype and abscission time of rose petals under different treatments. 0 h, untreatment; 8 h, 8 h in treatment of different solutions; 1 to 14 days, days after treatment; N.A., no abscission. Scale bars 10 cm. **(C, D)** Changes of pectinase and cellulase activities in rose AZ. Statistical significance between different treatment and control groups was tested using Duncan's test (*p < 0.05; **p < 0.01), biological replicates n=3.

metabolites were Global and overview maps (127 species), Amino acid metabolism (50 species), Biosynthesis of other secondary metabolites (46 species), Carbohydrate metabolism (29 species), and Metabolism of cofactors and vitamins (25 species). The remaining metabolites were annotated to Membrane transport, Signal transduction, Folding, sorting and degradation, Translation, Energy metabolism, Lipid metabolism, Metabolism of terpenoids and polyketides, and Nucleotide metabolism (Supplementary Table 4).

3.3 Identification of differentially accumulated metabolites

3.3.1 Screening and acquisition of DAMs

To systematically identify metabolites that were differentially accumulated in the AZ of petals in STS-treated flowers, differentially accumulated metabolites (DAMs) of different comparative combinations were screened based on three criteria: variable importance in the projection (VIP) indicates the contribution of metabolites to the grouping; fold change (FC) is the ratio of the mean quantitative value for all biological replicates of each metabolite in the comparison group; and the *p*-value was calculated with Student's *t*-test and indicates the degree of significance of the difference. The thresholds VIP > 1.0, FC > 1.2 or FC < 0.833, and *p*-value < 0.05 were set for screening DAMs. We identified 67 up-regulated and 40 down-regulated DAMs in the group STS24h *vs.* MOCK24h, 143 up-regulated and 72 down-regulated DAMs in the group ETH24h vs. MOCK24h, and 161 up-regulated and 92 down-regulated DAMs in the group ETH24h vs. STS24h (Figures 2A-C). In addition, 63 and 64 down-regulated DAMs, and 98 and 70 up-regulated DAMs were identified in the groups S_E24 h *vs.* MOCK24h and MOCK24h vs. Untreated, respectively (Supplementary Table 5). The DAMs in the different comparative groups were then annotated separately based on the KEGG pathway database (Supplementary Table 6). For the groups STS24h vs. MOCK24h, ETH24h vs. MOCK24h, and ETH24h vs. STS24h, five metabolic pathways (Global and overview maps, Amino acid metabolism, Biosynthesis of other secondary metabolites, Carbohydrate metabolism, and Metabolism of cofactors and vitamins) included significantly more DAMs than the other categories (Figure 2D). Similar results were observed for the groups S_E24h vs. MOCK24h and MOCK24h vs. Untreated (Supplementary Table 6). Therefore, we inferred that the metabolites that changed in accumulation during petal abscission in rose mainly originated from these five

10.3389/fpls.2022.1045270

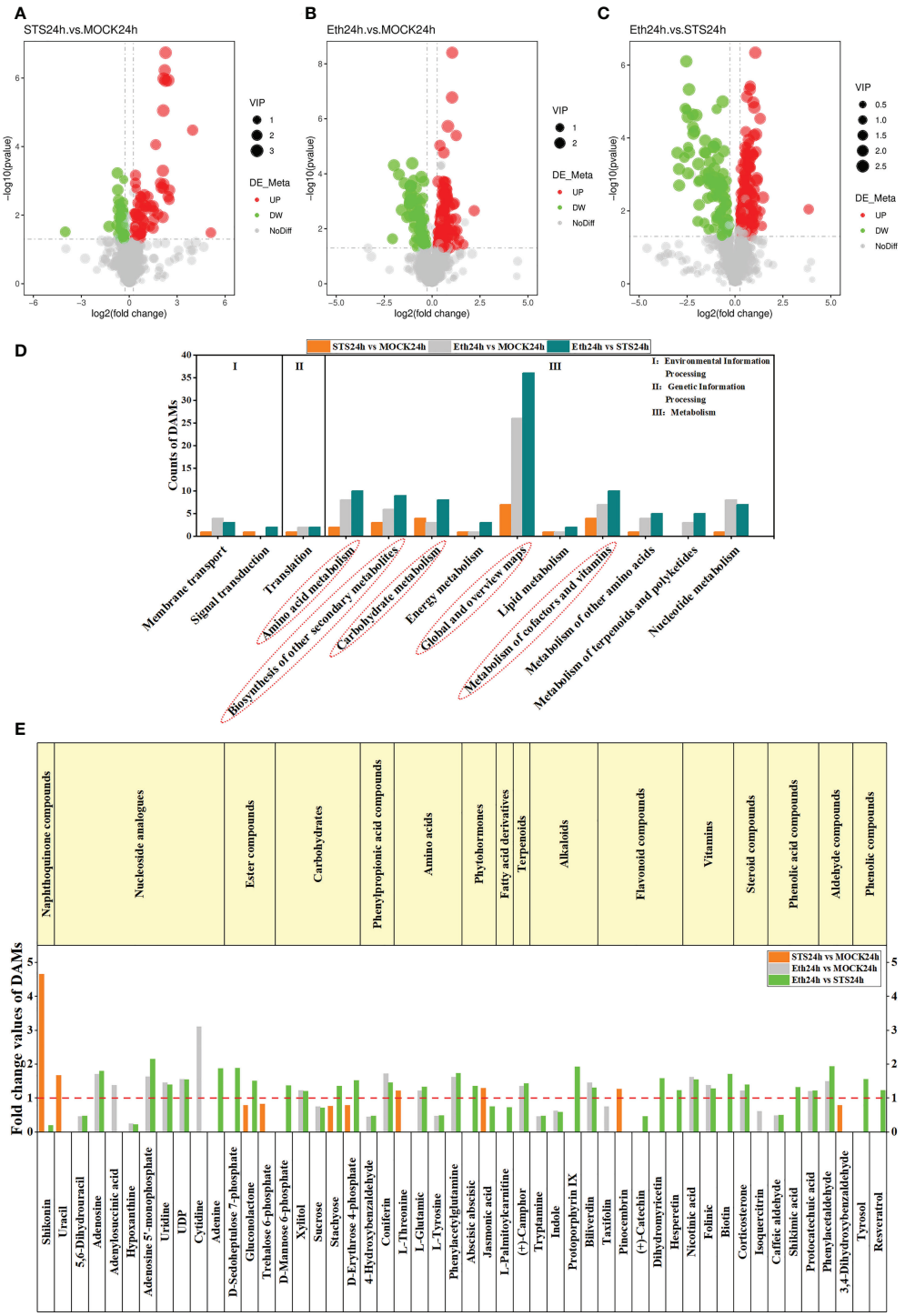

FIGURE 2
Analysis of DAMs in different comparative combinations. **(A–C)** Volcano plots of DAMs in groups STS24h vs. MOCK24h, ETH24h vs. MOCK24h and ETH24h vs. STS24h. Red represented up-regulated, green represented down-regulated. **(D)** KEGG enrichment analysis of DAMs in different comparative combinations. The content of the red dashed box was the five KEGG categories with a high number of DAMs. **(E)** Classification of the 50 DAMs and the FC values in groups STS24h vs. MOCK24h, ETH24h vs. MOCK24h and ETH24h vs. STS24h. The red dashed line was located at y-axis=1. The upper part of the dashed line indicated upward adjustment of metabolite content and the lower part indicated downward adjustment. The content of the yellow boxes indicated the different classes of metabolites.

metabolic pathways, and that most metabolites affected by STS were also concentrated among these pathways.

3.3.2 Classification of 50 DAMs from the five typical metabolic pathways

Next, we screened and classified the DAMs annotated with the aforementioned five metabolic pathways from the groups STS24h vs. MOCK24h, ETH24h vs. MOCK24h, and ETH24h vs. STS24h. Fifty metabolites were screened into 16 classes of compounds, namely, naphthoquinones (1), nucleotides (6), esters (3), carbohydrates (5), phenylpropanoids (2), amino acids (4), phytohormones (2), fatty acid derivatives (1), terpenoids (1), alkaloids (4), flavonoids (5), vitamins (3), steroids (2), phenolic acids (3), aldehydes (2), and phenolic compounds (2) (Figure 2E). The FC values of the 50 metabolites for the three groups are provided in Supplementary Table 7. Among these compounds, we observed that contents of shikonin (naphthoquinones) and jasmonic acid (phytohormones) were significantly higher in STS24h samples than in MOCK24h and ETH24h samples, and that gluconolactone (esters), stachyose (carbohydrates), and D-erythrose 4-phosphate (carbohydrates) were significantly lower in the STS24h samples than in the MOCK24h and ETH24h samples. No significant change was detected among these five metabolites in the group ETH24h vs. MOCK24h, indicating that these five metabolites changed mainly in response to STS treatment. In addition, in ETH24h samples, the contents of hypoxanthine (nucleosides), 5,6-dihydrouracil (nucleosides), uridine (nucleosides), UDP (nucleosides), sucrose (carbohydrates), 4-hydroxybenzaldehyde (phenylpropanoids), L-tyrosine (amino acids), tryptamine (alkaloids), indole (alkaloids), and caffeic aldehyde (phenolic acids) were substantially lower than those in the MOCK24h and STS24h samples; furthermore, accumulation of adenosine (nucleosides), adenosine 5′-monophosphate (nucleosides), xylitol (carbohydrates), coniferin (phenylpropanoids), L-glutamic acid (amino acids), phenylacetylglutamine (amino acids), (+)-camphor (terpenoids), biliverdin (alkaloids), nicotinic acid (vitamins), folinic acid (vitamin), corticosterone (steroidal compound), protocatechuic acid (phenolic acid), and phenylacetaldehyde (aldehyde) was much higher in the ETH24h samples than in the MOCK24h and STS24h samples. No differences were detected in the contents of the aforementioned 23 metabolites in the group STS24h vs. MOCK24h. Therefore, it was speculated that the effect of STS on petal abscission in rose may be less dependent on the production of these metabolites. In contrast, the content of the other 22 metabolites varied to different degrees in different comparisons between samples. Most of the nucleosides, amino acids, and alkaloids were affected by ethylene, whereas STS had almost no effect on these classes of metabolites (Figure 2E). In conclusion, these 50 metabolites may have different roles in the STS-mediated delay of petal abscission in rose.

3.3.3 KEGG enrichment analysis of 50 DAMs

The analysis of DAMs in the different comparative groups indicated that Global and overview maps, Amino acid metabolism, Biosynthesis of other secondary metabolites, Carbohydrate metabolism, and Metabolism of cofactors and vitamins comprised significantly more DAMs than the other categories. Therefore, the DAMs classified to these five categories in the different comparative groups were annotated separately with KEGG pathways in accordance with the significance criterion of p-value < 0.05. No significantly enriched KEGG pathways were detected in the group MOCK24h vs. Untreated. The Pentose phosphate pathway and Carbon metabolism pathway were significantly enriched in the group STS24h vs. MOCK24h. Here, the Pentose phosphate pathway is the part of the Carbon metabolism. Therefore the Pentose phosphate pathway was significantly enriched, so was Carbon metabolism pathway. Pyrimidine metabolism pathway and Purine metabolism pathway were significantly enriched in the group ETH24h vs. MOCK24h. Only Arginine and proline metabolism were significantly enriched in the group S_E24h vs. MOCK24h, whereas in the group ETH24h vs. STS24h Phenylalanine, tyrosine and tryptophan biosynthesis, Pentose phosphate pathway, and Zeatin biosynthesis were significantly enriched (Figures 5D–F and Supplementary Figure 4C). Among the enriched pathways, the Pentose phosphate pathway was enriched only in the groups STS24h vs. MOCK24h, S_E24h vs. MOCK24h, and ETH24h vs. STS24h. Only the top 20 pathways ranked by p-value are shown in Figures 5D-F and Supplementary Figure 4C. Given that the group MOCK24h *vs.* Untreated contained no significantly enriched KEGG pathways, no KEGG bubble plot was generated. The specific KEGG enrichment results for each comparison group were shown in Supplementary Table 8.

3.4 Transcriptome analysis of rose AZ under STS treatment

3.4.1 Quality assessment of transcriptome data and counting of DEGs

The phenotypic observations, determination of pectinases and cellulases activities in the petal AZ of rose, and metabolome analysis revealed distinct differences in the STS treatment compared with the MOCK and ETH treatment groups. Therefore, to identify the genes involved in the regulation of rose petal abscission that were affected by STS, transcriptome sequencing of five groups of samples (Untreated, MOCK24h, STS24h, ETH24h, and S_E24h) was performed. In total, six G clean reads were obtained with Q20 > 97%, Q30 > 92%, and the GC content ranged between 45% and 47%. Between 85% and 88% of the clean reads were mapped to the reference genome using HISAT2 software. The data quality of each sample met the

quality control criteria (Supplementary Table 9). On this basis, the transcriptome sequencing data were analyzed further. Differentially expressed genes (DEGs) in the different comparative groups were screened using the criteria p-value ≤ 0.05 and |log2 FC| ≥ 0. A total of 779 DEGs were up-regulated and 464 DEGs were down-regulated in the group STS24h vs. MOCK24h, 5353 DEGs were up-regulated and 4994 DEGs were down-regulated in the group ETH24h vs. MOCK24h, and 5089 DEGs were up-regulated and 4897 DEGs were down-regulated in the group ETH24h vs. STS24h (Figures 3A-C and Supplementary Table 10). In addition, 2587 and 1242 up-regulated DEGs and 3411 and 969 down-regulated DEGs were identified for the groups MOCK24h *vs.* Untreated and S_E24h *vs.* MOCK24h, respectively (Supplementary Figures 5A, B).

3.4.2 Transcription factors of rose AZ affected by STS

Among the screened DEGs, the expression of many transcription factors was indicated to have changed during the petal abscission process. Therefore, we performed transcription factor (TF) categorization analysis on the screened DEGs. The DEGs in the group MOCK24h vs. Untreated included 55 TF

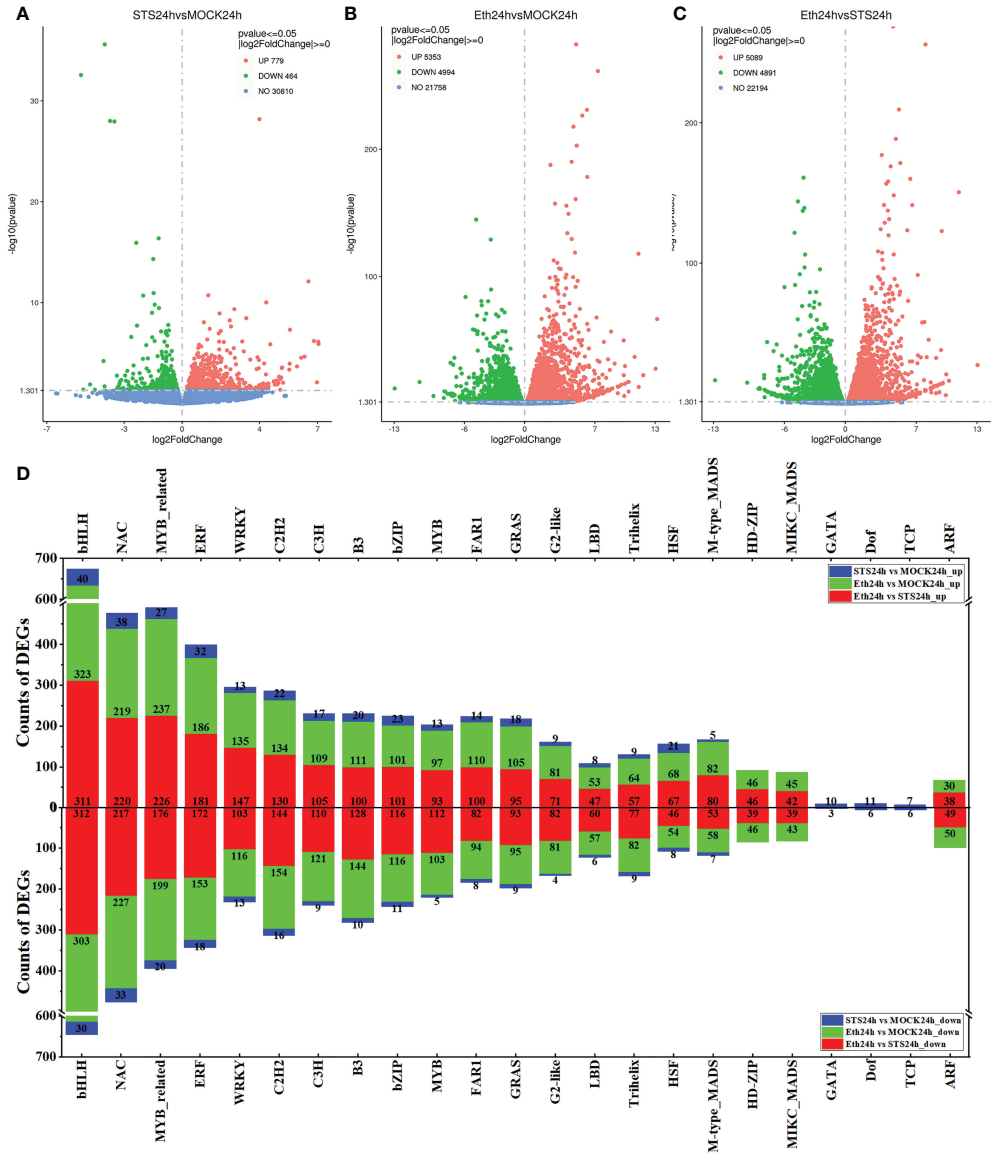

FIGURE 3
Volcano plots of DEGs and classification statistics of transcription factors. **(A–C)** Volcano plots. Red represented up-regulated, green represented down-regulated. **(D)** Classification statistics in the top 20 families of transcription factor.

families, those of the group STS24h vs. MOCK24h contained 50 TF families, the group ETH24h vs. MOCK24h included 57 TF families, the group S_E24h vs. MOCK24h DEGs encompassed 53 TF families, and DEGs from 56 TF families were detected in the group ETH24h *vs.* STS24h (Supplementary Table 11). To explore the TF families strongly influenced by STS during petal abscission, we compared the 20 top-ranked TF families by number of DEGs in each comparative group. In STS24h vs. MOCK24h, Top 20 TF families comprised bHLH (40 up-regulated, 30 down-regulated), NAC (38 up-regulated, 33 down-regulated), MYB_related (27 up-regulated, 20 down-regulated), ERF (32 up-regulated, 18 down-regulated), WRKY (13 up-regulated, 13 down-regulated), C2H2 (22 up-regulated, 16 down-regulated), C3H3 (17 up-regulated, nine down-regulated), B3 (20 up-regulated, 10 down-regulated), bZIP (23 up-regulated, 11 down-regulated), MYB (13 up-regulated, five down-regulated), FAR1 (14 up-regulated, eight down-regulated), GRAS (18 up-regulated, nine down-regulated), G2-like (nine up-regulated, four down-regulated), LBD (eight up-regulated, six down-regulated), Trihelix (nine up-regulated, nine down-regulated), HSF (21 up-regulated, eight down-regulated), M-type_MADS (five up-regulated, seven down-regulated), GATA (10 up-regulated, three down-regulated), Dof (11 up-regulated, six down-regulated), and TCP (seven up-regulated, six down-regulated) (Figure 3D). The number of DEGs associated with TFs in group Eth24h *vs.* STS24h was quite large. For example, the number of bHLH transcription factors reached 623, NAC transcription factors reached 437, MYB_related transcription factors reached 402, ERF transcription factors reached 353, C2H2 transcription factors reached 274 and WRKY-related transcription factors reached 250, while the number of these transcription family-related DEGs was still relatively large in group Eth24h vs. MOCK24h. Interestingly, we found significantly fewer bHLH (130), NAC (109), MYB_related (89), ERF (74), C2H2 (64) and WRKY (41) related DEGs in group S_E24h vs. MOCK24h than in group Eth24h vs. MOCK24h.This showed that when ethylene and STS were applied at the same time, STS inhibited the effect of ethylene. In summary, the effect of STS on the process of petal abscission in rose involved changes in the expression of a large number of transcription factors and STS could inhibit the regulation of a large number of transcription factors by ethylene.

3.4.3 DEGs related to phytohormone biosynthesis and signal transduction in STS-treated rose AZ

Phytohormone are vital regulators of plant growth and development and play an important role in organ abscission (Patharkar and Walker, 2018). To investigate whether the regulation of petal abscission by STS involved the roles of phytohormone, we analyzed the screened DEGs associated with auxin, ethylene, jasmonic acid, abscisic acid (ABA), salicylic acid, gibberellin, cytokinin, and brassinosteroids. The results showed that DEGs associated with the eight types of phytohormones were detected in almost all treatment (Figures 4A-D and Supplementary Figure 5C). Significantly more ethylene- and auxin-related DEGs were detected in the groups STS24h vs. MOCK24h, ETH24h vs. MOCK24h, and ETH24h vs. STS24h than genes associated with other phytohormones. In the group STS24h vs. MOCK24h, four auxin-related DEGs (2 up-regulated and 2 down-regulated) and 14 ethylene-related DEGs (4 up-regulated and 10 down-regulated) were detected. In the group ETH24h vs. MOCK24h, 87 auxin-related DEGs (30 up-regulated and 57 down-regulated) and 63 ethylene-related DEGs (36 up-regulated and 27 down-regulated) were identified. Among the DEGs for the group ETH24h vs. STS24h, 90 were auxin-related (30 up-regulated and 60 down-regulated) and 61 were ethylene-related (36 up-regulated and 25 down-regulated). These results indicated that the abscission process involved changes in multiple phytohormone-related genes, but the effects of STS and ethylene on phytohormones during petal abscission in rose were mainly focused on ethylene- and auxin-related genes.

3.4.4 Analysis of other DEGs possibly involved rose petal abscission in STS treatment

Organ abscission is a complex physiological process involving changes in the expression of many genes with diverse functions. Therefore, we classified the DEGs into gene classes that may be involved in the petal abscission process (Singh et al., 2020). The genes were classified into 21 categories, comprising defense-related genes (thaumatin-like protein, endochitinase, cytochrome P450, glutathione *S*-transferase, and heat shock protein), disease-resistance-related genes (ABC transporter, protein detoxification, and disease resistance protein), cell wall-related genes (xyloglucan endotransglucosylase/hydrolase, pectinesterase, pectate lyase, polygalacturonase, and cellulase), photosynthesis-related genes (peroxidase and chlorophyll), and other categories of genes (GDSL esterase/lipase, amino acid, sucrose, heavy metal, senescence, and NRT1/PTR family). The numbers of DEGs in the cytochrome P450, ABC transporter, and disease resistance protein-related categories were significantly greater in the five comparative groups (STS24h vs. MOCK24h, Eth24h vs. STS24h, Eth24h vs. MOCK24h, S_E24h vs. MOCK24h and MOCK24h vs. Untreated) than for the other gene categories (Figures 4E-H and Supplementary Figure 5D). Approximately two-thirds of the disease resistance protein-related DEGs were down-regulated in the groups ETH24h vs. MOCK24h and ETH24h vs. STS24h, indicating that ethylene had a greater inhibitory effect on the expression of this class of genes. The number of photosynthesis-related DEGs were 37 in the group MOCK24h vs. Untreated and 55 in the group ETH24h vs. STS24h, whereas the number of photosynthesis-related DEGs was lower in the group STS24h vs. MOCK24h. Unlike other comparative groups, only a small number of amino acid-related DEGs were detected in STS24h and S_E24h samples compared

10.3389/fpls.2022.1045270

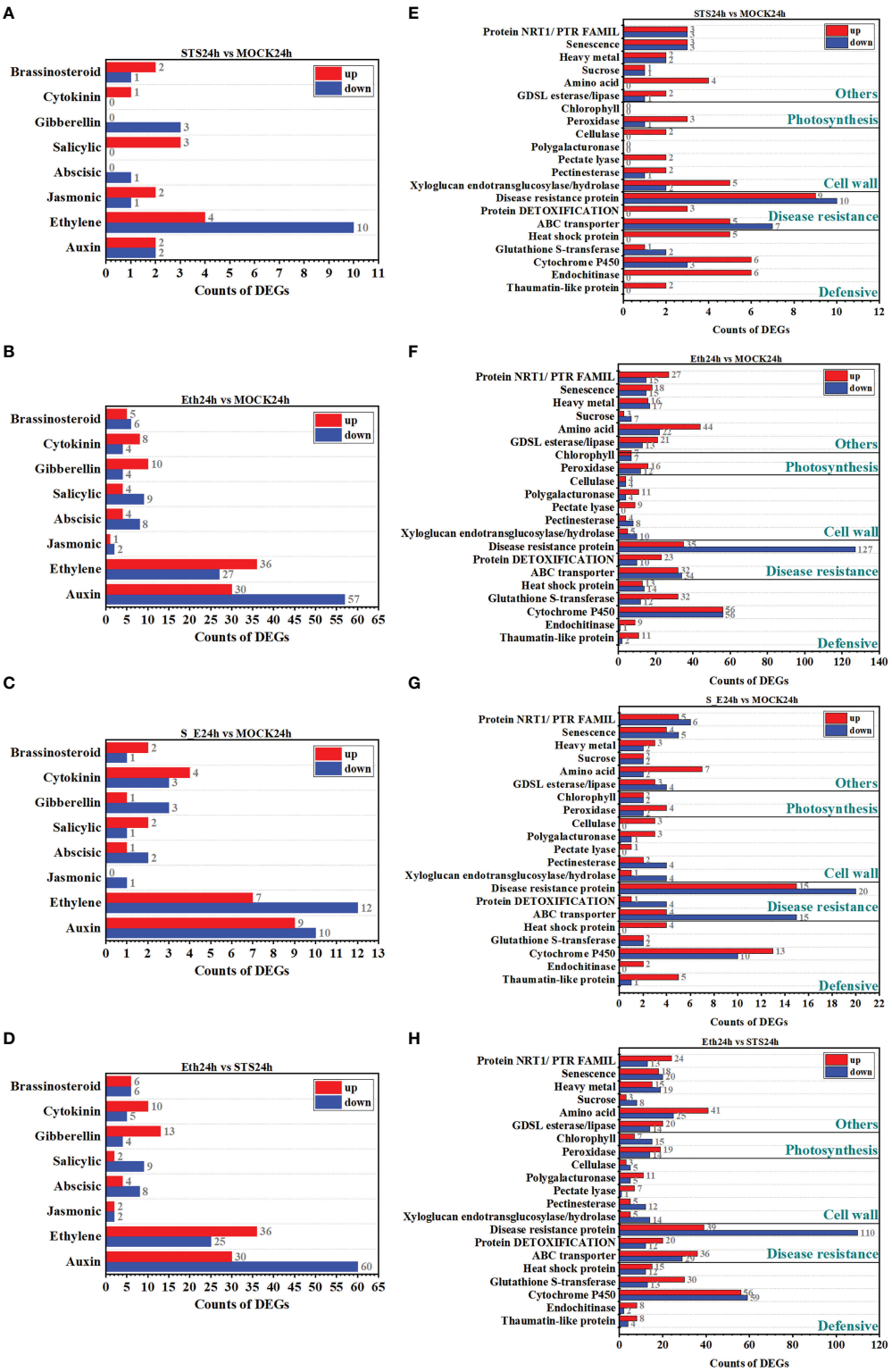

FIGURE 4
Classification of DEGs. **(A–D)** Classification of DEGs related to phytohormone. **(E–H)** Classification of different functionally relevant DEGs.

with MOCK24h, respectively. However, a greater number of amino acid-related DEGs were observed in the groups ETH24h vs. MOCK24h and ETH24h vs. STS24h. Therefore, ethylene might strongly affect the expression of amino acid-related genes during abscission, which was distinct from the effect of STS. In this study, cell wall-associated DEGs were detected in all comparative combinations. Combined with the estimations of pectinases and cellulases activities, this result suggested a strong link existed between cell wall degradation and STS-affected abscission in rose.

3.4.5 KEGG enrichment analysis of DEGs

Based on the screening results of DEGs, we conducted a KEGG pathway enrichment analysis in the five comparative groups. The 20 highest-ranked pathways by *p*-value were identified (Figures 5A-C and Supplementary Figures 4A, B). The specific KEGG enrichment results were shown in Supplementary Table 12. The pathways significantly enriched in group STS24h vs. MOCK24h were MAPK signaling pathway-plant, Plant hormone signal transduction, Phenylpropanoid biosynthesis, Nicotinate and nicotinamide metabolism, and Cysteine and methionine metabolism. Among them, MAPK signaling pathway-plant and Plant hormone signal transduction all belonged to the signal transduction class of KEGG pathways. MAPK signaling pathway-plant was also significantly enriched in the other four comparative groups, and the Plant hormone signal transduction pathway was also significantly enriched in the other three groups except for MOCK24h vs. Untreated. In addition, Phenylpropanoid biosynthesis was significantly enriched in group STS24h vs. MOCK24h; Nicotinate and nicotinamide metabolism was also significantly enriched in group S_E24h vs. MOCK24h; Cysteine and methionine metabolism was also significantly enriched in group Eth24h vs. STS24h. Therefore, in the process of petal abscission in rose, MAPK signaling pathway-plant, Plant hormone signal transduction, and Cysteine and methionine metabolism were associated with both STS and ethylene; while Phenylpropanoid biosynthesis and Nicotinate and nicotinamide metabolism pathways more depended on STS.

There were 15, 18, 9, and 19 significantly enriched KEGG pathways in the groups Eth24h vs. MOCK24h, Eth24h vs. STS24h, S_E24h vs. MOCK24h, and MOCK24h vs. Untreated, separately (Supplementary Table 12). According to the functional classification results of DEGs, a large number of photosynthesis-related DEGs were found in the four groups except for STS24h vs. MOCK24h. In the group MOCK24h vs. Untreated, the energy metabolism classes Photosynthesis, Photosynthesis - antenna proteins, and Carbon fixation in photosynthetic organisms were significantly enriched and all were associated directly with photosynthesis. In the groups ETH24h vs. MOCK24h (Photosynthesis), S_E24h vs. MOCK24h (Photosynthesis, Carbon fixation in photosynthetic organisms, and Nitrogen metabolism), and Eth24h vs. STS24h (Nitrogen metabolism), the specified KEGG pathways were directly associated with photosynthesis. Interestingly, no significant enrichment of photosynthesis-related KEGG pathways was detected in the group STS24h vs. MOCK24h. Based on these results, we inferred that the abscission of rose petals involved alteration of photosynthesis, and that the effect of STS was relatively less dependent on pathways involved in photosynthetic changes, which was consistent with the preceding results in KEGG enrichment analysis of DAMs.

3.5 Verification of DEGs from transcriptome data by qRT-PCR

To verify the reliability of the transcriptome data, we randomly selected 12 DEGs for qRT-PCR analysis based on the results of the transcriptomic and metabolomic analyses. The selected DEGs comprised *Rh112173500* (Gene ID: 112173500, F-box protein), *RhCYSC1* (Gene ID: 112181707, associated with carbon metabolism and amino acid biosynthesis), *RhIAA26* (Gene ID: 112186817, auxin response protein), *RhMYB108* (Gene ID: 112200084, MYB TF), *RhNAC072* (Gene ID: 112164521, NAC TF), *RhJAO2* (Gene ID: 112182989, associated with jasmonate synthesis), *RhETR2* (Gene ID: 112196585, ethylene receptor 2), *RhERF110* (Gene ID: 112187519, ethylene-responsive TF 110), *RhMGL* (Gene ID: 112176950, methionine gamma-lyase), *RhGLIP5* (Gene ID: 112181007, GDSL lipase), *RhMLP423* (Gene ID: 112197262, pathogenesis-associated protein), and *RhPAO4* (Gene ID: 112191920, bHLH TF). The changes in expression of these 12 DEGs in the AZ of rose petals during abscission under the different treatments showed good agreement between the transcriptome sequencing data and the qRT-PCR results (Figure 6 and Supplementary Table 13). All these genes showed different changes in expression trends under the different treatments, indicating that their expression during petal abscission in rose was differentially affected by STS and ethylene.

3.6 Comparison between KEGG enrichment analysis of DEGs and DAMs

3.6.1 Highly consistent result in KEGG enrichment analysis of DEGs and DAMs

To determine whether DEGs and DAMs in the different comparative groups were correlated in KEGG pathways, the KEGG pathways of DEGs were compared with those pathways involved in the five major classes of DAMs (Global and overview maps, Amino acid metabolism, Biosynthesis of other secondary metabolites, Carbohydrate metabolism, and Metabolism of cofactors and vitamins, Supplementary Table 14). All KEGG

10.3389/fpls.2022.1045270

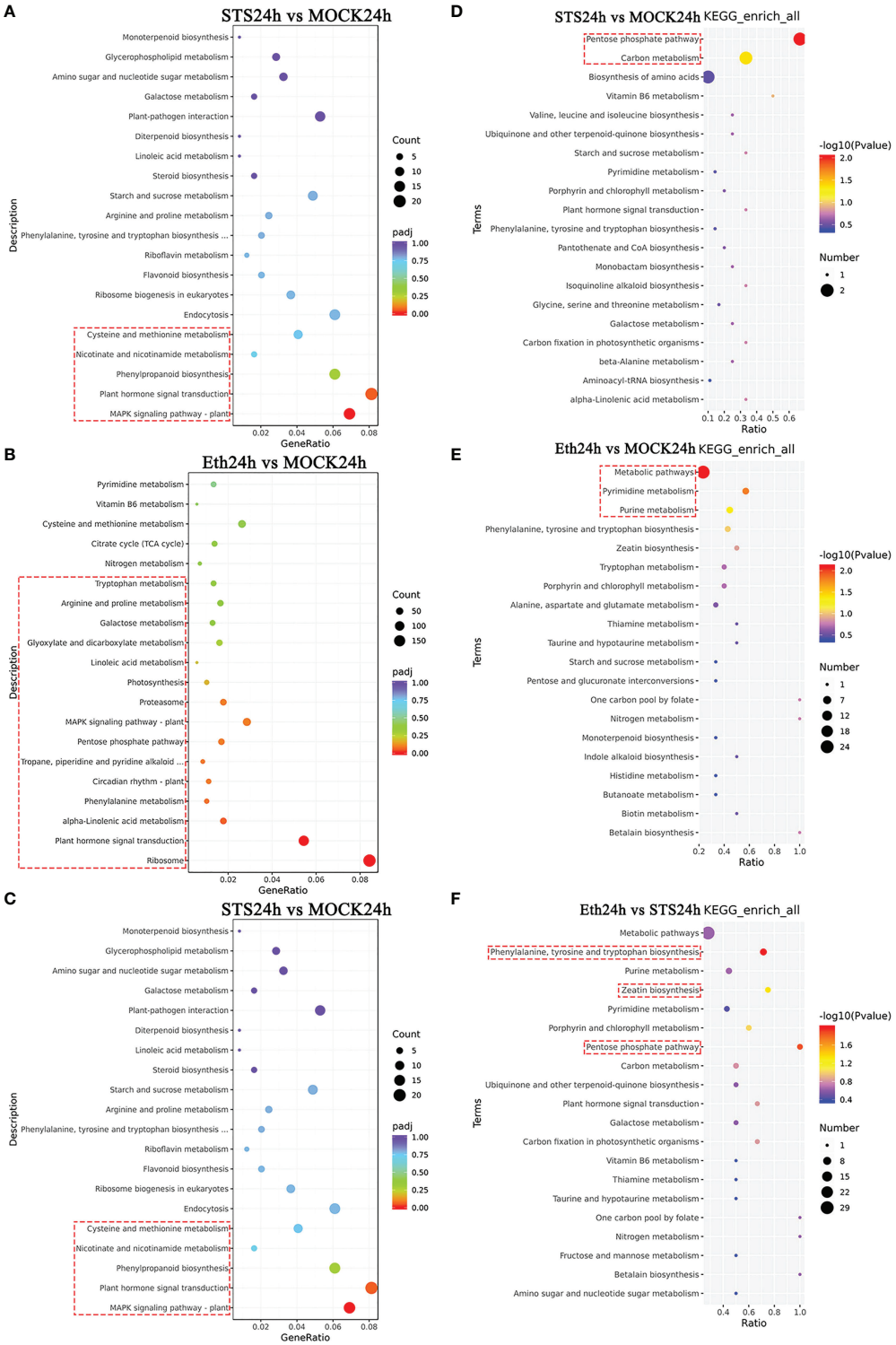

FIGURE 5
KEGG enrichment analysis of DAMs and DEGs. **(A–C)** KEGG enrichment analysis of 50 DAMs. **(D–F)** KEGG enrichment analysis of DEGs. The red dashed boxes indicated the KEGG pathways that were significantly enriched (p-value < 0.05).

pathways of DEGs were consistent with at least half of the KEGG pathways involved in the five major classes of metabolites. These results indicated that the KEGG pathway enrichment among transcriptomic DEGs was similar to the KEGG pathway annotation of metabolomic DAMs.

3.6.2 The typical KEGG pathway affected by STS

In order to verify the typical KEGG pathway affected by STS, we further analysed KEGG pathways of DEGs and DAMs. We found that the Pentose phosphate pathway was significantly enriched in both of DEGs and DAMs KEGG pathways in group Eth24h vs. STS24h, and gluconolactone, D-Sedoheptulose 7-phosphate and D-Erythrose 4-phosphate enriched to this pathway were differentially changed. In the group ETH24h vs. MOCK24h, Phenylalanine metabolism, Arginine and proline metabolism, and Tryptophan metabolism were associated with Amino acid metabolism, and the Pentose phosphate pathway, Glyoxylate and dicarboxylate metabolism, and Galactose metabolism were associated with Carbohydrate metabolism. The number of these significantly enriched KEGG pathways accounted for almost 85% of the KEGG pathways annotated for the five classes of DAMs for this group. Therefore, we hypothesized that amino acid metabolism and carbohydrate metabolism played a crucial role in the effect of ethylene on the abscission process in rose. Interestingly, amino acid biosynthesis involves the generation of D-Erythrose 4-phosphate, an intermediate product of the Pentose phosphate pathway (PPP). Based on this, we observed the variation patterns of DAMs in the Pentose phosphate pathway and amino acid biosynthesis (Figure 7). Among them, gluconolactone, D-Sedoheptulose 7-phosphate, D-Erythrose 4-phosphate, L-Glutamic acid, protocatechuic acid and shikimic acid were negatively related to STS and positively related to ethylene; L-Threonine, Indole and L-Tyrosine were positively related to STS and negatively related to ethylene. In conclusion, STS-delayed abscission of rose petal involved the pathways of the pentose phosphate pathway and amino acid biosynthesis.

3.7 Integral analysis of STS-affected DAMs and directly associated genes

The preceding identification of DAMs revealed that changes in the contents of shikonin (naphthoquinones), jasmonic acid (phytohormones), gluconolactone (esters), stachyose (carbohydrates), and D-erythrose 4-phosphate (carbohydrates) in AZ were strongly influenced by STS, but not significantly influenced by Ethylene (Figure 2D); therefore, we speculated that these five metabolites played an important role in the delayed petal abscission of rose by STS. Among them, shikonin and jasmonic acid were positively correlated with STS, gluconolactone, stachyose and D-Erythrose 4-phosphate were negatively correlated with STS (Figure 8A).

The production and changes in contents of metabolites are determined by the expression of the relevant genes in the corresponding metabolic pathways. The relevant KEGG pathways corresponding to these five metabolites were compared with the

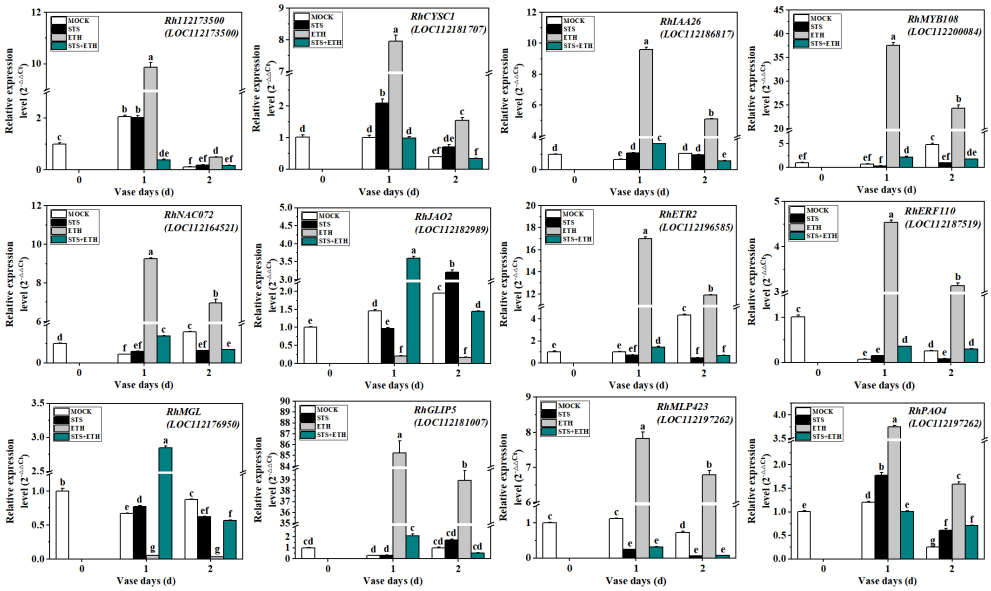

FIGURE 6
Validation of 12 DEGs by qRT-PCR. The experimental method used was $2^{-\triangle\triangle CT}$^2. *RhUBI2* was used as the internal reference gene. Different letters represent significant differences based on one-way ANOVA and Duncan's tests ($p < 0.05$).

10.3389/fpls.2022.1045270

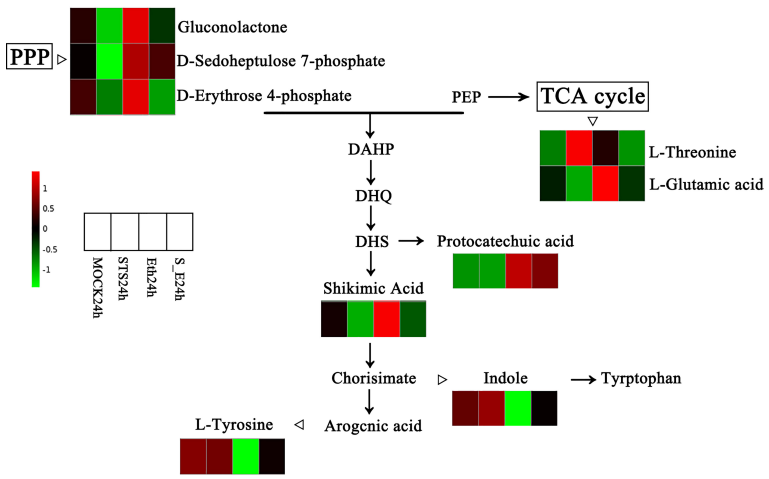

FIGURE 7
Changes of DAMs in the pentose phosphate pathway and amino acid biosynthesis. PPP, Pentose phosphate pathway; PEP, phosphoenolpyruvate; DAHP, 3-deoxy-α-arabinoheptulosonate-7-phosphate; DHQ, 3-dehydroquinate; DHS, 3-dehydroshikimate.

KEGG pathways for transcriptomic DEGs to identify the associated DEGs (Figure 8B and Supplementary Table 15). Shikonin is synthesized in the Ubiquinone and other terpenoid-quinone biosynthesis metabolic pathway, and four DEGs associated with shikonin were detected in this pathway (112168180, tyrosine transaminase 2; 112166004, NAD(P)H dehydrogenase (quinone); 112192149, 4-coumarate-CoA ligase 6; and 1121048780, 4-hydroxyphenylpyruvate dioxygenase). Stachyose is involved in Galactose metabolism and five associated DEGs were detected (112189773, phosphofructokinase 3; 112191944, cottonseed glycosylase 2; 112180851, galactose variable cyclase; 112179506, galactosidase; and 112176825, acidic β-fructosidase). Only one DEG (112185294, glucokinase) associated with gluconolactone in the Pentose phase pathway was detected. Jasmonic acid is associated with alpha-Linolenic acid metabolism and Plant hormone signal transduction; two associated DEGs (112196726, lipoxygenase 6; and 112189737, protein 1 containing the ZIM structural domain of jasmonic acid) were identified. D-Erythrose 4-phosphate is involved in six KEGG pathways. (1) Four DEGs were identified in the Pentose phosphate pathway (112179402, ribulose phosphate pyrophosphate kinase 1; 112171994, fructose diphosphate aldolase 2; 112189773, phosphofructokinase 3; and 112188495, glyceraldehyde-3-phosphate dehydrogenase); (2) Five DEGs were identified in Carbon metabolism (112167524, (*S*)-2-hydroxy-acid oxidase GLO1; 112186654, formate dehydrogenase; 112164572, serine-glyoxylate transaminase; 112186882, formylamine-like enzyme; and 112165571, (*S*)-2-hydroxy-acid oxidase GLO1); (3) Two DEGs (112192678, pyridoxal 5′-phosphate synthase subunit PDX1; and 112190654, inorganic pyrophosphatase 1) were identified in Vitamin B6 metabolism; (4) Four DEGs associated with Carbon fixation in photosynthetic organisms were identified (112196410, ribulose diphosphate carboxylase; 112179079, phosphokinase; 112188936, glyceraldehyde-3-phosphate dehydrogenase GAPA2; and 112189957, ribulose diphosphate carboxylase); (5) Seven DEGs involved in Biosynthesis of amino acids were detected (112181707, L-3-cyanoalanine synthase 2; 112186520, acetyl lactate synthase; 112188038, acetyl ornithine aminotransferase; 112175455, acetyl lactate synthase 2; 112192997, L-threonine aldolase 1; 112180616, glutamine synthetase cytoplasmic isozyme 2; and 112197711, glutamine synthetase leaf isozyme); (6) Five DEGs (112186992, 3-dehydroquinic acid dehydratase/manganate dehydrogenase; 112168180, tyrosine transaminase 2; 112175156, phospho-2-dehydro-3-deoxyheptulose aldolase 1; 112194607, tryptophan synthase; and 112186759, phospho-2-dehydro-3-deoxyheptulose aldolase 2) involved in Phenylalanine, tyrosine, and tryptophan biosynthesis were identified. The expression of these 39 genes showed opposite responses in the STS- and ETH-treated samples. A repressive effect of STS on ethylene was observed in the S_E samples. Significantly, the genes 112192149 (4-coumarate-CoA ligase 6), 112196726 (lipoxygenase 6), 112189737 (jasmonate ZIM domain-containing protein 1), and two glyceraldehyde-3-phosphate dehydrogenase genes (112188495 and 112188936) were key factors associated with the biosynthesis of shikonin, jasmonic acid, and D-erythrose 4-phosphate.

In summary, the changes in contents of the five metabolites were strongly associated with changes in the expression of 39 genes, which including five crucial factors related to the biosynthesis of the three metabolites. These genes may play important roles in STS-mediated inhibition of petal abscission in rose.

10.3389/fpls.2022.1045270

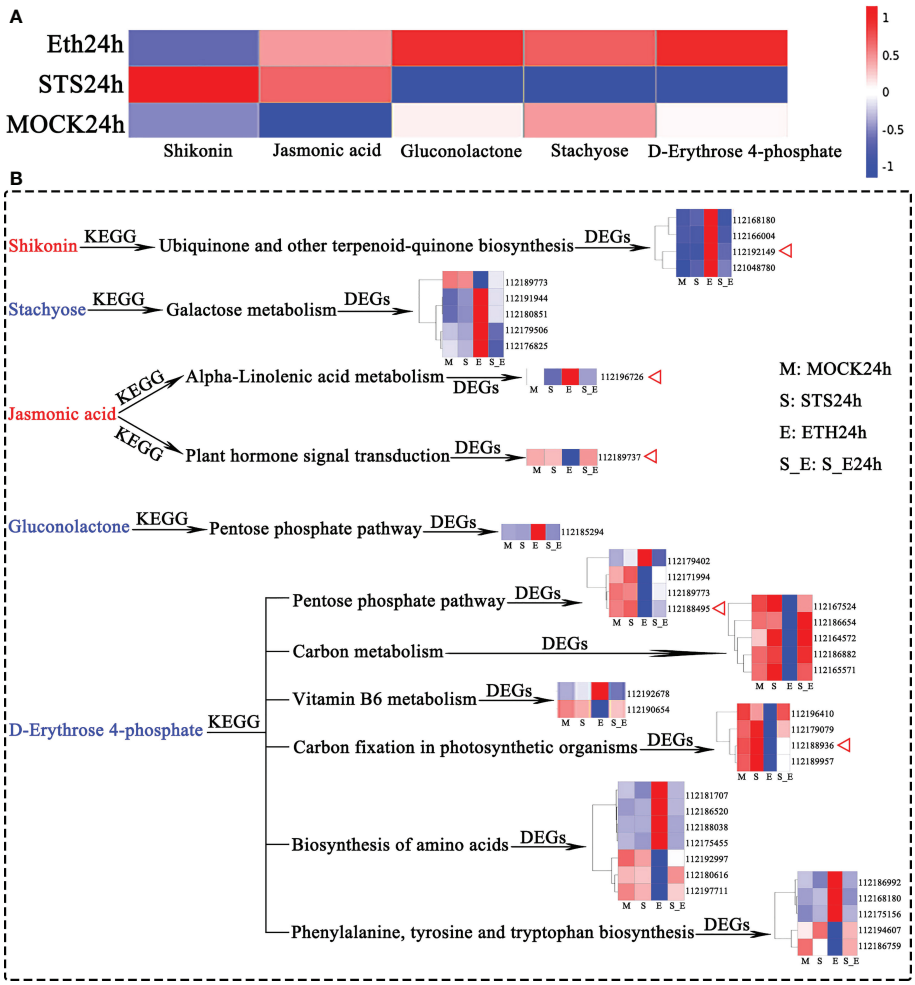

FIGURE 8
Analysis of DAMs and associated DEGs affected by STS. **(A)** Accumulation patterns of five metabolites in different samples. **(B)** DEGs associated with 5 DAMs. Red letter represented up-regulated metabolites affected by STS, blue letter represented down-regulated metabolites affected by STS. DEGs are shown for gene IDs.

4 Discussion

The abscission of tissues or organs is a normal developmental phenomenon in plants. However, premature abscission of flowers and fruits severely affects the economic value of a plant. Previous studies have demonstrated that ethylene promotes petal abscission and affects gene expression in the AZ (Singh et al., 2020). Inhibitors of ethylene synthesis or action are effective in mitigating the negative effects of ethylene on plant organ abscission. Therefore, we delayed petal abscission by treating cut flowers of the ethylene-sensitive rose 'Tineke' with the ethylene inhibitor STS. The changes in the petal abscission process were compared under the MOCK, STS, ETH, and S_E24h treatments. At the physiological level, we determined changes in the activities of the cell wall-related enzymes pectinase and cellulase in the AZ. In addition, metabonomic and transcriptomic analyses were conducted to explore the changes in metabolite accumulation and the underlying molecular mechanisms in the AZ during STS-affected abscission of rose petal.

4.1 Effect of STS on the cell wall in rose AZ

Degradation of the primary cell wall is a major cause of plant organ abscission, and is promoted by pectinase and cellulase activity (Lashbrook and Cai, 2008). In the present study, the

activities of pectinase and cellulase in the AZ under STS treatment were significantly lower than those of the MOCK and ETH-treated groups (Figures 1C, D). These results suggested that STS inhibited degradation of cell walls in the AZ during petal abscission and the effect was in contrast to that of ethylene. Transcriptomic analysis of DEGs revealed that, compared with the MOCK, STS affected the expression of 14 cell wall-related genes, including xyloglucan endotransglucosylase/hydrolase, pectinesterase, pectate lyase, and cellulase. Many cell wall-related genes were also affected by ethylene treatment. For example, the expression of 59 cell wall-related genes was changed in the group ETH24h vs. MOCK24h. In addition, the expression of 68 cell wall-related DEGs was changed in the group ETH24h vs. STS24h, whereas only 19 genes were differentially expressed in the group S_E vs. MOCK24h (Figures 4E-H). Interestingly, accumulation of gluconolactone, a metabolite associated with the cell wall, was affected by STS. Gluconolactone is able to inhibit cellulase activity in the Gramineae (Ma et al., 2022). However, in the current study, the gluconolactone content was significantly reduced under STS treatment compared with that of the MOCK and ETH treatments. These results suggested that STS affected the cell walls in the AZ during petal abscission of rose and, as an ethylene inhibitor, STS effectively alleviated the effect of ethylene on the cell wall.

4.2 Effects of STS on gene expression in rose AZ

Transcription factors play an important role in plant development and stress response (Niu and Fu, 2022). In this study, the DEGs affected by STS in the AZ of rose petals included a large number of TFs. The bHLH, NAC, MYB_related, ERF, WRKY, C2H2, C3H, B3, bZIP, MYB, FAR1, GRAS, G2-like, LBD, Trihelix, HSF, and M-type_MADS transcription factor families were found in the TFs with top 20 number of DEGs in each comparative combination (Figure 3D and Supplementary Table 11). In addition, the number of bHLH transcription factor family-associated DEGs was significantly more than other TFs in each comparison combination, and the number of bHLH family and NAC family DEGs was also the largest in group STS24h vs. MOCK24h. In the previous study, changes in the expression of some TFs (HSF, ARF, MYB, NAC, GRAS, SBP) were detected during rose petal abscission in response to ethylene treatment (Singh et al., 2020). And the petal abscission is characterized by complex transcriptional reprogramming, in which TF family members, such as Zinc finger, WRKY, ERF, and AUX/IAA, were differentially expressed in rose (Gao et al., 2016). The TF families HSF, MYB, NAC, GRAS, WRKY and ERF mentioned in above-mentioned study could be found in the top 20 TF families of all comparative combinations of DEGs. Besides of them, SBP TF family also present in other comparative combinations, although not in the top 20. In addition, a certain number of ARF-related TFs were present in each comparison group, 47 (17 up-regulated, 30 down-regulated) in group MOCK24h vs. Untreated; four (two up-regulated, two down-regulated) in group STS24h vs. MOCK24h; 80 (30 up-regulated, 50 down-regulated) in group ETH24h vs. MOCK24h, 21 (9 up-regulated, 12 down-regulated) in group S_E24h vs. MOCK24h, and 87 (38 up-regulated, 49 down-regulated) in group ETH24h *vs.* STS24h (Supplementary Table 11). Thus, the abscission of rose petals involves changes in a large number of transcription factors, and so was the role of STS in regulating the transcript levels of DEGs during abscission of rose petal.

Transcriptome sequencing results indicated that ethylene and auxin play a central role in the process of petal abscission in rose (Gao et al., 2016). Regarding phytohormone-related genes, STS and ethylene affected the expression of eight types of phytohormone-related genes, but predominantly on auxin- and ethylene-related DEGs (Figures 4A-D, Supplementary Figure 5C), and this further confirmed the previous research results (Gao et al., 2016). There were fewer auxin-related DEGs (19) and ethylene-related DEGs (19) in group S_E24h *vs.* MOCK24h than in group ETH24h vs. MOCK24h (63 auxin-related DEGs and 87 ethylene-related DEGs), suggesting that STS may mediate changes in auxin and ethylene-related gene expression through inhibition of ethylene function (Figures 4B, C). Meanwhile, in the results of metabolite content change analysis, we found that STS affected the content of jasmonic acid, and the expression of jasmonic acid-related genes also shew different expressions.

Among the functional classification of DEGs, the number of disease-resistant protein-associated DEGs was the most significant among all comparative combinations. There were 19 (9 up-regulated, 10 down-regulated), 162 (35 up-regulated, 127 down-regulated), and 35 (15 up-regulated, 20 down-regulated) regulated disease-resistant protein-like DEGs in groups STS24h vs. MOCK24h, ETH24h vs. MOCK24h, and S_E24h vs. MOCK24h, respectively (Figures 4E-G). In summary, the process of petal abscission in rose involved a lot of changes in the expression of genes related to plant disease resistance, and STS may be able to mitigate the negative effects of ethylene on plant disease resistance to some extent during petal abscission.

4.3 Expression analysis of DEGs by qRT-PCR in rose AZ

Combining the present results of transcriptomic and metabolomic analyses revealed that STS had significant effects on TFs, phytohormones, disease resistance, and amino acid

anabolism and so on during abscission. Therefore, we randomly selected 12 DEGs that showed strong changes in expression for further analysis (Figure 6).

First, we screened one F-box family member *Rh112173500* and one NAC-related gene *RhNAC072*. *Rh112173500* expression was down-regulated by STS and up-regulated by ethylene. F-box family proteins play an important role in the abscission of plant organs, but their function in the onset of abscission is unclear. *NAC072* is associated with ABA-regulated senescence mechanisms in Arabidopsis. Members of the NAC TF family have been well studied in rose, but little is known about the mechanisms involved in their regulation of petal abscission (Garapati et al., 2015; Li et al., 2016). In the present study, the expression of *RhNAC072* was inhibited by STS and promoted by ethylene. Second, the expression of *RhCYSC1*, a gene associated with amino acid biosynthesis and encoding a cysteine synthase, was up-regulated under both STS and ethylene treatment. Cysteine synthase is a crucial enzyme for L-cysteine synthesis, but L-cysteine has no effect on root abscission in the water fern *Azolla pinnata* (Yamasaki et al., 2019). The onset of the abscission process is often accompanied by changes in the cell membranes, and disruption of AZ cell membranes in the AZ is associated with lipase (Kucko et al., 2022). *RhGLIP5*, a lipase-related gene, may be associated with gibberellin (GA_3)-induced seed dormancy in *Leymus chinensis* (Li et al., 2021). In the AZ of rose petals, ethylene promoted the expression of *RhGLIP5*, whereas STS inhibited its expression. In addition, *RhIAA16*, a member of the AUX/IAA family in rose petal AZ, is involved in the positive regulation of the petal abscission process through an ethylene-independent pathway or upstream of the ethylene pathway (Gao et al., 2016). Interestingly, expression of a homologous family member, *RhIAA26*, distinguished other auxin-related genes from the antagonistic effect with ethylene, and the expression of *RhIAA26* was up-regulated under ethylene treatment, whereas STS had little effect on its expression. Moreover, the expression of *RhJAO2* (2-oxoglutarate-dependent dioxygenase) and *RhMGL* (methionine gamma-lyase) did not change under ethylene treatment but were up- or down-regulated under STS treatment. In conclusion, the expression of TFs, amino acid synthesis-related genes, cell membrane-related genes, and phytohormone-related genes were affected by STS in the AZ of rose petal. Further analyses were required to elucidate the molecular mechanisms of these genes in abscission process of rose petal.

The gene *RhMLP423* (pathogenesis-related protein) was selected among the 12 randomly screened DEGs. Its expression was down-regulated by STS and up-regulated by ethylene. In tobacco, *NtMLP423* regulates drought tolerance by increasing the ABA content under drought stress, and overexpression of *NtMLP423* reduces membrane damage and reactive oxygen species (ROS) accumulation (Liu et al., 2020). In animal cancer cells, STS promotes the accumulation of ROS (Ota et al., 2021). *RhMYB108* expression was down-regulated by STS treatment and up-regulated by ethylene. In cassava, the MYB transcription factor *MeMYB108* reduces leaf abscission under drought stress by inducing ROS scavenging (Wang et al., 2022). Whether ROS play a role that is affected by STS in the abscission of rose petals remains to be studied.

Polyamines (PAs) are cationic compounds that widely present in organisms and participate in fruit set (Alburquerque et al., 2006; Gomez-Jimenez et al., 2010). *PAO*, a gene associated with polyamine catabolism, is a stress-related gene. In present study, the expression of *RhPAO4* was down-regulated by STS and up-regulated by ethylene. Polyamines regulate ethylene biosynthesis in relation to nitric oxide (NO) and hydrogen peroxide (H_2O_2) during fruit abscission (Parra-Lobato and Gomez-Jimenez, 2011; Gil-Amado and Gomez-Jimenez, 2012). The gene *PAO4* is negatively correlated with salt stress and drought stress in tomato (Upadhyay et al., 2021). The expression of *ZmPAO2*, *3*, *4*, *5*, and *6* is increased in maize under drought stress (Pakdel et al., 2020). However, studies of the role of *PAO* genes in petal abscission of rose are presently lacking.

Ethylene response factors (AP2/ERFs) are associated with plant organ abscission (Yi et al., 2021). In the current study, we identified an ERF gene, *RhERF110*, that has not been reported previously in abscission-related studies. In cucumber, *CsERF110* is associated with sex determination and in Arabidopsis *AtERF110* regulates the timing of bolting (Zhu et al., 2013). We also screened an ethylene receptor gene, *RhETR2*, which is associated with abscission. The present qRT-PCR results showed that the expression of *RhERF110* and *RhETR2* was significantly down-regulated under STS treatment and significantly up-regulated in response to ethylene treatment. The functions of these genes in petal abscission of rose in response to STS treatment requires further investigation.

4.4 Integral effect of STS on DAMs and directly associated pathways, and genes

A combined analysis of metabolomic and transcriptomic KEGG enrichment results revealed a high degree of similarity between them. Meanwhile, STS exerted an effect on D-Erythrose 4-phosphate, an intermediate of the Pentose phosphate pathway, which is involved in the biosynthesis of various amino acids. And we found a differential gene *LOC112188495* (glyceraldehyde-3-phosphate dehydrogenase gene) in the Pentose phosphate pathway associated with D-Erythrose 4-phosphate biosynthesis (Figure 8B). Based on the expression pattern of the Pentose phosphate pathway and amino acid related DAMs, we found opposite trends in the effects of STS and ethylene on the contents of gluconolactone, D-Sedoheptulose 7-phosphate, D-Erythrose 4-phosphate, L-glutamic acid, protocatechuic acid, shikimic acid, L-Threonine, indole, and L-Tyrosine (Figure 7). Meanwhile, according to the classification results of amino acid- associated DEGs, four DEGs

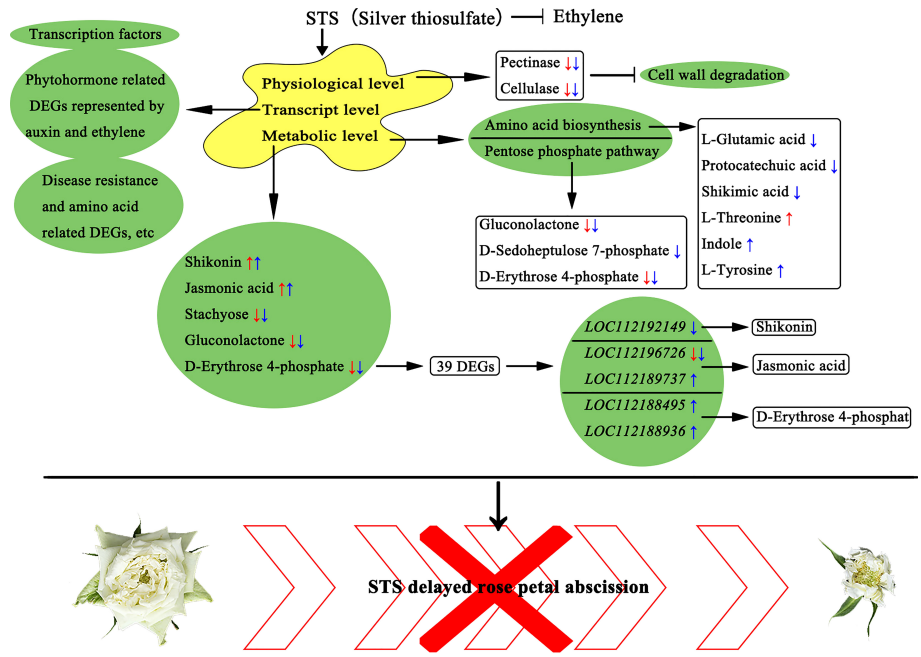

FIGURE 9
A proposed model of STS negatively influences petal abscission of rose. The red arrows indicated the up- or down- regulated in STS24h vs. MOCK24h; the blue arrows indicate the up- or down- regulated in STS24h vs. Eth24h. Scale bar, 5 cm.

were found in group STS24h vs. MOCK24h, 66 DEGs of this class were found in group ETH24h vs. MOCK24h, and nine DEGs were differentially expressed in group S_E24h vs. MOCK24h. Thus, we hypothesized that ethylene had a dramatic effect on the transcription and synthesis of amino acids during the petal abscission of rose, both at the metabolite level and at the gene level, STS eliminated this effect by inhibiting ethylene synthesis.

We identified 1120 metabolites in the AZ of rose petals. Most DAMs in the AZ were annotated with five metabolite categories, comprising Global and overview maps, Amino acid metabolism, Biosynthesis of other secondary metabolites, Carbohydrate metabolism, and Metabolism of cofactors and vitamins (Figure 2D). Subsequently, 50 DAMs from these five categories were screened (Figure 2E). Among these DAMs, the contents of five DAMs were significantly affected by STS but did not change significantly under ethylene treatment: shikonin (naphthoquinones), jasmonic acid (phytohormones), gluconolactone (esters), stachyose (carbohydrates), and D-erythrose 4-phosphate (carbohydrates). A KEGG pathway enrichment analysis of the DAMs and DEGs indicated that 39 DEGs may be associated with these five metabolites (Figure 8B). Meanwhile, these 39 DEGs belonged to 10 KEGG pathways. Among them, Ubiquinone and other terpenoid-quinone biosynthesis and Vitamin B6 metabolism belongs to Metabolism of cofactors and vitamins; Galactose metabolism belongs to Carbohydrate metabolism; alpha-Linolenic acid metabolism belongs to Lipid metabolism; Plant hormone signal transduction belongs to Signal transduction; Pentose phosphate pathway belongs to Carbohydrate metabolism; Carbon metabolism and Biosynthesis of amino acids belongs to Global and overview maps; Carbon fixation in photosynthetic organisms belongs to Energy metabolism; Phenylalanine, tyrosine and tryptophan biosynthesis belongs to Amino acid metabolism. Among the six shikonin-related DEGs, the gene *LOC112192149* encoded a 4-coumarate coenzyme A ligase 6 (4CL6), which was up-regulated in expression under STS treatment and down-regulated under ethylene treatment. The role of 4CL is to catalyze the synthesis of 4-coumaric acid coenzyme A followed by the ultimate synthesis of *p*-hydroxybenzoic acid, a precursor for shikonin biosynthesis (Suttiyut et al., 2022). Although the reactions involved in this process are obscure, 4CL is a crucial enzyme for paclitaxel synthesis. The initial steps of jasmonate biosynthesis involve members of several gene families, including phospholipases (PLA/PLD), lipoxygenases (LOX), allene oxide synthase (AOS) and allene oxide cyclases (AOC) (Singh et al., 2022). In the present study, the content of jasmonic acid was up-regulated by STS and was associated with two DEGs (*LOC112196726* and *LOC112189737*). *LOC112196726* encodes a lipoxygenase 6 (LOX6) and its expression was down-regulated by STS but up-regulated by ethylene. An additional jasmonic acid-related gene, *LOC112189737*, encodes a jasmonate ZIM domain-containing protein which expression was promoted by STS and

repressed by ethylene. In the Pentose phosphate pathway, D-erythrose 4-phosphate is generated from 3-phosphoglyceraldehyde, which in turn can be converted to 3-phosphoglyceric acid, and finally the interconversion of D-erythrose 4-phosphate and 3-phosphoglyceric acid occurs. Among the 27 DEGs associated with D-erythrose 4-phosphate, the expression of two glyceraldehyde-3-phosphate dehydrogenase genes (*LOC112188495* and *LOC112188936*) was up-regulated by STS and down-regulated by ethylene. In summary, five metabolites (shikonin, jasmonic acid, gluconolactone, stachyose, and D-erythrose 4-phosphate), and 39 DEGs were involved in the delay of petal abscission by STS. In addition, the genes 112192149 (4 coumaric acid-CoA ligase 6), 112196726 (lipoxygenase 6), 112189737 (jasmonic acid ZIM structural domain-containing protein 1), and two glyceraldehyde-3-phosphate dehydrogenase genes (112188495 and 112188936) were crucial factors related to the biosynthesis of shikonin, jasmonic acid, and D-erythrose 4-phosphate, so they probably may directly influence the changes in the three metabolic contents.

5 Conclusion

Above all, we speculated a model by which STS negatively influences petal abscission of rose (Figure 9). STS significantly delayed the petal abscission in phenotype and reduced the activity of two enzymes (pectinase and cellulase) associated with cell wall degradation in physiological level. STS significantly affected the contents of five metabolites, namely shikonin, jasmonic acid, gluconolactone, stachyose, and D-erythrose 4-phosphate, and 39 DEGs associated with these five metabolites were screened, among them five DEGs (*LOC112192149*, *LOC112196726*, *LOC112189737*, *LOC112188495*, and *LOC112188936*) were probably directly associated with the biosynthesis of shikonin, jasmonic acid, and D-erythrose 4-phosphate. Meanwhile, STS had an effect on gluconolactone, D-Sedoheptulose 7-phosphate and D-Erythrose 4-phosphate in the pentose phosphate pathway and affected changes in various amino acid biosynthesis-related metabolites, including L-Glutamic acid, protocatechuic acid, shikimic acid, L-Threonine, indole, and L-Tyrosine. In addition, STS affected the expression changes of a large number of transcription factors, phytohormone related DEGs represented by auxin and ethylene, and DEGs related to disease resistance and amino acid biosynthesis.

Data availability statement

The original contributions presented in the study are publicly available. This data can be found here: NCBI, PRJNA880356.

Author contributions

JZ, HP, YZ, YH, ZQ, and CX conceived and designed the experiments. JZ, TD, and WW collected the rose accessions and participated in the material preparation. JZ, DS, and HF performed the experiments and did the formal analysis. JZ and HP analyzed the data and drafted the manuscript. All authors contributed to the article and approved the submitted version.

Funding

This research was supported by National Nature Science Foundation of China to HP (Grant no. 31860572) and National Nature Science Foundation of China to CX (Grant no. 32060498).

Acknowledgments

We sincerely thank the editors and reviewers for their contributions. We are grateful to the staff of Beijing Novogene Technology Co., Ltd (Beijing, China) for their support in metabolite determination and analysis and transcriptome detection and analysis.

Conflict of interest

The authors declare that the research was conducted in the absence of any commercial or financial relationships that could be construed as a potential conflict of interest.

Publisher's note

Supplementary material

The Supplementary Material for this article can be found online at: https://www.frontiersin.org/articles/10.3389/fpls.2022.1045270/full#supplementary-material

References

Adal, A. M., Doshi, K., Holbrook, L., and Mahmoud, S. S. (2021). Comparative RNA-seq analysis reveals genes associated with masculinization in female *Cannabis sativa*. *Planta.* 253, 17. doi: 10.1007/s00425-020-03522-y

Alburquerque, N., Egea, J., Burgos, L., Martinez-Romero, D., Valero, D., and Serrano, M. (2006). The influence of polyamines on apricot ovary development and fruit set. *Annals. Appl. Biol.* 149, 27–33. doi: 10.1111/j.1744-7348.2006.00067.x

Çelikel, F. G., Reid, M. S., and Jiang, C. (2020). Postharvest physiology of cut gardenia jasminoides flowers. *Scientia. Hortic.* 261, 108983. doi: 10.1016/j.scienta.2019.108983

Gao, Y., Liu, Y., Liang, Y., Lu, J., Jiang, C., Fei, Z., et al. (2019). *Rosa hybrida* RhERF1 and RhERF4 mediate ethylene- and auxin-regulated petal abscission by influencing pectin degradation. *Plant J.* 99, 1159–1171. doi: 10.1111/tpj.14412

Gao, Y., Liu, C., Li, X., Xu, H., Liang, Y., Ma, N., et al. (2016). Transcriptome profiling of petal abscission zone and functional analysis of an Aux/IAA family gene RhIAA16 involved in petal shedding in rose. *Front. Plant Sci.* 7. doi: 10.3389/fpls.2016.01375

Garapati, P., Xue, G., Munne-Bosch, S., and Balazadeh, S. (2015). Transcription factor ATAF1 in arabidopsis promotes senescence by direct regulation of key chloroplast maintenance and senescence transcriptional cascades. *Plant Physiol.* 168, 1122–112+. doi: 10.1104/pp.15.00567

Gil-Amado, J. A., and Gomez-Jimenez, M. C. (2012). Regulation of polyamine metabolism and biosynthetic gene expression during olive mature-fruit abscission. *Planta.* 235, 1221–1237. doi: 10.1007/s00425-011-1570-1

Gomez-Jimenez, M. C., Paredes, M. A., Gallardo, M., and Sanchez-Calle, I. M. (2010). Mature fruit abscission is associated with up-regulation of polyamine metabolism in the olive abscission zone. *J. Plant Physiol.* 167, 1432–1441. doi: 10.1016/j.jplph.2010.05.020

John-Karuppiah, K.-J., and Burns, J. K. (2010). Expression of ethylene biosynthesis and signaling genes during differential abscission responses of sweet orange leaves and mature fruit. *Am. Soc Hortic. Sci.* 135, 456–464. doi: 10.21273/JASHS.135.5.456

Kato, M., Kanda, M., and Ichimura, K. (2022). Effects of pulse treatments with sucrose, silver thiosulfate complex (STS) and calcium chloride on the vase life and soluble carbohydrate and aurone levels in cut snapdragon flowers. *Hortic. J.* 91, 112–121. doi: 10.2503/hortj.UTD-304

Kim, J., Chun, J., and Tucker, M. (2019). Transcriptional regulation of abscission zon-es. *Plants-Basel.* 8, 154. doi: 10.3390/plants8060154

Kishimoto, K. (2021). Effect of post-harvest management on scent emission of carnation cut flowers. *Hortic. J.* 90, 341–348. doi: 10.2503/HORTJ.UTD-268

Kılıç, T., Kazaz, S., Şahin, E. G. E., and Uran, M. (2020). Extension of the vase life of cut sunflower by different vase solutions. *Ornamental. Hortic.* 26, 45–50. doi: 10.1590/2447-536x.v26i1.2108

Krause, M. R., Santos, M., Moreira, K. F., Tolentino, M. M., and Mapeli, A. M. (2021). Extension of the vase life of *Lilium pumilum* cut flowers by pulsing solution containing sucrose, citric acid and silver thiosulfate. *Ornamental. Hortic.* 27, 344–350. doi: 10.1590/2447-536x.v27i3.2330

Kucko, A., Alche, J. D., Tranbarger, T. J., and Wilmowicz, E. (2022). The acceleration of yellow lupine flower abscission by jasmonates is accompanied by lipid-related events in abscission zone cell. *Plant Sci.* 316, 111173. doi: 10.1016/j.plantsci.2021.111173

Lashbrook, C. C., and Cai, S. (2008). Cell wall remodeling in arabidopsis stamen abscission zones: Temporal aspects of control inferred from transcriptional profiling. *Plant Signaling behavior.* 3, 733–736. doi: 10.4161/psb.3.9.6489

Liang, Y., Jiang, C., Liu, Y., Gao, Y., Lu, J., Aiwaili, P., et al. (2020). Auxin regulates sucrose transport to repress petal abscission in rose (*Rosa hybrida*). *Plant Cell.* 32, 3485–3499. doi: 10.1105/tpc.19.00695

Li, X., Li, X., Li, M., Yan, Y., Liu, X., and Li, L. (2016). Dual function of NAC072 in ABF3-mediated ABA-responsive gene regulation in arabidopsis. *Front. Plant Sci.* 7. doi: 10.3389/fpls.2016.01075

Liu, X., Cheng, L., Li, R., Cai, Y., Wang, X., Fu., X., et al. (2022). The HD-zip transcription factor SlHB15A regulates abscission by modulating jasmonoyl-isoleucine biosynthesis. *Plant Physiol.* 189, 2396–2412. doi: 10.1093/plphys/kiac212

Liu, H., Ma, X., Liu, S., Du, B., Cheng, N., Wang, Y., et al. (2020). The *Nicotiana tabacum l.* major latex protein-like protein 423(NtMLP423) positively regulates drought tolerance by ABA-dependent pathway. *BMC Plant Biol.* 20, 475. doi: 10.1186/s12870-020-02690-z

Liu, J., Zhang, Z., Li, H., Lin, X., Lin, S., Joyce, D. C., et al. (2018). Alleviation of effects of exogenous ethylene on cut 'Master' carnation flowers with nano-silver and silver thiosulfate. *Postharvest. Biol. Technol.* 143, 86–91. doi: 10.1016/j.postharvbio.2018.04.017

Livak, K. J., and Schmittgen, T. D. (2001). Analysis of relative gene expression data using real-time quantitative PCR and the 2(-delta delta C(T)) method. *Methods* 25, 402–408. doi: 10.1006/meth.2001.1262

Li, B., Zhang, P., Wang, F., Li, R., Liu, J., Wang, Q., et al. (2021). Integrated analysis of the transcriptome and metabolome revealed candidate genes involved in GA(3)-induced dormancy release in *Leymus chinensis* seeds. *Int. J. Mol. Sci.* 22, 4161. doi: 10.3390/ijms22084161

Ma, Z., Huang, Y., Zhang, Z., Liu, X., Xuan, Y., Liu, B., et al. (2022). Comparative genomic analysis reveals cellulase plays an important role in the pathogenicity of setosphaeria turcica f. sp. *Zeae*. *Front. Microbiol.* 13. doi: 10.3389/fmicb.2022.925355

Meir, S., Philosoph-Hadas, S., Sundaresan, S., Selvaraj, K. S. V., Burd, S., Ophir, R., et al. (2010). Microarray analysis of the abscission-related transcriptome in the tomato flower abscission zone in response to auxin depletion. *Plant Physiol.* 154, 1929–1956. doi: 10.1104/pp.110.160697

Naing, A. H., Soe, M. T., Yeum, J. H., and Kim, C. K. (2021). Ethylene acts as a negative regulator of the stem-bending mechanism of different cut snapdragon cultivars. *Front. Plant Sci.* 12. doi: 10.3389/fpls.2021.745038

Nakano, T., Fujisawa, M., Shima, Y., and Ito, Y. (2014). The AP2/ERF transcription factor SlERF52 functions in flower pedicel abscission in tomato. *J. Exp. Botany.* 65, 3111–3119. doi: 10.1093/jxb/eru154

Niu, X., and Fu, D. (2022). The roles of BHLH transcription factors in plant development and environmental response. *Int. J. Mol. Sci.* 23, 3731. doi: 10.3390/ijms23073731

Ota, A., Tajima, M., Mori, K., Sugiyama, E., Sato, V. H., and Sato, H. (2021). The selective cytotoxicity of silver thiosulfate, a silver complex, on MCF-7 breast cancer cells through ROS-induced cell death. *Pharmacol. Rep.* 73, 847–857. doi: 10.1007/s43440-021-00260-0

Pakdel, H., Hassani, S. B., Ghotbi-Ravandi, A. A., and Bernard, F. (2020). Contrasting the expression pattern change of polyamine oxidase genes and photosynthetic efficiency of maize (*Zea mays l.*) genotypes under drought stress. *J. Biosci.* 45, 73. doi: 10.1007/s12038-020-00044-3

Parra-Lobato, M. C., and Gomez-Jimenez, M. C. (2011). Polyamine-induced modulation of genes involved in ethylene biosynthesis and signalling pathways and nitric oxide production during olive mature fruit abscission. *J. Exp. Botany.* 62, 4447–4465. doi: 10.1093/jxb/err124

Patharkar, O. R., and Walker, J. C. (2018). Advances in abscission signaling. *J.Exp. Bot.* 69, 733–740. doi: 10.1093/jxb/erx256

Patterson, S. E., and Bleecker, A. B. (2004). Ethylene-dependent and -indepenent processes associated with floral organ abscission in arabidopsis. *Plant Physiol.* 134, 194–203. doi: 10.1104/pp.103.028027

Ricci, A., Capriotti, L., Mezzetti, B., Navacchi, O., and Sabbadini, S. (2020). Adventitious shoot regeneration from *In vitro* leaf explants of the peach rootstock Hansen 536. *Plants-Basel.* 9, 755. doi: 10.3390/plants9060755

Singh, P., Bharti, N., Singh, A. P., Tripathi, S. K., Pandey, S. P., Chauhan, A. S., et al. (2020). Petal abscission in fragrant roses is associated with large scale differential regulation of the abscission zone transcriptome. *Sci. Rep.* 10, 17196. doi: 10.1038/s41598-020-74144-3

Singh, P., Maurya, S. K., Pradhan, L., and Sane, A. P. (2022). The JA pathway is rapidly down-regulated in petal abscission zones prior to flower opening and affects petal abscission in fragrant roses during natural and ethylene-induced petal abscission. *Scientia. Hortic.* 300, 111072. doi: 10.1016/j.scienta.2022.111072

Smith, E., and Whiting, M. (2010). Effect of ethephon on sweet cherry pedicel fruit retention force and quality is cultivar dependent. *Plant Growth Regul.* 60, 213–223. doi: 10.1007/s10725-009-9435-3

Son, K. C., Byoun, H. J., and Yoo, M. H. (2003). Effect of pulsing with $AgNO_3$ or STS on the absorption and distribution of silver and the vase life of cut rose 'Red sandra'. *Acta Hortic.* 624, 365–372. doi: 10.17660/ActaHortic.2003.624.50

Suttiyut, T., Auber, R. P., Ghaste, M., Kane, C. N., McAdam, S. A. M., Wisecaver, J. H., et al. (2022). Integrative analysis of the shikonin metabolic network identifies new gene connections and reveals evolutionary insight into shikonin biosynthesis. *Hortic. Res.* 9, uhab087. doi: 10.1093/hr/uhab087

Upadhyay, R. K., Fatima, T., Handa, A. K., and Mattoo, A. K. (2021). Differential association of free, conjugated, and bound forms of polyamines and transcript abundance of their biosynthetic and catabolic genes during Drought/Salinity stress in tomato (*Solanum lycopersicum l.*) leaves. *Front. Plant Sci.* 12. doi: 10.3389/fpls.2021.743568

Wang, B., Li, S., Zou, L., Guo, X., Liang, J., Liao, W., et al. (2022). Natural variation MeMYB108 associated with tolerance to stress-induced leaf abscission linked to enhanced protection against reactive oxygen species in cassava. *Plant Cell Rep.* 41, 1573–1587. doi: 10.1007/s00299-022-02879-6

Want, E. J., Masson, P., Michopoulos, F., Wilson, I. D., Theodoridis, G., Plumb, R. S., et al. (2013). Global metabolic profiling of animal and human tissues *via* UPLC-MS. *Nat. Protoc.* 8, 17–32. doi: 10.1038/nprot.2012.135

Yamasaki, H., Ogura, M. P., Kingjoe, K. A., and Cohen, M. F. (2019). D-Cysteine-Induced rapid root abscission in the water fern *Azolla pinnata*: Implications for the linkage between d-amino acid and reactive sulfur species (RSS) in plant environmental responses. *Antioxidants.* 8, 411. doi: 10.3390/antiox8090411

Yi, J., Wang, Y., Ma, X., Zhang, J., Zhao, M., Huang, X., et al. (2021). LcERF2 modulates cell wall metabolism by directly targeting a UDP-glucose-4-epimerase gene to regulate pedicel development and fruit abscission of litchi. *Plant J.* 106, 801–816. doi: 10.1111/tpj.15201

Zhu, L., Liu, D., Li, Y., and Li, N. (2013). Functional phosphoproteomic analysis reveals that a serine-62-Phosphorylated isoform of ethylene response Factor110 is involved in arabidopsis bolting. *Plant Physiol.* 161, 904–917. doi: 10.1104/pp.112.204487

Frontiers in
Plant Science

Cultivates the science of plant biology and its applications The most cited plant science journal, which advances our understanding of plant biology for sustainable food security, functional ecosystems and human health.

Discover the latest Research Topics

See more →

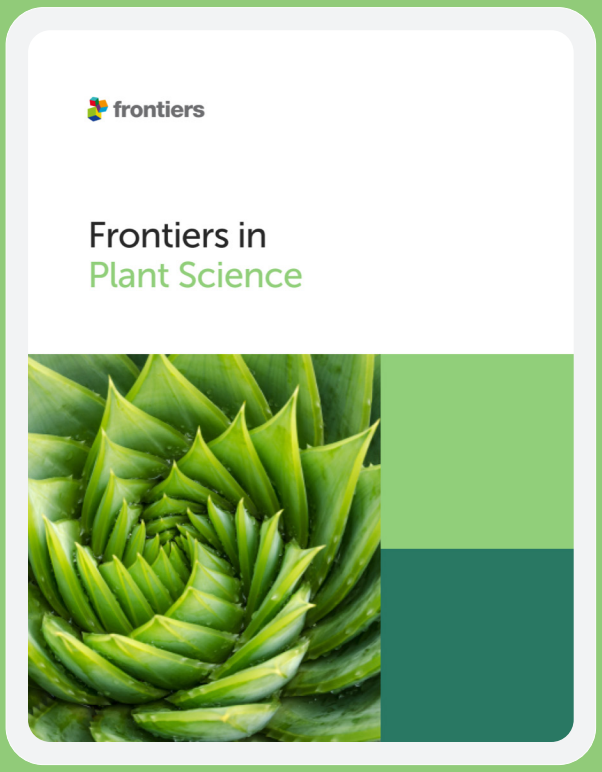

Frontiers

Avenue du Tribunal-Fédéral 34
1005 Lausanne, Switzerland
frontiersin.org

Contact us

+41 (0)21 510 17 00
frontiersin.org/about/contact